NASA CR-163,578

A Reproduction

OF

NASA CR-163,578

(NASA-CR-163578) PHASE 2 AND 3 WIND TUNNEL TESTS OF THE J-97 POWERED, EXTERNAL AUGMENTOR V/STOL MODEL (De Havilland Aircraft Co. of Canada Ltd.) 174 p
HC A08/MF A01

CSCL 01A G3/02

N80-31350

Uncla
16917

THE DE HAVILLAND AIRCRAFT OF CANADA LIMITED

DHC-DND 80-1

PHASE 2 AND 3 WIND TUNNEL TESTS OF THE J-97 POWERED, EXTERNAL AUGMENTOR V/STOL MODEL

MARCH 1980

DE HAVILLAND AIRCRAFT OF CANADA LIMITED

DHC-DND 80-1

PHASE 2 AND 3 WIND TUNNEL TESTS OF THE J-97 POWERED, EXTERNAL AUGMENTOR V/STOL MODEL

NASA Contract No. NASW 2797

DSS Contract Serial No. 2SR77-00008

Prepared & Submitted by .....
D.B. Garland J.L. Harris

Approved by .....
D.C. Whittley

1. SUMMARY

Further static and forward speed tests have been made in the 40 x 80 foot wind tunnel at the Ames Research Center, NASA, of a large-scale, ejector-powered V/STOL aircraft model. Modifications had been made to the model following earlier tests primarily to improve longitudinal acceleration capability during transition from hovering to wing-borne flight. A rearward deflection of the fuselage augmentor thrust vector was shown to be beneficial in this regard. Other augmentor modifications were tested, notably the removal of both endplates, which improved acceleration performance at the higher transition speeds. The model tests again demonstrated minimal interference of the fuselage augmentor on aerodynamic lift. A flapped canard surface also showed negligible influence on the performance of the wing and of the fuselage augmentor.

2. CONTENTS

TABLES

3. INTRODUCTION

Initial static and wind tunnel tests of the large-scale model of the DHC 'external-augmentor' V/STOL concept were undertaken in 1977-78 and reported in References 1, 2 and 3. Two further wind tunnel tests have now been completed, the results from which have been combined to form the present test report. The model is fully described in References 4 and 5. Descriptions of the concept together with an overview of test results have been published in References 6 and 7.

The objectives addressed in these latest tests were to investigate the effects of the following:

(a) Vectoring of the fuselage augmentor thrust (the augmentor nozzles were deflected rearward by 12½°).

(b) Fuselage augmentor throttling (the diffuser area ratio was reduced from 1.6 to 0.5 at forward speed).

(c) Thrust transfer from fuselage augmentor nozzles to a rear propulsion nozzle (individual fuselage augmentor nozzles were 'blanked-off' in several arrangements).

(d) Removal of fuselage augmentor endplates at forward speed (normally required statically to maintain a high thrust augmentation ratio).

(e) Fuselage augmentor inlet vanes (two different arrangements to improve flow into the augmentor at high forward speed).

(f) Leading-edge slat on outboard wing panels (to eliminate a previously observed wing stall).

(g) Canard surface interference on wing and fuselage augmentor.

(h) 'Wing-borne' configuration (i.e. fuselage augmentor seal and all fuselage augmentor nozzle thrust transferred to the rear propulsion nozzle, the wing augmentor remaining operational).

The research work described here was conducted by De Havilland Aircraft of Canada (DHC) in cooperation with the Ames Research Center, NASA: the work was funded jointly by the Canadian Department of National Defence and NASA and undertaken with the support of the facilities of the Ames Research Center.

4. DESCRIPTION OF MODEL AND TESTS

4.1 Model

A three-view drawing of the model is given in Figure 1. Photographs of the model in the 40 x 80 foot wind tunnel at the Ames Research Center are reproduced as Figures 2 and 3. Tables 1, 2 and 3 list pertinent geometrical data.

The model geometry is the same as in the earlier tests, with the following exceptions:-

(a) Deflected fuselage augmentor nozzles.

The fuselage augmentor nozzles were 'twisted' through $12\frac{1}{2}^{o}$ to provide an axial component of thrust to improve longitudinal acceleration during transition. Figure 4 shows how a 'twisted' segment was inserted into the basic nozzle to achieve the desired thrust deflection.

To maintain control over the flow at the augmentor endplates, the nozzle-to-endplate spacing has been retained at ¼ pitch, hot. The inlet fairings and endplate locations have been modified accordingly, as shown in Figure 5. Two nozzles have been removed at the aft end of the augmentor to allow the rear endplate to remain within the existing augmentor door. This slightly decreased the fuselage/wing thrust split ratio, a favourable trend for improving transition.

(b) Hinged fuselage augmentor doors.

A revised door attachment scheme (Figure 6) was introduced to allow a wide range of diffuser area ratio and

yet still provide an essentially air-tight hinge. This feature will be most useful for future static tests when augmentor optimization will be pursued.

(c) Inlet turning vanes for fuselage augmentor.

Two designs of vanes were tested in an attempt to improve flow through the fuselage augmentor at forward speed These are shown in Figure 7.

(d) Augmentor inlet cover plates.

As part of the transition studies, a longitudinally shortened augmentor was tested. Figure 8 shows how covers with inlet fairings were installed over the forward and rear quarters of the augmentor inlet leaving only the middle half of the augmentor operational. Nozzles under the covers were blanked-off. Augmentor endplates were removed and the augmentor door fixed at the required DAR by strut braces at the lower end of the doors.

(e) Leading edge slat for outboard wing panel.

A simple slat was attached to the outboard wing panels to extend the angle of attack range before leading edge stall occurred. Details are given in Figure 9.

(f) Canard surface.

A canard with leading edge slat and a plain flap (Figure 10) was mounted as shown in Figure 1. The flap was remotely controllable over the range 0^{o} to 30^{o} and the canard incidence could be manually set in increments of 10^{o} in the range $\pm 30^{o}$.

(g) Sealed augmentor.

For tests representing the case where the fuselage augmentor was shut down, inlet covers were installed, the augmentor doors were removed and replaced with plywood panels in the 'closed door' position (see Figure 11). All the fuselage augmentor nozzles were blanked-off and a propulsion nozzle of equivalent area fitted to the rear end of the fuselage duct. The wing augmentor remained operational.

(h) Revised augmentor exit rake.

A new augmentor exit rake was made with pitot and static tubes inclined 15° to align with the expected fuselage augmentor efflux direction (Figure 12).

(i) Fuselage base instrumentation.

A false base was installed, as shown in Figure 13, containing surface static pressure taps and thermocouples.

4.2 Thrust Loading

As noted in Reference 3, the design thrust loading for the model was 60 lb/ft.^{2} At the elevated temperatures generated in the 40 x 80 foot wind tunnel (up to 135°F) the maximum nozzle pressure ratio was limited to 2.5 (compared with the standard day design value of 3.5) and the thrust loading was correspondingly reduced to 35 lb/ft.^{2} Some of the later tests in the wind tunnel were further restricted by noise abatement requirements and an even lower thrust loading was necessary. The full scale, or equivalent, flight dynamic head is inversely proportional to the model thrust

loading so that appropriate factors may be applied to the tunnel q to obtain equivalent full-scale dynamic head.

4.3 Reference Pressure Ratio

The J97 engine thrust was set during tests by reference to a reading of the static pressure in the fuselage duct located just upstream of the first fuselage augmentor nozzle off-take (see location PF1 in Figure 14). This pressure is expressed as a Reference Pressure Ratio

$$RPR = \frac{PF1}{p_a}$$

and is used throughout this report. The total pressure measured at the exit plane of the fuselage augmentor nozzles was approximately 9.6% greater than the reference static pressure, PF1. Hence with RPR = 2.30 (a value used for most of the forward speed tests) the average nozzle pressure ratio (NPR) was 2.52.

4.4 Data Reduction

For all force and moment data, the thrust of the small trim nozzle in the rear fuselage was subtracted from the balance values. The inlet momentum drag of the J97 engine was not subtracted.

Wind tunnel boundary corrections were based on aerodynamic or effective lift (the total lift less the reactive lift components of the static augmented thrusts of the fuselage and wing augmentors). Effective lift coefficient is given by:

$$C_{L_{eff}} = C_L - C_{J_{AUG_F}} \cos(\alpha - \theta_F) - C_{J_{AUG_W}} \sin(\alpha + \delta_F) - C_{J_{NR}} \sin\alpha$$

The following boundary corrections were then made:

$$\alpha = \alpha_u + 0.3538\ C_{L_{aero}}$$

$$C_D = C_{D_u} + 0.0062\ \left(C_{L_{aero}}\right)^2$$

The corrected coefficient data were then used to compute the force ratios

$$L/T_H,\ D/T_H,\ M/T_H\bar{c}$$

where T_H is the augmented thrust of the model in the "hovering" configuration, i.e. the sum of the fuselage augmentor thrust and the wing augmentor thrust. The former is the value determined from static test measurements with the nozzles deflected aft 12.5 degrees, all nozzles operating, endplates on and diffuser area ratio = 1.6. It includes a small loss due to negative base thrust (see Section 5). The wing augmentor thrust is the value determined from static test measurements with the wing/flap fairing off. This fairing gives rise to a small loss in thrust at large deflection angles (see Reference 8) which is discounted in the evaluation of T_H.

Note that the gross wing area used to define force and moment coefficients is the area of the complete wing, including the forward part containing the fuselage augmentor, plus the projected area of the complete wing within the fuselage. The gross area of the wing without the forward part is 98.80 sq. ft.

5. STATIC TEST RESULTS

For static tests in the wind tunnel working section, the model was mounted on the standard balance struts and was therefore about 18 feet above the tunnel floor, well out of ground effect. The overhead tunnel doors were opened wide to minimize recirculation effects and run times were kept short to reduce build-up of tunnel q.

The quantities of interest derived from the present static tests were the gross thrust augmentation ratio

$$\phi_{G_{F+B}} = \sqrt{L_{F+B}^2 + D_F^2} \Big/ X_{N_F}$$

and the average jet efflux angle

$$\theta_{F+B} = \tan^{-1}\left(\frac{-D_F}{L_{F+B}}\right)$$

where $L_{(F+B)} = L - L_W$)
$D_F = D - D_W + X_{N_R}$) suffix F relates to fuselage augmentor
$L_W = \phi_{G_W} . X_{N_W} \sin \delta_F$) suffix W relates to wing augmentor
$D_W = -\phi_{G_W} X_{N_W} \cos \delta_F$) the wing augmentor thrust components at the model static test attitude of $\alpha = 0^c$

and X_{N_R} = the rear propulsion nozzle thrust, if any.

The fuselage augmentor nozzle thrust, X_{N_F}, was assumed to be 25/27 of the previously determined value for the VTOL 1 configuration (as in Reference 1), since two nozzles had been removed from each nozzle array for the present configuration (as shown in Figure 5).

The subscript 'F + B', meaning 'fuselage augmentor plus base', signifies that the base thrust effect is included in

the calculated augmentation ratio and efflux angle. Base thrust data became available only in the VTOL 3 test program when the pressure instrumentation was added (see Figure 13). The base thrust arises from a small base pressure, negative in free-air, which is generated between the two fuselage augmentor effluxes. Subsequent static tests (Reference 8) have shown, however, that the negative base pressure causes an increase in thrust augmentation of the fuselage augmentor which almost offsets the base thrust. Nevertheless, the subscript 'F + B' is retained to indicate that the data refer to the complete 'fuselage augmentor plus base' configuration.

Figures 15 and 16 present $\phi_{G_{F+B}}$ and θ_{F+B} respectively versus RPR for each of the configurations tested. A summary of the results at RPR = 2.3 is given in Table 6.

For the basic augmentor, i.e., DAR = 1.6, endplates on and full set of 25 nozzles operating, $\phi_{G_{F+B}}$ was determined to be about 1.50 to 1.57 in the VTOL 2 tests at RPR = 2.30. The scatter was partly due to the degree of endplate flow attachment generated by the jet efflux from the first and last nozzles of the array. The clearance between these nozzles and the endplates was initially too large and some experimentation was done in this area.

Cold flow tests at DHC had shown that a 15° efflux deflection (or thrust vectoring) of the fuselage augmentor thrust would be obtained if the nozzle angle was a few degrees less ($12\frac{1}{2}^{\circ}$ was actually chosen for the J97 powered model).

This arose from the augmentor internal flow having to cross the diffuser isobars non-orthogonally (viz. 90 - 12.5 = 77.5° initially), as shown in Figure 17. The collected efflux angle data of Figure 16 indicate a deflection of about 15° for the basic augmentor.

The collected static test data also show the effects of diffuser area ratio, removing front or both endplates, blanki off alternate nozzles, blanking-off all but the centre half o the nozzles, etc. These changes reflect naturally in the forward speed data.

Figure 18 shows a comparison between the deflected augmentor nozzle results of the present tests with those of the undeflected nozzle tests of the VTOL 1 augmentor (Reference 3) With base thrust effects included, the augmentation ratio $\phi_{G_{F+B}}$ is seen to decrease by about 5 counts due to the nozzl deflection of 12.5 degrees.

Installation of the augmentor exit rake had no discernibl effect on thrust augmentation ratio but caused small reduction in jet deflection ar-'e (as shown in Figure 19). The reasons for this are not fully understood.

It should be noted that the derivation of $\phi_{G_{F+B}}$ is more direct (and reliable) for configurations with $\delta_c = 0^\circ$ because in such cases, it is not necessary to make assumptions with respect to the thrust of the wing augmentor.

6. FORWARD SPEED RESULTS

6.1 Presentation of Transition Performance

An important area of interest at the present stage of development relates to the optimization of acceleration capability from hover to wing-borne flight during which the fuselage augmentor is progressively shut down and eventually sealed with appropriate folding doors. The rear propulsion nozzle is correspondingly increased in area to accept the transferred fuselage augmentor nozzle thrust. The angle of attack range during transition is important, too, as is the pitching moment. However, the moment is amenable to change by configuration layout and by appropriate 'blanking' of fuselage augmentor nozzles during transition.

A limited number of configurations have been tested in the wind tunnel to explore the effects of flap angle, diffuser area ratio, and thrust transfer on transition characteristics. These are listed in Table 7. The force data for these configurations are presented in Figures 20 through 48 in the format

L/T_H vs α

L/T_H vs D/T_H

L/T_H vs $M/T_H \bar{c}$

The denominator, T_1, is the take-off thrust in the hovering configuration as defined in Section 4.4.

These data relate to a fuselage augmentor with nozzle angle (δ_N) deflected 12½° rearward relative to the vertical datum of the aircraft. The data may be interpreted in either of two ways:

(i) nozzle angle δ_N = 12½° and fixed, this being the basis of analysis (or interpretation) presented here.

(ii) nozzle angle variable, in which case the results provide a set of data for one value of δ_N only, in a possible range of -10° to +40°, say.

For a VTOL aircraft, it is necessary that T_H be greater than the take-off weight to allow for vertical acceleration and for excess thrust for control and trim purposes. When comparing the various transition configurations, a value of T_H/W = 1.10 has been taken as a typical reference value. The drag ratio, D/T_H, during transition, is obtained from the wind tunnel data at a lift ratio given by

$$L/T_H = \frac{W}{1.10W} = 0.91$$

since L = W if negligible vertical acceleration is used once the VTOL aircraft has started to pick up forward speed. This also assumes that the hovering or take-off level of thrust is maintained during the transition maneuver.

From the drag ratio D/T_H the longitudinal acceleration is given by

$$Acc^n = -D/W = -1.10\left(\frac{D}{T_H}\right) \quad (acc^n \text{ in g's})$$

This value of acceleration has been plotted to show transition performance (Figures 49 through 55) as a function of forward speed. In these figures the forward speed is the value equivalent to that for a VTOL aircraft having the same aerodynamic characteristics as the present model but operating at its design value of thrust loading,

$$\text{i.e. } \left(T_{H}/_{S}\right)_{\text{Design}} = 60 \text{ lb/ft}^2$$

The wind tunnel model would have given this loading at standard day conditions with a J97 engine operating at its design pressure ratio (NPR = 3.5). Due to the high temperatures encountered in the wind tunnel the model was operated at a reduced power setting which generated a thrust loading less than the design value, as described in Section 4.2. The wind tunnel tests were conducted at correspondingly lowered wind speeds to generate the same jet thrust coefficient, $C_{J_{AUG}}$, as the 'full-scale aircraft'.

Table 8 gives a summary of transition performance, i.e. acceleration, angle of attack and pitching moment for $T_{H}/_{L}$ = 1.10 and $T_{H}/_{S}$ = 60 lb/ft^2 as described above. The table also records the model configuration, its identification code and the figure number of the force data plot.

6.2 Basic Augmentor Configuration

The 'basic' augmentor is that used for hovering. It generates the greatest thrust augmentation. In these tests therefore, the configuration is defined by all nozzles operating (but deflected 12½°), endplates on and diffuser area ratio set to 1.60.

Tests were conducted with flap deflections of 0, 30 and 45°. The augmentor exit rake was installed for some test and affected test results as described below. The effect of flap angle on acceleration and angle of attack in level flight is shown in Figure 49. It can be seen that a large flap deflection permits a greater acceleration but requires a large nosedown model attitude. A representative, practical deflection is probably about 30° and will allow acceleration up to about 130 knots (Figure 49(b), rake-off data) with a nose down attitude (α) not exceeding -13°.

Interference effects of the augmentor exit rake on performance at forward speed were unexpectedly large in the VTOL 2 tests (see Figure 50(a) and (b)) although much useful information on augmentor exit flow distribution was collected. (See Section 6.9.) In the VTOL 3 tests, the interference was smaller (Figure 50(c)) but the rake was removed for most of the tests.

6.3 Intermediate Augmentor Configurations

These fall into three categories

(a) reductions in diffuser area ratio
(b) removal of one or both endplates
(c) thrust transfer (by blanking some augmentor nozzles and increasing propulsion nozzle area).

The tested configurations (see Table 7) often combined all three modifications as attempts were made to maximize acceleration capability and to simplify the augmentor configuration.

In the first category, reduction of DAR, Figures 51(a) and (b) show no favourable effect with the 'full nozzle set' augmentor at $\delta_F = 45^o$ but some advantage at high speed with the 'alternate nozzles blanked' configuration. The acceleration data reflect the relative magnitudes of the major force components, viz. augmentor inlet momentum drag, propulsion nozzle thrust and drag due to lift. It should be noted that the nose down attitude is reduced as augmentor thrust is reduced (by throttling or thrust transfer). Aerodynamic lift then replaces jet lift.

With augmentor endplates off, the effect of reducing DAR is very small. Figures 52(a), (b) and (c) show test results with the three different nozzle configurations, i.e. full nozzles, alternate nozzles and 'centre' nozzles.

The case with only the front endplate off (Figure 53) falls somewhere between the endplates on and endplates off test results. Reducing DAR with the full nozzle set at $\delta_F = 30^o$ lowered the acceleration capability in the speed range of interest.

In the second category, removal of one or both endplates, a significant improvement in acceleration performance was produced by removing the front endplate. (See Figures 54(a) and (b)). It is presumed that the increased deflection of the fuselage augmentor efflux (see Section 5) gave rise to this improvement. There was some benefit obtained by removing both endplates, a result of some considerable practical significance.

In the third category, thrust transfer, a benefit was recorded above about 100 knots (see Figure 55(a)) with alternate nozzles blanked-off and with $\delta_F = 30^\circ$. There was no improvement, however, with the flap set at 45°, (Figure 55(b)). The best results were obtained with the "centre nozzles" configuration and endplates off (Figure 55(c)). Inlet fairings or covers over the blanked-off nozzles at the front and back of the augmentor (Figure 8) had no effect on the test data.

Some representative test data of intermediate transition configurations are given in Figure 56 in the more usual force coefficient format. These may be compared with the wing-borne data shown in Figure 61.

6.4 Augmentor Sealed (Wing-Borne) Configuration

This configuration is one where all the fuselage augmentor nozzle area has been blanked-off and replaced with equivalent propulsion nozzle area in the rear fuselage. The wing augmentor was operating as usual but the fuselage augmentor doors were "retracted" (in practice, replaced with plywood panels to simulate the retracted position, see Figure 11). The fuselage augmentor inlets were sealed with close-fitting light alloy covers, simulating intake doors on a VTOL aircraft in the closed position.

The test data (Figure 57) show an acceleration capability of about 0.4g at 100 knots. Performance is best at the lower flap angles but angle of attack becomes rather large in that case. A good compromise would be $\delta_F = 40^\circ$

at $\alpha = +10^{\circ}$ at 100 knots. The corresponding lift coefficient is $C_L = 1.6$ and the equivalent wing loading is $W/S = 54.5$ lb/ft^2 based on gross wing area.

6.5 Summarized Acceleration Capability

The maximum recorded accelerations for the best configurations are shown in Figure 58 together with the associated angles of attack. Also shown are the accelerations available within the α limits of $\pm 10^{\circ}$. These test data applied to a full-scale aircraft would allow acceleration to 110 knots in about 10 seconds, covering about 1000 feet horizontally in the process. At 110 knots, transition from jet-borne to wing-borne flight could be achieved with a constant flap angle of 30° without exceeding the $\pm 10^{\circ}$ attitude limitations.

6.6 Pitch Trim

The major components of the pitching moment arise from the deflected wing augmentor flap (nose down moments) and the fuselage augmentor inlet flow (nose up moment). At low forward speed the resultant moment would be minimized by appropriate choice of aircraft layout and trimmed out by jet reaction methods (using either the fuselage augmentor or separate 'puff-pipes'). At higher speeds, a tailplane or canard surface would provide the primary trim control.

Pitching moments of the present model layout are shown in Figure 59 to give an idea of present magnitudes and are compared with the available contribution from the present canard surface (or an equivalent tailplane) at an effective surface lift coefficient of 1.0.

6.7 Effect of Wing Leading-Edge Slat

The outer wing panels showed a pronounced leading edge stall during the VTOL 1 tests, the stalling angle being a function of flap angle primarily. For the subsequent wind tunnel tests, a simple L/E slat (see Figure 9) was added. It provided excellent control of flow over the wing, as indicated by tufts, up to $\alpha = 24^{\circ}$ or so. The flow on the slat upper surface was also attached. Test data are reproduced in Figure 60. The improvement due to slat is evident at the larger angles of attack. This is more clearly seen when the test data are plotted with the reactive thrust components removed (see Section 6.8, Figure 74).

6.8 Interference Effects of Fuselage Augmentor

6.8.1 Longitudinal

In the VTOL 3 wind tunnel tests some runs were made with the fuselage augmentor nozzles blanked-off and the augmentor closed and sealed (see Figure 11). A conical propulsion nozzle of equal area was fitted to allow for transfer of the augmentor nozzle thrust. The interference effects of the fuselage augmentor could then be obtained directly by difference between 'augmentor-on' and 'augmentor-sealed' configurations. (Unfortunately, there was insufficient test time available to examine directional characteristics with augmentor-sealed.)

The longitudinal data, in coefficient form, for the augmentor-sealed or 'wing-borne' configuration are

given in Figure 61 for flap angles of 15^{o}, 30^{o} and 45^{o}. The "effective lift coefficient" is given in Figure 62 for the same flap angles and for the three jet coefficients, $C_{J_{N_W}}$, at which the tests were made. Cross-plots of $C_{L_{eff}}$ at $\alpha = 0^{o}$ versus δ_F and $C_{J_{N_W}}$ are given in Figure 63. Lift curve slopes are plotted in Figure 64. Note that effective lift is defined as "total lift minus static, augmented lift", as defined in Section 4.4.

In Figure 65 is given $C_{L_{eff}}$ versus α for the 'augmentor-on' configuration, the jet-borne configuration with basic augmentor, i.e. full nozzle set, DAR = 1.6 and endplates on. The comparisons in Figures 66 and 67 show very small interference effects of the fuselage augmentor on lift.

Drag data for the wing-borne configuration are given in Figure 68 in the form $C_{D_{eff}}$ versus $C_{L_{eff}}^{2}$ for the three flap angles and three jet coefficients. The slope of these curves is approximately $1/\pi A$. The effect of flap angle is fairly small, as shown in Figure 69.

The definition of $C_{D_{eff}}$ parallels that of $C_{L_{eff}}$, i.e. $C_{D_{eff}} = C_D - C_{J_{AUG_F}} \sin(\alpha - \theta_F) - C_{J_{AUG_W}} \cdot \cos(\alpha + \delta_F) - C_{J_{N_R}} \cos \alpha$.

The comparative drag data with augmentor operating are given in Figures 70, 71 and 72 for the VTOL 1, 2 and 3 tests respectively. A comparison of the three tests

is given in Figure 73. The slope is seen to be about $1/\pi A$ provided the outboard wing leading-edge slat is on, as more clearly indicated in Figure 74.

6.8.2 Lateral

Some indication of the effect of fuselage augmentor on lateral data can be obtained from the effects of changing power setting, or $C_{J_{AUG}}$. Figures 75(a) and (b) show a small dependence on $C_{J_{AUG}}$ of all three lateral/directional coefficients.

The effect of thrust vectoring the fuselage augmentor efflux was small (Figure 76) as was the effect of removing the augmentor endplates (Figure 77).

6.9 Augmentor Exit Rake Results

6.9.1 Exit Distributions

The fuselage augmentor exit rake (see Figure 12) was installed for some of the runs to obtain exit total and static pressure distributions, from which were calculated velocity distributions. These, in turn, provided integrated thrust and mass flow data. Due to turbulence in the exit flow the rake thrust readings are higher than the true (balance) values (this was discussed in Reference 3). However, for comparative purposes the rake data are quite valuable.

The longitudinal distribution of exit thrust is first shown (Figures 78 and 79) for the VTOL 2 and VTOL 3 tests respectively with 'basic' augmentor. The degree of flow attachment at front and rear endplates is indicated by

the thrust level at each end of the augmentor at q = 0. At forward speed the exit thrust increases noticeably especially the rear 70% of the augmentor length. The VTOL 2 results show some thrust reduction over the front 30%, an effect also noted in the VTOL 1 tests. The VTOL 3 results show a general improvement over VTOL 2 both in the front and rear portions of the augmentor for reasons not fully understood.

A summation of the longitudinal thrust distribution gives the total rake thrust which may be divided by the fuselage augmentor nozzle thrust to give an augmentation ratio $\phi_{G_{RAKE}}$. The magnitude is high, due to turbulence, but the variation with RPR and forward speed is indicative of the real trends. Figure 80 shows results for the basic augmentor from both VTOL 2 and VTOL 3 tests.

The effect of angle of attack is quite small (Figure 81) especially for the VTOL 3 configuration (even though nominally the same as the VTOL 2 configuration).

6.9.2 Augmentor Inlet Vanes

During the VTOL 1 wind tunnel tests (Reference 3) some degradation in fuselage augmentor exit velocity distribution had been recorded at forward speed (using the exit rake). This was tentatively attributed to a flow separation near the front inlet region. Subsequent tests (in VTOL 2 and VTOL 3) with inlet vanes arranged to improve flow attachment on the high-curvature inlet regions were not successful in improving exit distributions significantly. However,

surface and stand-off tufts showed a notable change of flow direction and improvement in flow smoothness when the front endplate was removed (Run 8 of VTOL 3). The exit rake, unfortunately, was not installed for these tests. Further tuft studies in the region just ahead of the front endplate showed a flow separation from the outer edge of the front endplate (when installed) which was carried up over the wing leading-edge and into the fuselage augmentor. This is illustrated in Figure 82. The problem is believed to be much alleviated with the front endplate removed.

6.10 Canard Characteristics and Interference Effects

6.10.1 Longitudinal

Tests to investigate the magnitude of interference generated by a canard surface were made in both VTOL 2 and VTOL 3 wind tunnel programs.

Longitudinal data in coefficient format are given in Figures 83 and 84. In Figure 85 the lift and moment data are plotted versus α for the two canard incidences, $i_c = \pm 10^\circ$. The generated pitching moment increment for $\Delta i_c = 20^\circ$ was $\Delta C_M = 0.090$. With a canard moment arm of $\ell_{c/\bar{c}} = 0.92$, the corresponding lift increment would be $\Delta C_L = 0.10$. However, the measured increment was only 0.05, indicating that the downwash from the canard caused a download on the wing in the manner described in Reference 9, for example. Interference of this type may also reduce the net canard pitching moment if the downwash affects mostly that part of the wing ahead of the moment reference centre.

Figure 86 shows the effect of canard incidence change for the power-off, augmentor open configuration. These results are similar but contain several anomalous variations.

From the intersection points of the canard on/off pitching moment curves, where the canard angle of attack is zero, the upwash at the canard location can be obtained from

$$\epsilon_c = -(\alpha_w + i_c)$$

The available data are plotted in Figure 87 and show $\frac{\partial \epsilon_c}{\partial \alpha} \approx 0.5$ from the VTOL 3 tests for the configuration tested at $C_{J_{AUG}} \approx 1.25$. The effect of C_J on upwash at the canard is very small, as indicated by the intersections in Figures 83(a), (b) and (c).

Figure 88 shows the effect of canard flap deflection on C_L, C_D and C_M.

6.10.2 Lateral/Directional

Lateral data were collected with the canard at a high lift setting, viz. $i_c = + 10^o$ and $\delta_c = + 30^o$. A comparison, with canard-off data, (Figure 89) shows a small increase in C_l and a larger increase in C_n.

Figure 90 shows no change in the effect of yaw on longitudinal coefficients when the canard was installed. The comparison tests were made with $\alpha = 0$ and $\delta_F = 30^o$ with positive and negative lift on the canard. There was no observable effect of the canard on the augmentor performance.

7. CONCLUSIONS

(i) Rearward deflection of the fuselage augmentor nozzle thrust direction by about 15^{o} resulted in much improved longitudinal acceleration capability.

(ii) Reducing diffuser area ratio was not an effective means of increasing acceleration capability for the configuration with all augmentor nozzles operating. Some benefit at high speed was noted for the case where one half of the augmentor nozzles were operating. With augmentor endplates removed the effect of reducing DAR was small but favourable.

(iii) Removing the front augmentor endplate had a beneficial effect on acceleration due to the rearward deflection of fuselage augmentor efflux caused thereby.

(iv) Removing both endplates, a significant practical case, also caused an improvement in acceleration, especially at high forward speed.

(v) Thrust transfer from fuselage augmentor to rear propulsion nozzle was most beneficial when the front and rear quarters of the augmentor were shut down and augmentor endplates were removed. This configuration provided a good acceleration capability to full scale speeds in excess of 140 knots.

(vi) The wing-borne configuration or jet-flap mode (i.e. fuselage augmentor sealed and thrust transferred to the rear propulsion nozzle) demonstrated excellent acceleration capability at low speed - nearly 0.4g with $\delta_F = 40^\circ$ and $\alpha = +10^\circ$ at 100 knots full-scale.

(vii) Interference effects of the fuselage augmentor on lift characteristics of the model were again shown to be minimal. The influence of intake momentum on drag and pitching moment was as expected. Similar effects on lateral/directional derivatives are strong but well ordered. Further study is required in this area.

(viii) Tests of a canard surface mounted below the wing chord datum showed no adverse effects on the fuselage augmentor operation. The downwash from the lifting canard apparently unloads the wing somewhat. The upwash at the canard due to the wing gave a value of $\left(\partial\epsilon_c/\partial\alpha\right)$ about 0.5.

(ix) A leading-edge slat added to the outer wing panels extended the low induced drag characteristics of the model to high angles of attack. The induced drag factor 'k' was approximately 1.0 over a wide range of angle of attack and jet coefficient both 'jet-borne' and 'wing-borne'.

(x) A fuselage augmentor exit rake showed an increase of exit thrust with forward speed and quite small effects of angle of attack. A source of interference on exit thrust was believed to be a flow separation emanating from the front augmentor endplates.

8. REFERENCES

1. Garland, D.B. — Static Tests of the J97 Powered External Augmentor V/STOL Wind Tunnel Model. DHC Report DHC-DND 77-4, February 1978.

2. Aoyagi, K. Aiken, T.N. — Wind-Tunnel Investigation of a Large-Scale VTOL Aircraft Model with Wing Root and Wing Thrust Augmentors. NASA TM 78589, September 1979.

3. Garland, D.B. Whittley, D.C. — Phase I Wind Tunnel Tests of the J97 Powered, External Augmentor V/STOL Model. DHC Report DHC-DND 79-4, September 1979.

4. Garland, D.B. — Description and Test Specification for J97 Powered, External Augmentor V/STOL Wind Tunnel Model. DHC Report DHC-DND 77-3, December 1977.

5. Garland, D.B. — Specification for Phase 2 Static and Wind Tunnel Tests of J97 Powered, External Augmentor V/STOL Model (with Phase 3 Test Specificat. Addendum). DHC Report DHC-DND 78-2, November 1978.

6. Garland, D.B. — Transition Characteristics of the External Augmentor V/STOL Aircraft Concept. Proc. V/STOL Aircraft Aerodynamics Symposium, Naval Postgraduate School, Monterey, California, May 1979.

7. Whittley, D.C. Koenig, D.G. — Large Scale Model Tests of a New Technology V/STOL Concept. AIAA Paper No. 80-0233, January 1980.

8. Gilbertson, F.L.
Love, R.H.

Static Tests of the J-97 Powered, External Augmentor V/STOL Model at the Ames Research Center, NASA DHC-DND 80-2 April 1980

9. Paulson, J.W.
Thomas, J.L.

Summary of Low-Speed Longitudinal Aerodynamics of Two Powered, Close-Coupled Wing-Canard, Fighter Configurations.

NASA TP 1535,
December 1979.

9. NOTATION

A = aspect ratio

$\bar{c}$ = mean aerodynamic chord (m.a.c.)

C_D, C_{D_C} = corrected drag coefficient

$C_{D_{eff}}$ = effective drag coefficient (see Section 6.8.1)

C_{D_U} = uncorrected drag coefficient

$C_{J_{AUG}}$ = T_H/qS

$C_{J_{AUG_F}}$ = X_{AUG_F}/qS

$C_{J_{AUG_W}}$ = X_{AUG_W}/qS

$C_{J_{NF}}$ = X_{N_F}/qS

$C_{J_{NR}}$ = X_{N_R}/qS

$C_{J_{NW}}$ = X_{N_W}/qS

C_L = lift coefficient

$C_{L_{aero}}$ = $C_{L_{eff}}$, effective lift coefficient (see Section 4.4)

C_{L_T} = tail (or canard) lift coefficient

C_l = rolling moment coefficient

C_m = pitching moment coefficient (see Table 1)

C_n = yawing moment coefficient

Cy = side force coefficient

D = balance drag force

D_F = drag component of fuselage augmentor thrust (q = 0)

D_R = drag component of rear nozzle thrust (q = 0)

D_W	=	drag component of wing augmentor thrust (q = 0)
DAR	=	diffuser area ratio
DHC	=	The De Havilland Aircraft of Canada, Limited
E/P	=	endplate
i_c	=	canard incidence
k	=	induced drag factor
L	=	lift force
L_F	=	lift component of fuselage augmentor thrust (q = 0)
L_R	=	lift component of rear nozzle thrust (q = 0)
L_W	=	lift component of wing augmentor thrust (q = 0)
L/E	=	leading-edge
M	=	pitching moment
mac	=	mean aerodynamic chord (= $\bar{c}$)
NPR	=	fuselage augmentor nozzle pressure ratio
p	=	fuselage augmentor nozzle pitch
p_a	=	ambient pressure
PF1	=	reference pressure in J97 exhaust duct
q	=	wind tunnel dynamic head (lb/ft^2)
RPR	=	reference pressure ratio ($PF1/p_a$)
S	=	gross wing area
Ta	=	ambient temperature
t/c	=	thickness/chord ratio
T_H	=	$(X_{AUG_F} + X_{AUG_W} + X_{BASE})$ at q = 0
W	=	aircraft weight
X_{AUG_F}	=	fuselage augmentor thrust ($= \phi_{G_F} \cdot X_{N_F}$)
X_{AUG_W}	=	wing augmentor thrust ($= \phi_{G_W} \cdot X_{N_W}$)

X_{N_F} = fuselage augmentor nozzle thrust

X_{N_R} = rear (propulsive) nozzle thrust

X_{N_W} = wing augmentor nozzle thrust

$\alpha, \alpha_{c'}, \alpha_w$ = wing angle of attack, corrected for tunnel wall constraint

α_u = uncorrected angle of attack

β = sideslip angle

δ_c = canard flap deflection angle

δ_F = wing augmentor flap deflection angle

δ_N = fuselage augmentor nozzle deflection angle (measured from z axis)

ϵ_c = downwash angle at canard location

ϕ_{G_F} = (X_{AUG_F}/X_{N_F}) at $q = 0$

$\phi_{G_{F+B}}$ = $(X_{AUG_F} + X_{BASE})/X_{N_F}$ at $q \neq 0$

$\phi_{G_{RAKE}}$ = Fuselage augmentor exit thrust as obtained by rake survey / X_{N_F}

ϕ_{G_W} = X_{AUG_W}/X_{N_W} at $q = 0$

TABLE 1 GEOMETRY OF J-97 POWERED, EXTERNAL AUGMENTOR V/STOL MODEL

Wing	
Area, gross	141 ft^2
Area, net	97 ft^2
Span	15.25 ft.
Aspect ratio	1.65
t/c	6%
m.a.c.	12.68 ft.
Chord on Fuselage Centreline	16.92 ft.
Fuselage	
Overall length	approx. 28 ft.
Fin	
Area	22.4 ft^2
Span (above fuselage top)	4.33 ft.
Aspect ratio	0.84
Canard	
Area (exposed/gross)	15.0/24.2 ft^2
Span	8.83 ft.
Aspect ratio	3.23
Tail volume coefficient (gross)	0.158

Moment reference centre (wing leading edge joint, on wing chord datum)
Distance ahead of rear strut location $\bar{x}$ = 44.0"
(also equal to 47.2% of m.a.c.)

TABLE 2 GEOMETRY OF FUSELAGE AUGMENTOR

Augmentor	
Chordwise length	= 92 in.
Throat width (L_T)	= 10.5 in.
Exit width (L_E)	= variable
Diffuser area ratio (L_E/L_T)	= variable
Length (min) (L)	= 34 in.
Mean nozzle width ($\bar{t}$)	= 0.457 in.
Augmentor length ratio ($L/\bar{t}$)	= 74
Nozzles	
Total geometric exit area (per side)	= 42.3 in.^{2}
Number of nozzles (per side)	= 25
Area (per nozzle)	= 1.693 in.^{2}
Aspect ratio (AR)	= 60
Span (b_N)	= 10.12 in.
Thickness at exit (t_N)	= 0.167 in.
Pitch (p)	= 3.68 in.
Pitch ratio ($p/\bar{t}$)	= 8.0

TABLE 3 GEOMETRY OF WING AUGMENTOR

Span (per wing)			= 69.5 in.
Total nozzle area (per wing)			= 11.5 in.^{2}
Bay spans	24.25	22.75	22.5 in.
Nozzle area/bay	4.88	3.73	2.88 in.^{2}
Mean nozzle width $\bar{t}$	0.201	0.164	0.128 in.
Number of nozzles (N)	15	17	22
Area per nozzle (A_N)	0.325	0.219	0.131 in.^{2}
Pitch (p)	1.60	1.32	1.01 in.
Nozzle span (b)	3.61	2.96	2.29 in.
Nozzle thickness (t)	.091	.074	.057 in.
Nozzle aspect ratio (AR)	40	40	40
Throat (mid span) (L_T)	4.17	3.40	2.65 in.
Exit (mid span) (L_E)	6.67	5.44	4.24 in.
Diffuser area ratio L_E/L_T	1.60	1.60	1.60
Nozzle inlet area/exit area	5.0	5.0	5.0
Augmentor length (mid span) (L)	17.3	14.7	12.1 in.
$L/\bar{t}$	86	90	95

TABLE 4 RUN HISTORY VTOL-2 TESTS (T-538) Sheet 1

RUN NO.	MODEL CONFIGURATION								TEST CONDITION				REMARKS
	δ_F	WING SLAT	CANARD ι_c	DAR	E/P's	AUG. NOZZLES	AUG. INLET	EXIT RAKE	RPR	q	α	β	
1	30°	OFF	OFF	1.6	ON	FULL	ST'D	OFF	-	0	~	~	Weight Tare
2									~	0	0	0	
3									2.3	5	~		
4										10			
5										15			
6										15			Run 5 cont'd.
7										25			
8										40			
9		ON								10			
10										25			
11										40			
12								ON	~	0	0	0	
13										5	~		
14										10			
15									2.3	0	0	0	
16									~	0			E/P Adjustments
17										0			
18									2.3	5	~	0	Repeat of Run 13
19										10			Repeat of Run 14
20										15			
21										25			
22										40			
23									~	25	0		

TABLE 4

RUN HISTORY VTOL-2 TESTS (T-538)

SHEET 2

RUN NO.	MODEL CONFIGURATION								TEST CONDITION				REMARKS
	δ_F	WING SLAT	CANARD i_c	DAR	E/P's	AUG. NOZZLES	AUG. INLET	EXIT RAKE	RPR	q	α	β	
24	30	ON	OFF	1.6	ON	FULL	ST'D	ON	~	10	0	0	
25									2.3			~	
26									1.5			~	
27							Vanes On		2.3	25	~	0	
28										40			
29										10			
30										5			
31	0°						ST'D	OFF	~	0	0	0	
32									2.3	15	~		
33										25			
34										40			
35									~	40	0		
36									~	25			
37									~	10			
38									~	0	0	0	Nozzle Welded
39									2.3	15	~		Repeat of Run 32
40								ON	~	0	0	0	Rake On But No Dat
41									2.3	15	~		
42									~	0	0	0	Repeat of Run 40
43									2.3	25	~		
44										40			
45	45°								2.3	5	~	0	
46										10			

TABLE 4 RUN HISTORY VTOL-2 TESTS (T-538) SHEET 3

RUN NO.	MODEL CONFIGURATION								TEST CONDITION				REMARKS
	δ_F	WING SLAT	CANARD i_c	DAR	E/P's	AUG. NOZZLES	AUG. INLET	EXIT RAKE	RPR	q	α	β	
47	45°	ON	OFF	1.6	ON	FULL	ST'D	ON	2.3	15	~	0	
48										25			
49										40			
50						HALF ALTERNATE			2.3	10	~	0	
51									~	0	0		
52									2.3	25	~		
53										40	~		
54	30°		0°						2.3	15	~	0	Short Span Canard I
55										25			Fwd Location
56										40			
57			OFF						2.3	15	~	0	
58										25			
59										40			
60				0.5					~	0	0	0	
61									2.3	40	~		
62										25			
63										15			
64	45°								2.3	15	~	0	
65										25			
66										40			
67				0.5		FULL			~	0	0	0	
68									2.3	40	~		
69										25			

TABLE 4

RUN HISTORY VTOL-2 TESTS (T-538)

RUN NO.	MODEL CONFIGURATION								TEST CONDITION				REMARKS
	δ_F	WING SLAT	CANARD i_c	DAR	E/P's	AUG. NOZZLES	AUG. INLET	EXIT RAKE	RPR	q	α	β	
70	45°	ON	OFF	0.5	ON	FULL	ST'D	ON	2.3	15	~	0	
71										10			
72										5			

TABLE 5

RUN HISTORY VTOL-3 TESTS (T-542)

SHEET 1

RUN NO.	MODEL CONFIGURATION								TEST CONDITION				REMARKS
	δ_F	WING SLAT	CANARD i_c	DAR	E/P's	AUG. NOZZLES	AUG. INLET	EXIT RAKE	RPR	q	α	β	
1	30°	ON	OFF	1.6	ON	FULL	ST'D	ON	~	0	0	0	
2									2.3	40	~		
3										25			
4										15			
5													
6							VANES ON		2.3	40		0	Weight Tare
7					FRONT OFF		ST'D	OFF	~	0	0	0	
8													DUFF RUN
9									2.3	40	~	0	
10										25			
11										15			
12										10			
13					OFF				~	0	0	0	
14									2.3	40	~		
15										25			
16										15			
17									-	-	-	-	WEIGHT TARE
18				1.0					~	0	0	0	
19									2.3	40	~		
20										25			
21										15			
22					FRONT OFF				~	0	0	0	
23									2.3	40	~		

TABLE 5 RUN HISTORY VTOL-3 TESTS (T-542) SHEET 2

RUN NO.	MODEL CONFIGURATION								TEST CONDITION				REMARKS
	δ_F	WING SLAT	CANARD i_c	DAR	E/P's	AUG. NOZZLES	AUG. INLET	EXIT RAKE	RPR	q	α	β	
24	30°	ON	OFF	1.0	FRONT OFF	FULL	ST'D	OFF	2.3	25	~	0	
25										15			
26				1.6	ON				~	0	0	0	
27									2.3	40	~		
28										25			
29										15			
30										10			
31						HALF ALTERNATE			~	0	0	0	
32									~	0	0	0	REAR CAL. NOZZLE
33									2.3	40	~		
34										25			
35										15			
36										15	0	~	
37										25			
38										40			
39									2.0	32	~	0	NOISE ABATEMENT cf RUN 33
40										12			NOISE ABATEMENT cf RUN 35
41			ON						-	-	-	-	WEIGHT TARE
42			-10°						2.0	20	~	0	
43											0	~	
44									1.0		~	0	POWER-OFF
45			+10°						2.0	20	~	0	δ_c = 0° and vari

TABLE 5 RUN HISTORY VTOL-3 TESTS (T-542) SHEET 3

RUN NO.	MODEL CONFIGURATION								TEST CONDITION				REMARKS
	δ_F	WING SLAT	CANARD i_c	DAR	E/P's	AUG. NOZZLES	AUG. INLET	EXIT RAKE	RPR	q	α	β	
46									2.0	20	0	~	
47	30^o	ON	$+10^o$	1.6	ON	HALF ALTERNATE	ST'D	OFF	2.0	20	0	~	$\delta c = 30^o$
48									1.0		~	0	POWER-OFF
49			OFF		FRONT OFF				~	0	0	0	
50									2.0	32	~		
51										20			
52										12			
53					OFF				~	0	0	0	
54									2.0	32	~		
55										20			
56										12			
57										20	0	~	
58				1.0					~	0	0	0	
59									2.0	32	~		
60										20			
61										12			
62				0.5					~	0	0	0	
63									2.0	32	~		
64										20			
65						HALF-				12			
66				1.0		CENTRE	ST'D		~	0	0	0	
67									2.0	32	~		
68										20			
69										12			

TABLE 5 RUN HISTORY VTOL-3 TESTS (T-542) SHEET 4

RUN NO.	MODEL CONFIGURATION								TEST CONDITION				REMARKS
	δ_F	WING SLAT	CANARD i_c	DAR	E/P's	AUG. NOZZLES	AUG. INLET	EXIT RAKE	RPR	q	α	β	
70	30°	ON	OFF	1.0	OFF	HALF CENTRE	COVERS ON	OFF	~	0	0	0	
71									2.0	32	~		
72										20			
73										12			
74				1.6					~	0	0	0	
75									2.0	32	~		
76										20			
77				0.5					~	0	0	0	
78									2.0	32	~		
79										20			
80										12			
81	30°			FUSELAGE AUGMENTOR SEALED					~	0	0	0	
82									2.0	32	~		
83										20			
84										12			
85													WEIGHT TARE
86	45°								2.0	0	0	0	
87									2.0	32	~		
88										20			
89										12			
90	15°								2.0	32	~		
91										20			
92										12			

TABLE 6 - STATIC PERFORMANCE SUMMARY - VTOL 2 TESTS

Sheet 1

RUN NO.	δ_F	DAR	RAKE	NOZZLES	END-PLATES	REMARKS	AT RPR = 2.3	
							$\emptyset_{GF+B}$	Θ_{F+B}
2	30	1.6	OFF	FULL	ON		1.54	13.8
12	30	"	ON	"	"		1.57	12.2
15	"	"	"	"	"	Inlet Gaps Sealed with RTV	1.50	13.3
16	"	"	"	"	"	Reduced Nozzle/End-Plate Clearance	1.52	11.3
17	"	"	"	"	"	" " " " "	1.54	11.4
31	0	"	OFF	"	"		1.51	15.0
38	"	"	"	"	"	Some Inlet Fairing Screws Tightened	1.51	14.8
40	"	"	ON	"	"	Some Force Data Not Acquired	1.51	12.2
42	"	"	"	"	"	Repeat of Run 40	1.51	13.0
51	45	"	"	ALTERNATE	"		1.48	4^o
60	30	0.5	"	"	"		0.87	2^o
67	45	"	"	FULL	"		0.86	10.0

TABLE 6 - STATIC PERFORMANCE SUMMARY - VTOL 3 TESTS
(Cont'd.)

RUN NO.	δ_F	DAR	RAKE	NOZZLES	END-PLATES	REMARKS	AT RPR = 2.3	
							ϕG_{F+B}	θ_{F+B}
1	30	1.6	ON	FULL	ON		1.55	14.6
7	"	"	OFF	"	FRONT OFF		1.42	22.7
13	"	"	"	"	BOTH OFF		1.37	15.5
18	"	1.0	"	"	"		1.26	12.9
22	"	"	"	"	FRONT OFF		1.27	13.8
26	"	1.6	"	"	ON		1.55	15.8
31	"	"	"	ALTERNATE	"		1.41	8.3
32	"	"	"	"	"	Rear Calibration Nozzle Installed	1.46	9.3
49	"	"	"	"	FRONT OFF		1.32	20.0
53	"	"	"	"	BOTH OFF		1.24	15.0
58	"	1.0	"	"	"		1.24	9.6
62	"	0.5	"	"	"		0.93	10.0
66	"	1.0	"	CENTRE	OFF	Inlet Covers Off	1.08	11.3
70	"	"	"	"	"	Inlet Covers On	1.08	12.6
74	"	1.6	"	"	"	" " "	1.08	13.7
77	"	0.5	"	"	"	" " "	0.86	14.5

TABLE 7

TRANSITION CONFIGURATIONS TESTED

(T538 & T542; VTOL 2 AND 3 TESTS)

FUSELAGE AUGMENTOR CONFIGURATION			DIFFUSER AREA RATIO			
NOZZLES	END-PLATES	REMARKS	1.6	1.0	0.5	0
FULL SET	ON		0, 0R 30, 30R 45R			
	FRONT OFF		30	30		
	BOTH OFF		30	30		
½ ALTERNATE	ON		30, 30R 45R		3 OR 45R	
	FRONT OFF		30			
	BOTH OFF		30	30	30	
½ CENTRE	BOTH OFF	NO INLET COVERS		30		
	BOTH OFF	WITH INLET COVERS	30	30	30	
AUGMENTOR SEALED	REMOVED	POWER ON				15 30 45
	REMOVED	POWER OFF				0 30

NOTES: (i) NUMERALS SHOWN REFER TO FLAP ANGLES TESTED.

(ii) LETTER 'R' INDICATES EXIT RAKE ON.

TABLE 8 SUMMARY OF TRANSITION PERFORMANCE, $T_{H/L} = 1.10$, $T_{H/S} = 60\ LB/FT^2$

IDENT. NO.	RUN NO'S	CONFIGURATION						FULL-SCALE V_∞ (KNOTS)					FIG. NO.
		δ_f	NOZZ.	DAR	RAKE	END-PLATES	OTHER	50	71	87	112	142	
2-1	3-8	30°	FULL	1.6	OFF	ON	ACCEL $\frac{TN}{}$ ALPHA $M/T_{H\bar{c}}$	.292 2.0 .105	.237 5.2 .100	.198 8.3 .095	.094 11.6 .080	.077 14.3 .045	20
2-2	9-11	30°	FULL	1.6	OFF	ON	WING SLAT ADDED	– – –	.249 6.2 .095	– – –	.088 11.1 .070	.083 13.2 .035	21
2-3	18-22	30°	FULL	1.6	ON	ON		.325 7.7 .100	.220 9.5 .100	.154 11.2 .100	.017 13.5 .090	.182 15.2 .060	22
2-4	28-30	30°	FULL	1.6	ON	ON	INLET VANES ON	.314 7.3	.220 9.1	– – –	.017 14.0	.176 15.0	–
2-5	32-34	0°	FULL	1.6	OFF	ON		– – –	– – –	.022 3.8 .265	.088 3.0 .305	.253 0.5 .350	23
2-6	41-44	0°	FULL	1.6	ON	ON		– – –	– – –	.014 2.6 .110	.149 0.4 .155	.333 1.0 .200	24
2-7	45-49	45°	FULL	1.6	ON	ON		.424 14.7 .060	.358 17.8 .055	.270 19.3 .040	.127 21.0 .015	.083 22.5 .020	25

SHEET

TABLE 8 SUMMARY OF TRANSITION PERFORMANCE, $^{T_H}/_{L} = 1.10$, $^{T_H}/_{S} = 60\ ^{LB}/_{FT^2}$

IDENT. NO.	RUN NO'S	CONFIGURATION						FULL-SCALE V_∞ (KNOTS)					FIG. NO.
		δ_F	NOZZ.	DAR	RAKE	END-PLATES	OTHER	50	71	87	112	142	
2-8	50 53	45°	ALT.	1.6	ON	ON	ACCEL $\frac{TN}{}$ ALPHA $M/T_H\ \bar{c}$	– – –	.105 2.2 .015	– – –	.028 12 4 .045	.160 16.0 .085	26
2-9	57-59	30°	ALT	1.6	ON	ON		– – –	– – –	.094 2.5 .065	.036 5.1 .050	.110 10.0 .015	27
2-10	61-63	30°	ALT	0.5	ON	ON		– – –	– – –	.064 12.5 .035	.057 3.1 .085	.011 3 2 .155	28
2-11	64-66	45°	ALT	0.5	ON	ON		– – –	– – –	.030 5.9 .090	.020 3.7 .160	.073 9.6 .250	29
2-12	68-72	45°	FULL	0.5	ON	ON		– – –	.028 1.9 .050	0 4.5 .085	.072 9.2 .145	.204 13.5 .245	30
3-1	3-4	30°	FULL	1.6	ON	ON		– – –	– – –	.154 10.3 .115	.033 13.3 .105	.127 15.0 .075	31
3-2	9-12	30°	FULL	1.6	OFF	FRONT OFF		– – –	.248 1.0 .092	.215 5.0 .090	.116 8.3 .055	.050 10.8 0	32

SHEI

TABLE 8 SUMMARY OF TRANSITION PERFORMANCE, $T_{H/L} = 1.10$, $T_{H/S} = 60\ LB/FT^2$

IDENT. NO.	RUN NO'S	CONFIGURATION						FULL-SCALE V_∞ (KNOTS)					FIG. NO.
		δ_F	NOZZ.	DAR	RAKE	END-PLATES	OTHER	50	71	87	112	142	
3-3	14-16	30°	FULL	1.6	OFF	BOTH	ACCEL TN	–	–	.132	.050	.088	33
						OFF	ALPHA	–	–	5.5	8.0	11.0	
							M/T_H $\bar{c}$	–	–	.070	.045	0	
3-4	19-21	30°	FULL	1.0	OFF	BOTH		–	–	.121	.050	.083	34
						OFF		–	–	4.3	8.0	10.2	
								–	–	.033	0	.057	
3-5	23-25	30°	FULL	1.0	OFF	FRONT		–	–	.105	.044	.088	35
						OFF		–	–	3.3	7.0	10.2	
								–	–	.040	.005	.055	
3-6	27-30	30°	FULL	1.6	OFF	ON		–	.259	.171	.061	.099	36
								–	8.0	8.7	11.8	13.9	
								–	.135	.135	.115	.085	
3-7	33-35	30°	ALT	1.6	OFF	ON		–	–	.132	.088	.050	37
								–	–	4.0	4.2	8.9	
								–	–	.080	.062	.030	
3-8	50-52	30°	ALT	1.6	OFF	FRONT		–	–	171	.127	.022	38
						OFF		–	–	8.0	0.5	5.2	
								–	–	.030	.013	.075	
3-9	54-56	30°	ALT	1.6	OFF	BOTH		–	–	.143	.112	.028	39
						OFF		–	–	8.0	0.5	5.2	
								–	–	.020	.020	.080	

SHEET 3

TABLE 8 SUMMARY OF TRANSITION PERFORMANCE, $T_H/_L = 1.10$, $T_H/_S = 60\ LB/_{FT^2}$

IDENT. NO.	RUN NO'S	CONFIGURATION						FULL-SCALE V_∞ (KNOTS)					FIG. NO.
		δ_F	NOZZ.	DAR	RAKE	END-PLATES	OTHER	50	71	87	112	142	
3-10	59-61	30°	ALT	1.0	OFF	BOTH OFF	ACCEL $\frac{TN}{}$ ALPHA $M/T_H\ \bar{c}$	— — —	— — —	.118 9.5 .008	.118 0.7 .033	.039 4.5 .092	40
3-11	63-65	30°	ALT	0.5	OFF	BOTH OFF		— — —	— — —	.094 12.8 .026	.114 3 2 .069	.055 2.6 .136	41
3-12	67-69	30°	CENTRE	1.0	OFF	BOTH OFF		— — —	— — —	.132 11.3 .029	.143 3.0 .073	.086 3.2 .137	42
3-13	71-73	30°	CENTRE	1.0	OFF	BOTH OFF	INLET COVERS ON	— — —	— — —	.132 12.6 .010	.143 4.2 .054	.110 2.4 .126	43
3-14	75,76	30°	CENTRE	1.6	OFF	BOTH OFF		— — —	— — —	— — —	.149 4.0 .037	.088 2.0 .105	44
3-15	78-80	30°	CENTRE	0.5	OFF	BOTH OFF		— — —	— — —	.143 13.5 .030	.171 4.2 .085	.121 2.1 .157	45
3-16	82-84	30°	—	—	OFF	BOTH OFF	FUSELAGE AUGMENTOR SEALED	— — —	— — —	.374 20.2 .054	.432 9.3 .126	.407 2.0 .210	46

TABLE 8 SUMMARY OF TRANSITION PERFORMANCE, $T_{H/L} = 1.10$, $T_{H/S} = 60\ LB/FT^2$

IDENT. NO.	RUN NO'S	CONFIGURATION						FULL-SCALE V_∞ (KNOTS)					FIG. NO.
		δ_F	NOZZ.	DAR	RAKE	END-PLATES	OTHER	50	71	87	112	142	
3-17	87-89	45°	—	—	OFF	BOTH	ACCEL $\frac{TN}{}$	—	—	.347	.363	.294	47
						OFF	ALPHA	—	—	14.2	3.4	3.2	
							$M/T_H\ \bar{c}$	—	—	.104	.190	.292	
3-18	90-92	15°	—	—	OFF	BOTH		—	—	.336	.446	.451	48
						OFF		—	—	24.5	15.8	9.2	
								—	—	.020	.026	.075	

DHC EXTERNAL AUGMENTOR V/STOL CONCEPT

G.A. OF J-97 POWERED MODEL

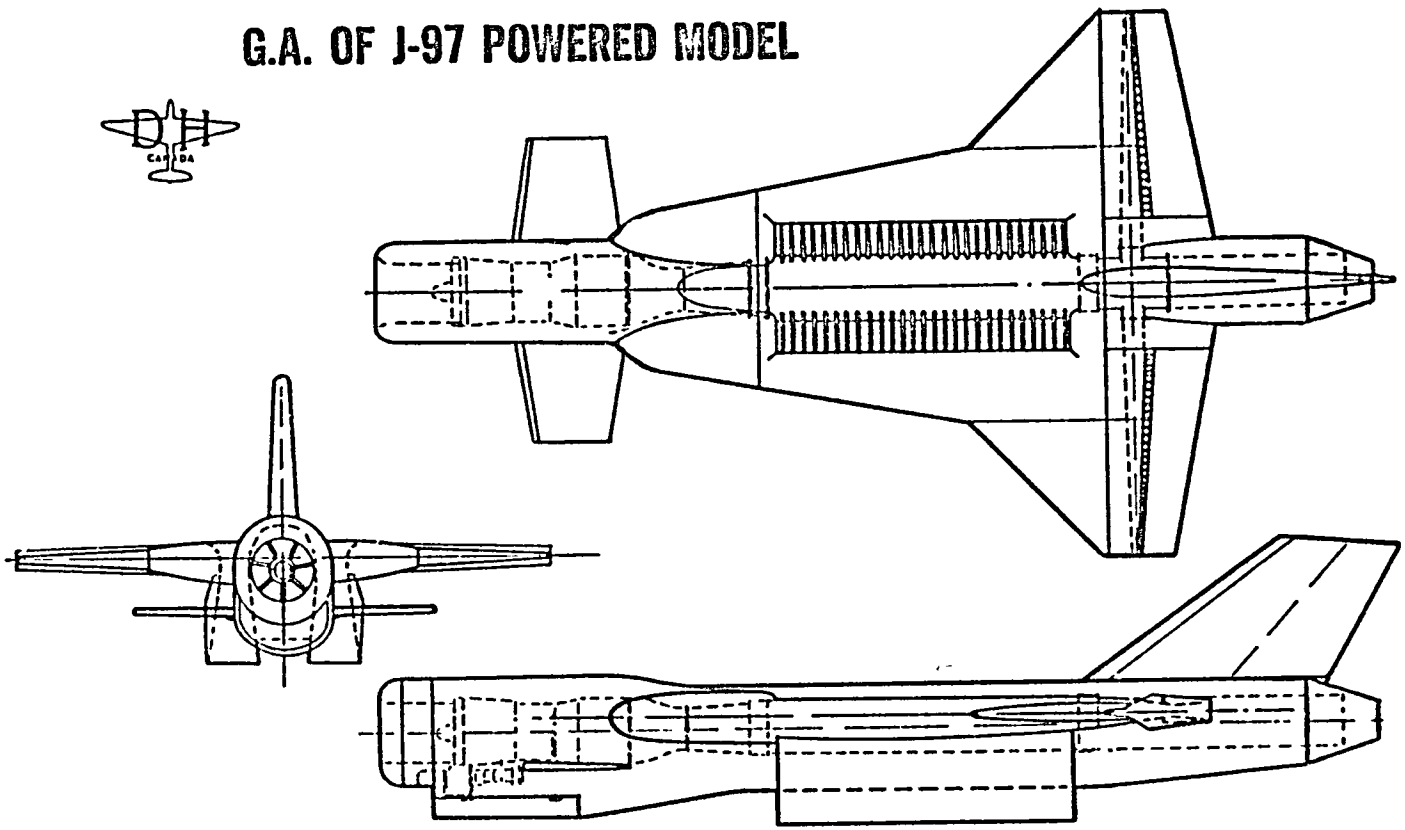

DHC CANADA

Fig. 1

CANADA

Fig. 2

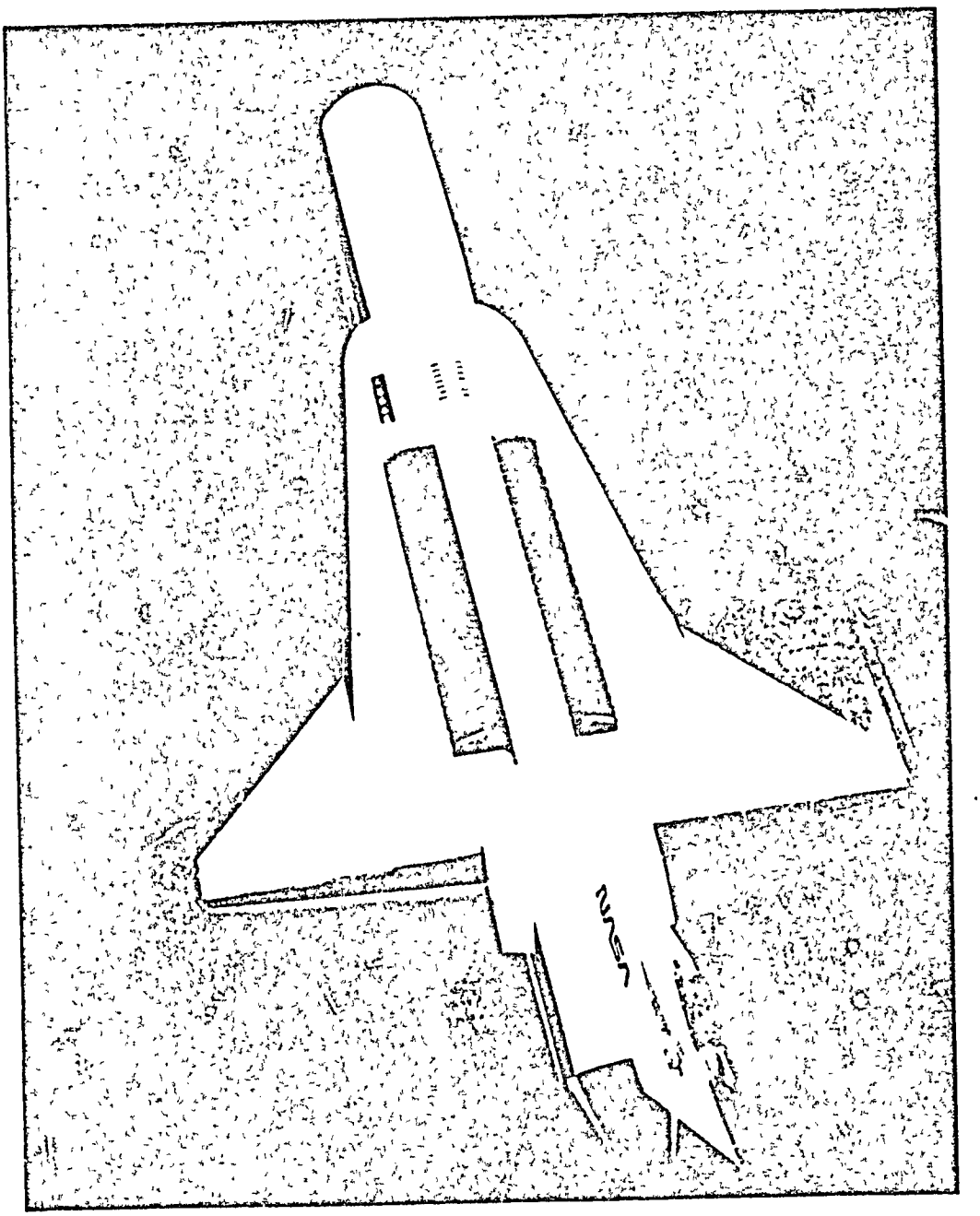

OVERHEAD VIEW OF MODEL IN TUNNEL

CANADA

Fig. 3

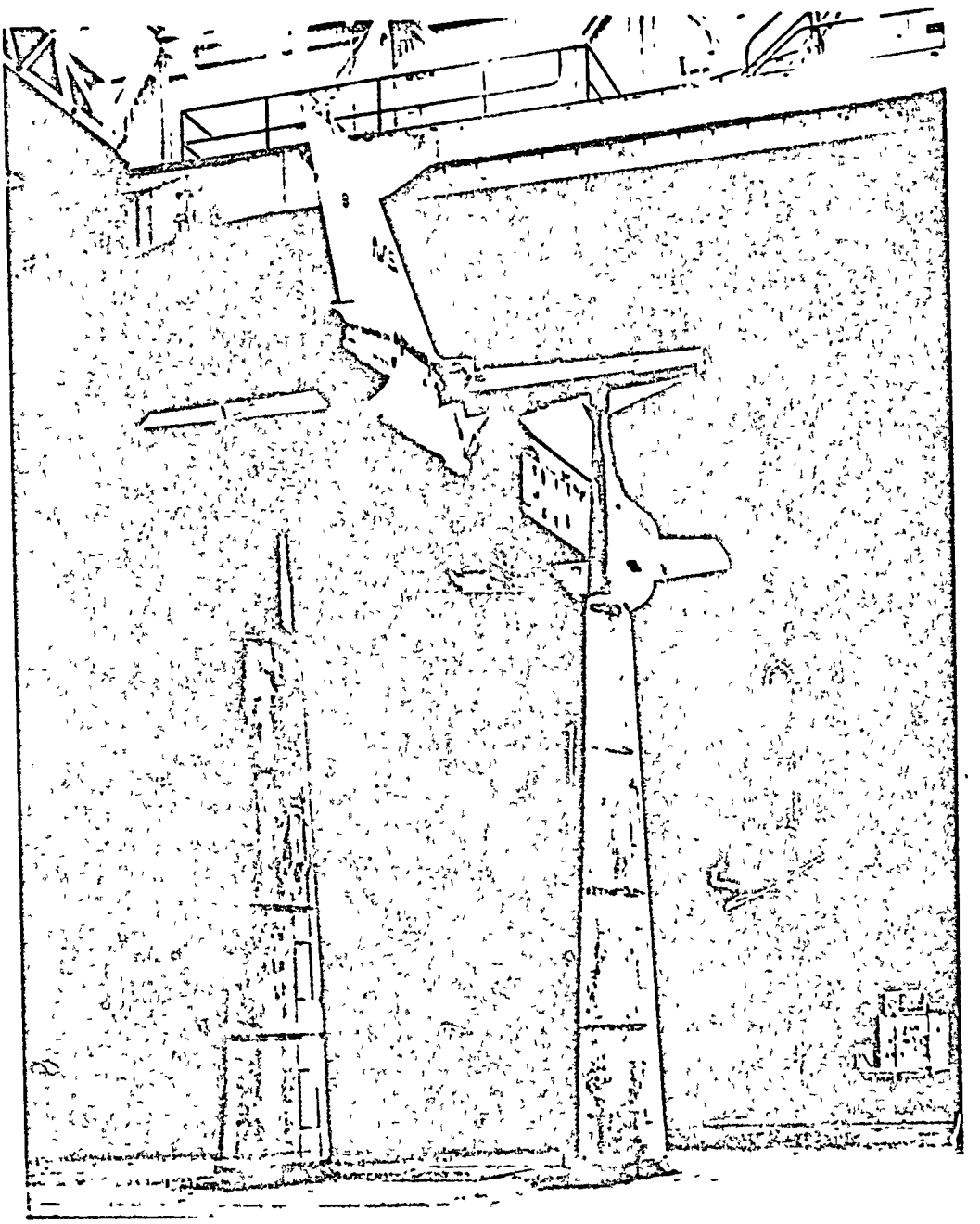

REAR VIEW OF MODEL IN TUNNEL

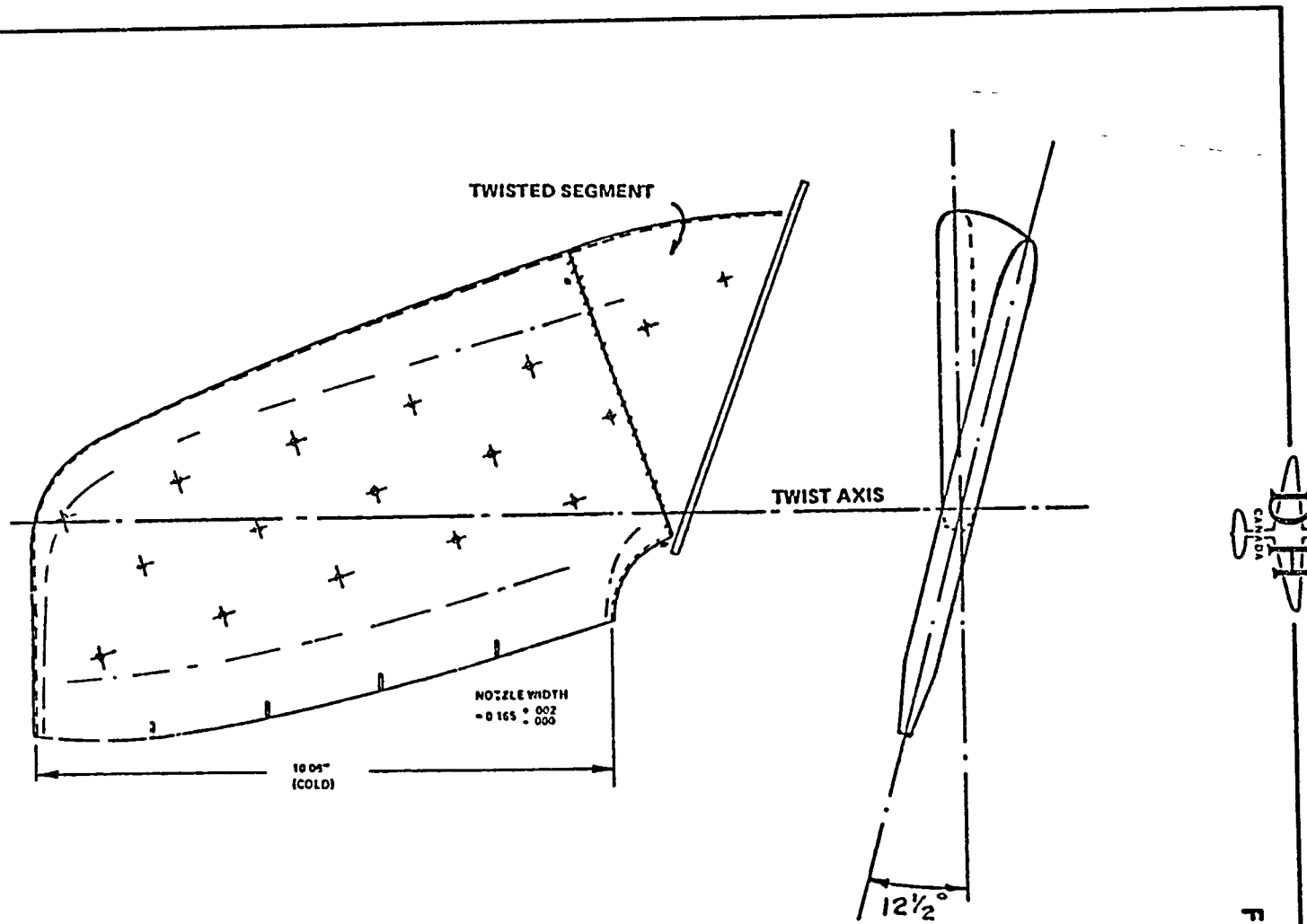

FUSELAGE AUGMENTOR NOZZLE, TWISTED 12½°

Fig. 4

Fig. 5

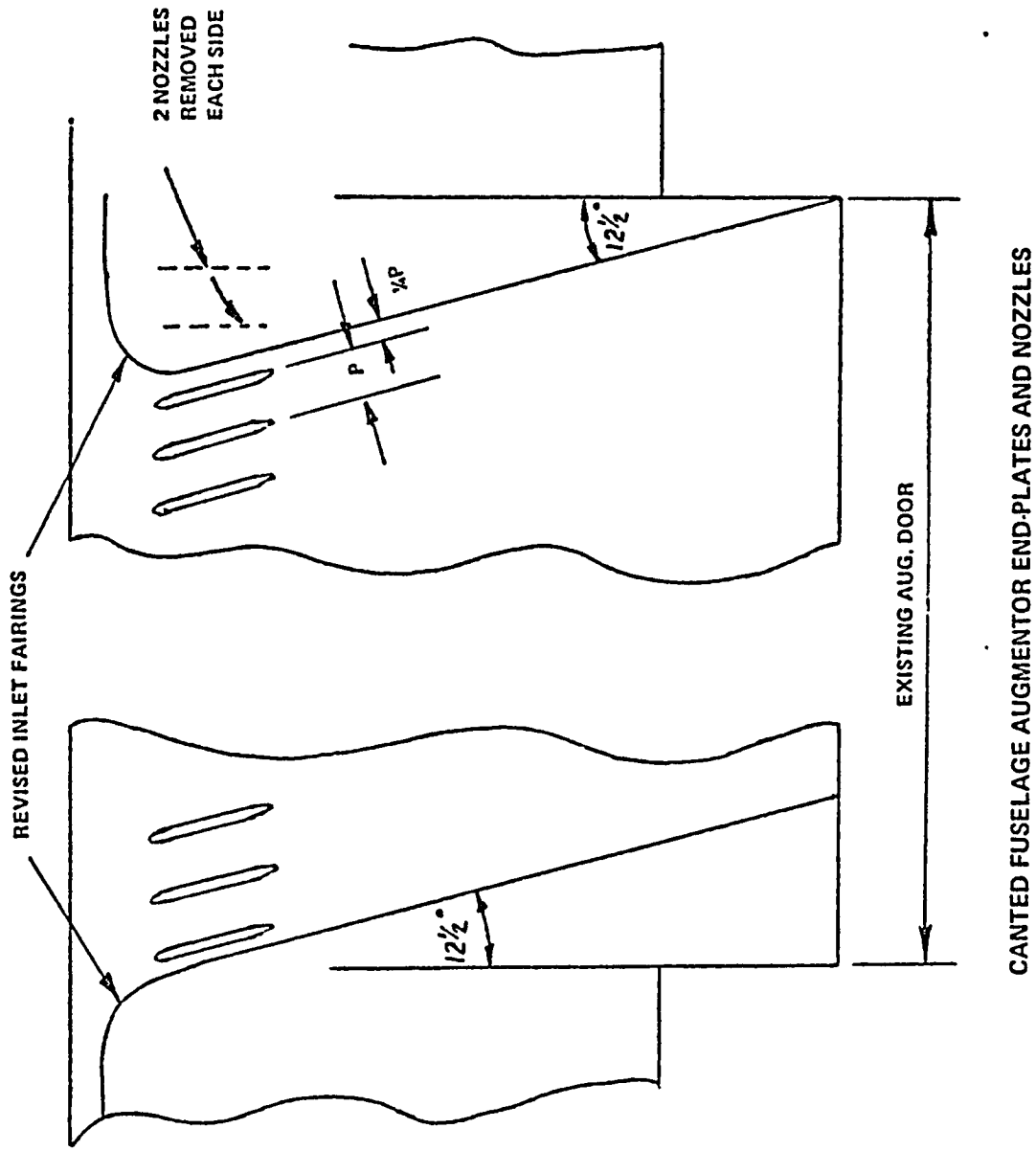

CANTED FUSELAGE AUGMENTOR END-PLATES AND NOZZLES

Fig. 6

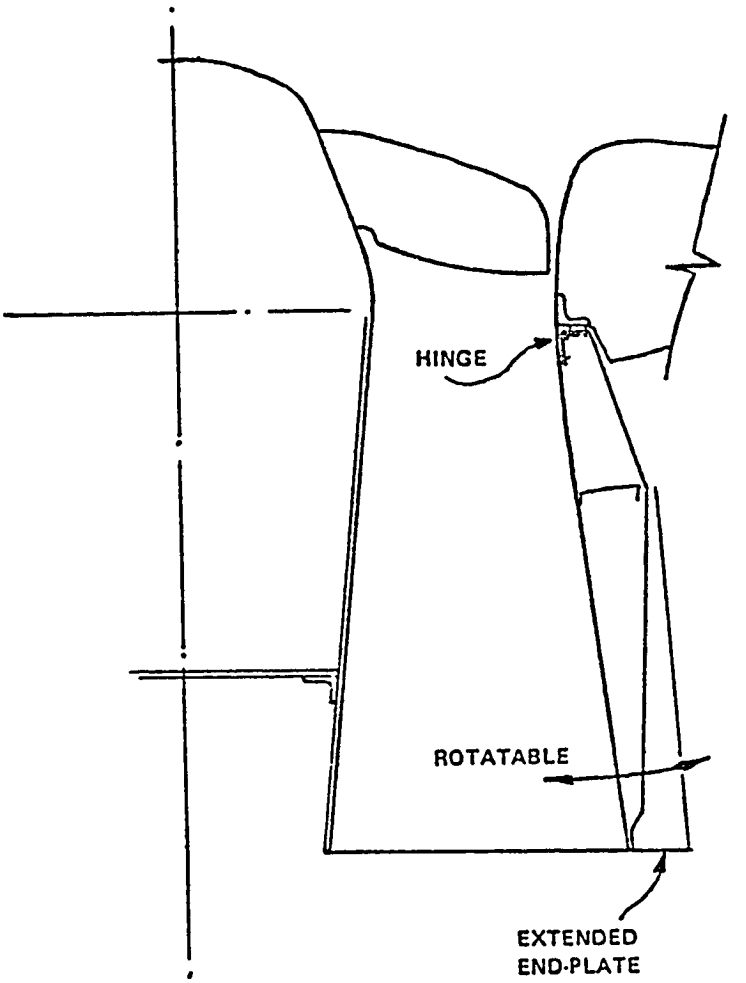

HINGED FUSELAGE AUGMENTOR DOOR

Fig. 7(a)

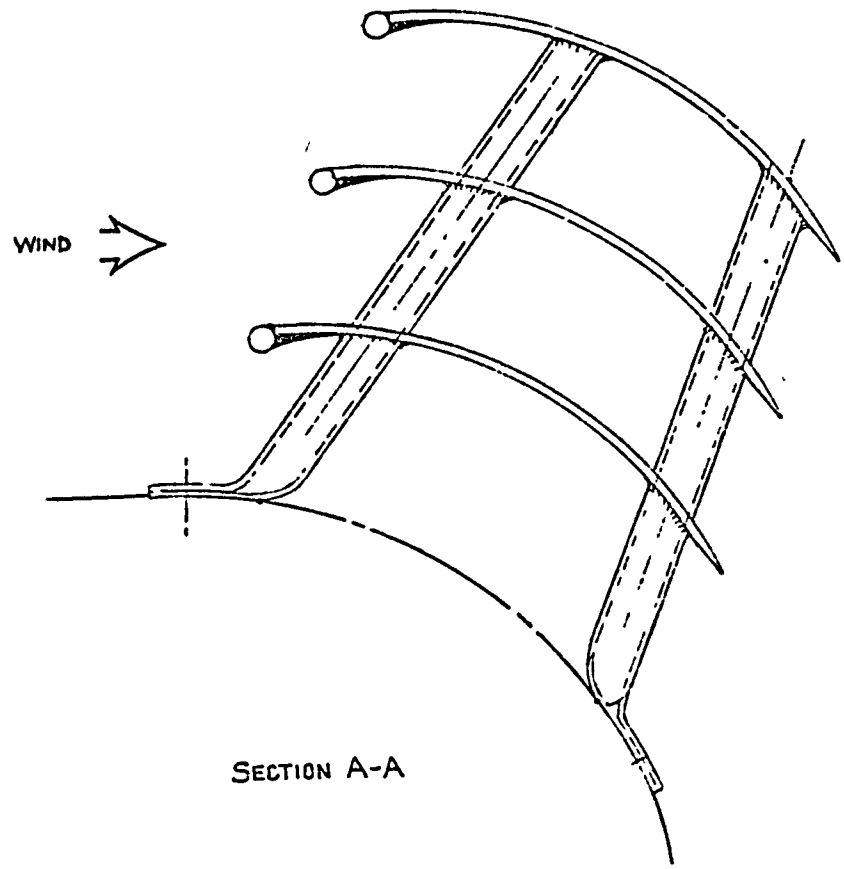

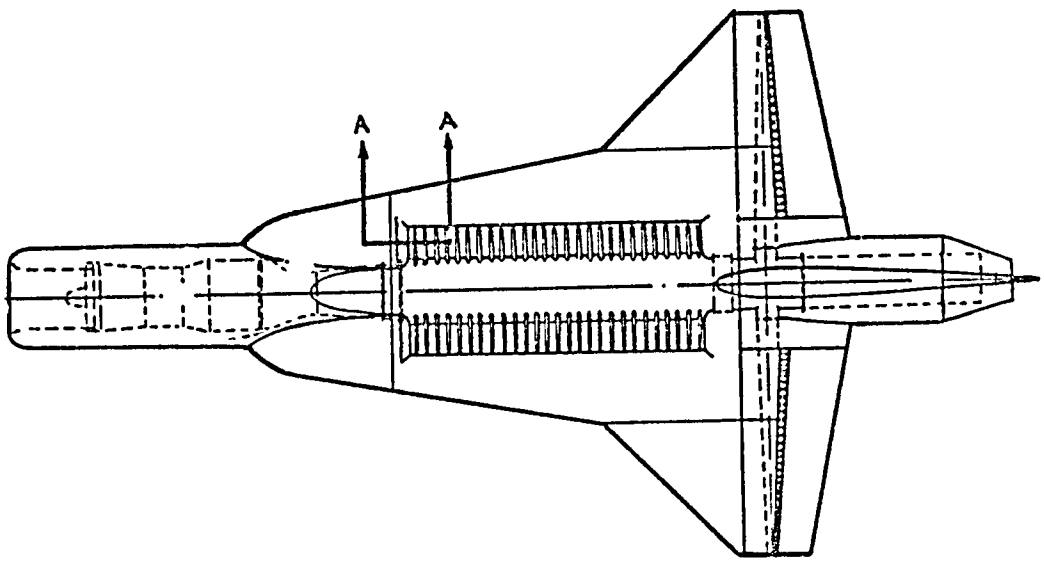

INLET FLOW-TURNING VANES (VTOL-2 TESTS)

Fig. 7(b)

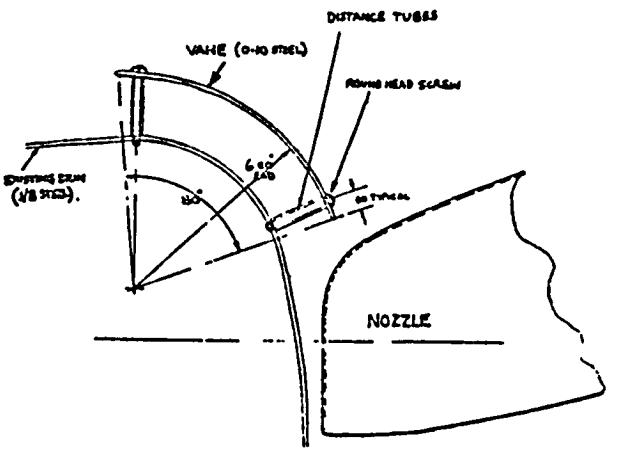

SECTION 'A-A'

SECTION THROUGH AUGMENTOR (OUTBOARD)

* LOOKING FORWARD - L.H SIDE *

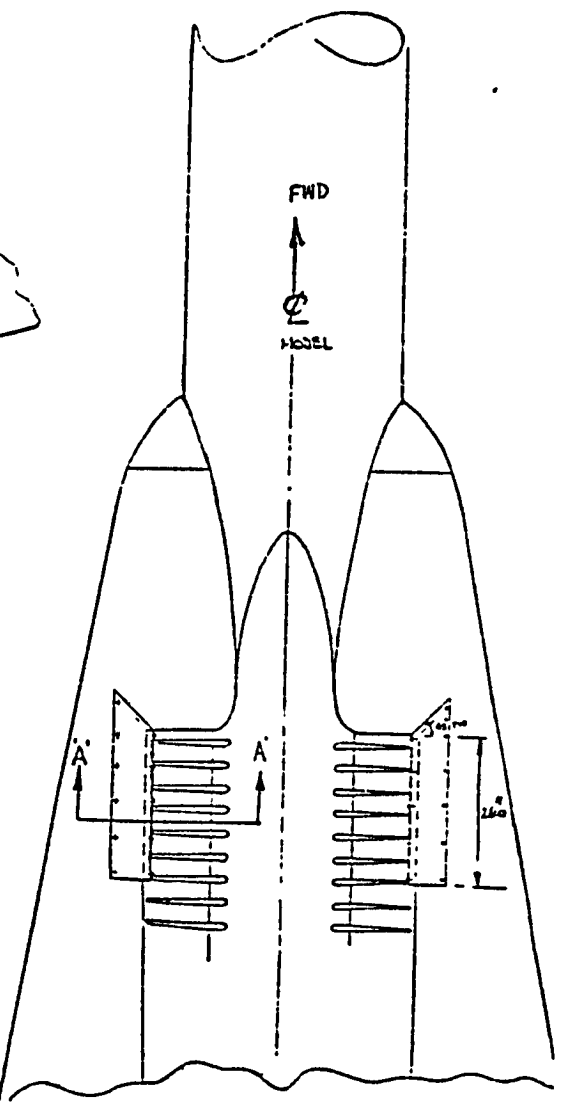

INLET VANE (VTOL-3 TESTS)

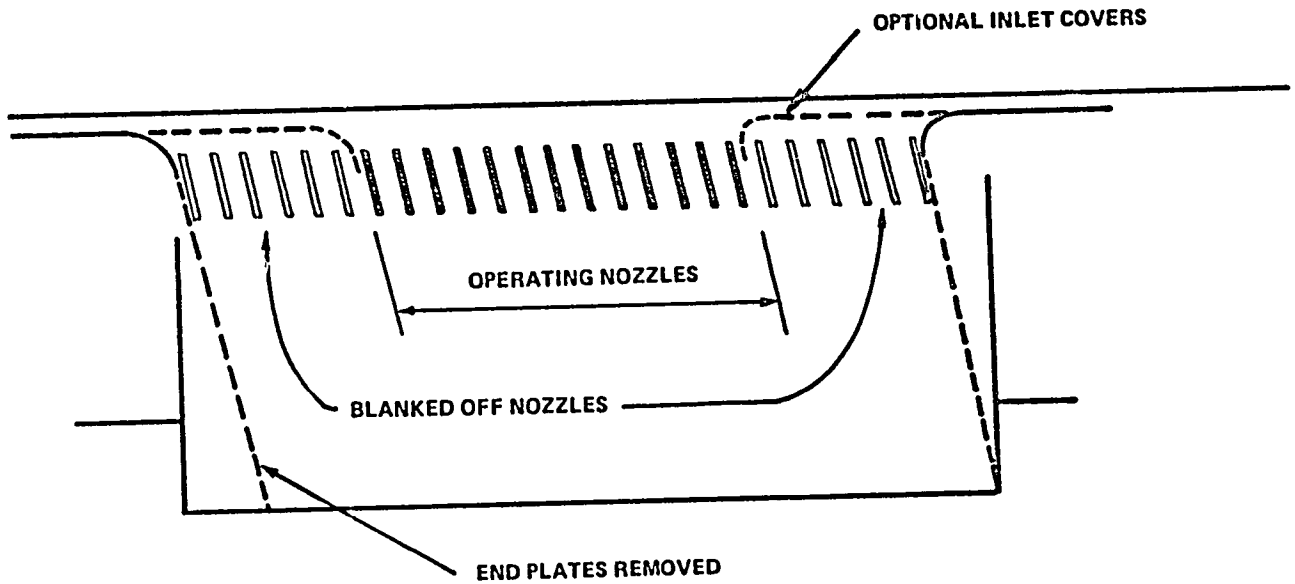

FUSELAGE AUGMENTOR WITH REDUCED CHORDWISE LENGTH ("HALF-CENTRE" CONFIGURATION)

Fig. 8

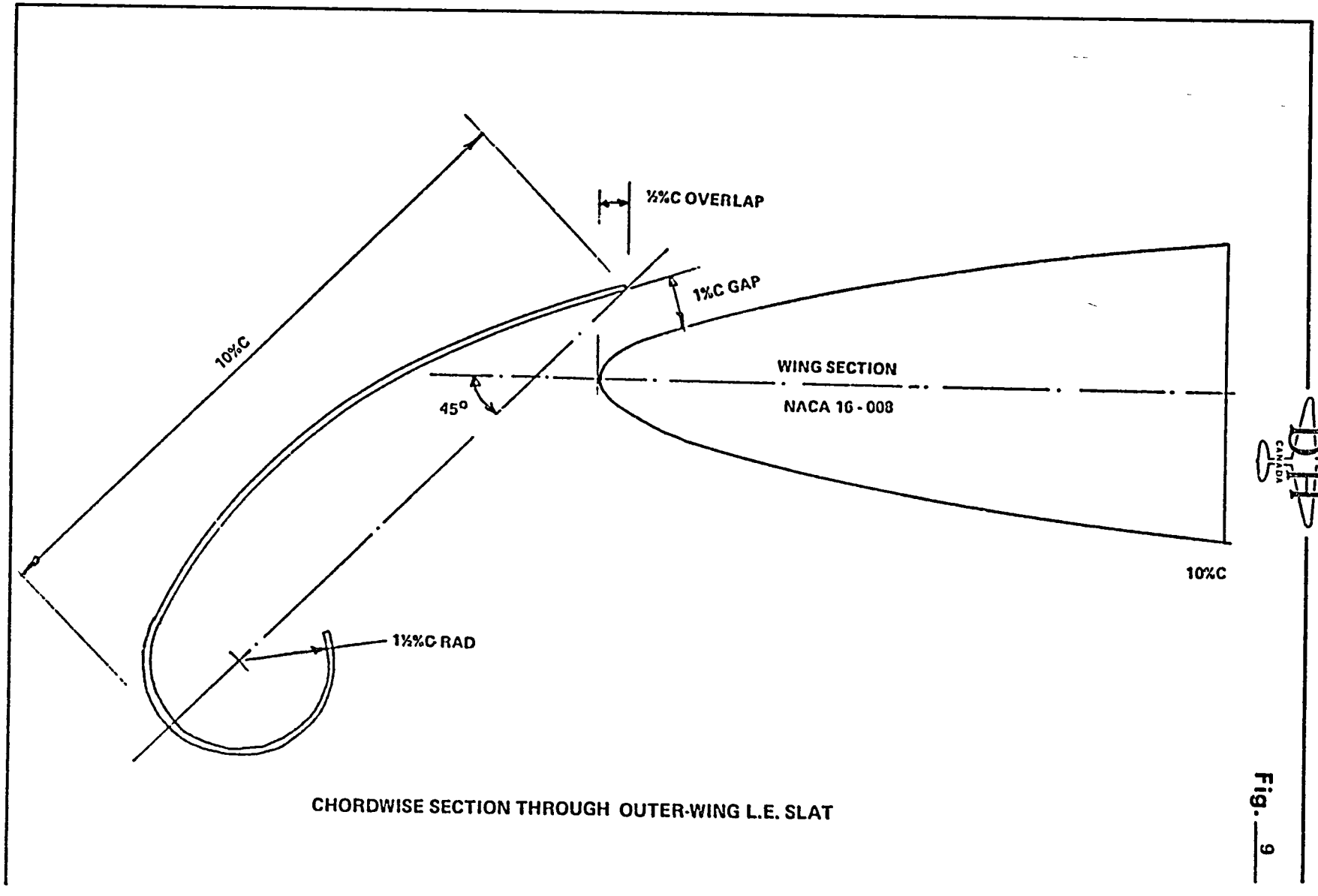

CHORDWISE SECTION THROUGH OUTER-WING L.E. SLAT

Fig. 9

Fig. 10

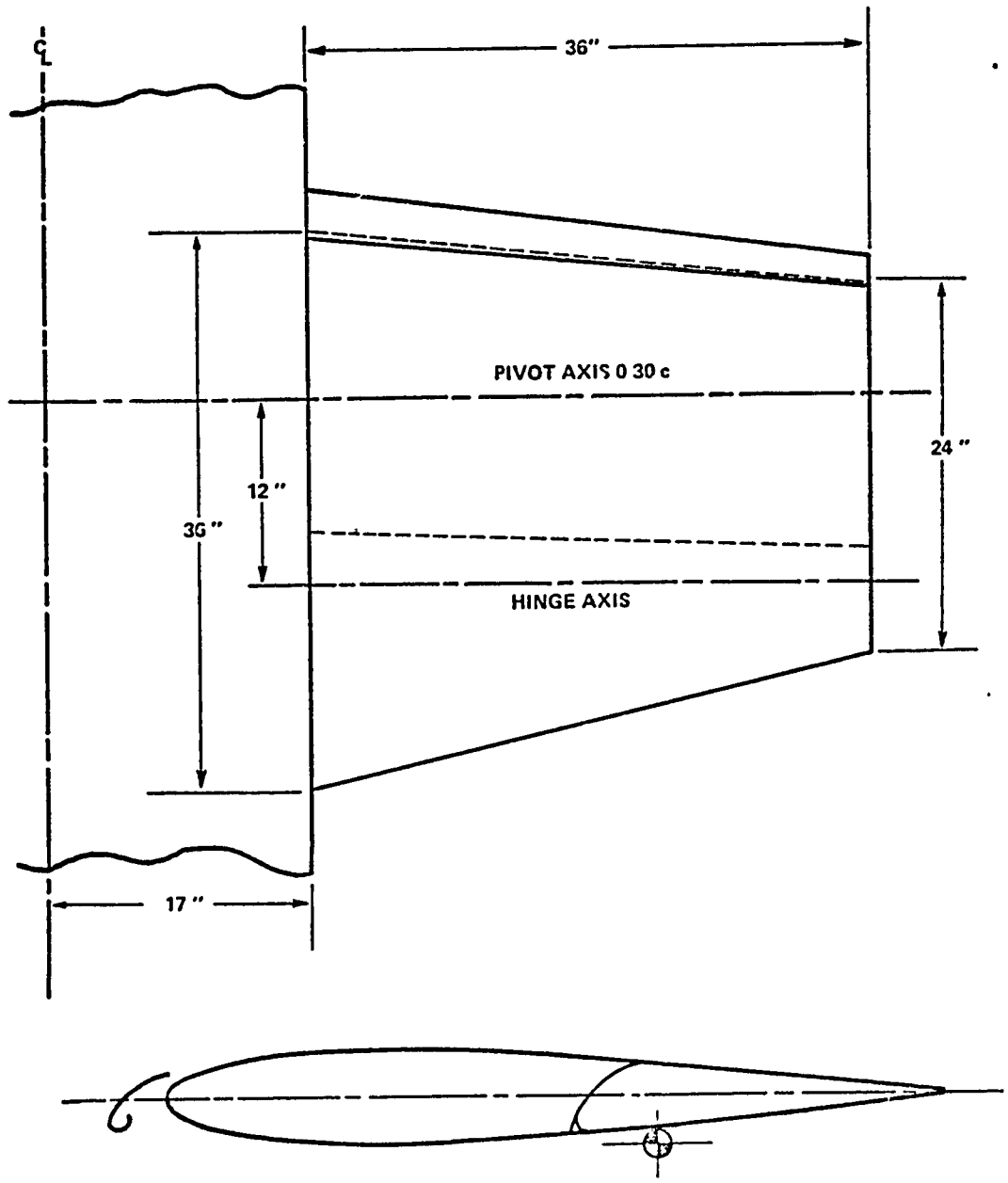

CANARD PLANFORM AND SECTION

Fig. 11

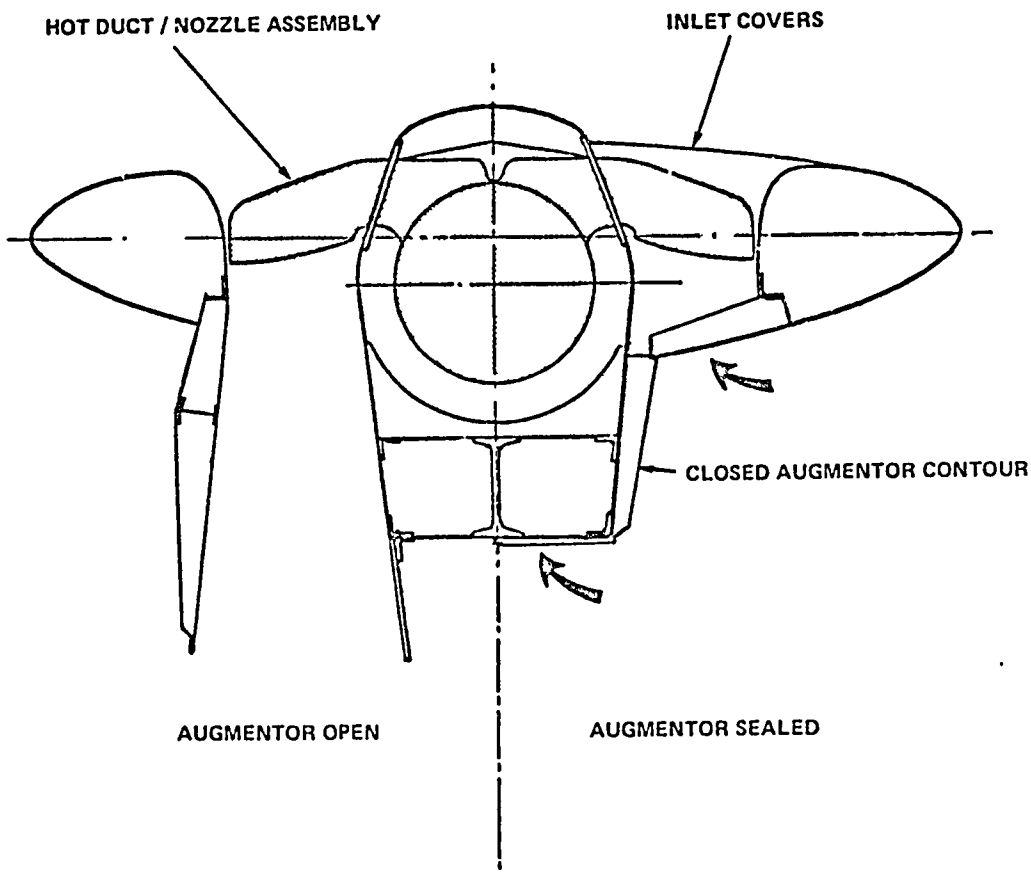

SECTION THROUGH FUSELAGE AUGMENTOR,
SHOWING SEALED AUGMENTOR CONFIGURATION

CANADA

Fig. 12

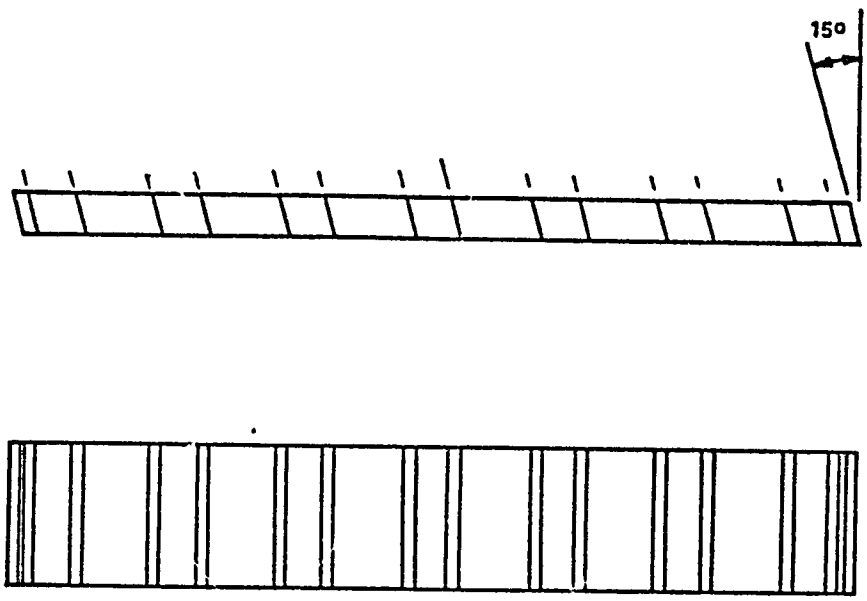

AUGMENTOR EXIT RAKE WITH CANTED PROBES

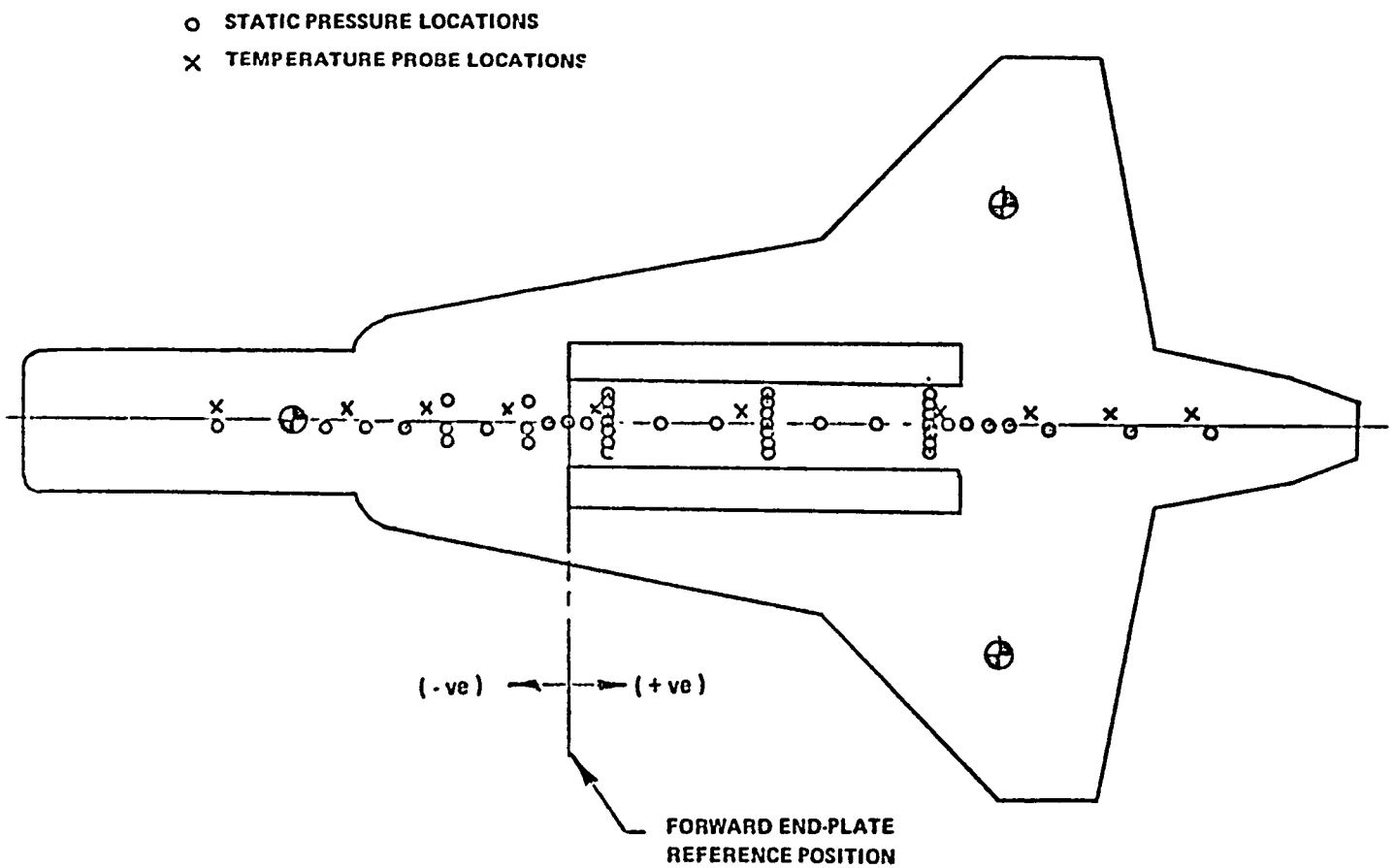

LOWER FUSELAGE INSTRUMENTATION
(VTOL 3)

Fig. 13

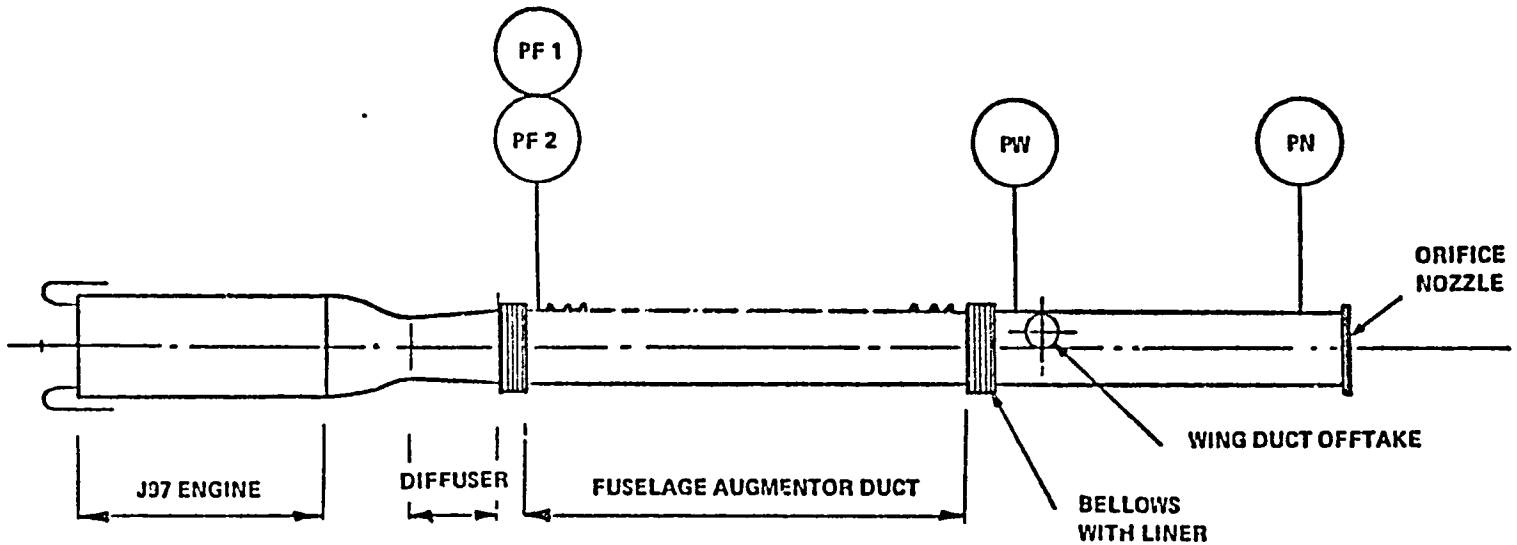

LOCATION OF DUCT STATIC PRESSURE TAPS

Fig. 14

Fig. 15(a)

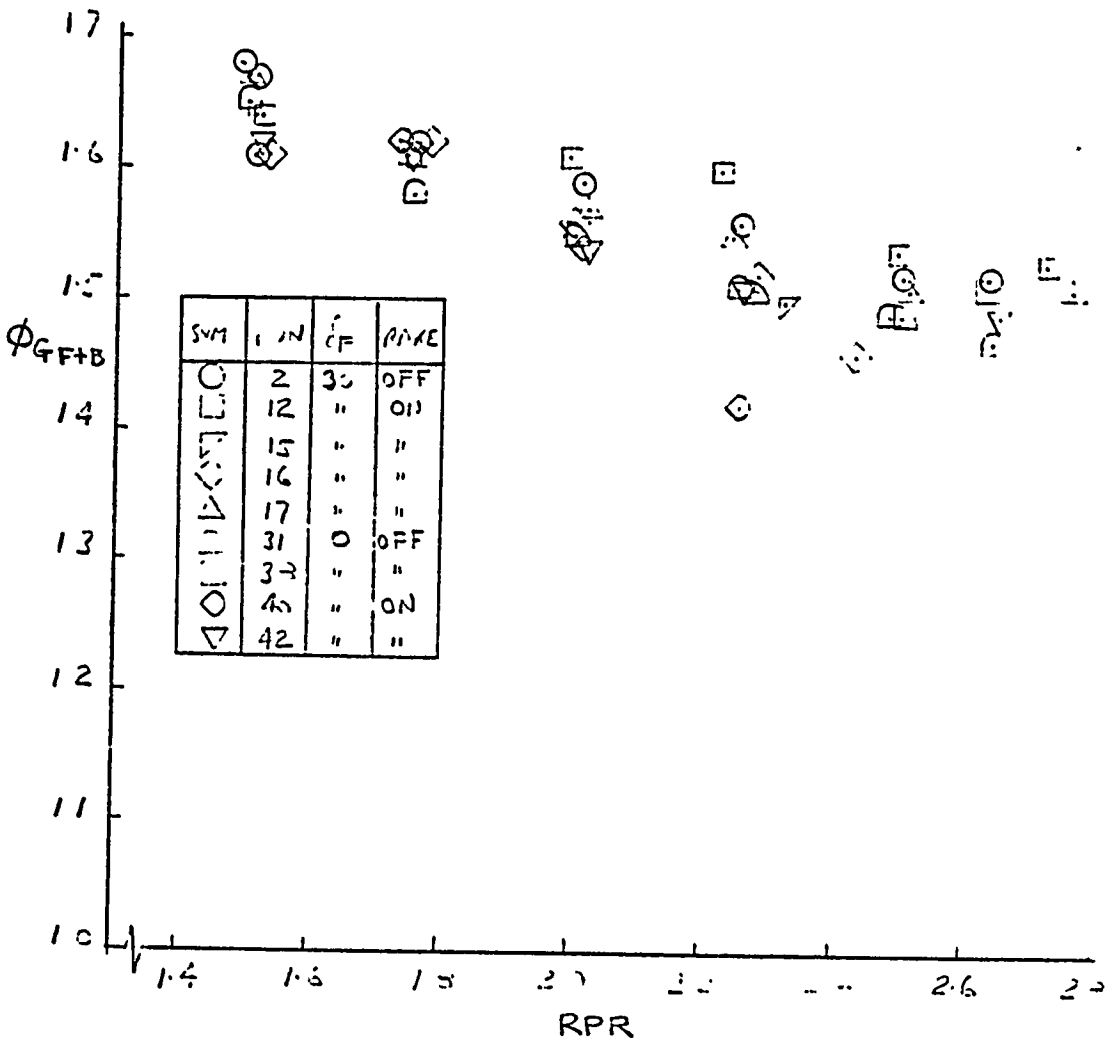

FUSELAGE AUGMENTOR STATIC THRUST AUGMENTATION RATIO

FULL NOZZLE SET DAR = 1.6 END-PLATES ON
(BASE THRUST INCLUDED)
VTOL-2 TESTS

Fig. 15(b)

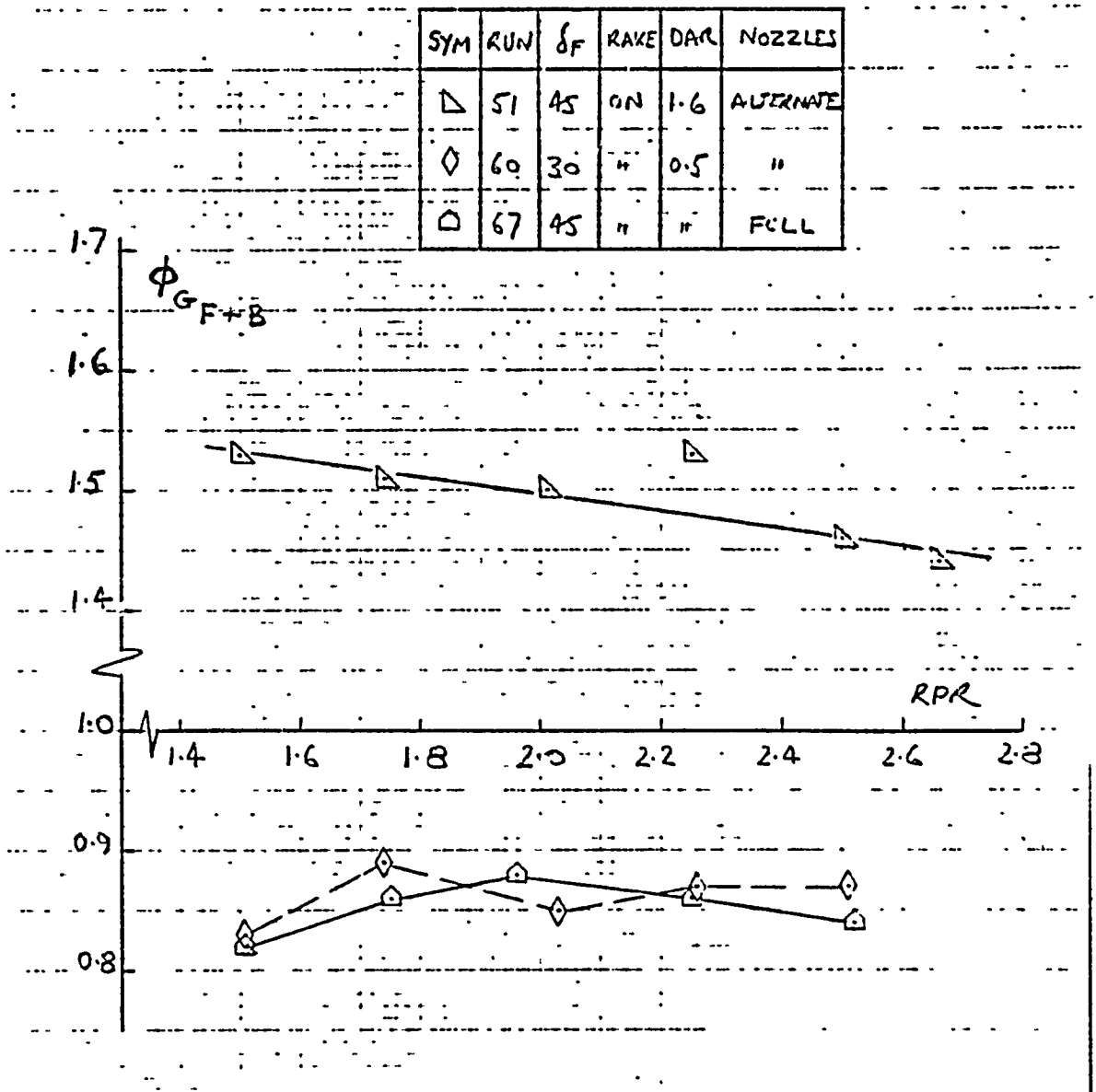

FUSELAGE AUGMENTOR STATIC THRUST AUGMENTATION RATIO

Fig. 15(c)

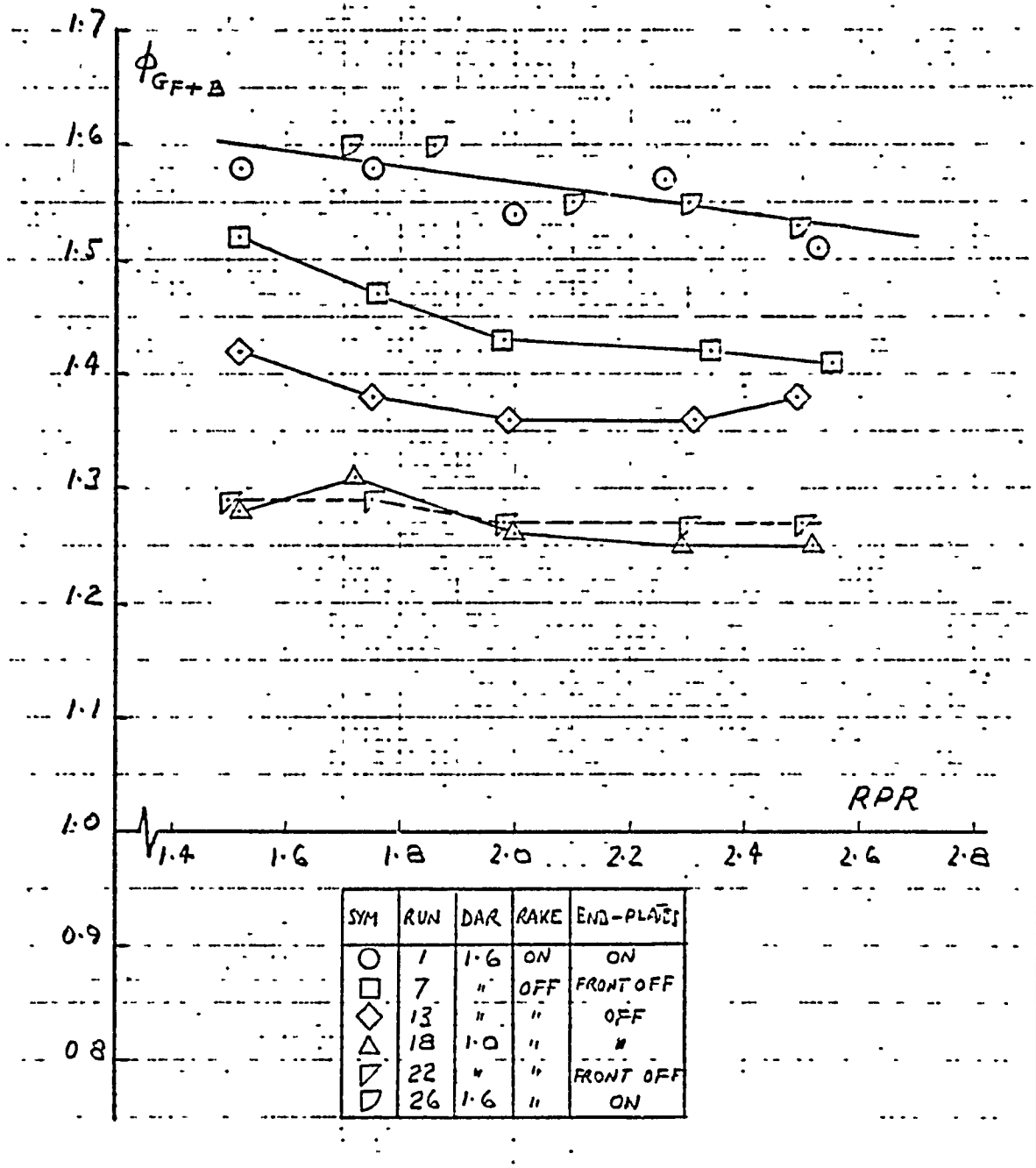

SYM	RUN	DAR	RAKE	END-PLATES
○	1	1·6	ON	ON
□	7	"	OFF	FRONT OFF
◇	13	"	"	OFF
△	18	1·0	"	"
▽	22	"	"	FRONT OFF
▷	26	1·6	"	ON

STATIC THRUST AUGMENTATION - VTOL 3 TESTS
FULL NOZZLE SET

Fig. 15(d)

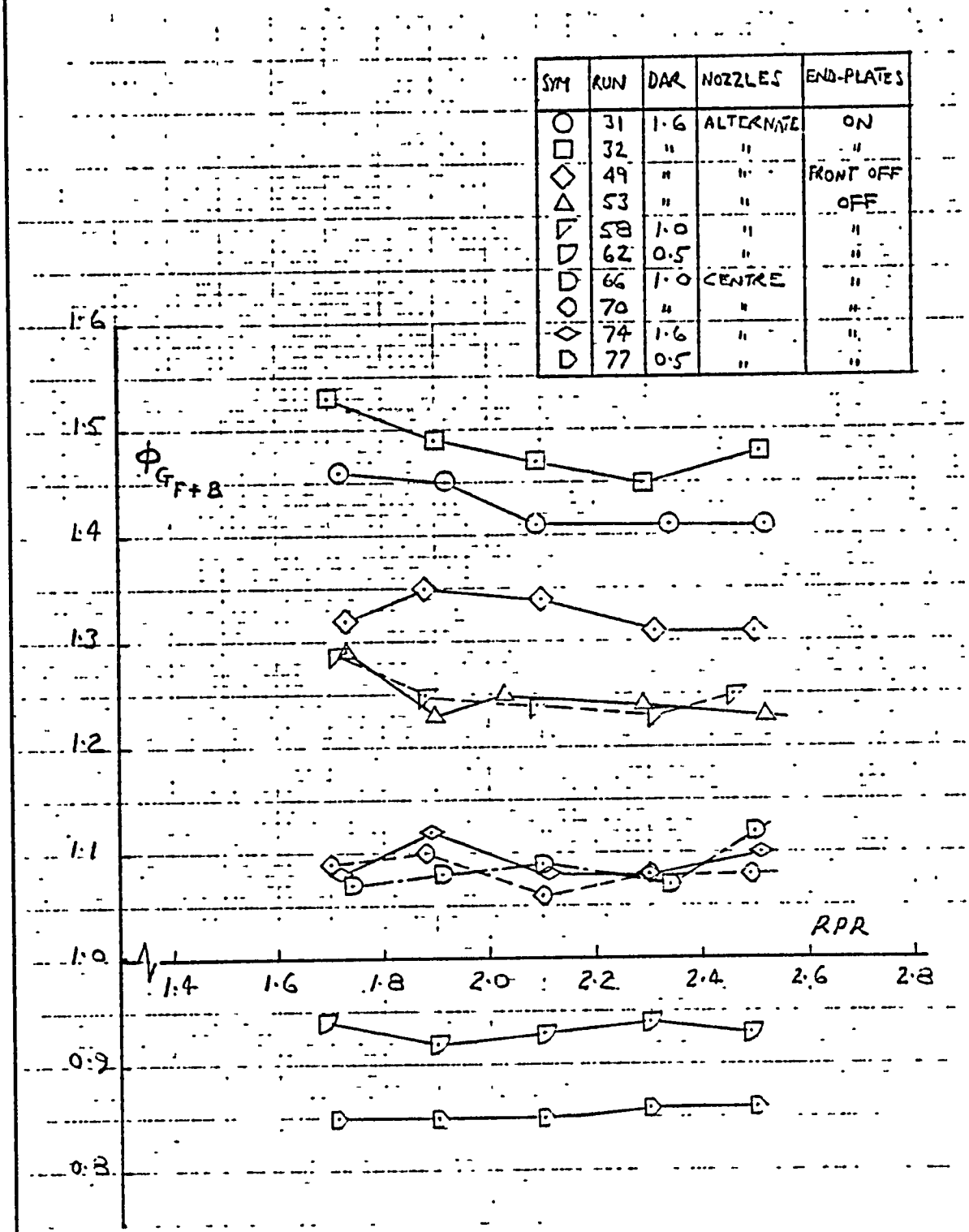

STATIC THRUST AUGMENTATION - VTOL 3 TESTS
HALF NOZZLE TESTS (RAKE OFF)

ORIGINAL PAGE IS
OF POOR QUALITY

Fig. 16(a)

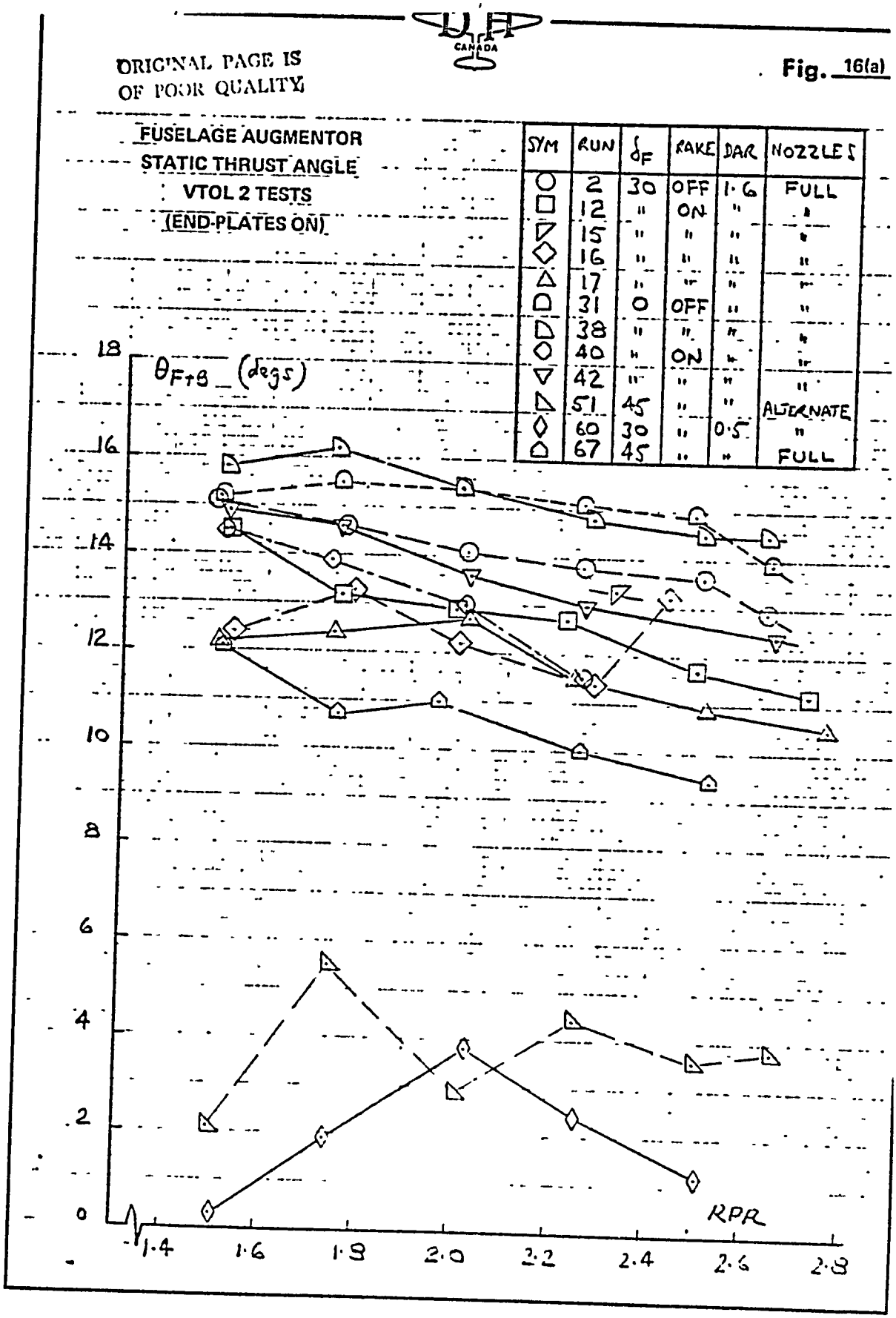

Fig. 16(b)

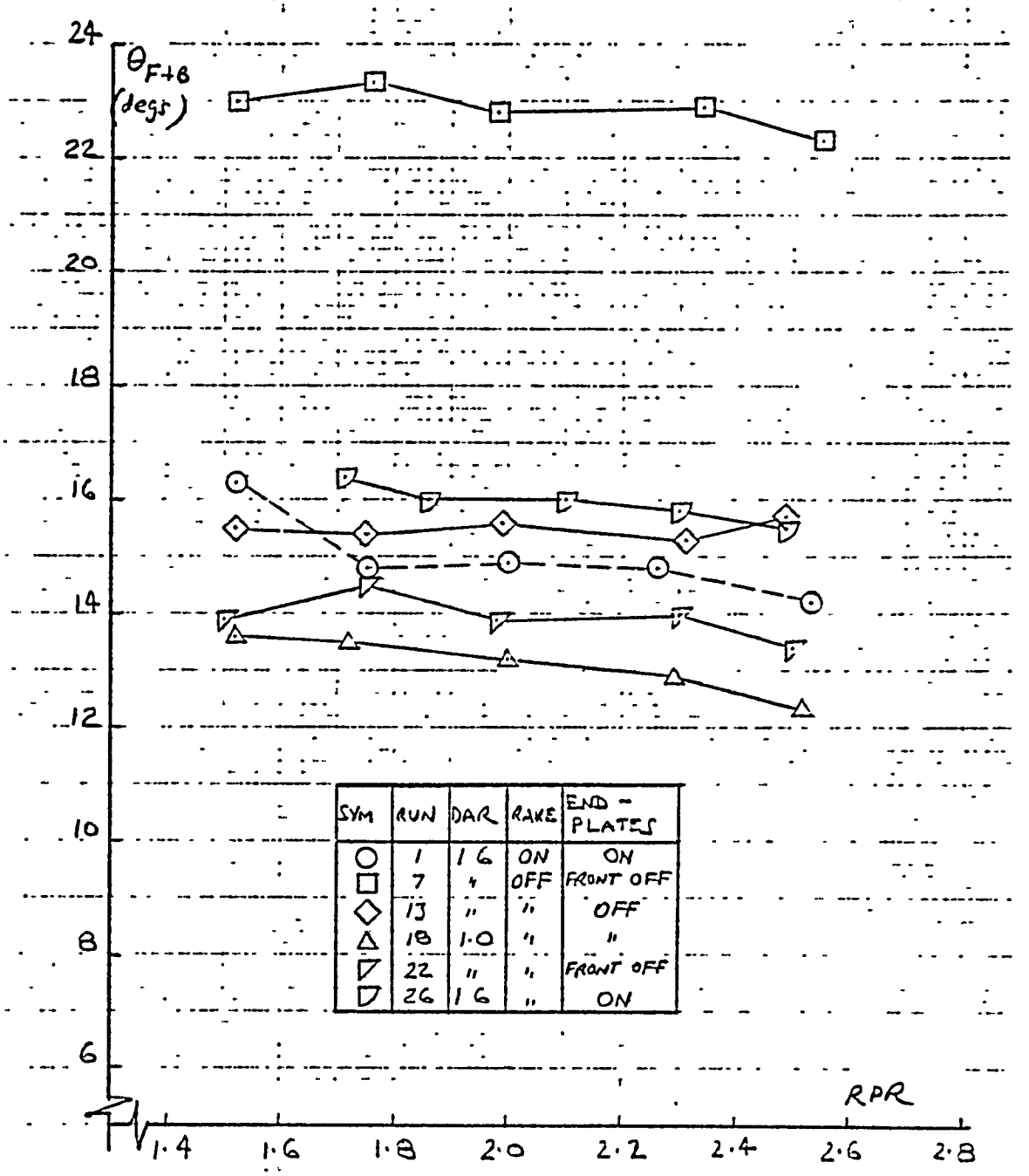

FUSELAGE AUGMENTOR STATIC THRUST ANGLE - VTOL 3 TESTS
FULL NOZZLE SET

Fig. 16(c)

FUSELAGE AUGMENTOR STATIC THRUST ANGLE - VTOL 3 TESTS

HALF NOZZLE TESTS (RAKE OFF)

SYM	RUN	DAR	NOZZLES	END-PLATES
○	31	1·6	ALTERNATE	ON
□	32	"	"	"
◇	49	"	"	FRONT OFF
△	53	"	"	OFF
◸	58	1·0	"	"
◸	62	0·5	"	"
◻	66	1·0	CENTRE	"
◇	70	"	"	"
◇	74	1·6	"	"
◻	77	0·5	"	"

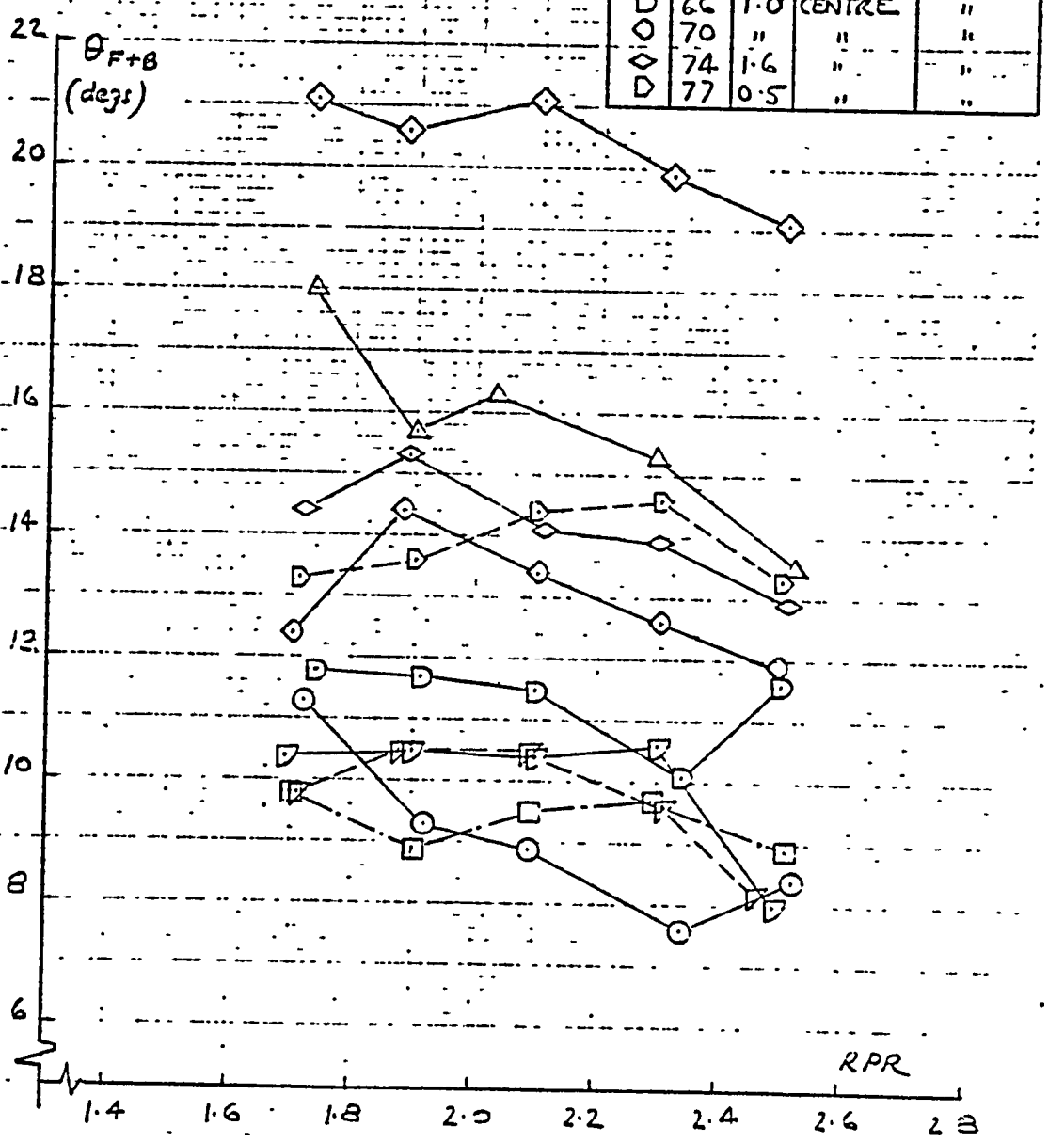

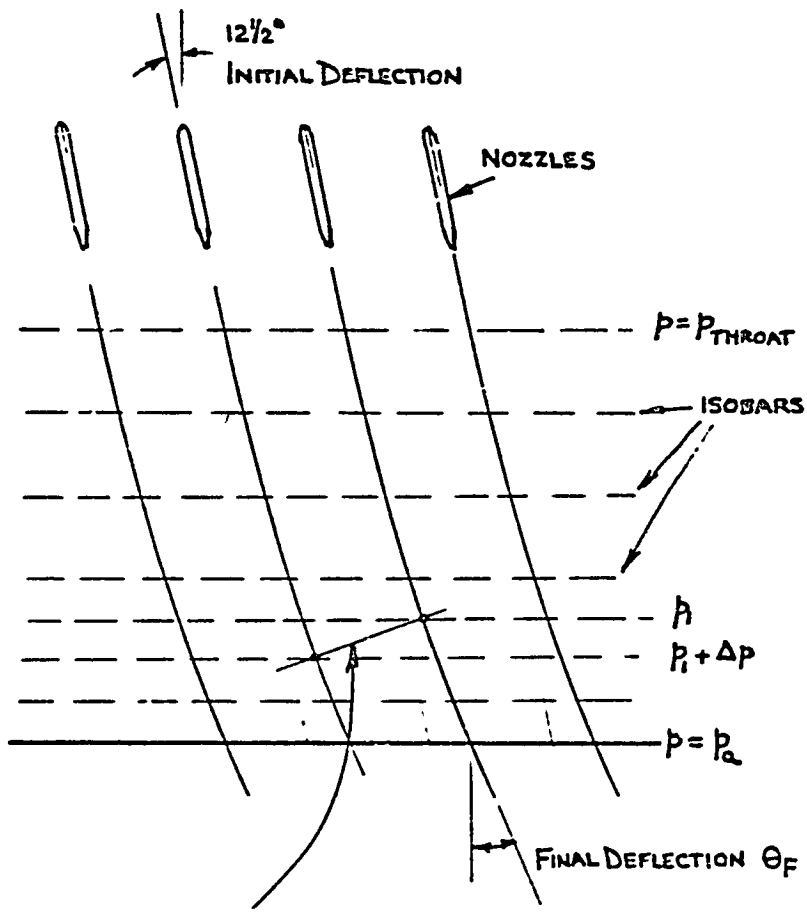

MECHANISM OF FLOW DEFLECTION
IN
FUSELAGE AUGMENTOR DIFFUSER

Fig. 18

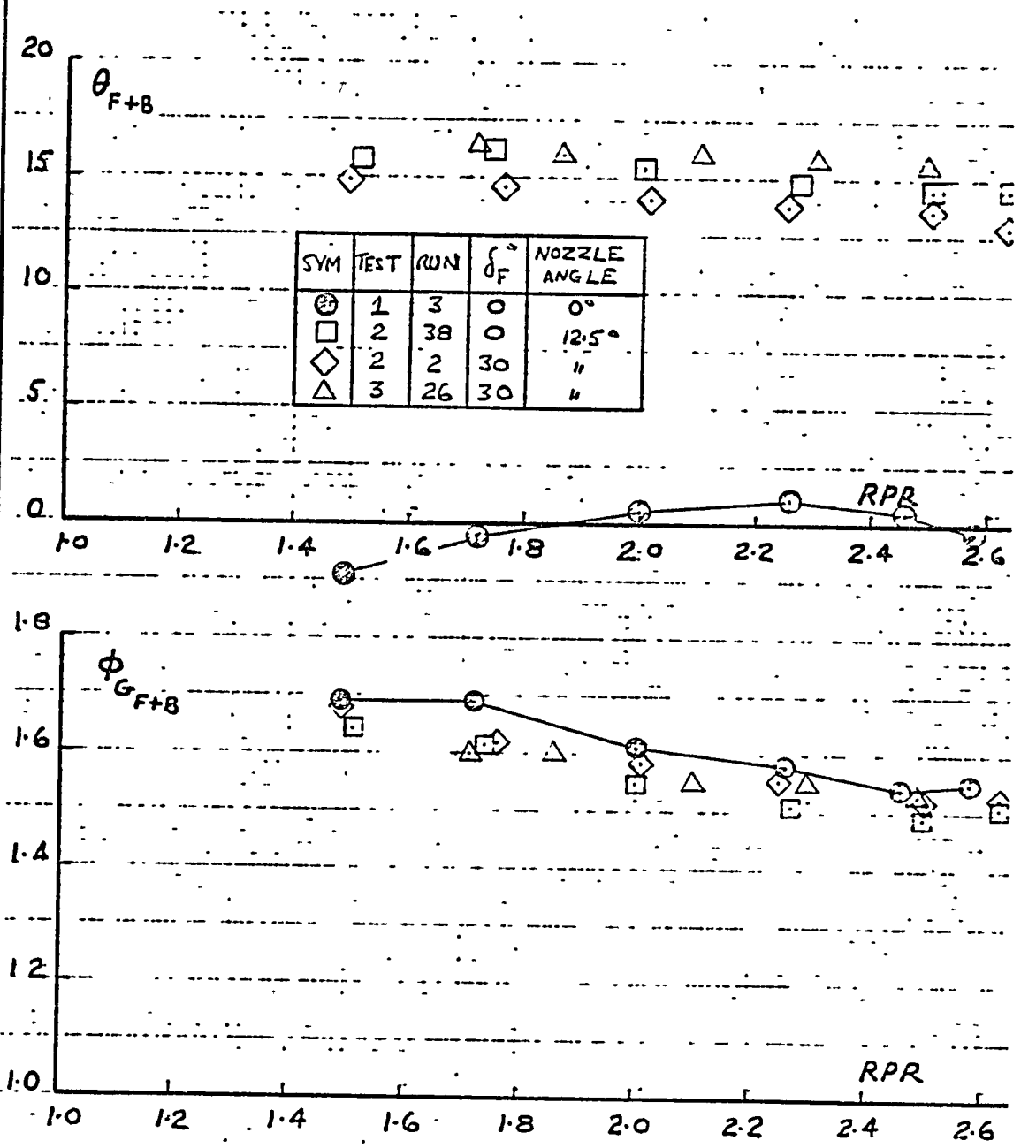

EFFECT OF FUSELAGE AUGMENTOR NOZZLE ANGLE ON STATIC PERFORMANCE

DAR = 1.6; FULL NOZZLE SET; EXIT RAKE OFF

Fig. 19

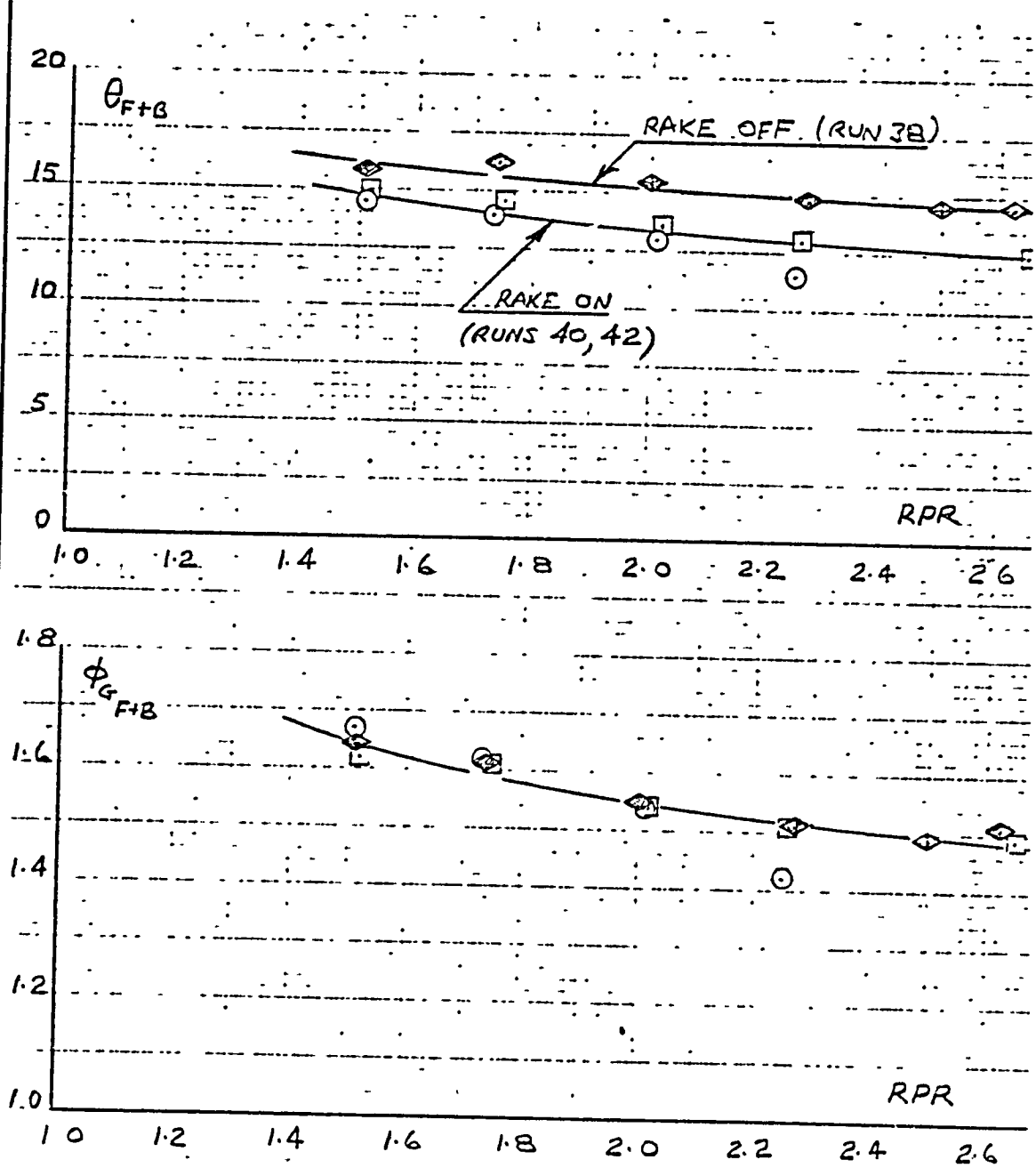

EFFECT OF RAKE ON STATIC PERFORMANCE (VTOL 2 TESTS)

DAR = 1.6; FULL NOZZLE SET

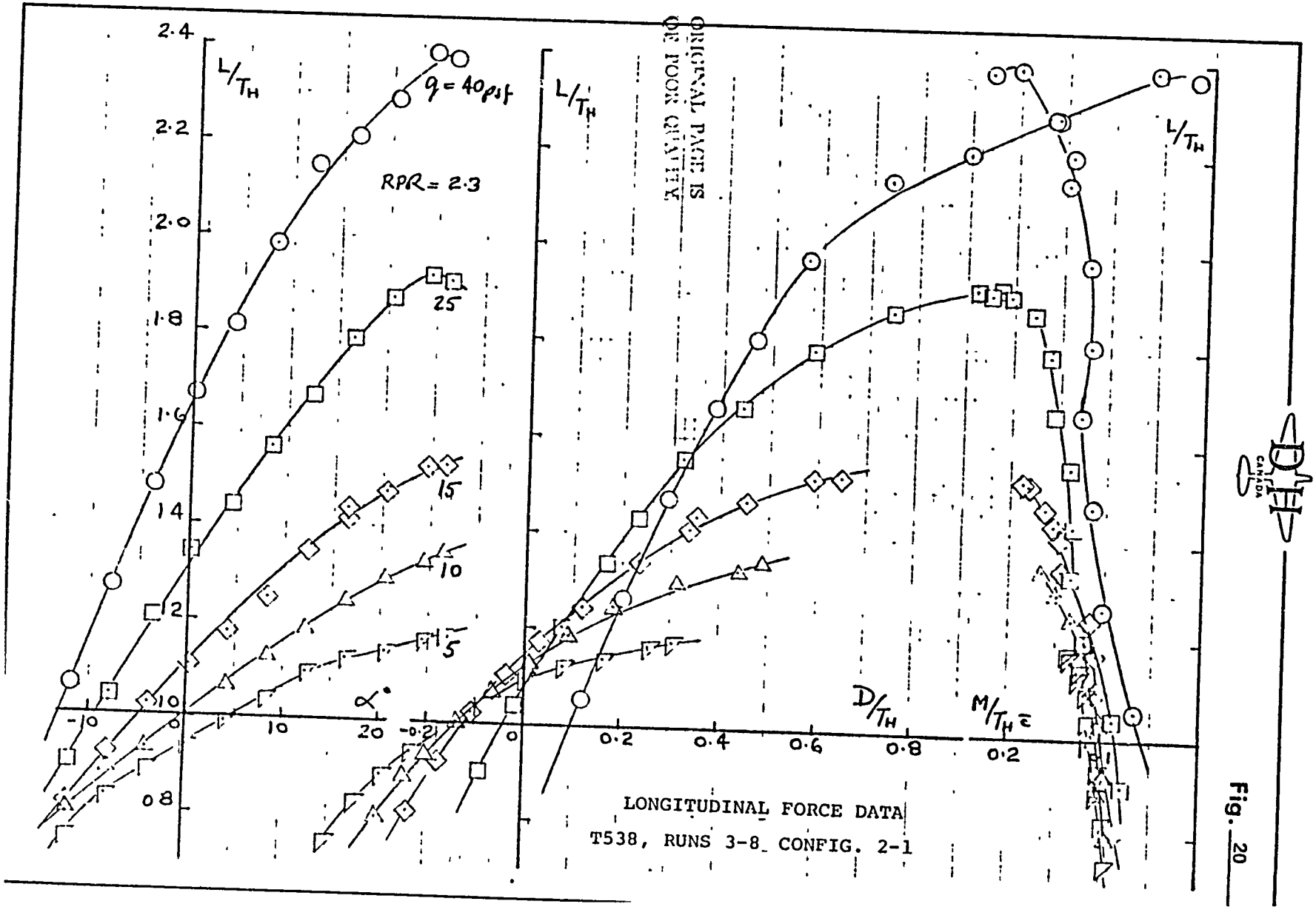
2.4
2.2
2.0
1.8
1.6
1.4
1.2
1.0
0.8
L/T_H
q = 40 psf
RPR = 2.3
25
15
10
5
-10
0
10
20
α°
-0.2
0
0.2
0.4
0.6
0.8
D/T_H
M/T_H c
0.2
L/T_H
L/T_H
ORIGINAL PAGE IS
OF POOR QUALITY
LONGITUDINAL FORCE DATA
T538, RUNS 3-8 CONFIG. 2-1

Fig. 20

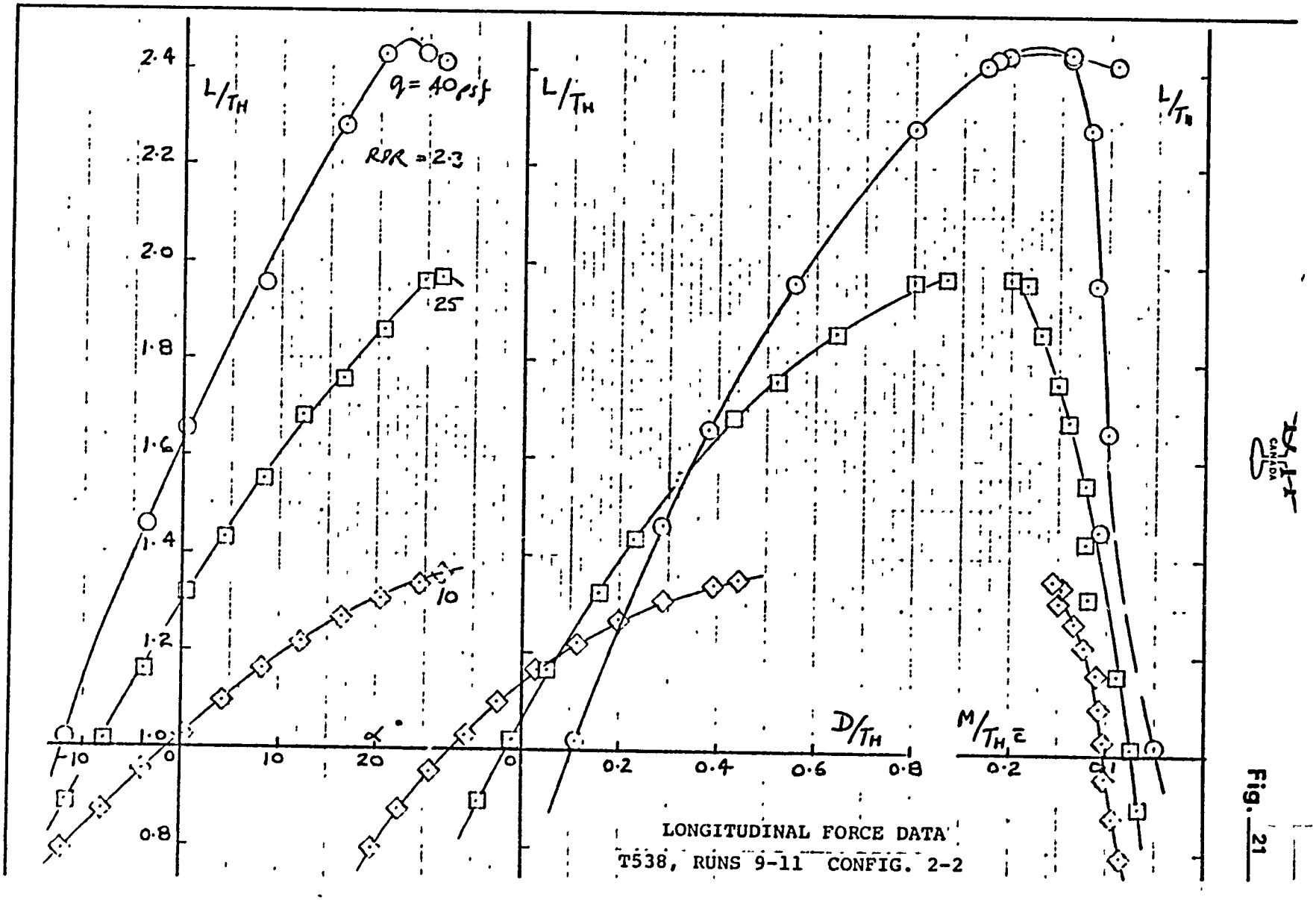

LONGITUDINAL FORCE DATA
T538, RUNS 9-11 CONFIG. 2-2

Fig. 21

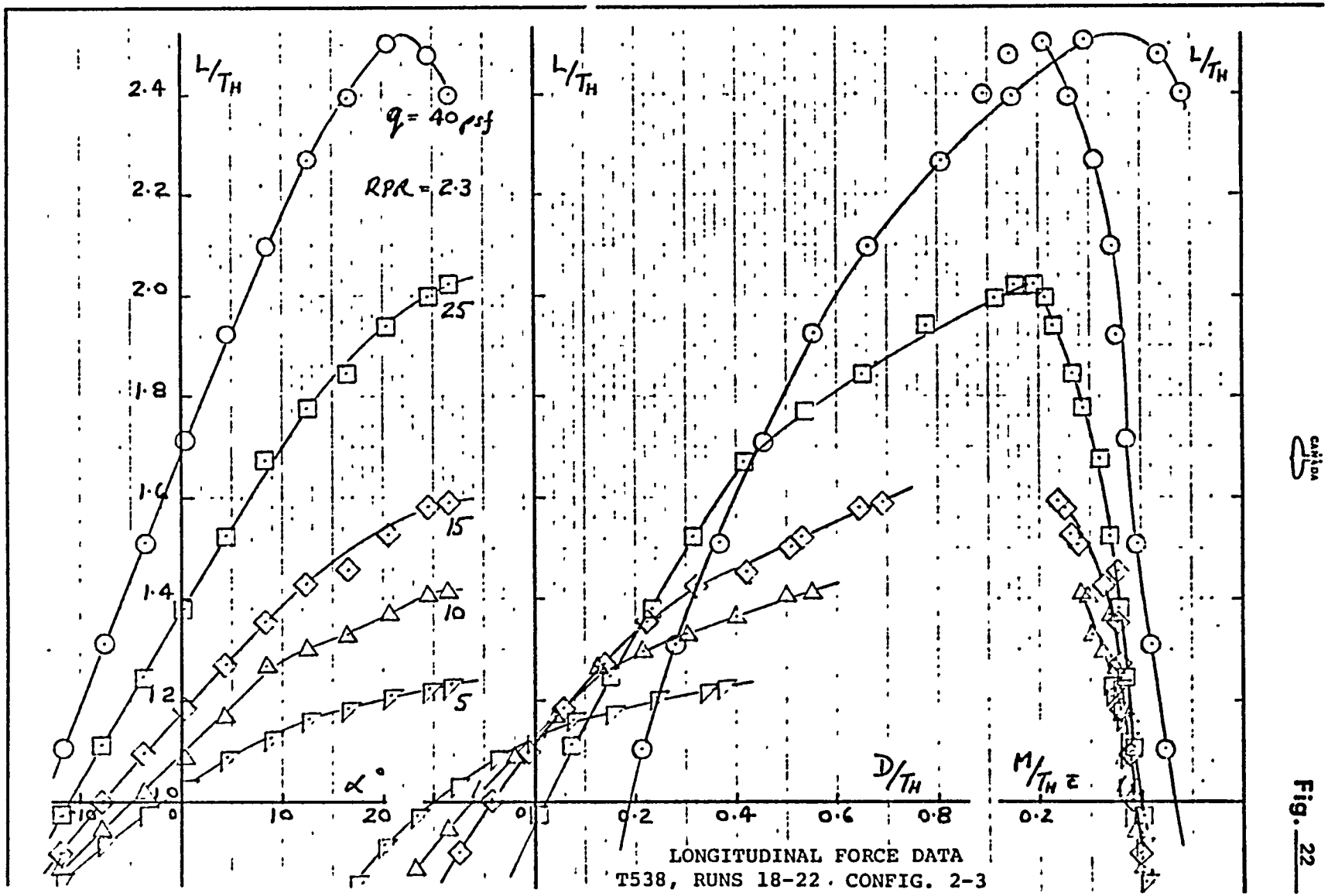

LONGITUDINAL FORCE DATA
T538, RUNS 18-22 . CONFIG. 2-3

Fig. 22

Fig. 23

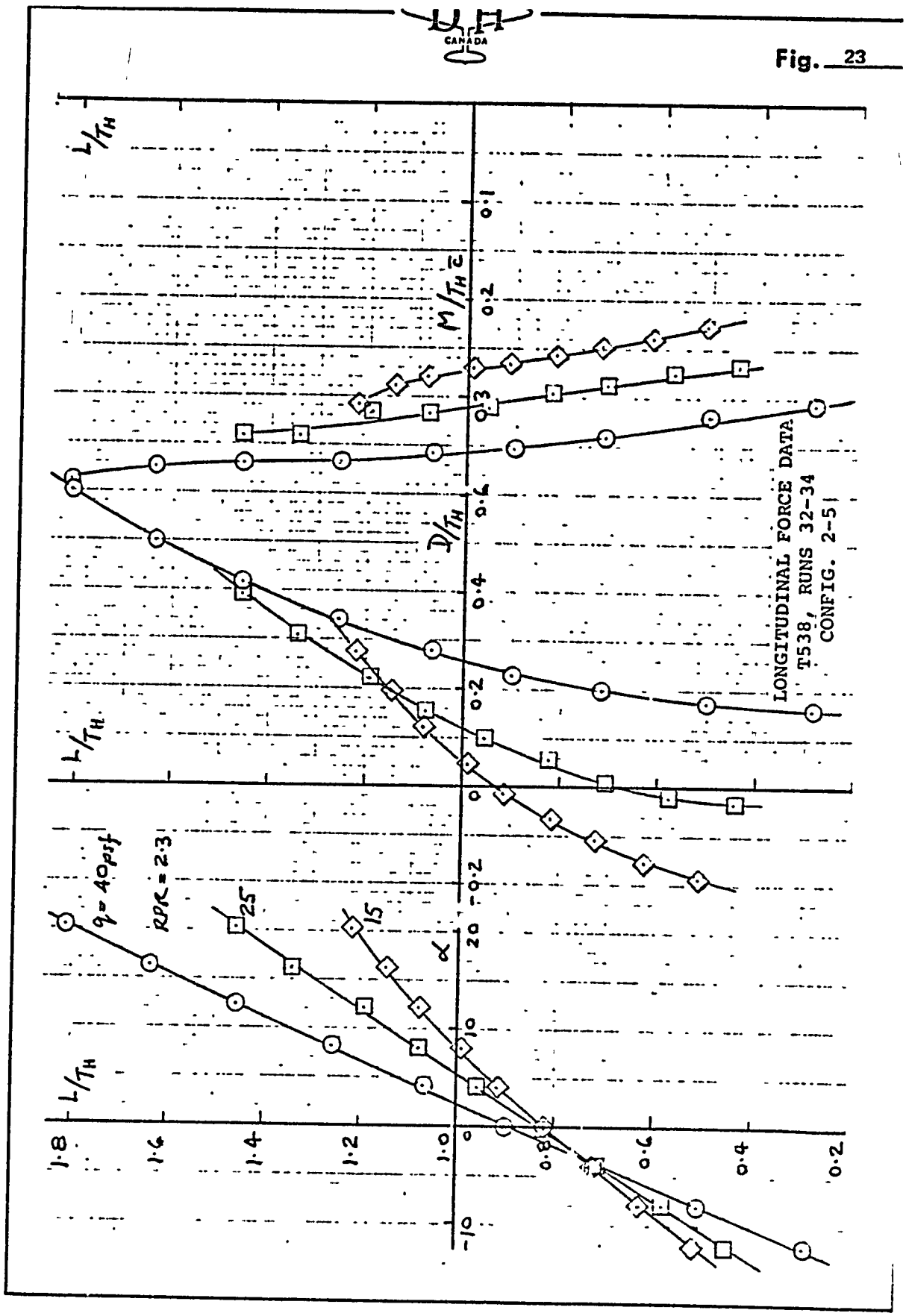
CANADA
LONGITUDINAL FORCE DATA
T538, RUNS 32-34
CONFIG. 2-5
L/TH
M/TH c̄
D/TH
L/TH
L/TH
q = 40 psf
RPK = 2.3
25
15
α
1.8
1.6
1.4
1.2
1.0
0.8
0.6
0.4
0.2
0.1
0.2
0.3
0.6
0.4
0.2
0
-0.2
20
10
0
-10

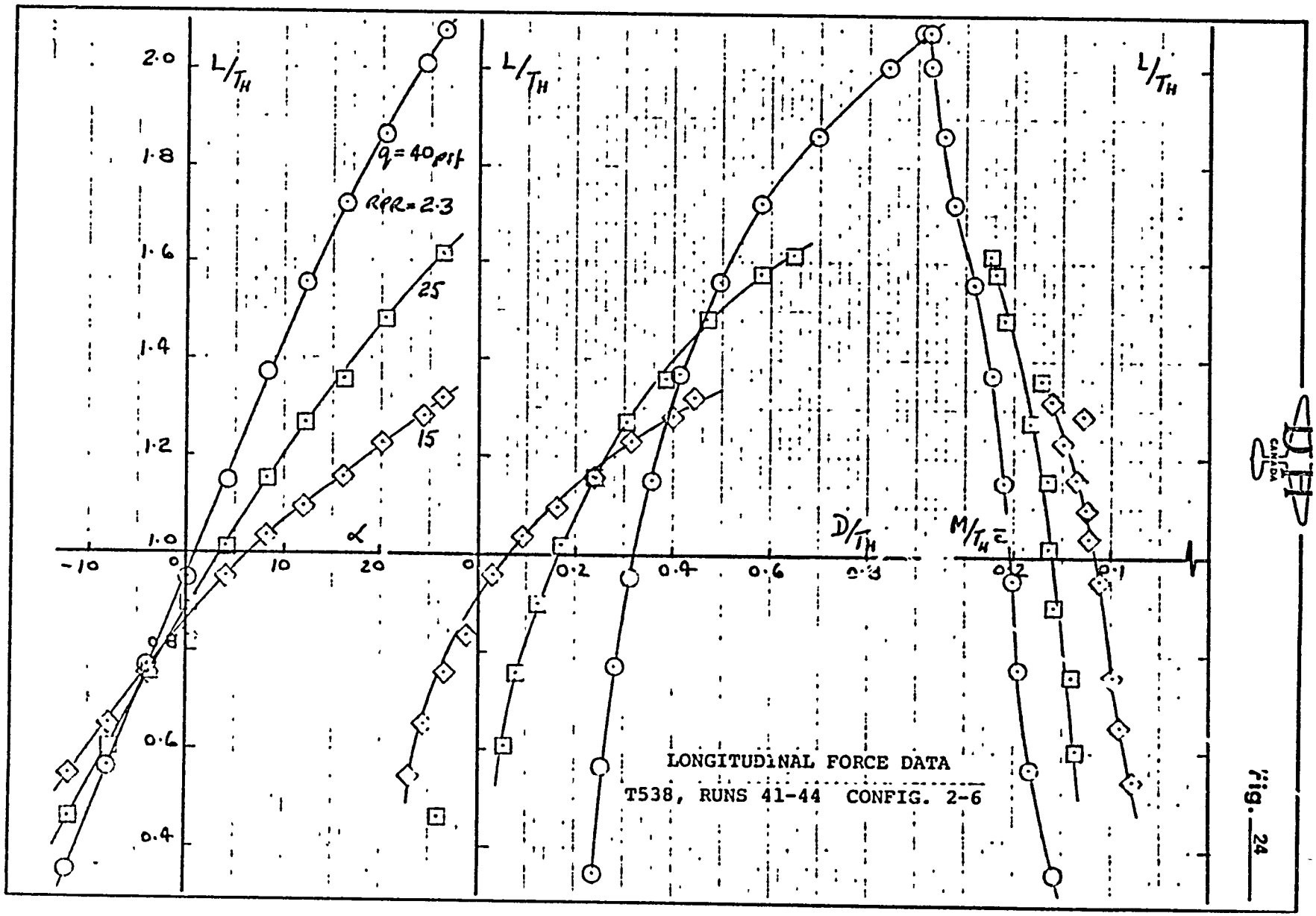
L/T_H
2.0
1.8
1.6
1.4
1.2
1.0
0.6
0.4
q = 40 psf
RPR = 2.3
25
15
α
-10
0
10
20
L/T_H
0
0.2
0.4
0.6
D/T_H
L/T_H
M/T_H ℓ
0.2
0.1
LONGITUDINAL FORCE DATA
T538, RUNS 41-44 CONFIG. 2-6

Fig. 24

Fig. 25
LONGITUDINAL FORCE DATA
T538, RUNS 45-49 CONFIG. 2-7
ORIGINAL PAGE IS
OF POOR QUALITY
L/T_H
D/T_H
M/T_H ℓ
α
q = 40 psf
RPR = 2.3
25
15
10
5
0
CANADA

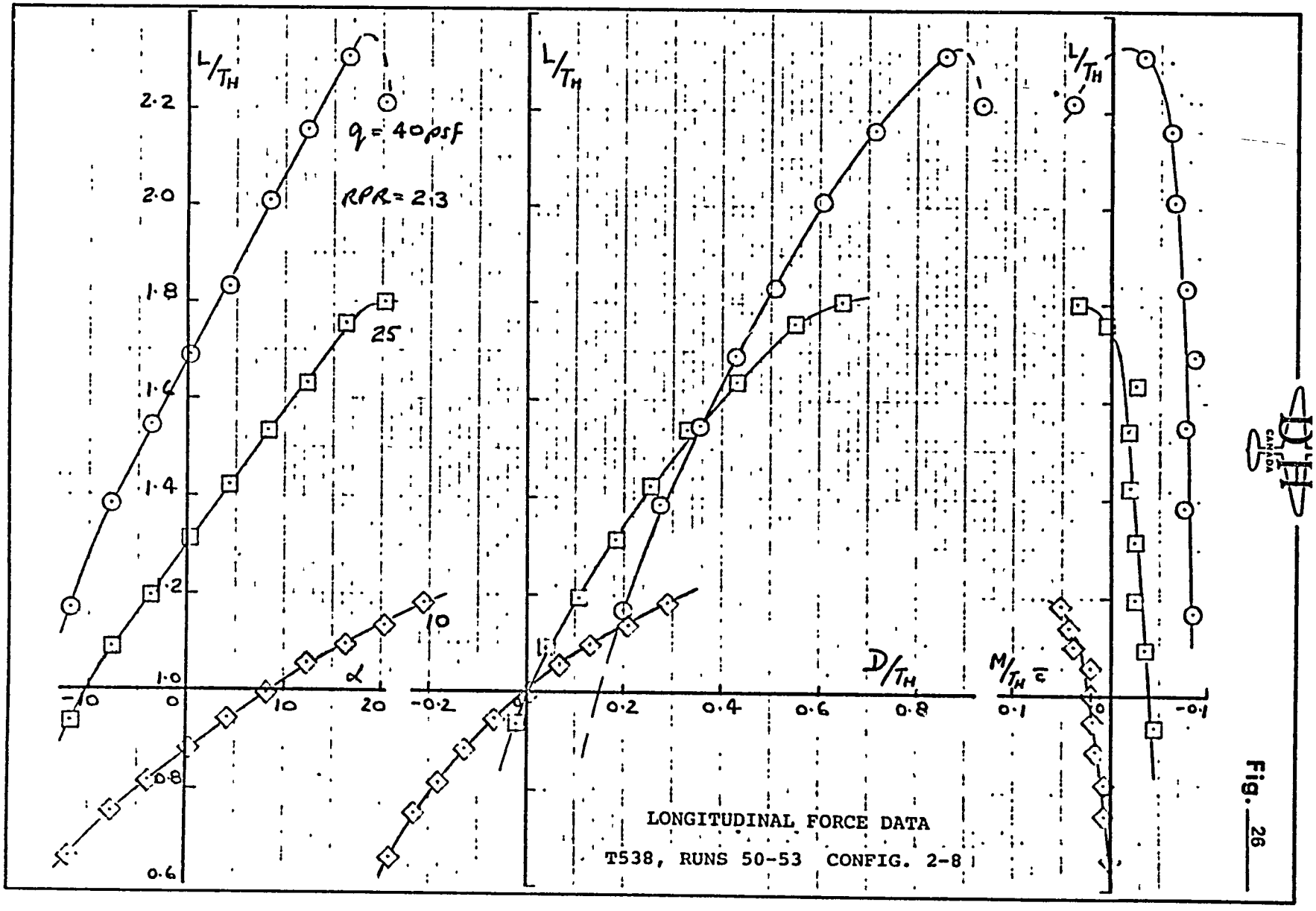

LONGITUDINAL FORCE DATA

T538, RUNS 50-53 CONFIG. 2-8

Fig. 26

Fig. 27

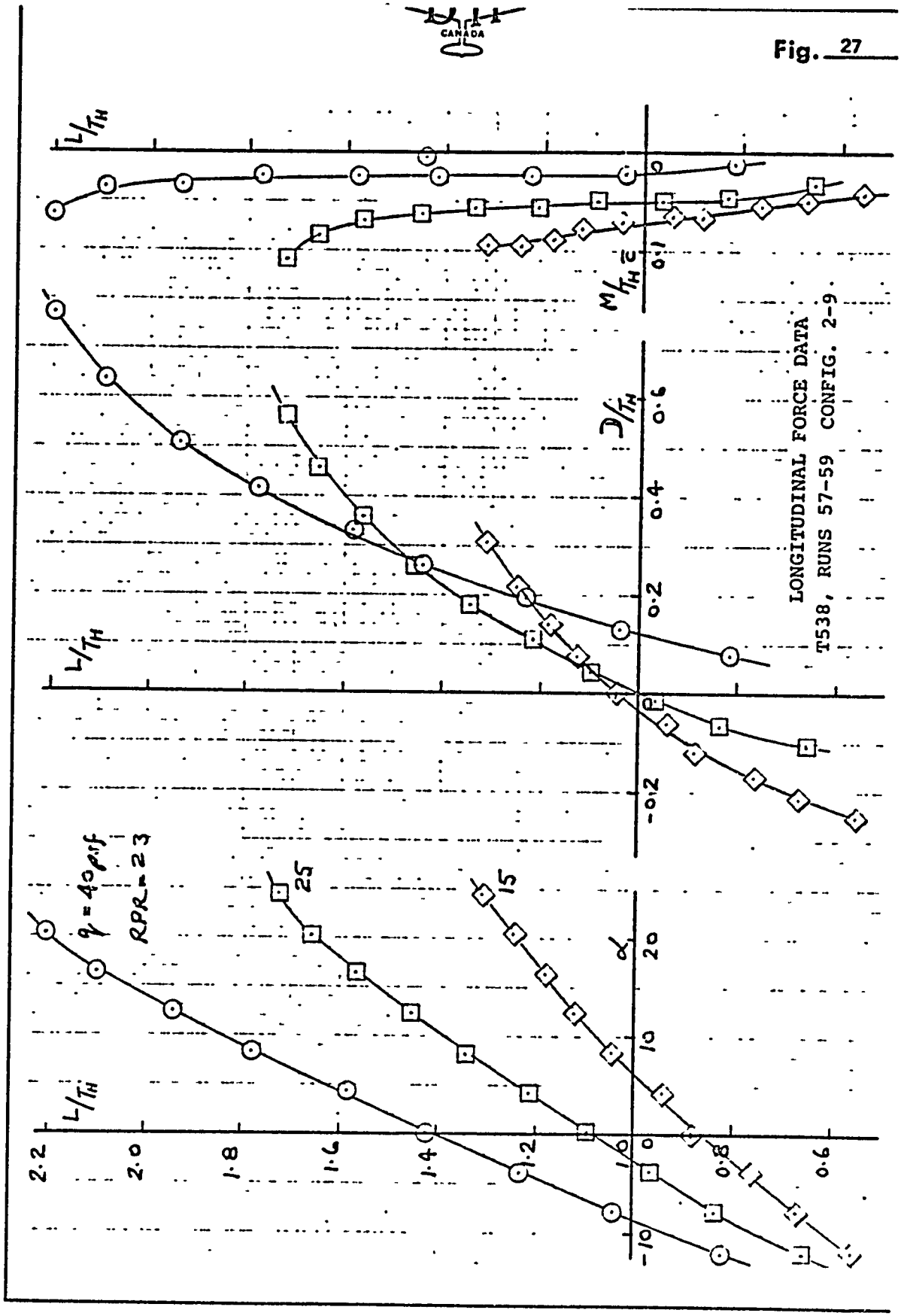
CANADA
LONGITUDINAL FORCE DATA
T538, RUNS 57-59 CONFIG. 2-9.
L/TH
D/TH
α
η = 40 psf
RPR = 23
25
15
2.2
2.0
1.8
1.6
1.4
1.2
1.0
0.8
0.6
0.4
0.2
0
-0.2
20
10
-10

Fig. 28

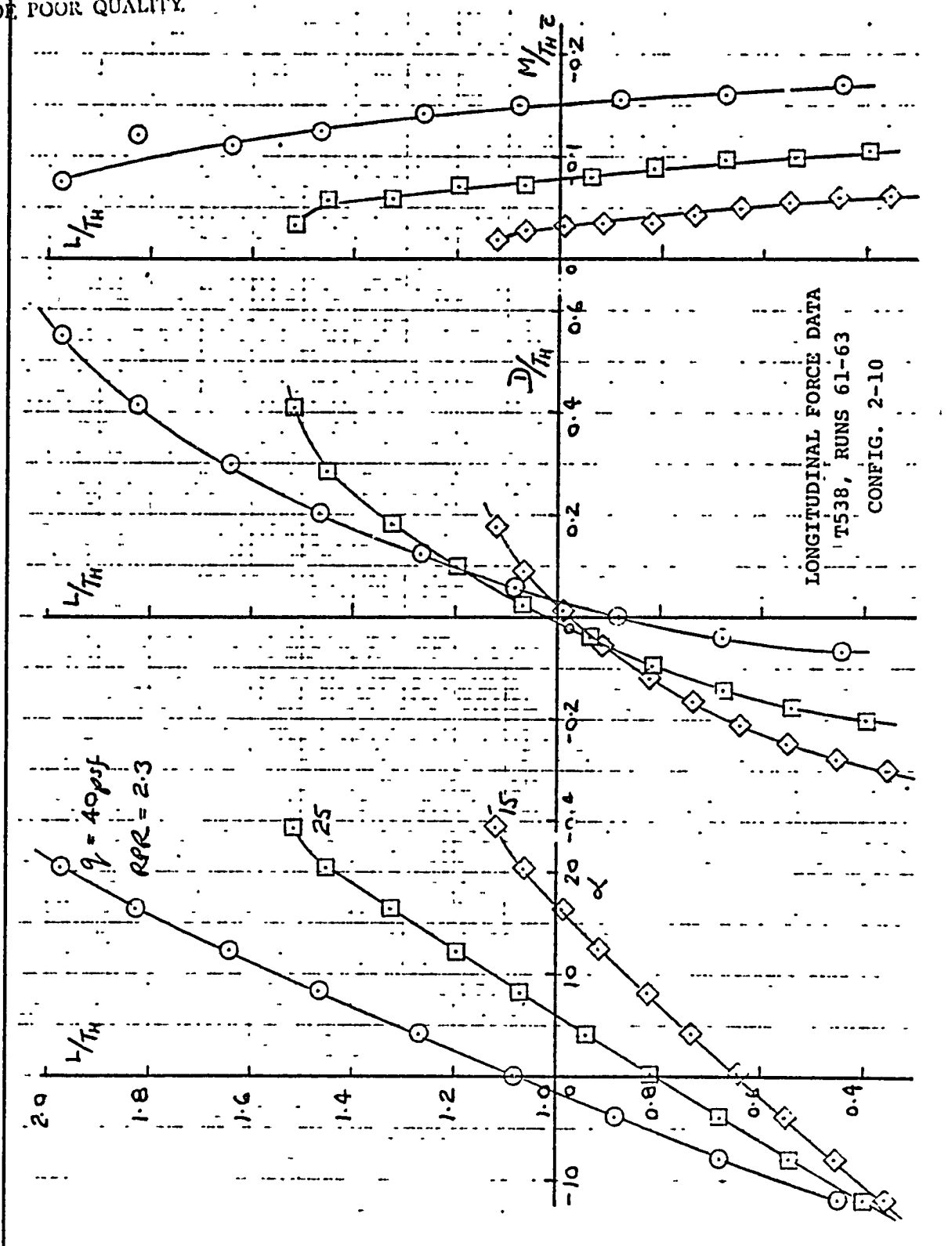

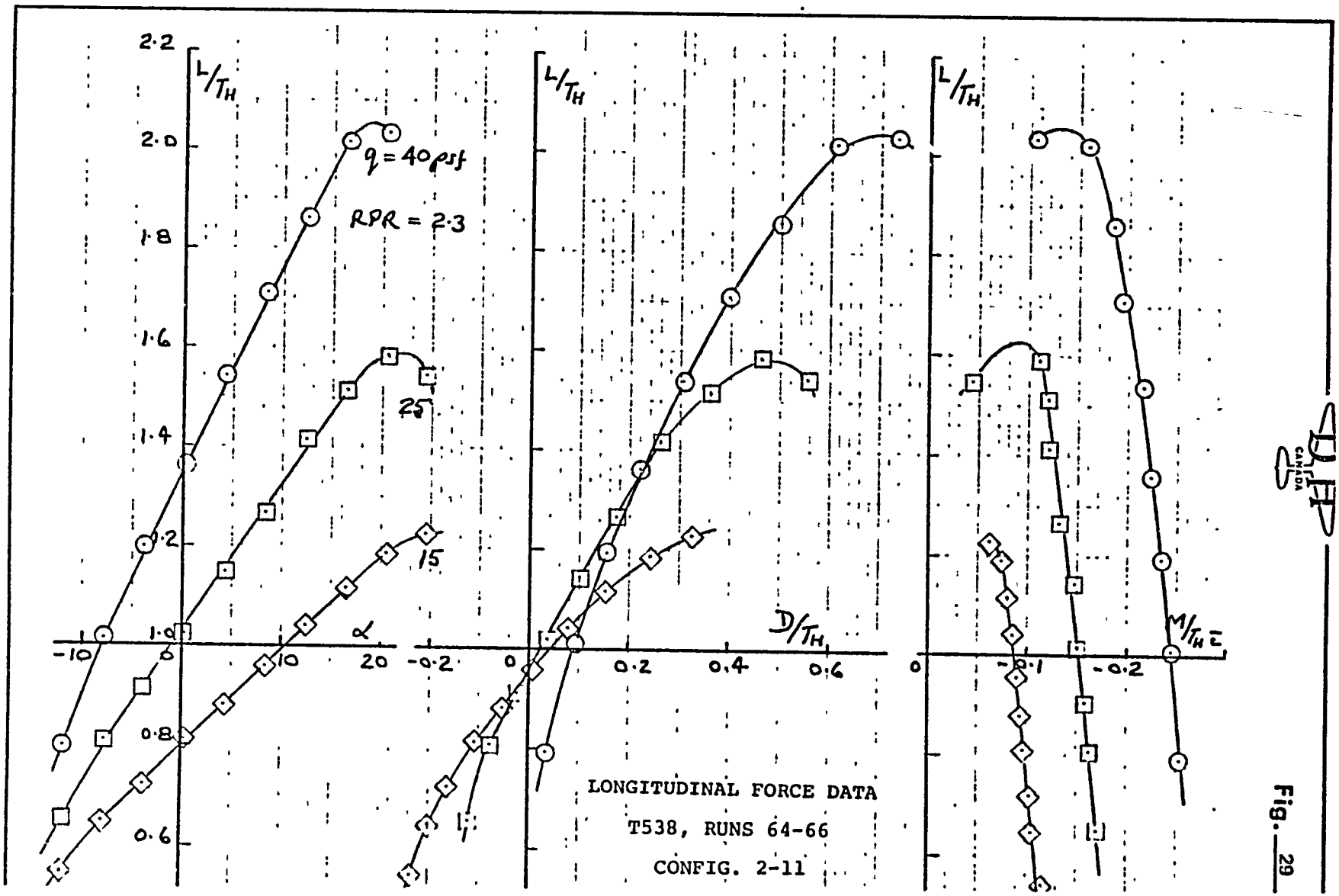

LONGITUDINAL FORCE DATA

T538, RUNS 64-66

CONFIG. 2-11

Fig. 29

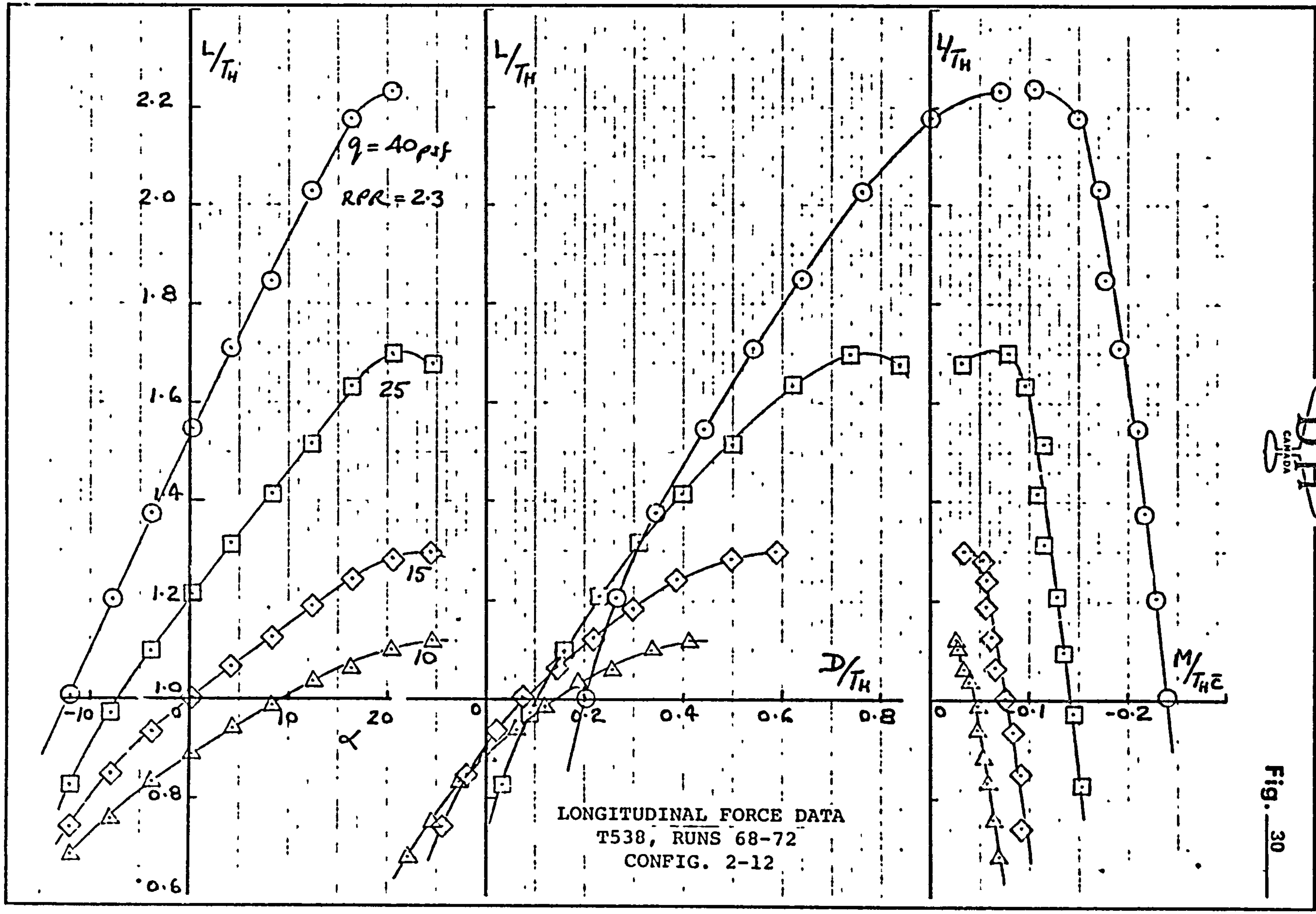

L/T_H
2.2
2.0
1.8
1.6
1.4
1.2
1.0
0.8
0.6
-10
0
10
20
α
q = 40 psf
RPR = 2.3
25
15
10
L/T_H
0
0.2
0.4
0.6
0.8
D/T_H
L/T_H
0
-0.1
-0.2
M/T_H c̄
LONGITUDINAL FORCE DATA
T538, RUNS 68-72
CONFIG. 2-12

Fig. 30

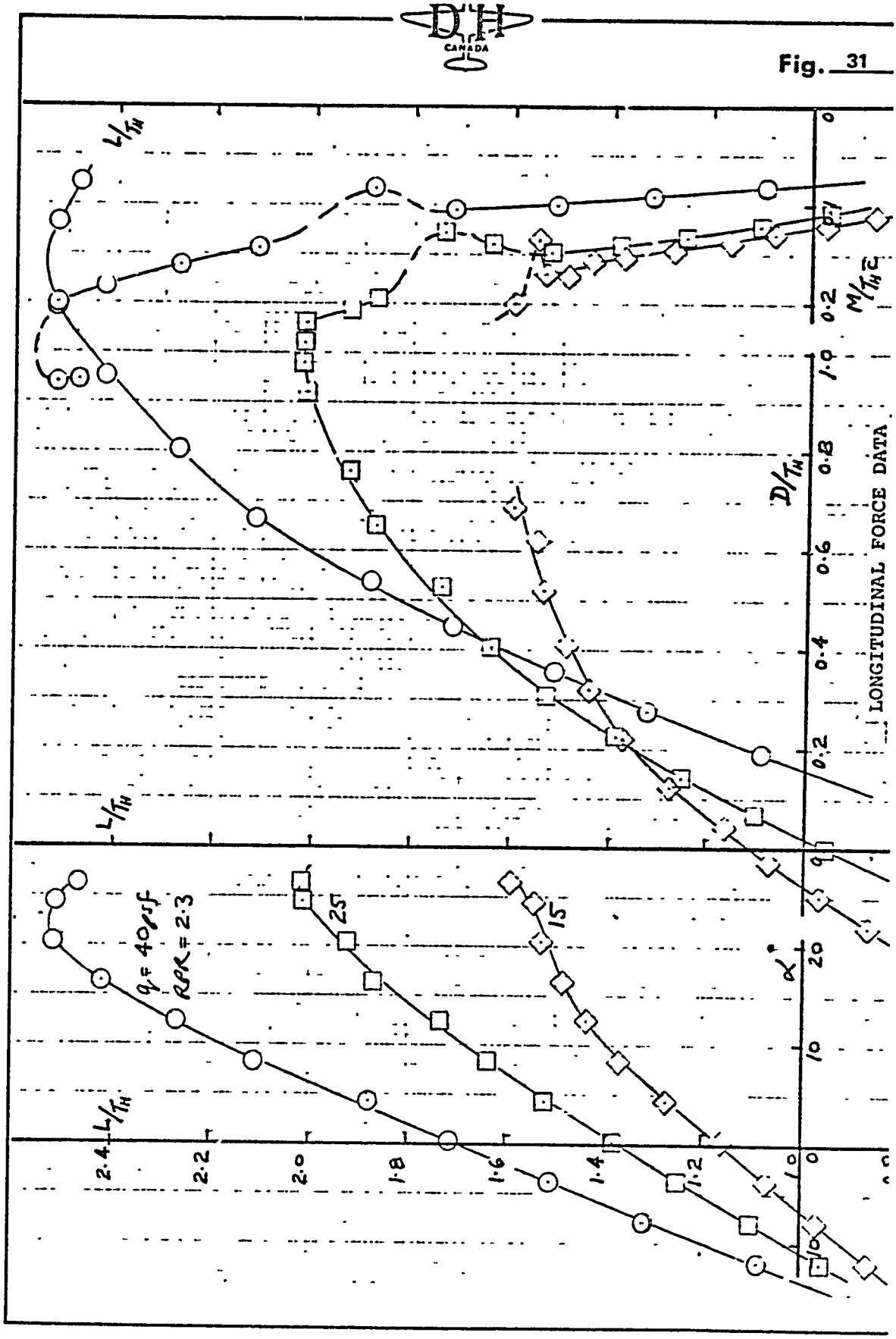
Fig. 31
LONGITUDINAL FORCE DATA
L/TH
D/TH
M/TH c
α°
q = 40 psf
RPK = 2.3
25°
15°

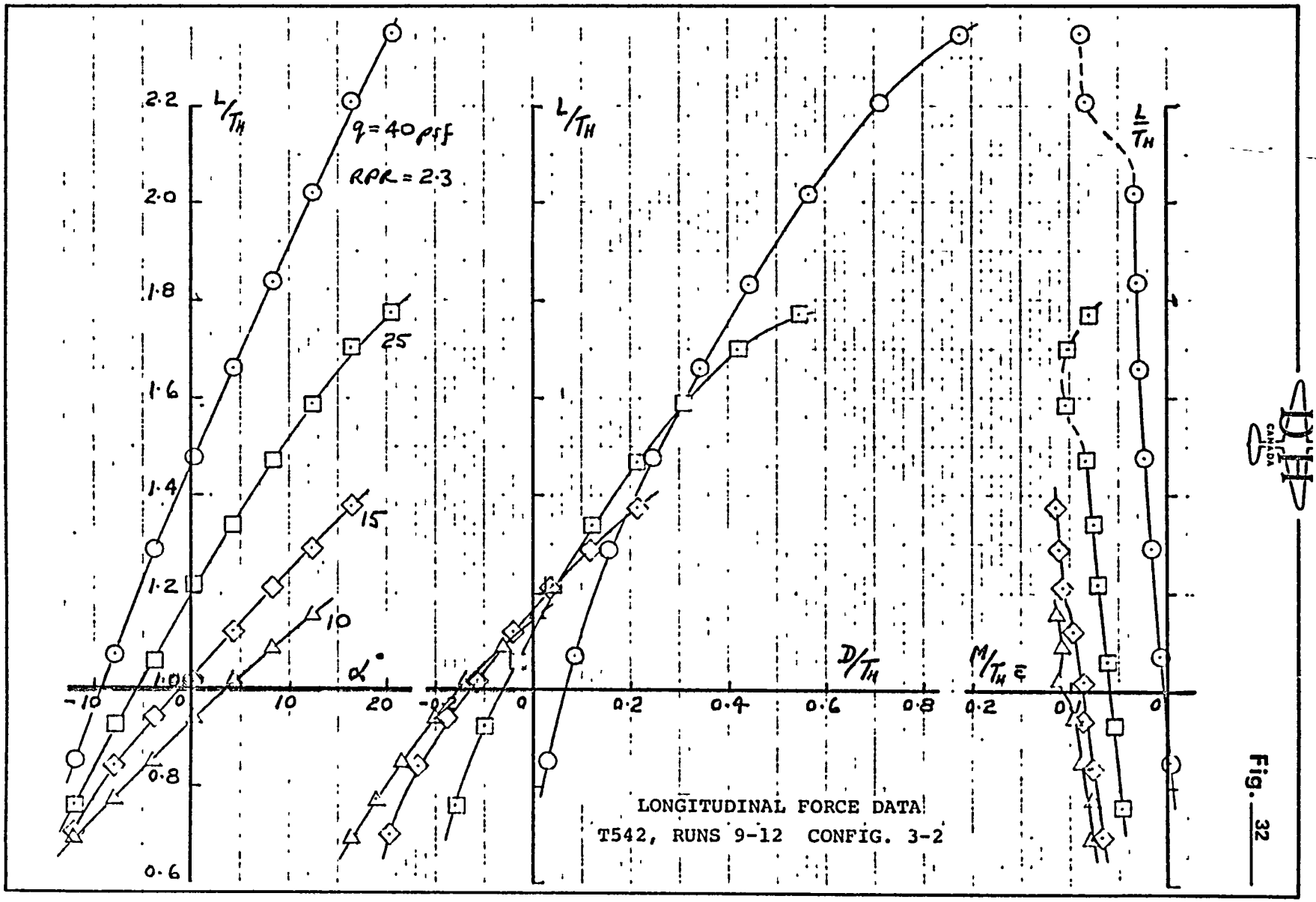

LONGITUDINAL FORCE DATA
T542, RUNS 9-12 CONFIG. 3-2

Fig. 32

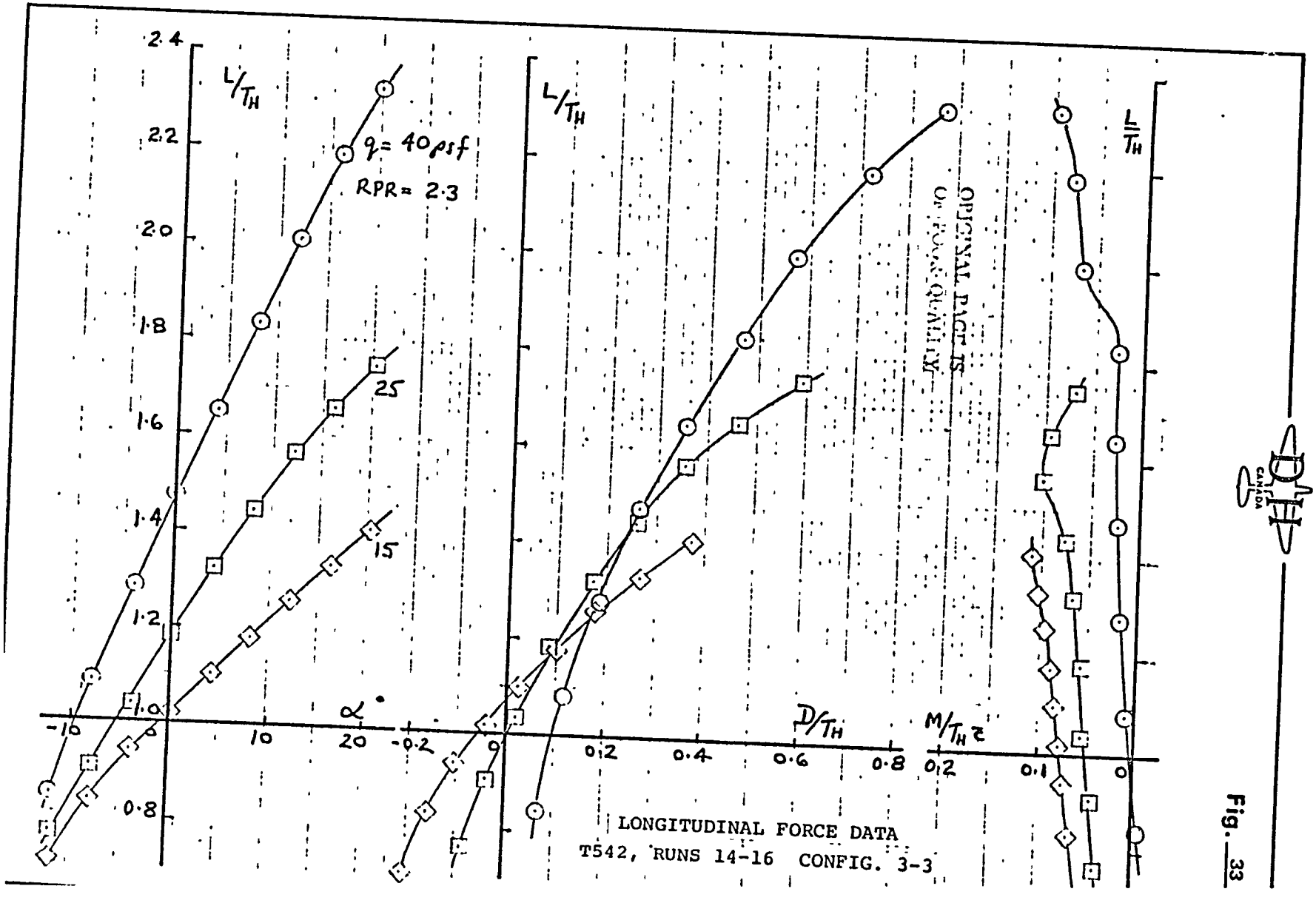

LONGITUDINAL FORCE DATA
T542, RUNS 14-16 CONFIG. 3-3

Fig. 33

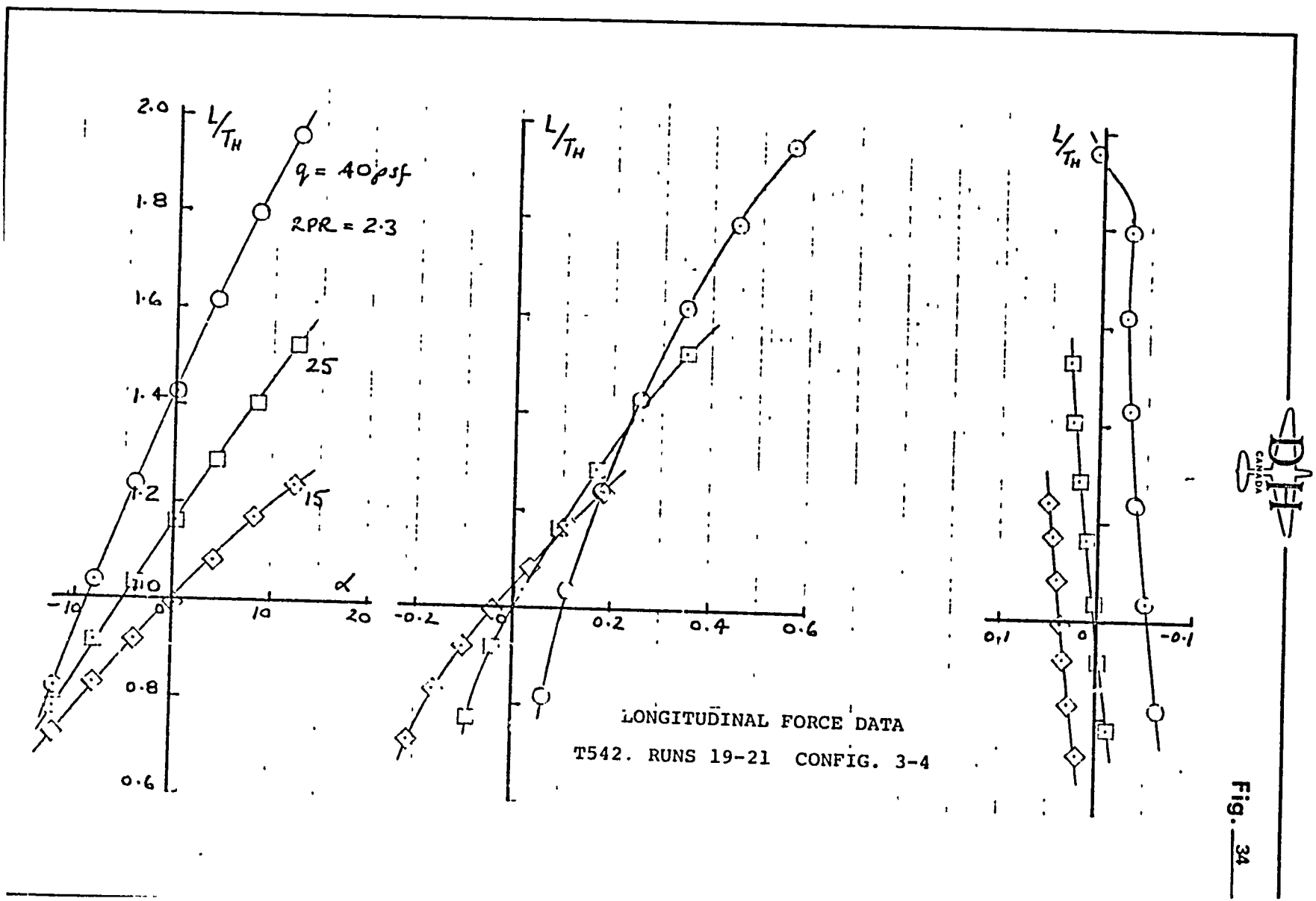

LONGITUDINAL FORCE DATA

T542. RUNS 19-21 CONFIG. 3-4

Fig. 34

Fig. 35

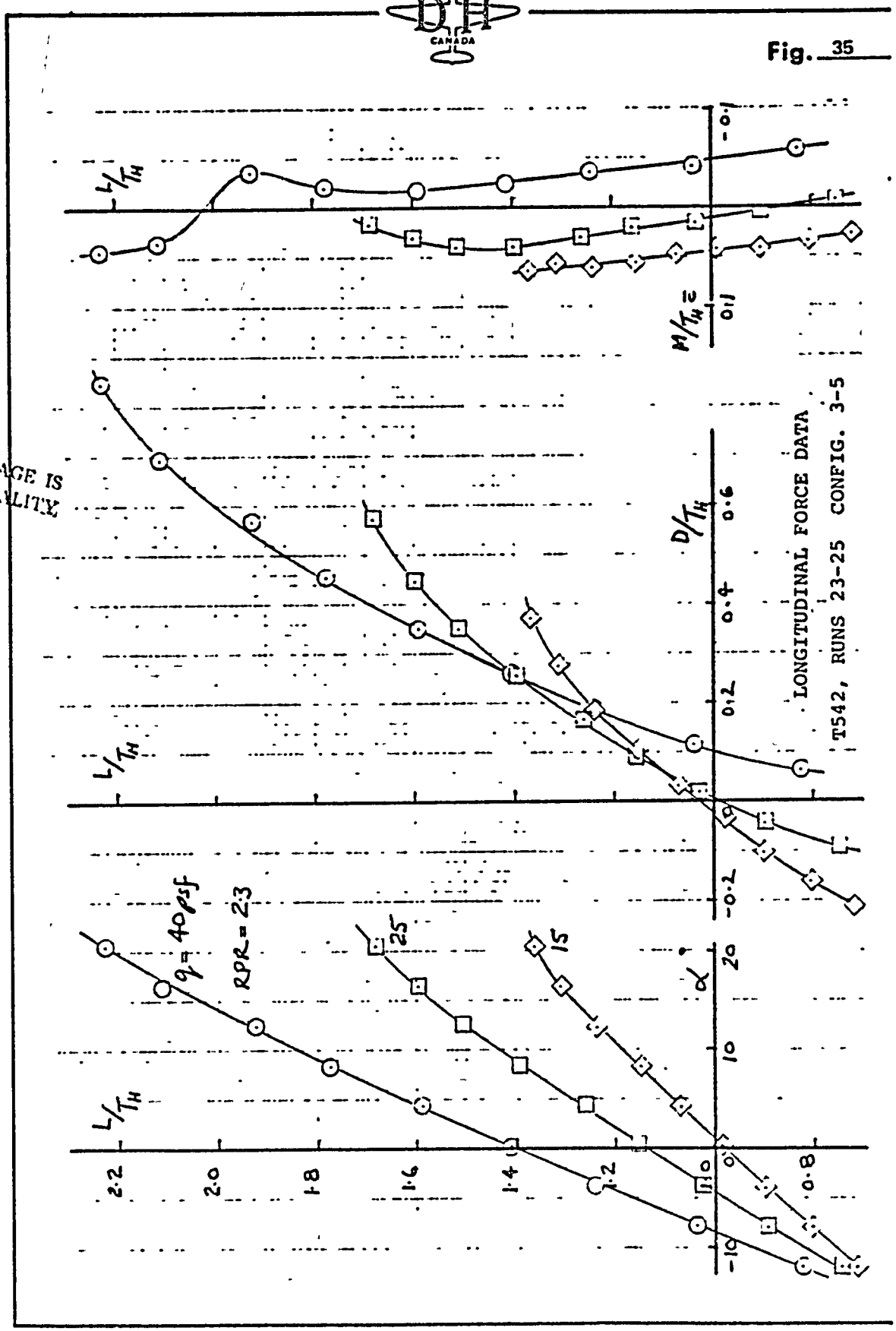

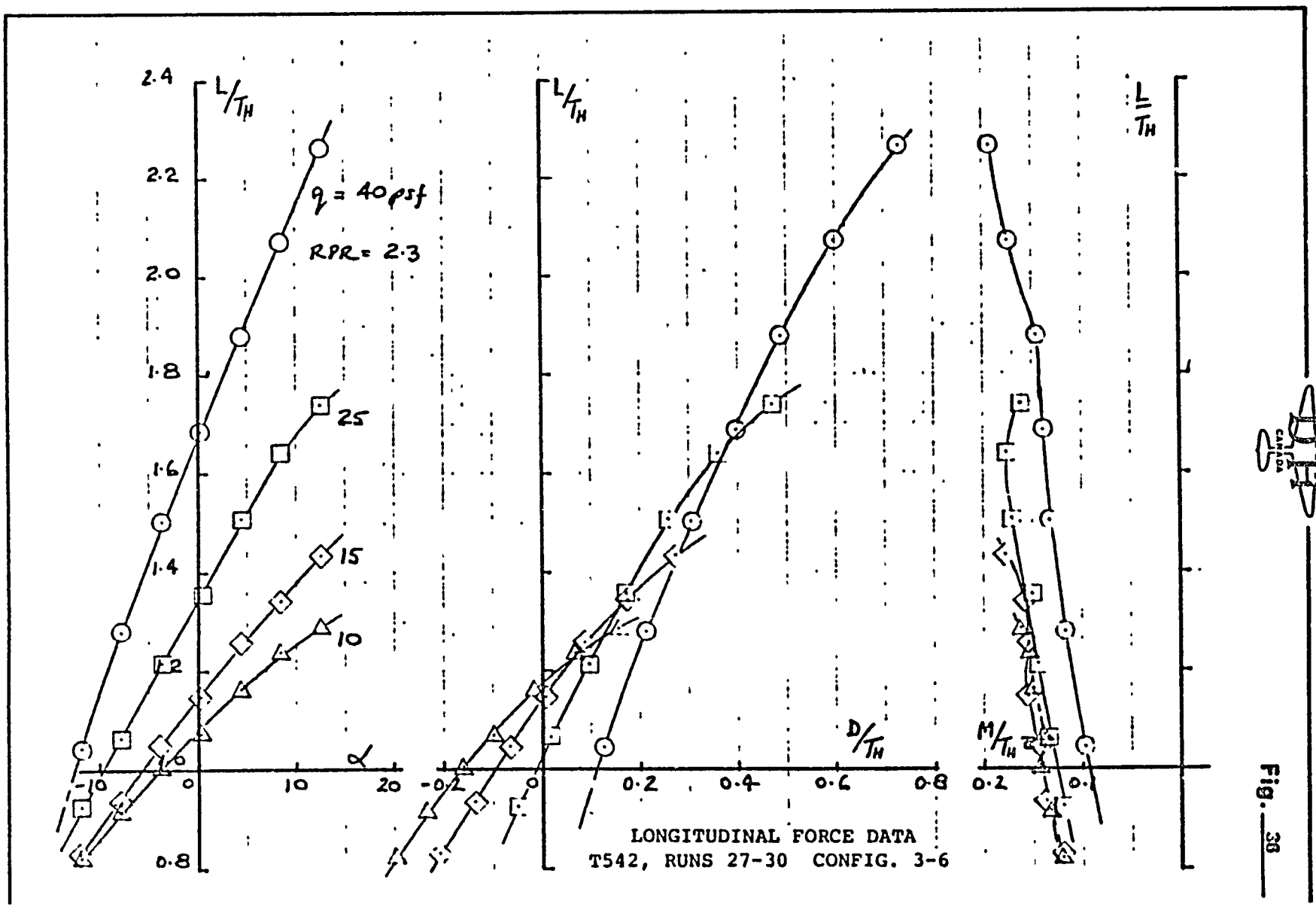

LONGITUDINAL FORCE DATA
T542, RUNS 27-30 CONFIG. 3-6

Fig. 39

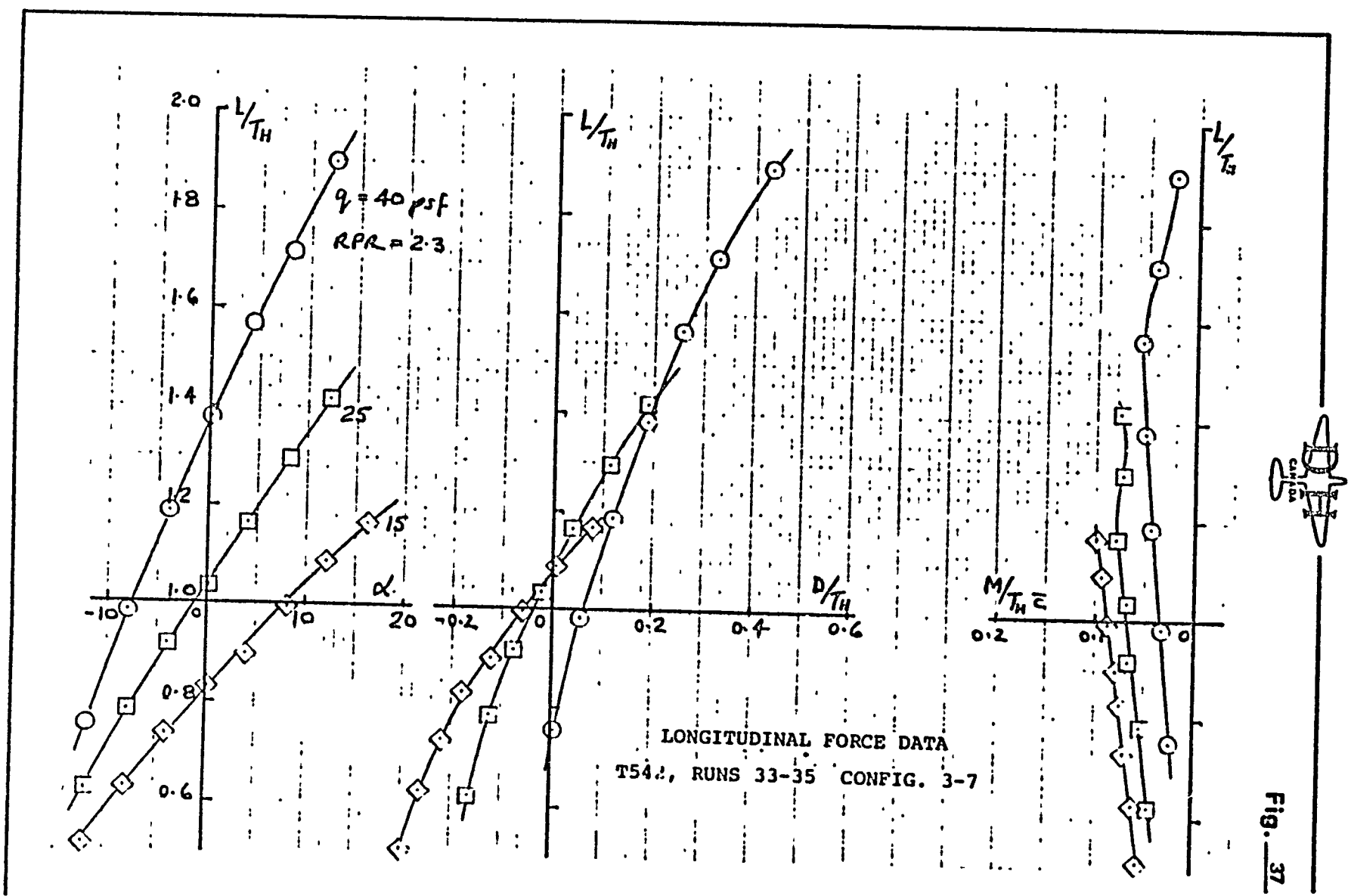

LONGITUDINAL FORCE DATA

T54J, RUNS 33-35 CONFIG. 3-7

Fig. 37

Fig. 38

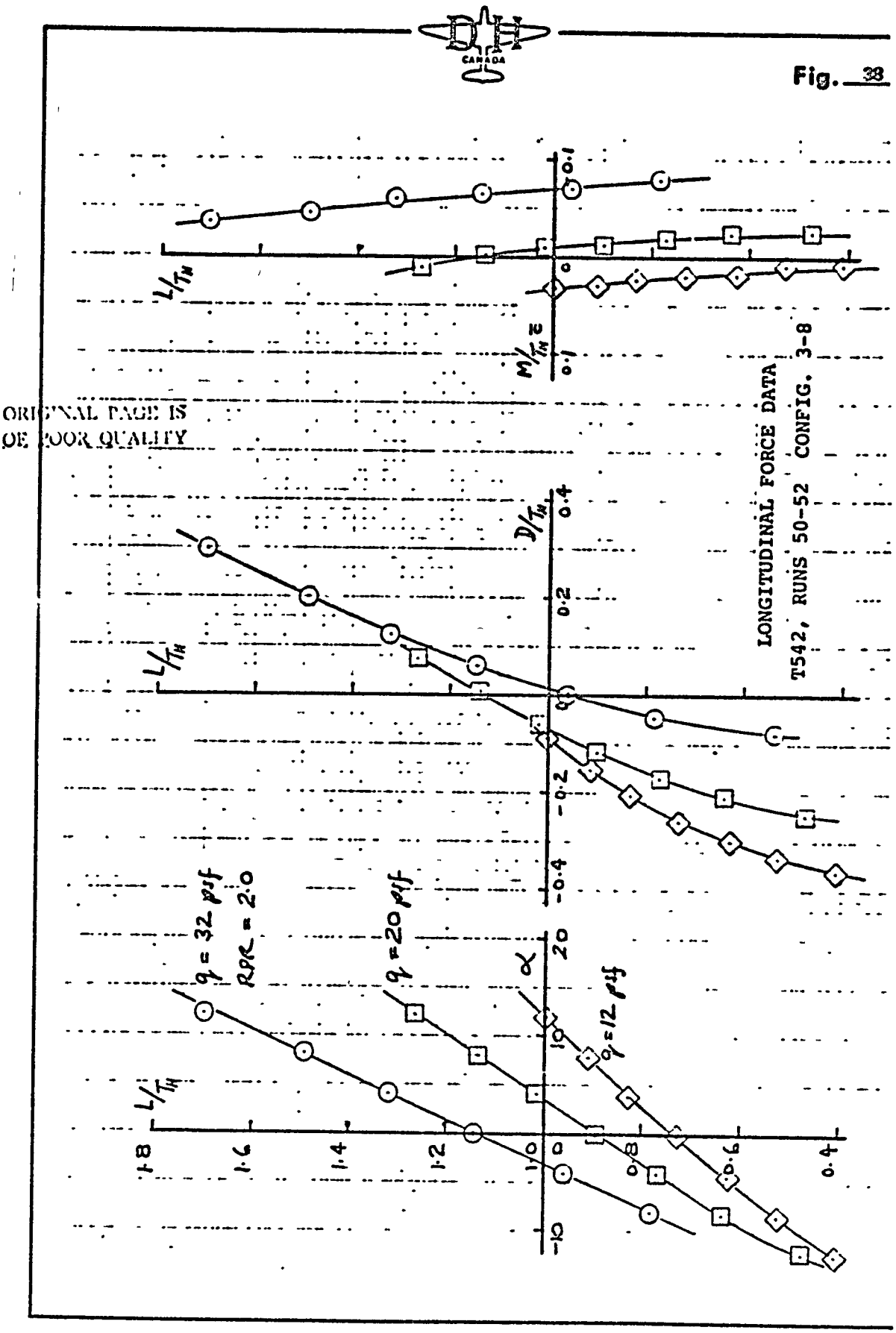

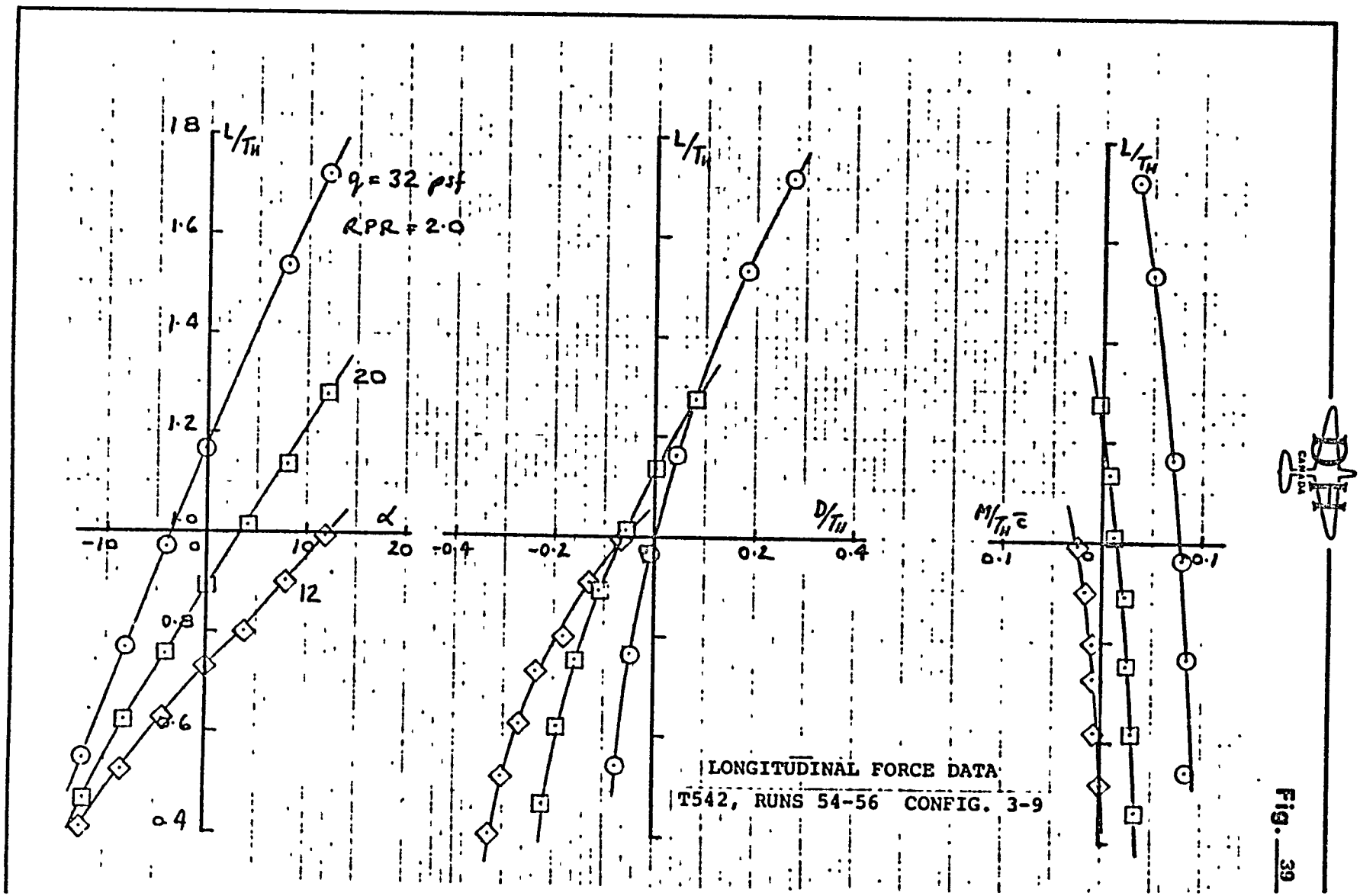

LONGITUDINAL FORCE DATA
T542, RUNS 54-56 CONFIG. 3-9

Fig. 39

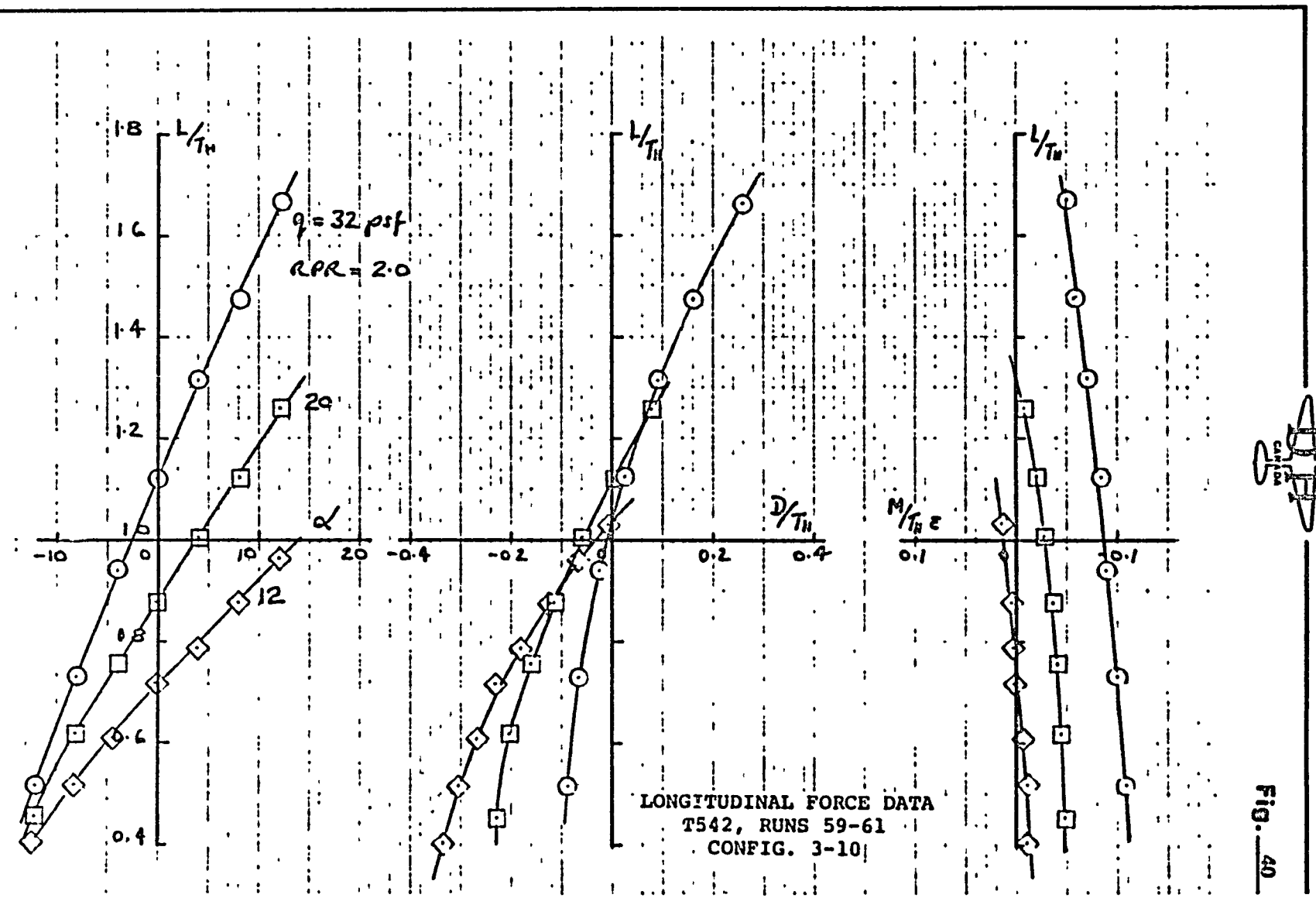

LONGITUDINAL FORCE DATA
T542, RUNS 59-61
CONFIG. 3-10

Fig. 40

Fig. 41

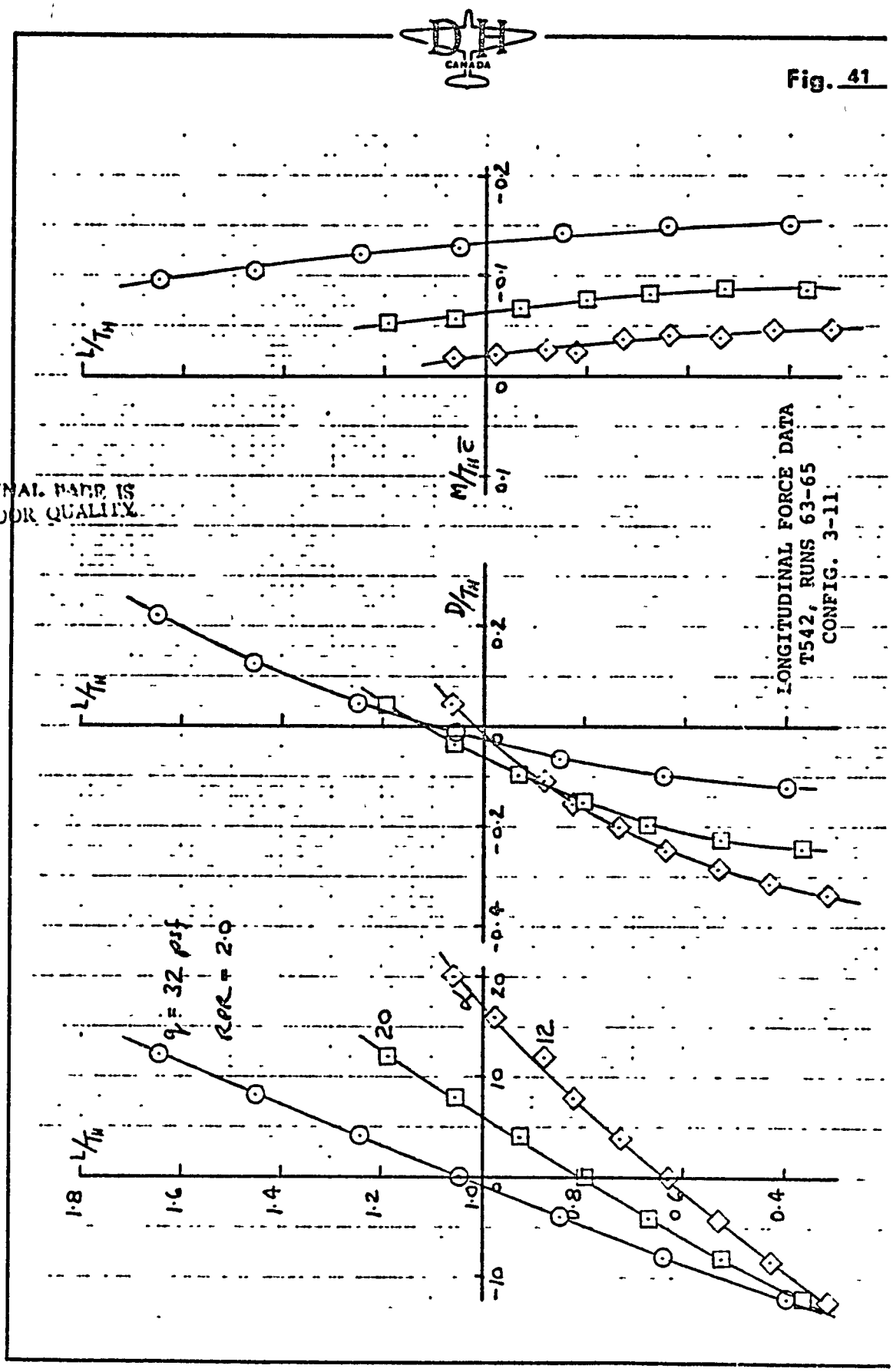

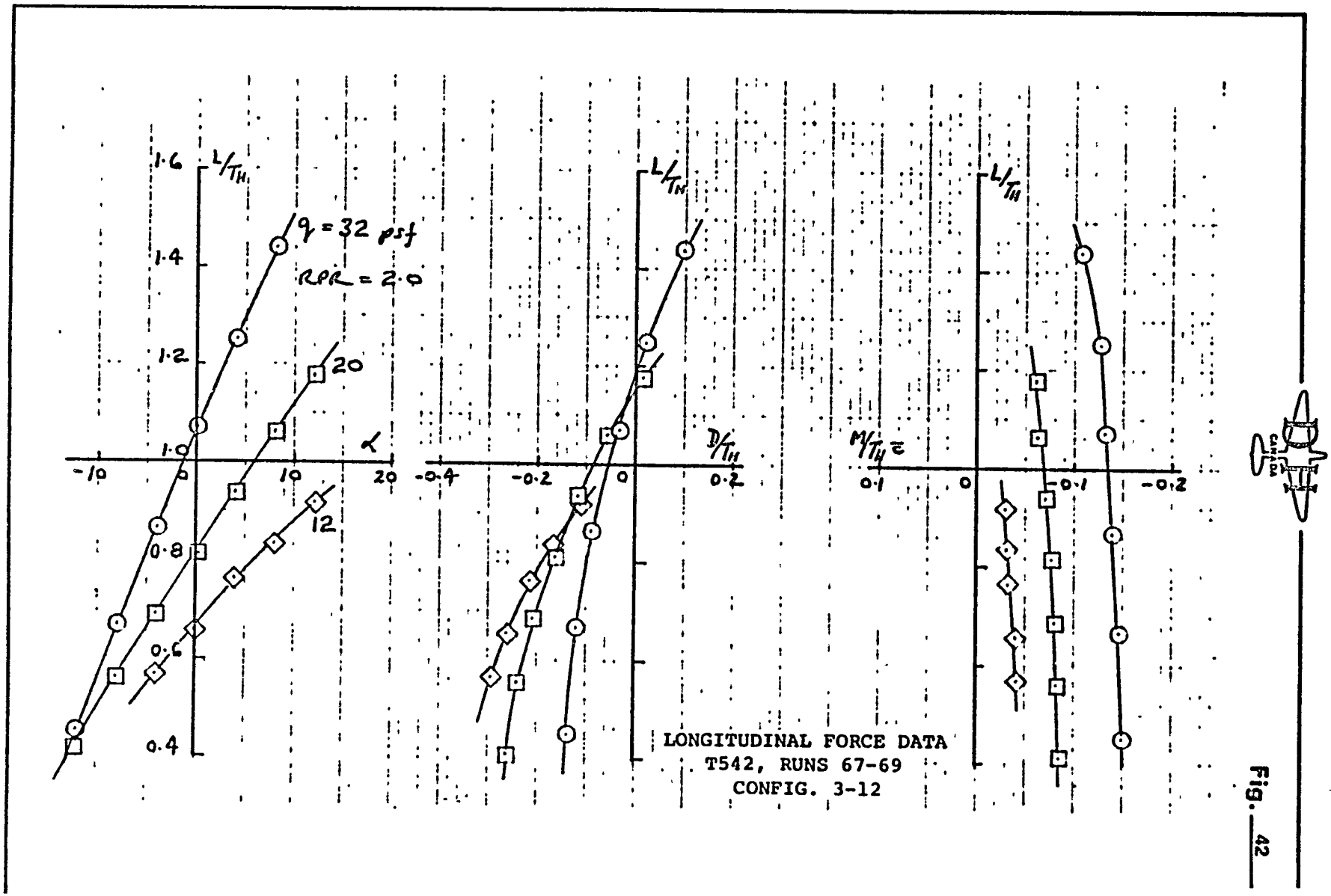

LONGITUDINAL FORCE DATA
T542, RUNS 67-69
CONFIG. 3-12

Fig. 42

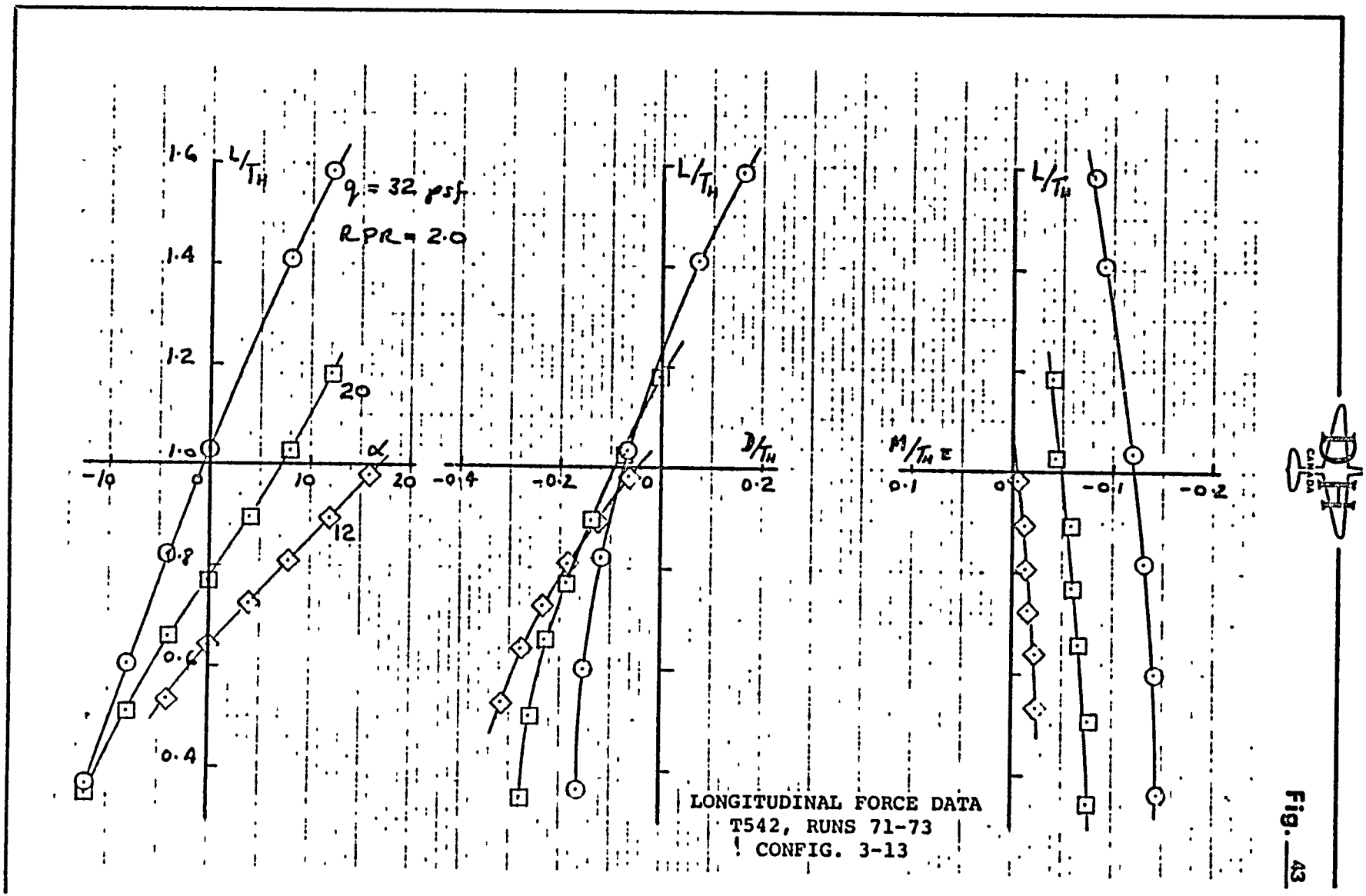

LONGITUDINAL FORCE DATA
T542, RUNS 71-73
CONFIG. 3-13

Fig. 43

Fig. 4

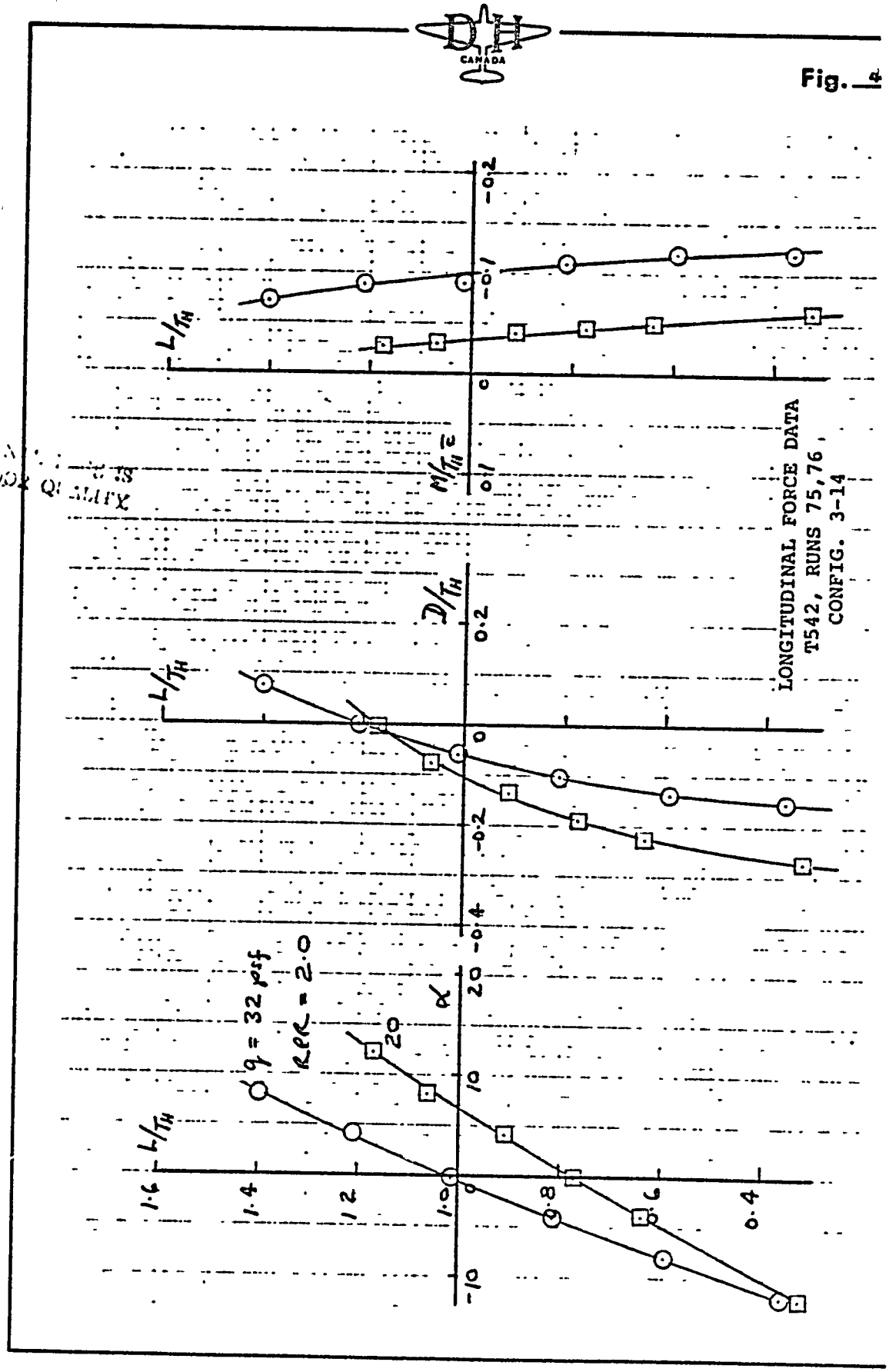
L/TH
M/TH ε
D/TH
α
q = 32 psf
RRC = 2.0
LONGITUDINAL FORCE DATA
T542, RUNS 75,76,
CONFIG. 3-14

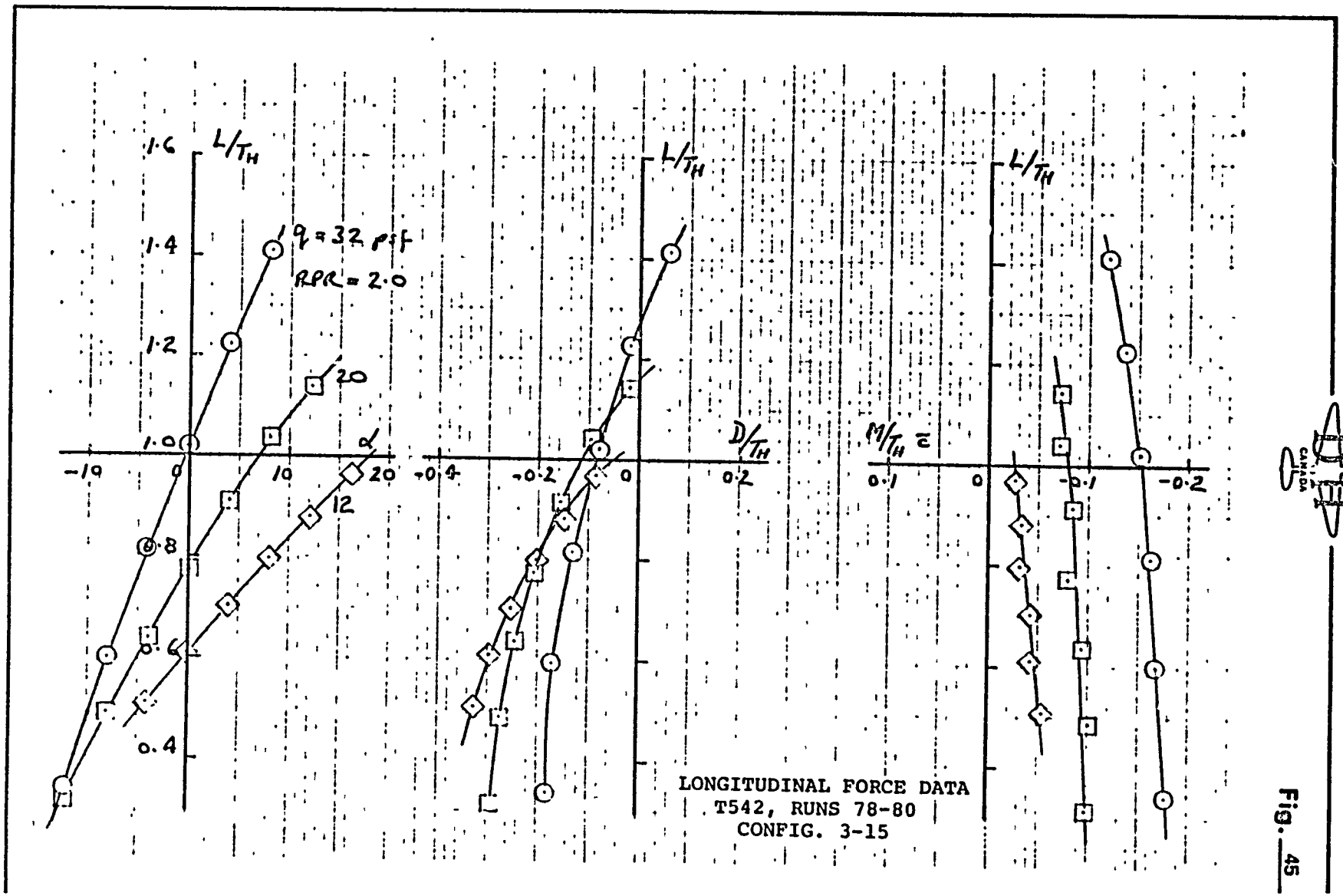

LONGITUDINAL FORCE DATA
T542, RUNS 78-80
CONFIG. 3-15

Fig. 45

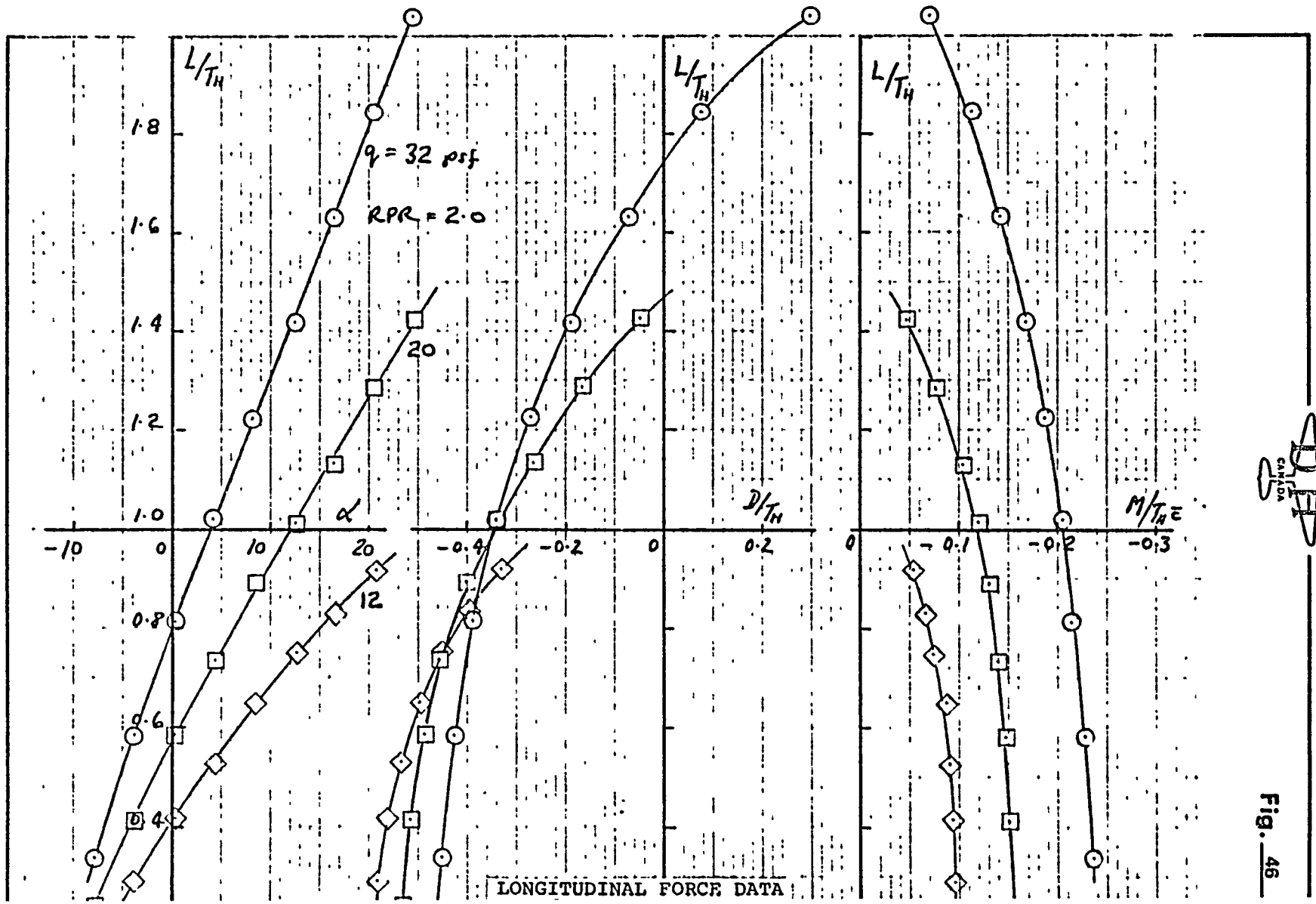
L/T_H
1.8
1.6
1.4
1.2
1.0
0.8
0.6
0.4
q = 32 psf
RPR = 2.0
20
12
α
-10
0
10
20
D/T_H
-0.4
-0.2
0
0.2
M/T_H ℓ
0
-0.1
-0.2
-0.3
LONGITUDINAL FORCE DATA

Fig. 46

Fig. 47

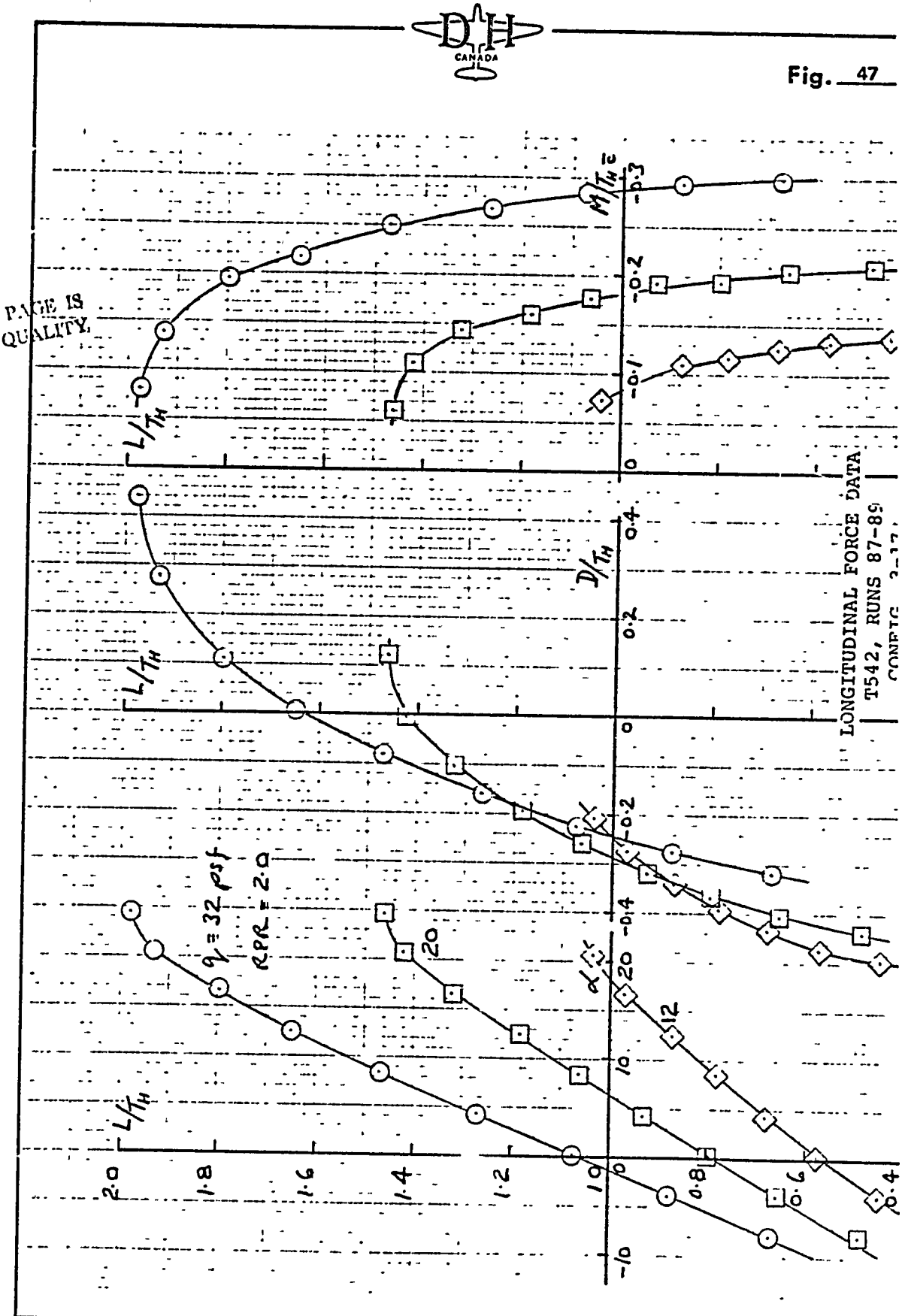

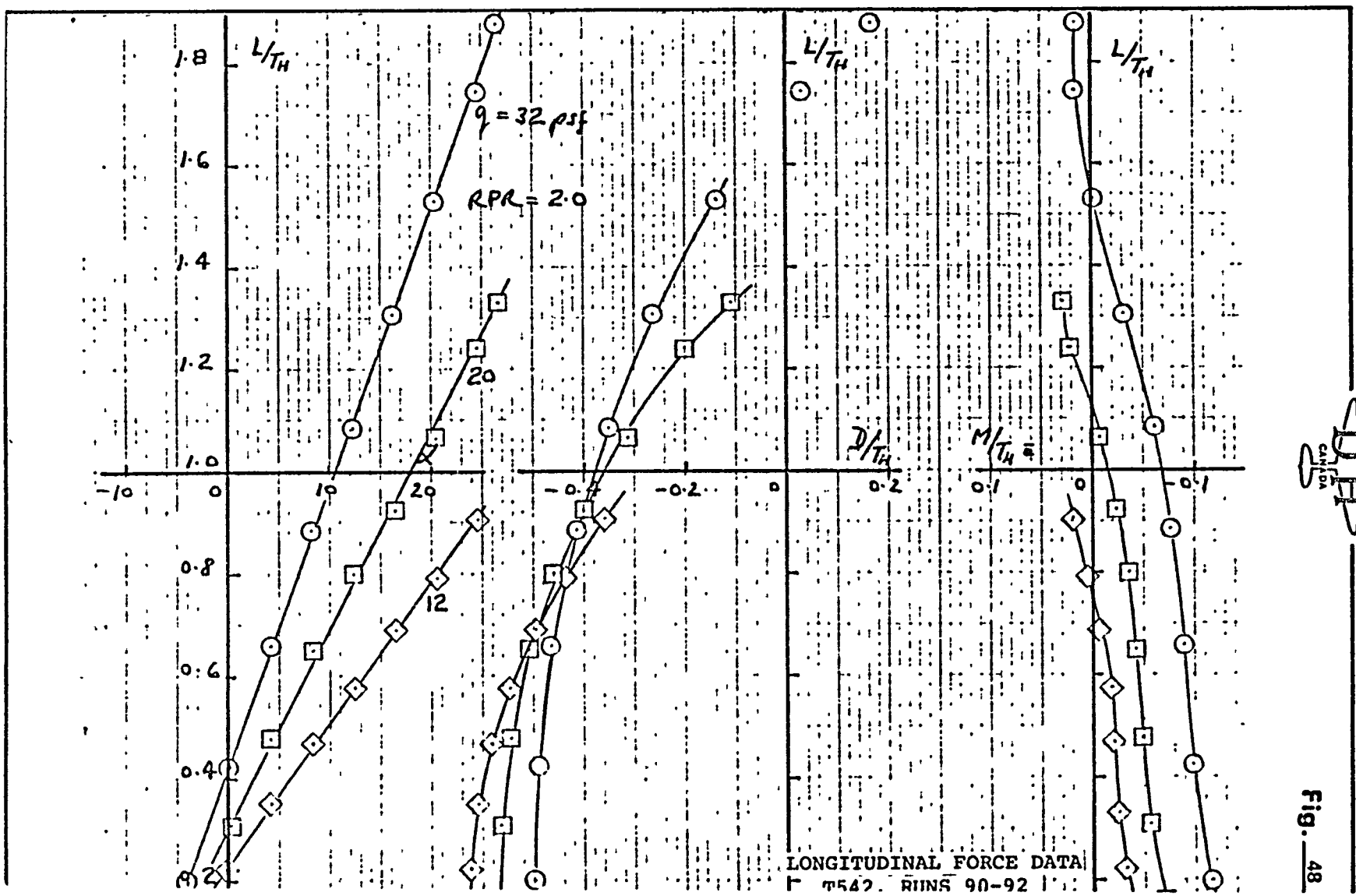

LONGITUDINAL FORCE DATA
T-542, RUNS 90-92

Fig. 48

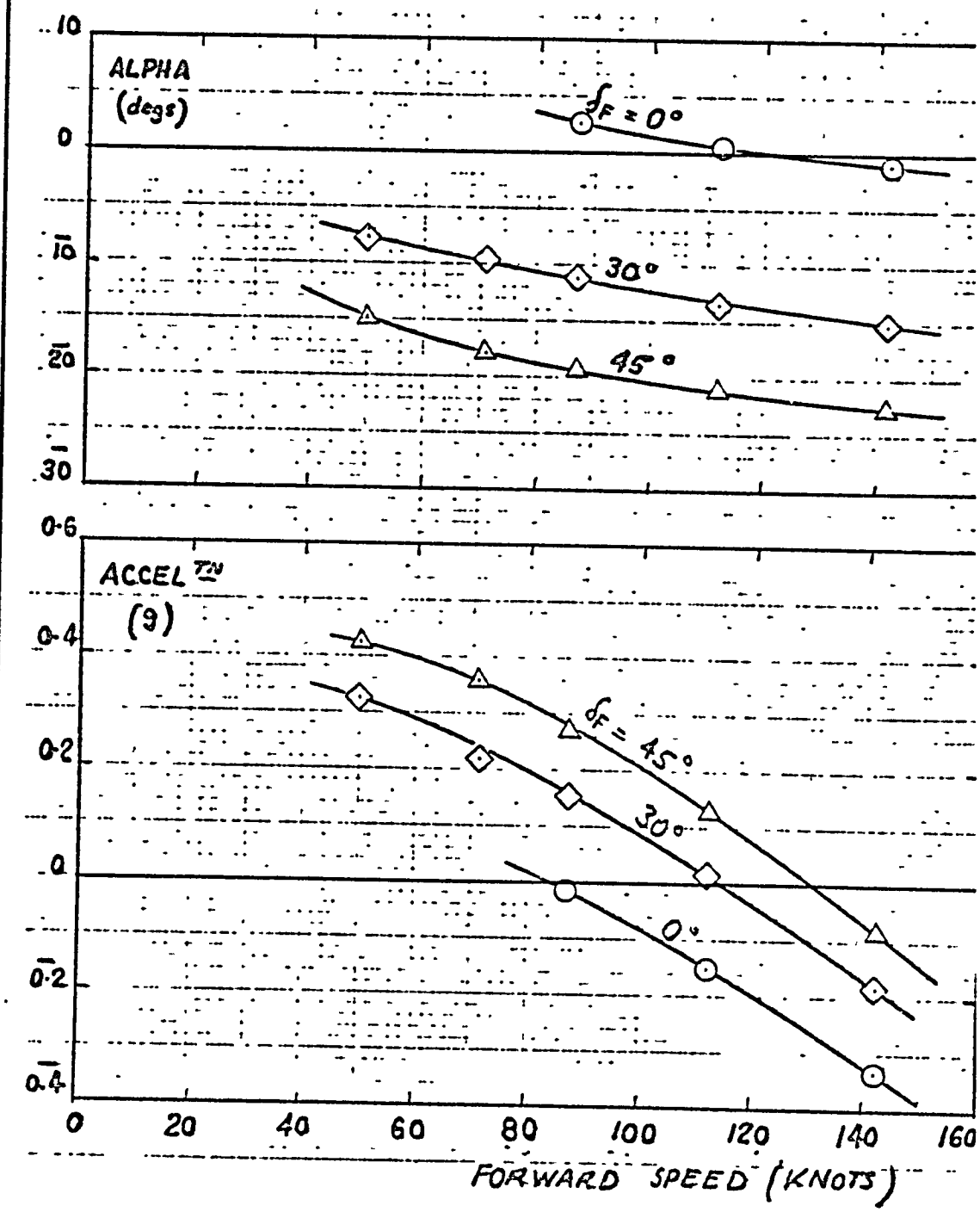

EFFECT OF FLAP ANGLE, BASIC AUGMENTOR
RAKE ON

T_H/L = 1.10 T_H/S = 60 LB/FT^2

Fig. 49(b)

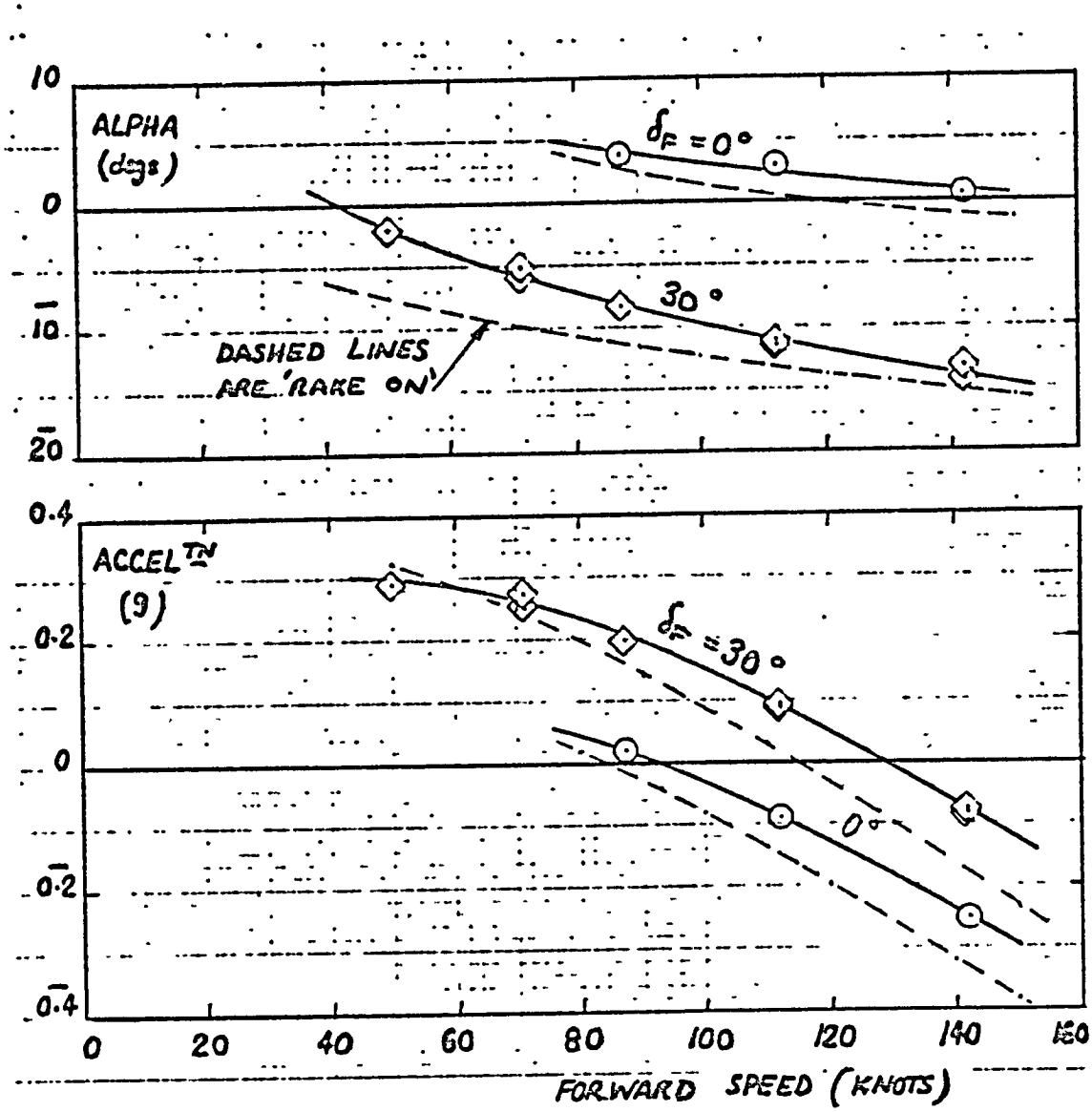

EFFECT OF FLAP ANGLE, BASIC AUGMENTOR
RAKE OFF

$T_H/L = 1{\cdot}10$; $T_H/S = 60$ LB/FT^2

Fig. 50(a)

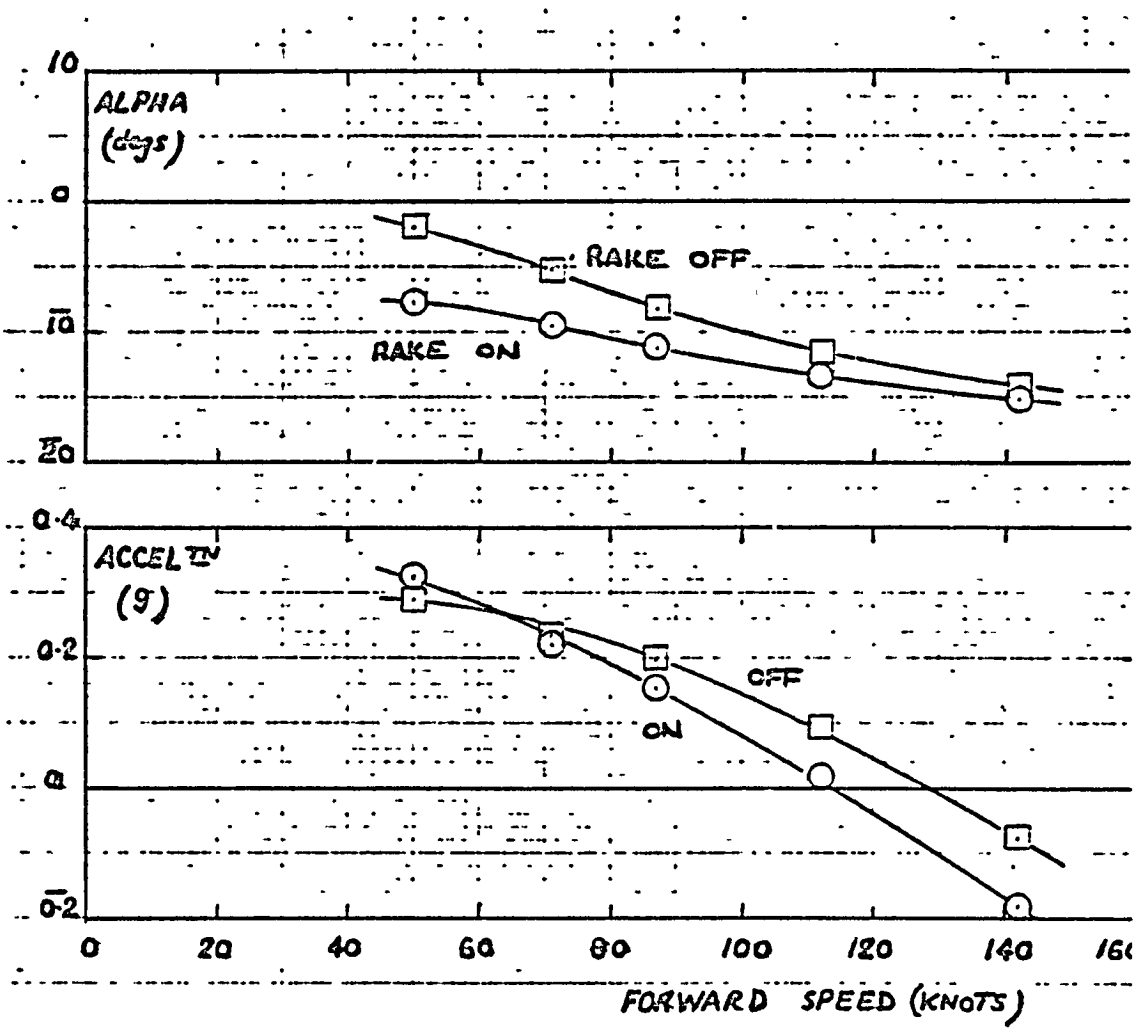

EFFECT OF EXIT RAKE, BASIC AUGMENTOR, VTOL 2 TESTS

END-PLATES ON $\delta = 30°$

$T_H/L = 1{\cdot}10$; $T_H/S = 60$ LB/FT^2

Fig. 50(b)

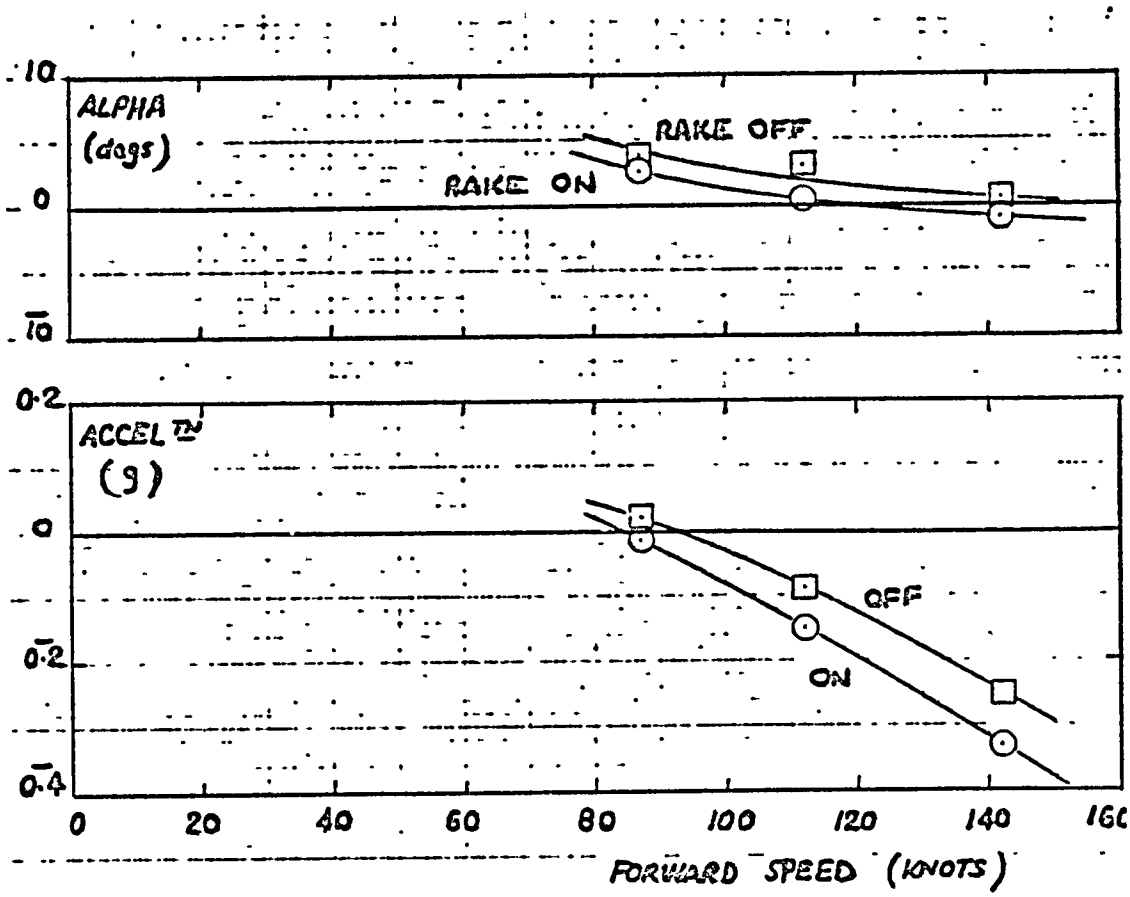

EFFECT OF RAKE; BASIC AUGMENTOR; VTOL 2 TESTS

END-PLATES ON $\delta_F = 0°$

$T_H/L = 1{\cdot}10$ $T_H/S = 60$ LB/FT^2

Fig. 50(c)

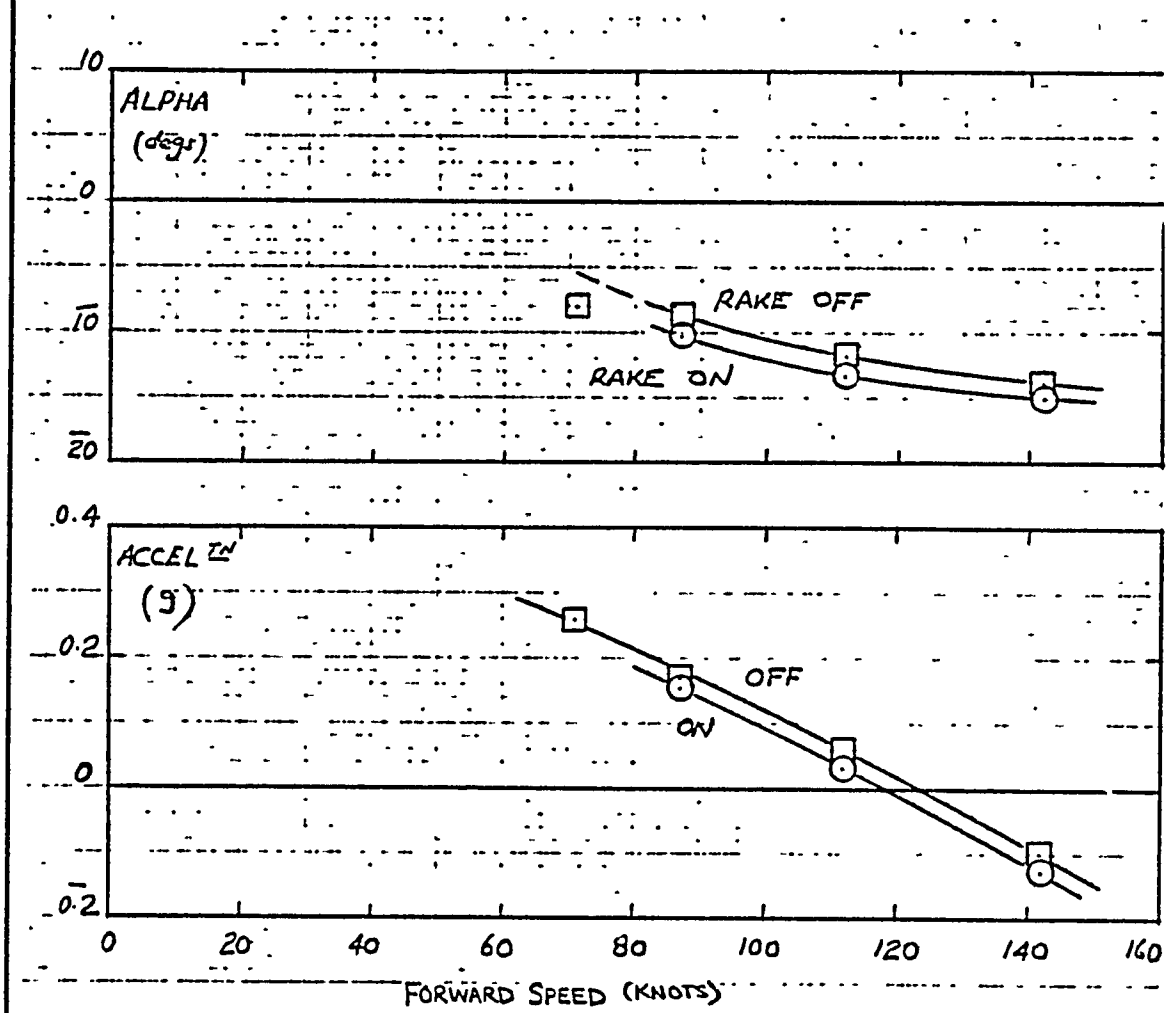

EFFECT OF EXIT RAKE, BASIC AUGMENTOR, VTOL 3 TESTS

END-PLATES ON $\delta_F = 30°$

$T_H/L = 1{\cdot}10$ $T_H/S = 60$ LB/FT²

Fig. 51(a)

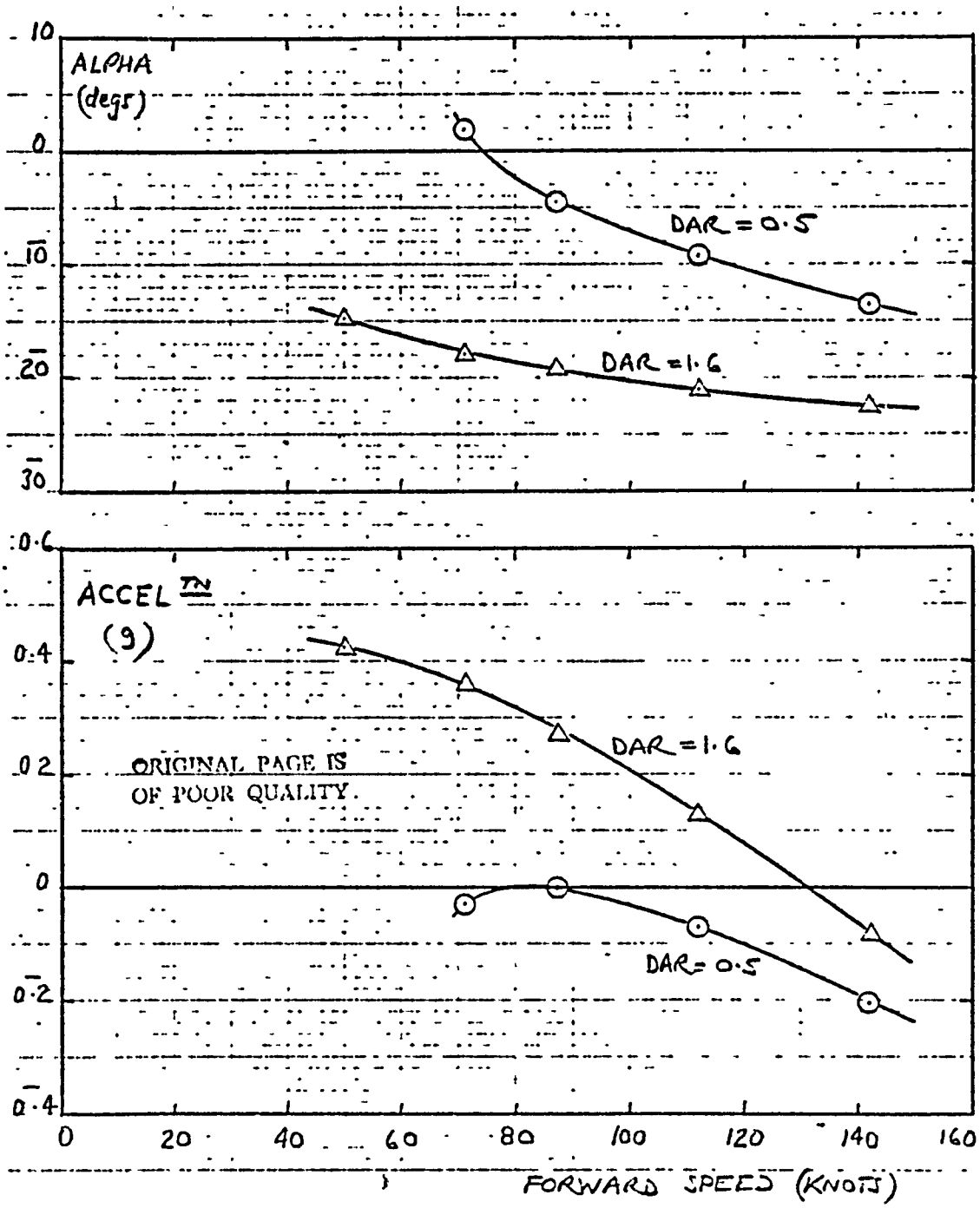

EFFECT OF DIFFUSER AREA RATIO, END-PLATES ON
FULL NOZZLE SET $\delta_F = 45°$ RAKE ON
$T_H/L = 1{\cdot}10$; $T_H/S = 60$ LB/FT²

Fig. 51

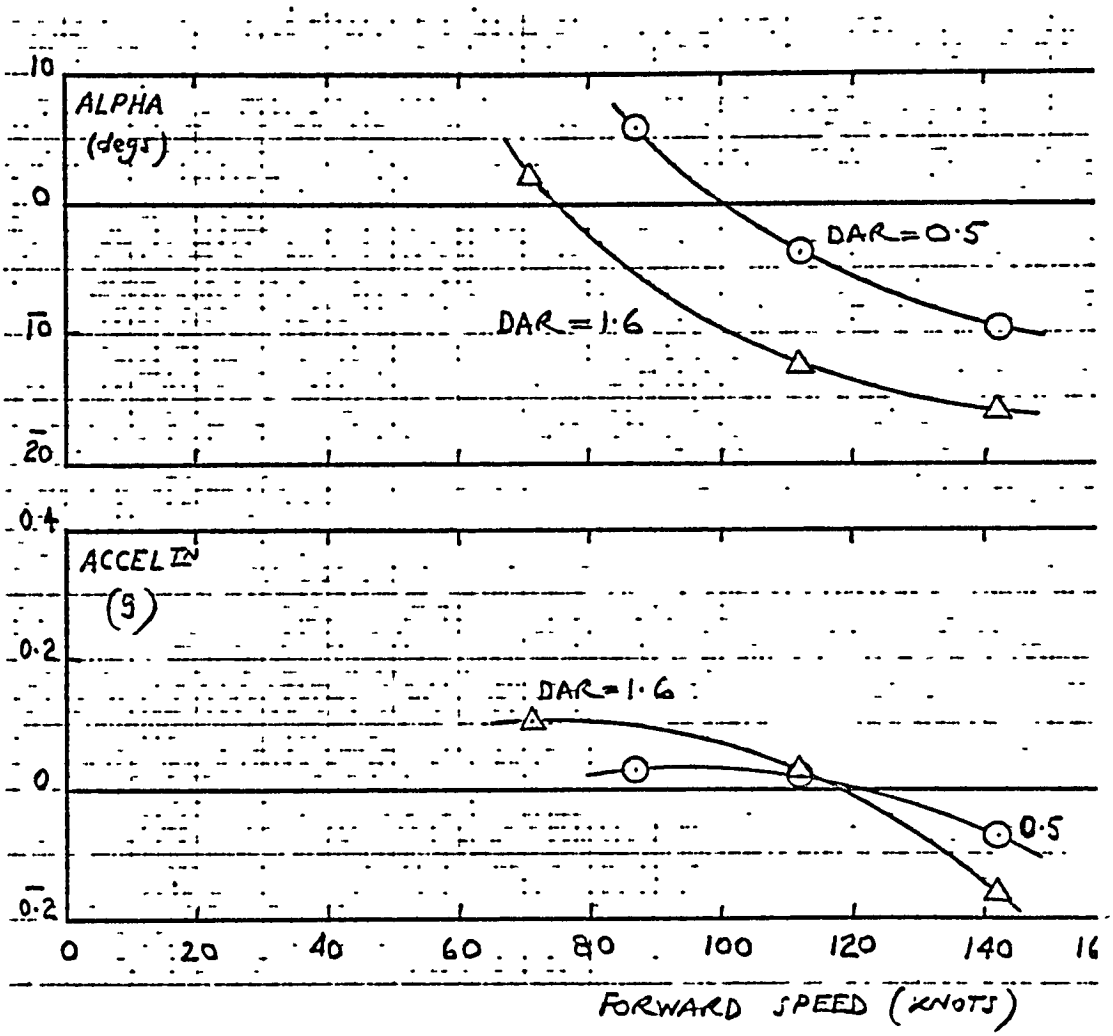

EFFECT OF DIFFUSER AREA RATIO END-PLATES ON
ALTERNATE NOZZLES BLANKED RAKE ON

$\delta_F = 45°$; $T_{H/L} = 1.10$; $T_{H/S} = 60$ lb/ft²

Fig. 52(a)

EFFECT OF DIFFUSER AREA RATIO, END-PLATES OFF

FULL NOZZLE SET ; $\delta_F = 30°$; RAKE OFF

$T_H/L = 1.10$; $T_H/S = 60$ LB/FT^2

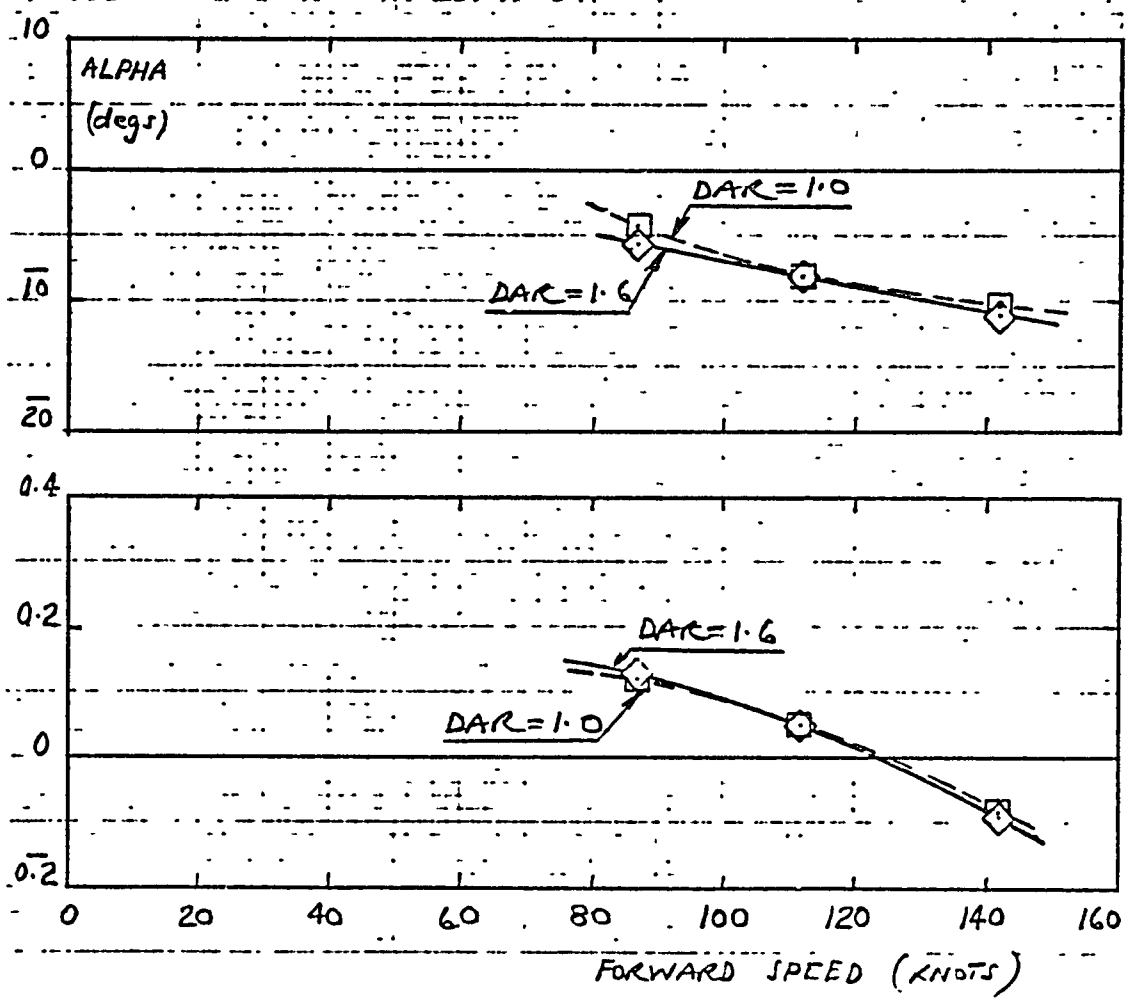

Fig. 52(b)

ORIGINAL PAGE IS
OF POOR QUALITY

EFFECT OF DIFFUSER AREA RATIO, END-PLATES OFF

δ_F = 30°; ALTERNATE NOZZLES BLANKED; RAKE OFF

T_H/L = 110; T_H/S = 60 LB/FT²

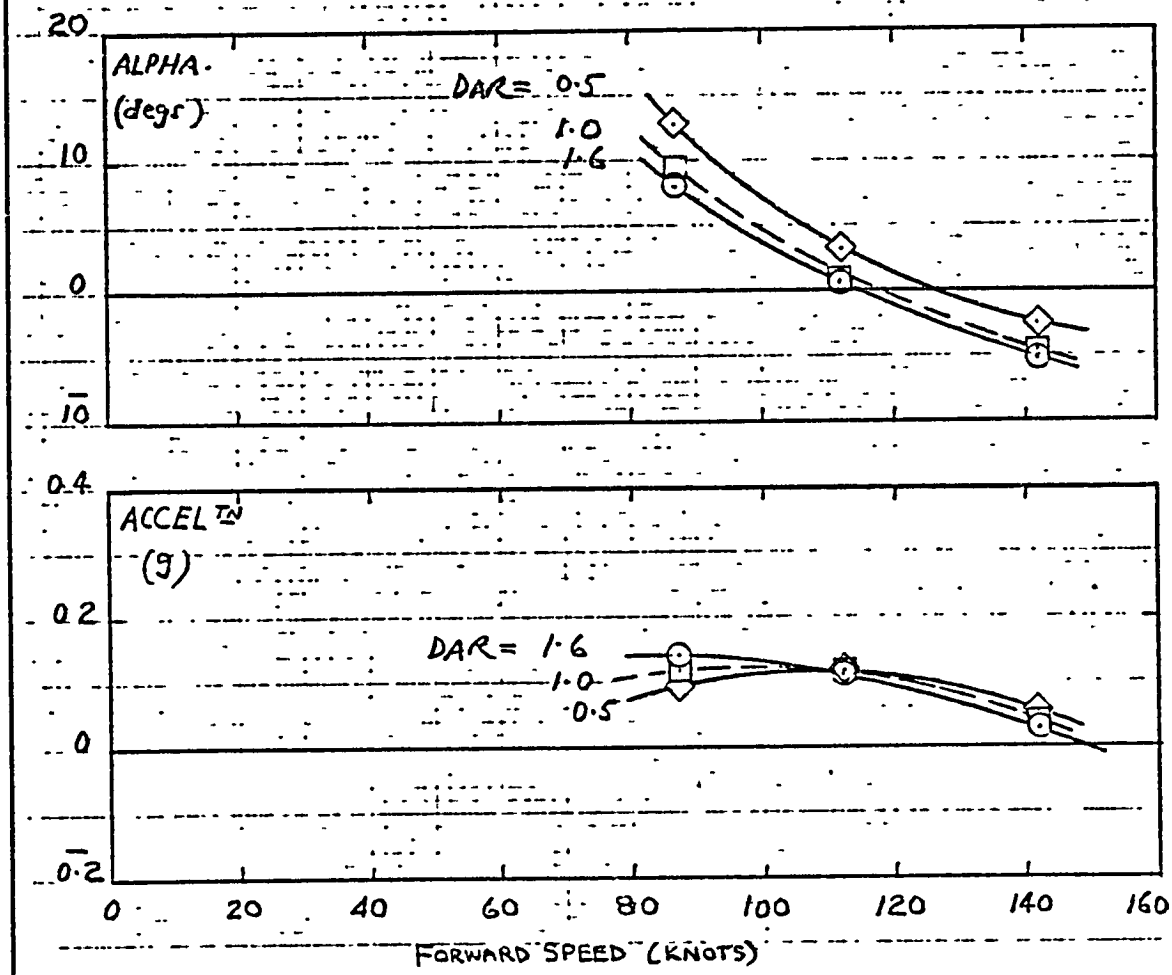

Fig. 5

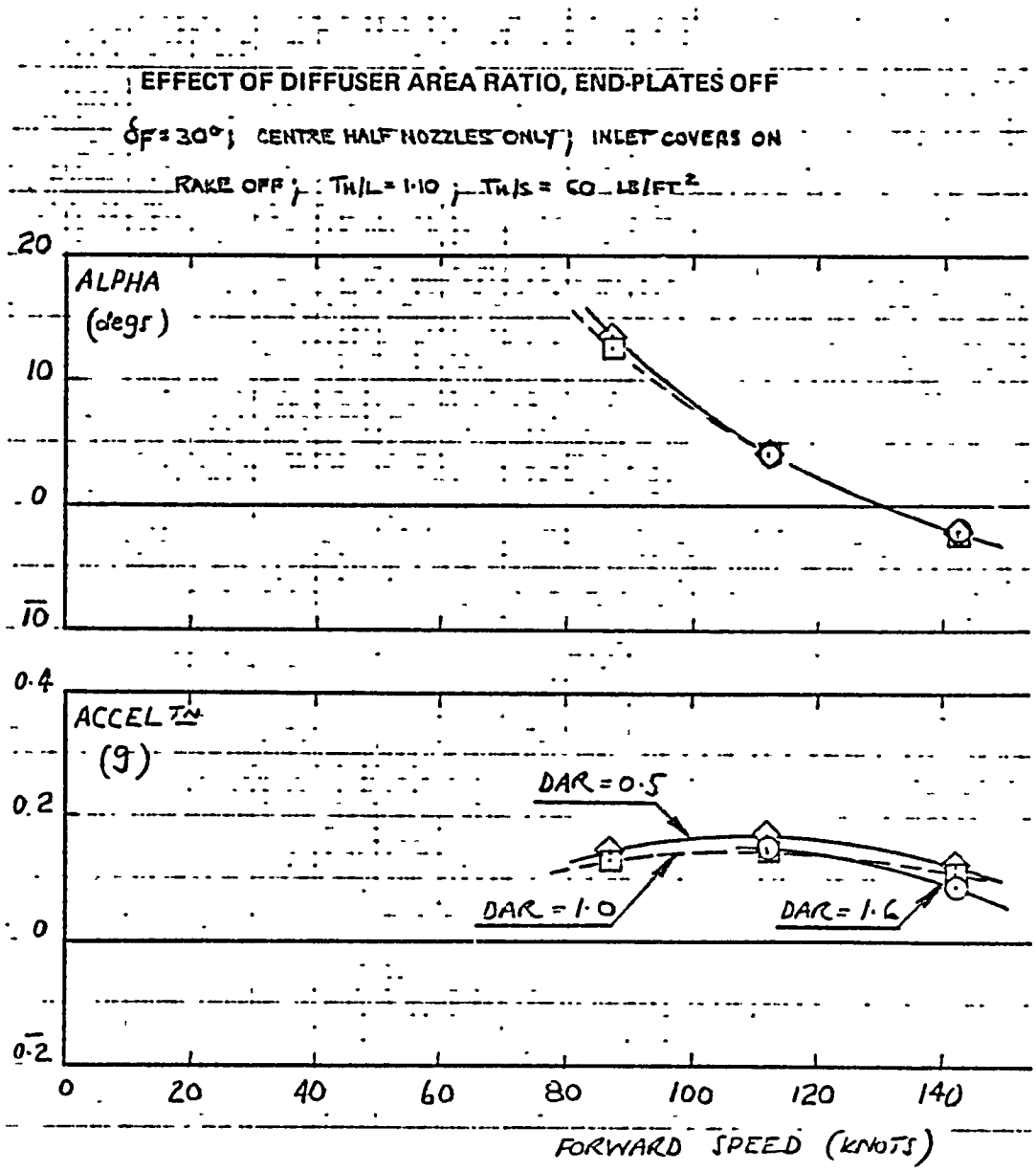
EFFECT OF DIFFUSER AREA RATIO, END-PLATES OFF
δF = 30°; CENTRE HALF NOZZLES ONLY; INLET COVERS ON
RAKE OFF; TH/L = 1·10; TH/S = 60 LB/FT²
20
ALPHA
(degs)
10
0
10
0·4
ACCEL TN
(g)
0·2
0
0·2
DAR = 0·5
DAR = 1·0
DAR = 1·6
0
20
40
60
80
100
120
140
FORWARD SPEED (KNOTS)

Fig. 53

EFFECT OF DIFFUSER AREA RATIO, FRONT END-PLATE OFF

FULL NOZZLE SET ; $\delta_F = 30°$; RAKE OFF

TH/L = 1·10 ; TH/S = 60 LB/FT²

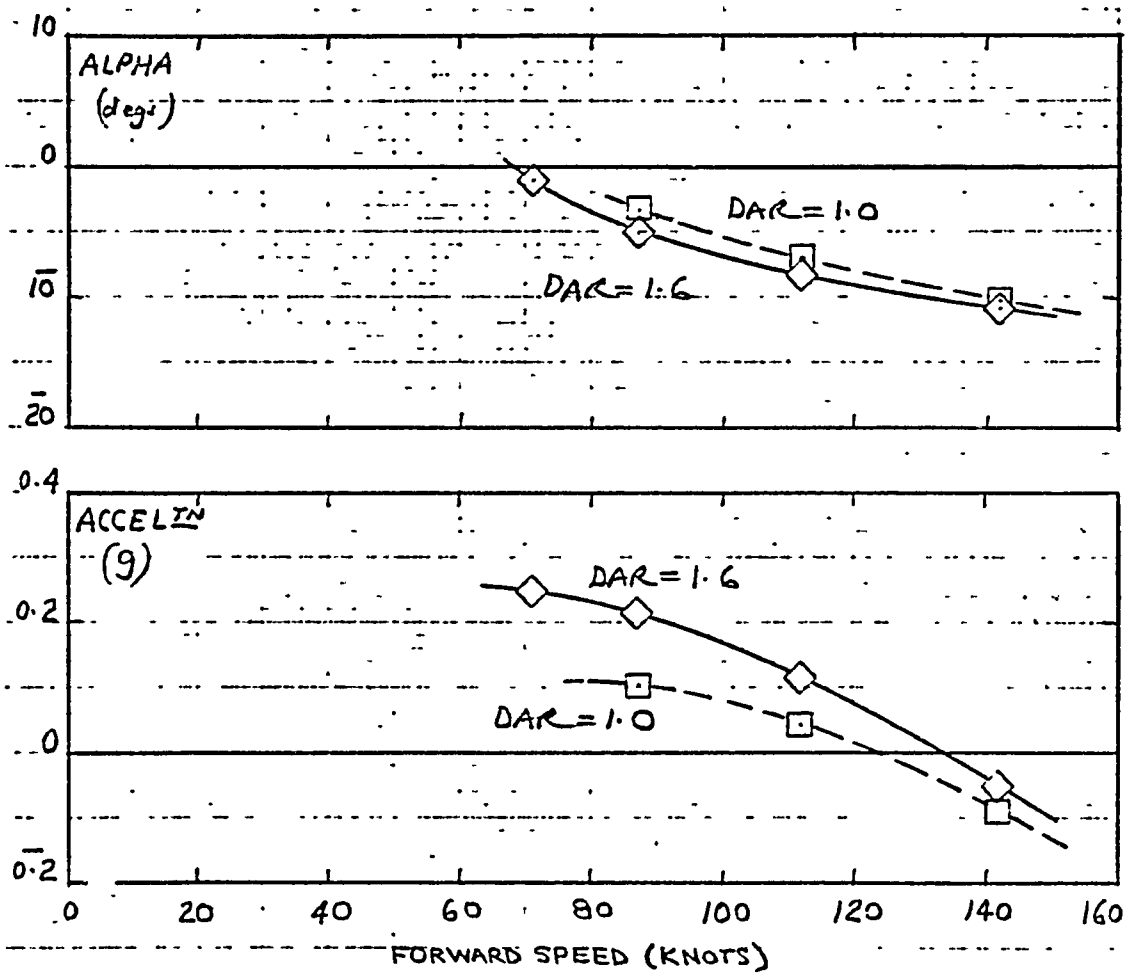

Fig. 54(a)

EFFECT OF AUGMENTOR END-PLATES, BASIC AUGMENTOR

$\delta_F = 30°$; RAKE OFF ; $T_H/L = 1.10$; $T_H/S = 60$ LB/FT^2

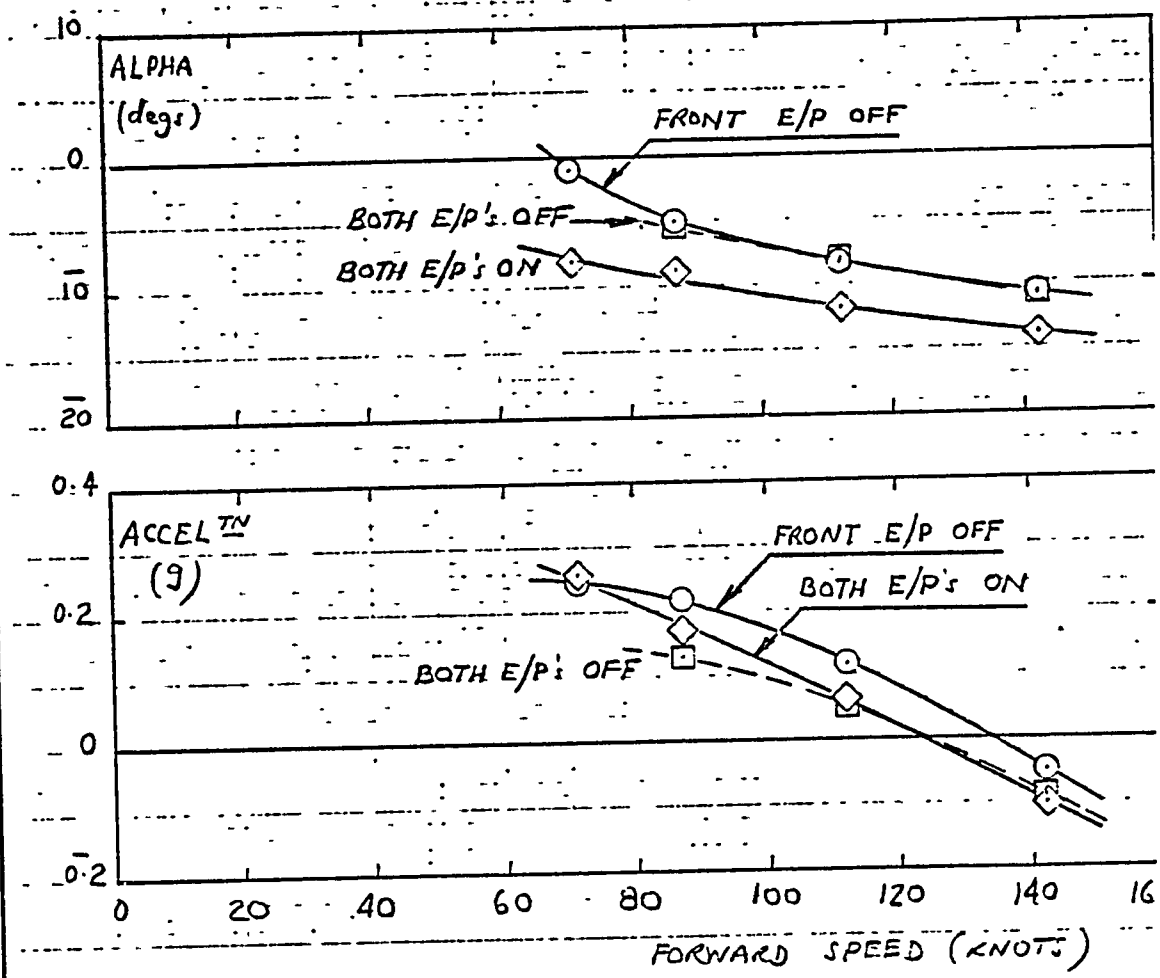

Fig. 54(b)

EFFECT OF AUGMENTOR END-PLATES, ALTERNATE NOZZLES BLANKED

δ_F = 30° ; RAKE OFF ; DAR = 1·6

T_H/L = 1·10 ; T_H/S = 60 LB/FT²

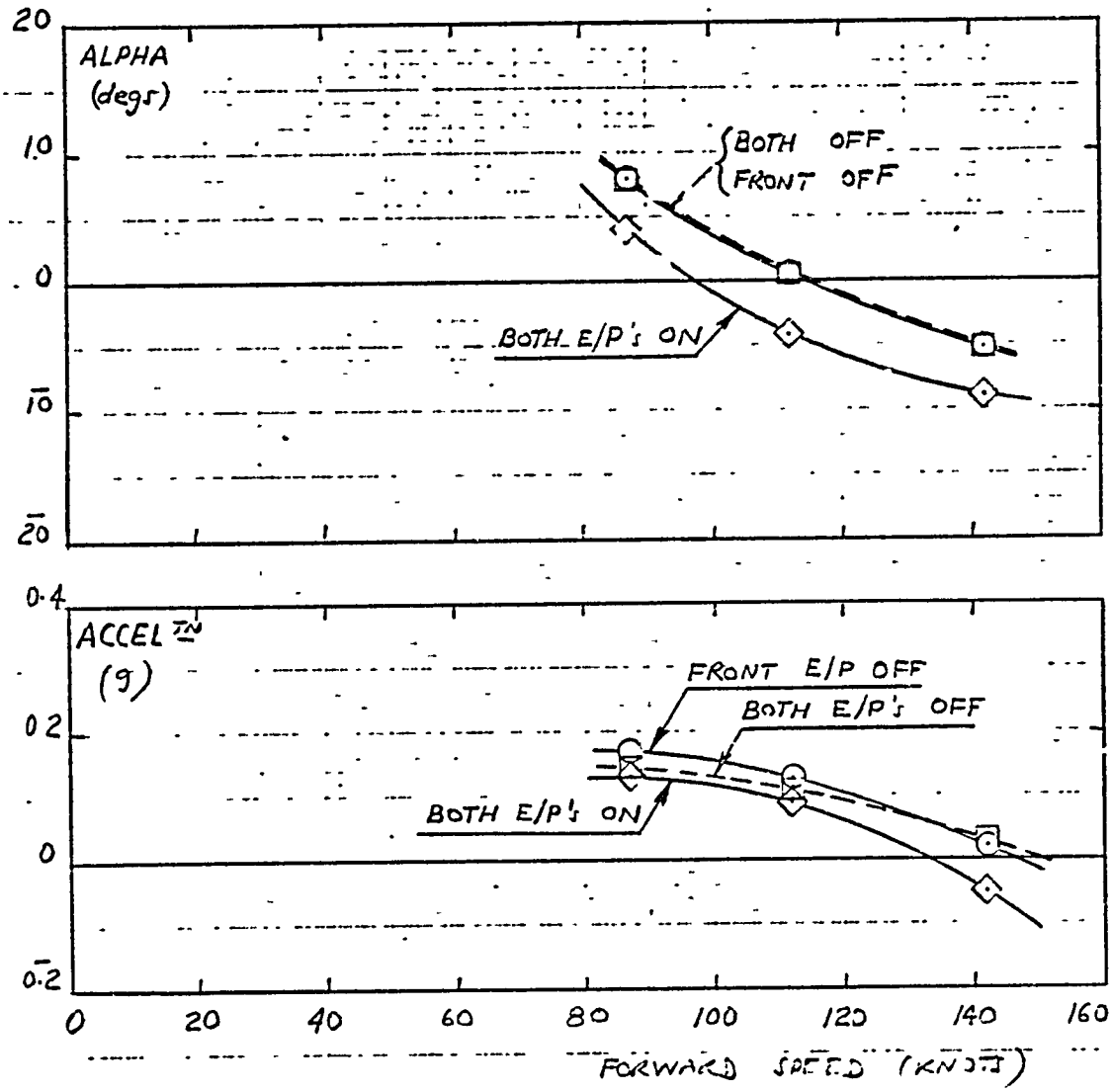

Fig. 55(a

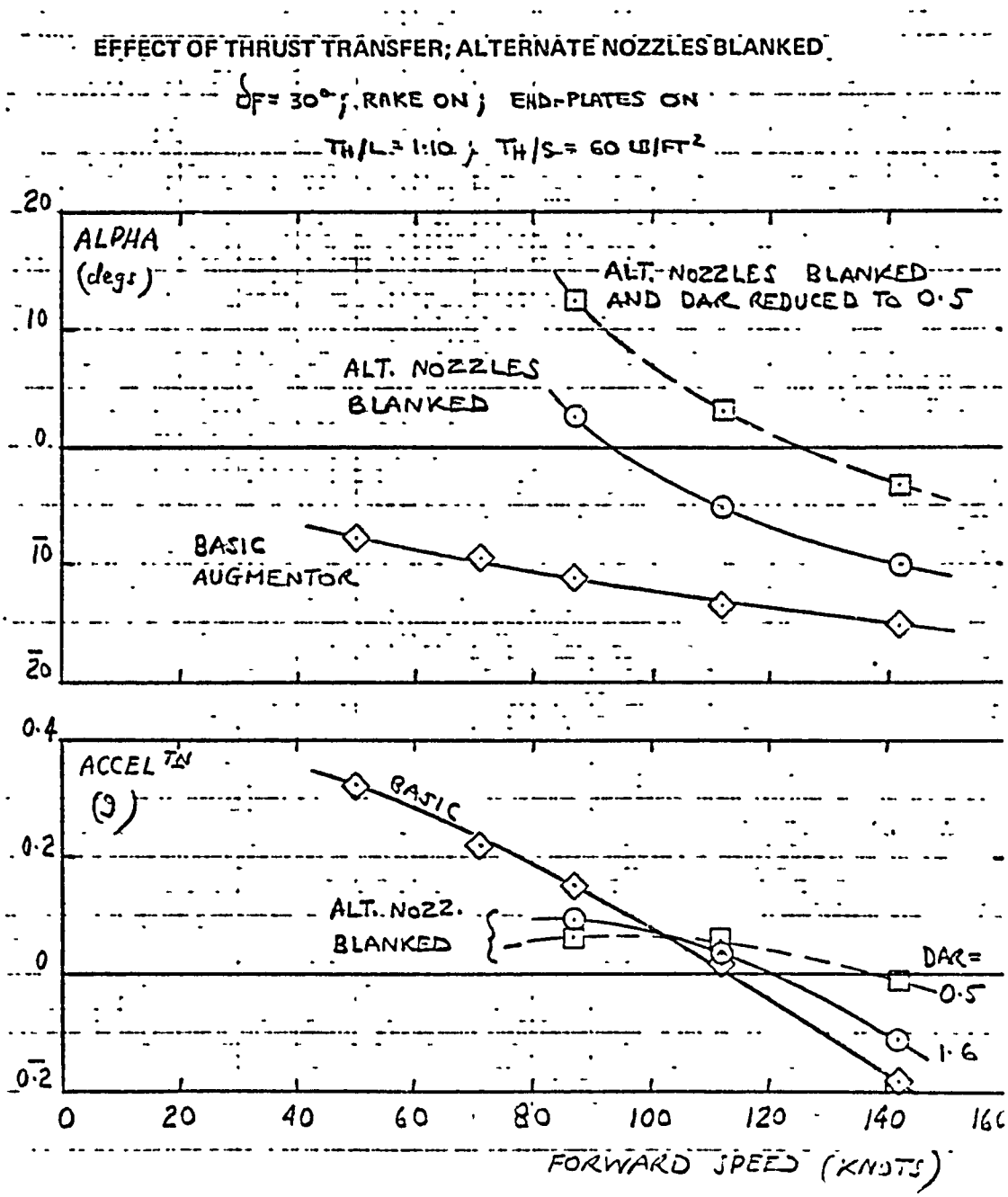
EFFECT OF THRUST TRANSFER; ALTERNATE NOZZLES BLANKED
δF = 30°; RAKE ON; END-PLATES ON
TH/L = 1:10; TH/S = 60 LB/FT²
ALPHA (degs)
ALT. NOZZLES BLANKED AND DAR REDUCED TO 0·5
ALT. NOZZLES BLANKED
BASIC AUGMENTOR
20
10
0
10
20
ACCEL TN (g)
0·4
0·2
0
0·2
BASIC
ALT. NOZZ. BLANKED
DAR = 0·5
1·6
0
20
40
60
80
100
120
140
160
FORWARD SPEED (KNOTS)

Fig. 55(b)

EFFECT OF THRUST TRANSFER; ALTERNATE NOZZLES BLANKED

$\delta_F = 45°$; RAKE ON; E/P's ON

$T_H/L = 1.10$; $T_H/S = 60$ lb/ft²

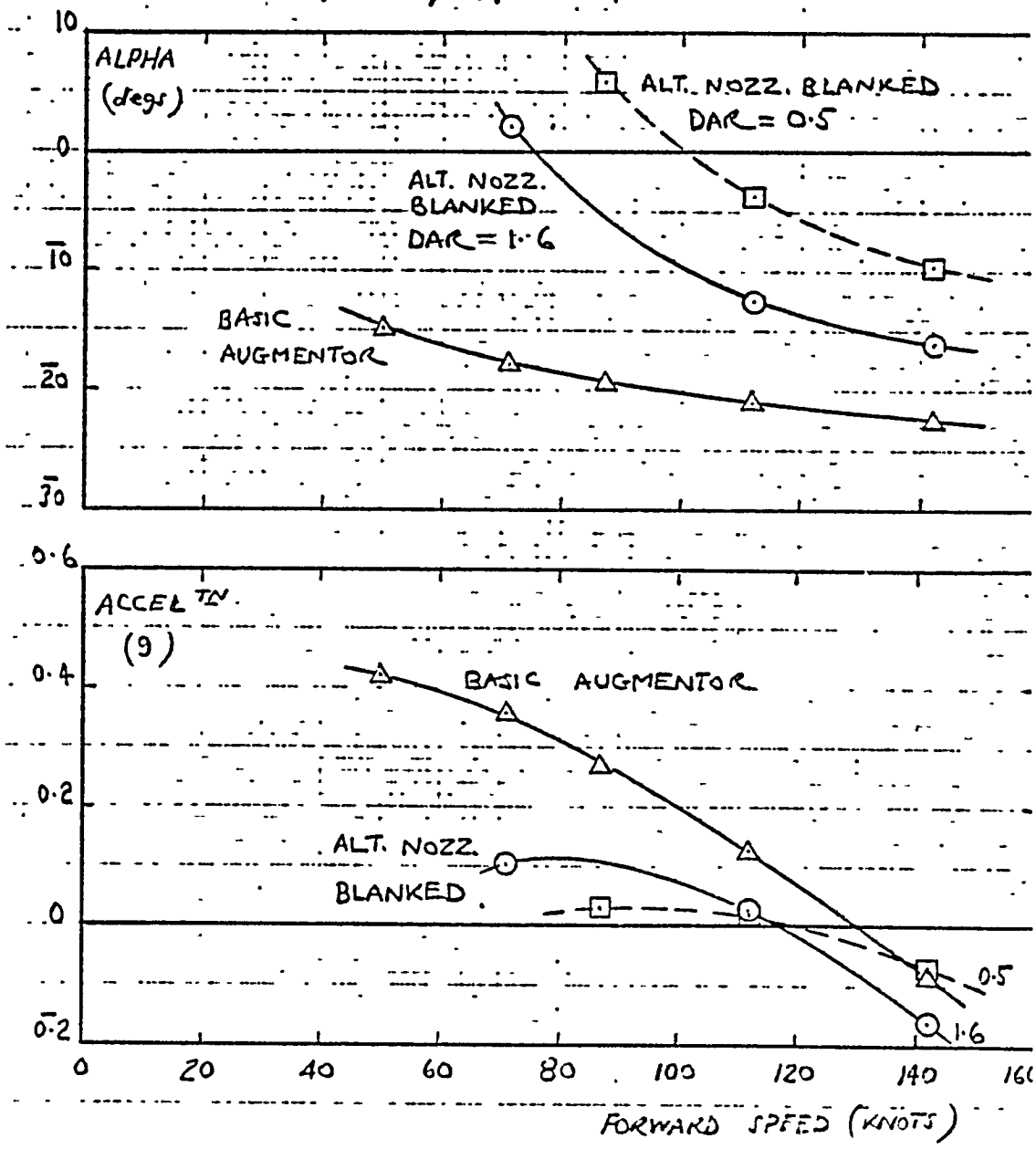

Fig. 55(c)

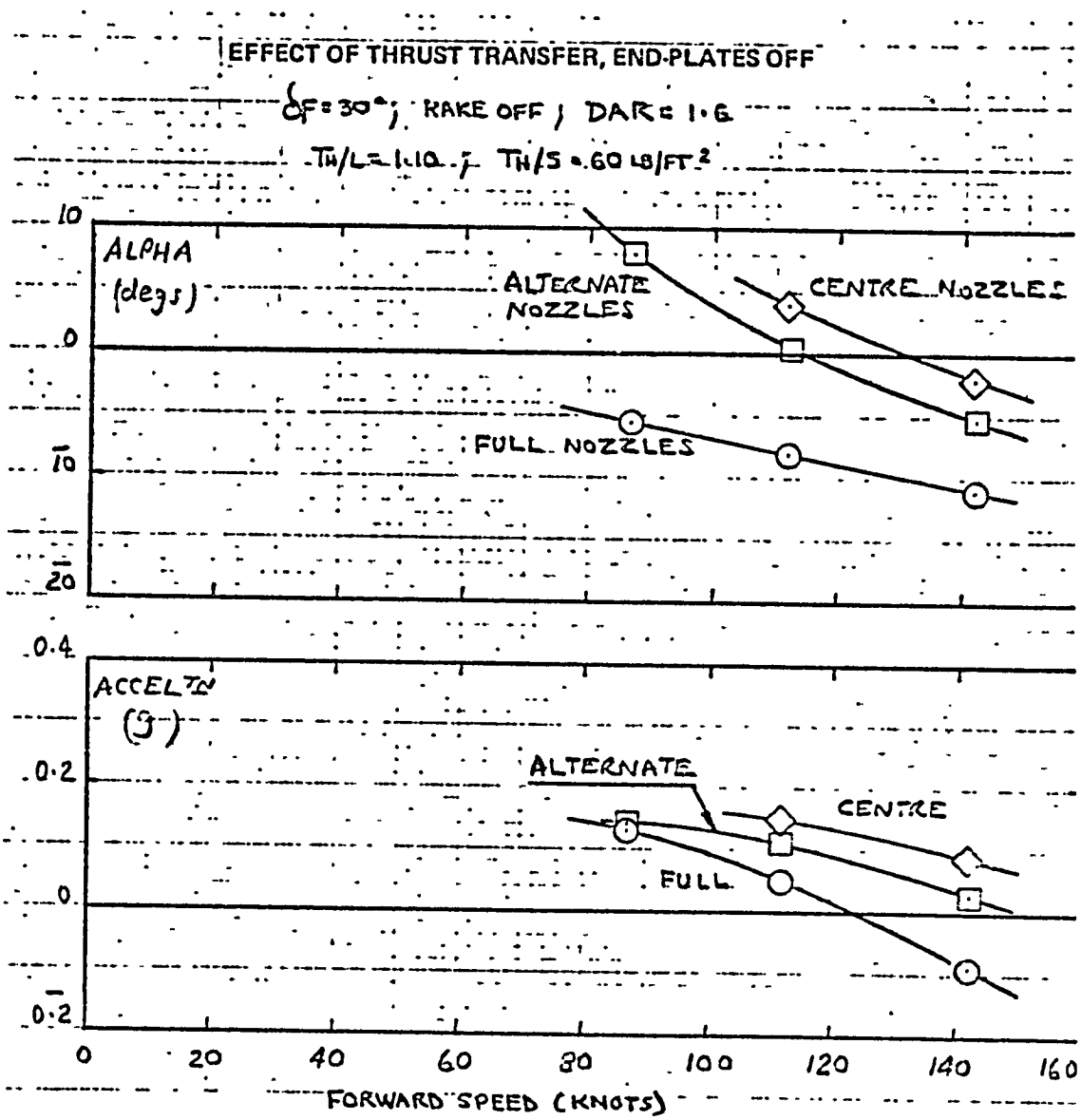
EFFECT OF THRUST TRANSFER, END-PLATES OFF
δF = 30° ; RAKE OFF ; DAR = 1·6
TH/L = 1·10 ; TH/S = 60 LB/FT²
ALPHA (degs)
10
0
10
20
ALTERNATE NOZZLES
CENTRE NOZZLES
FULL NOZZLES
0·4
ACCELTN (g)
0·2
0
0·2
ALTERNATE
CENTRE
FULL
0
20
40
60
80
100
120
140
160
FORWARD SPEED (KNOTS)

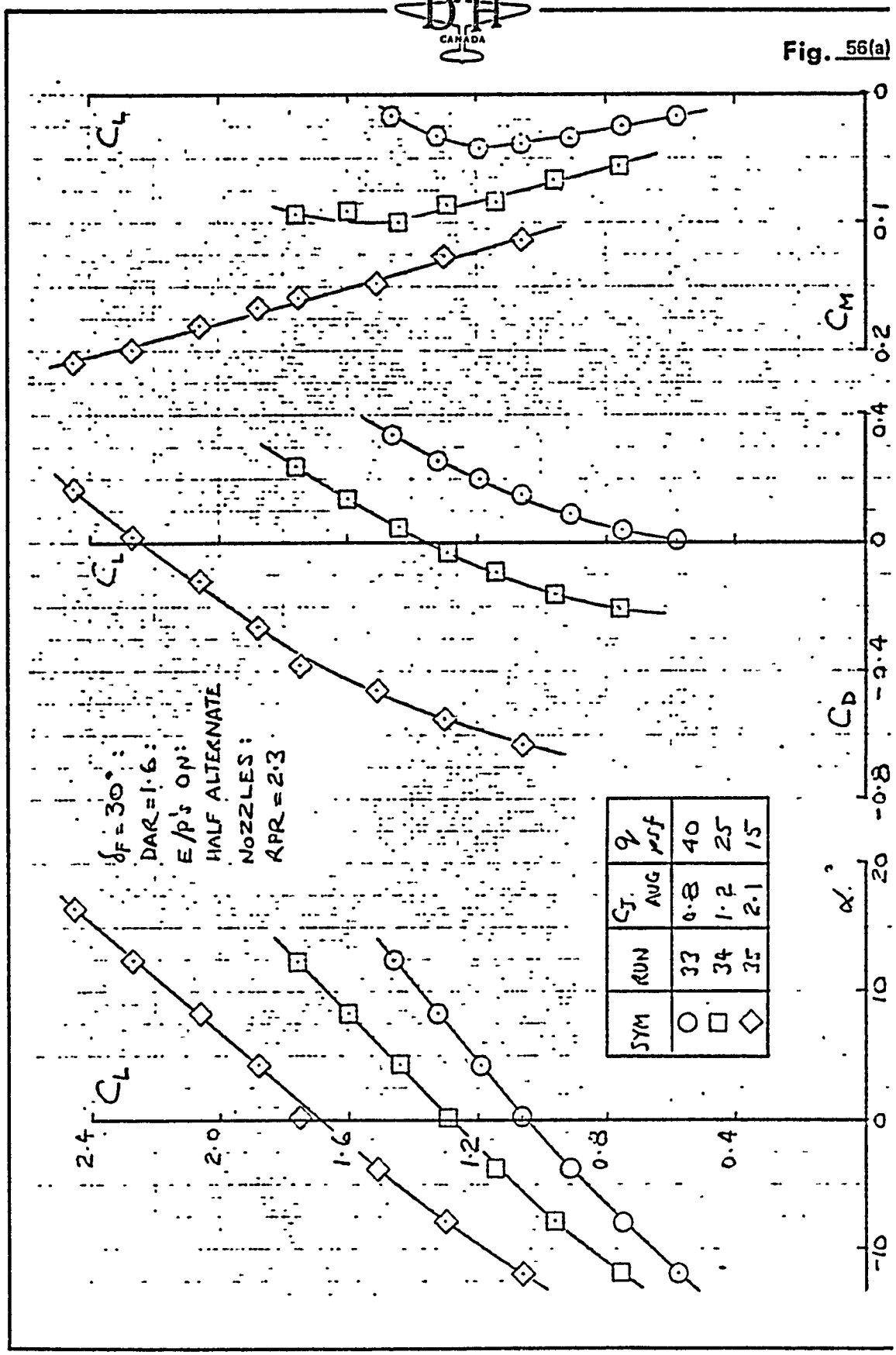
Fig. 56(a)
CANADA
C_L
C_M
C_L
C_D
C_L
α°
$\delta_F = 30°$;
DAR = 1·6 ;
E/P's ON:
HALF ALTERNATE
NOZZLES :
RPR = 2·3
SYM
RUN
C_T AUG
q psf
33 0·8 40
34 1·2 25
35 2·1 15
2·4
2·0
1·6
1·2
0·8
0·4
0
0·1
0·2
0·4
0
-0·4
-0·8
20
10
0
-10

Fig. 5c

CANADA
C_L
C_D
C_m
α°
2.4
2.0
1.6
1.2
0.4
SYM
RUN
$C_{T_{AUG}}$
q_{psf}
78 0.8 32
79 1.3 20
80 22 12
δ_F 30°
DAR = 0.5
E/P.S. OFF
HALF CENTRE
NO ZLES:
R_{RL} = 2.0
ORIGINAL PAGE IS
OF POOR QUALITY

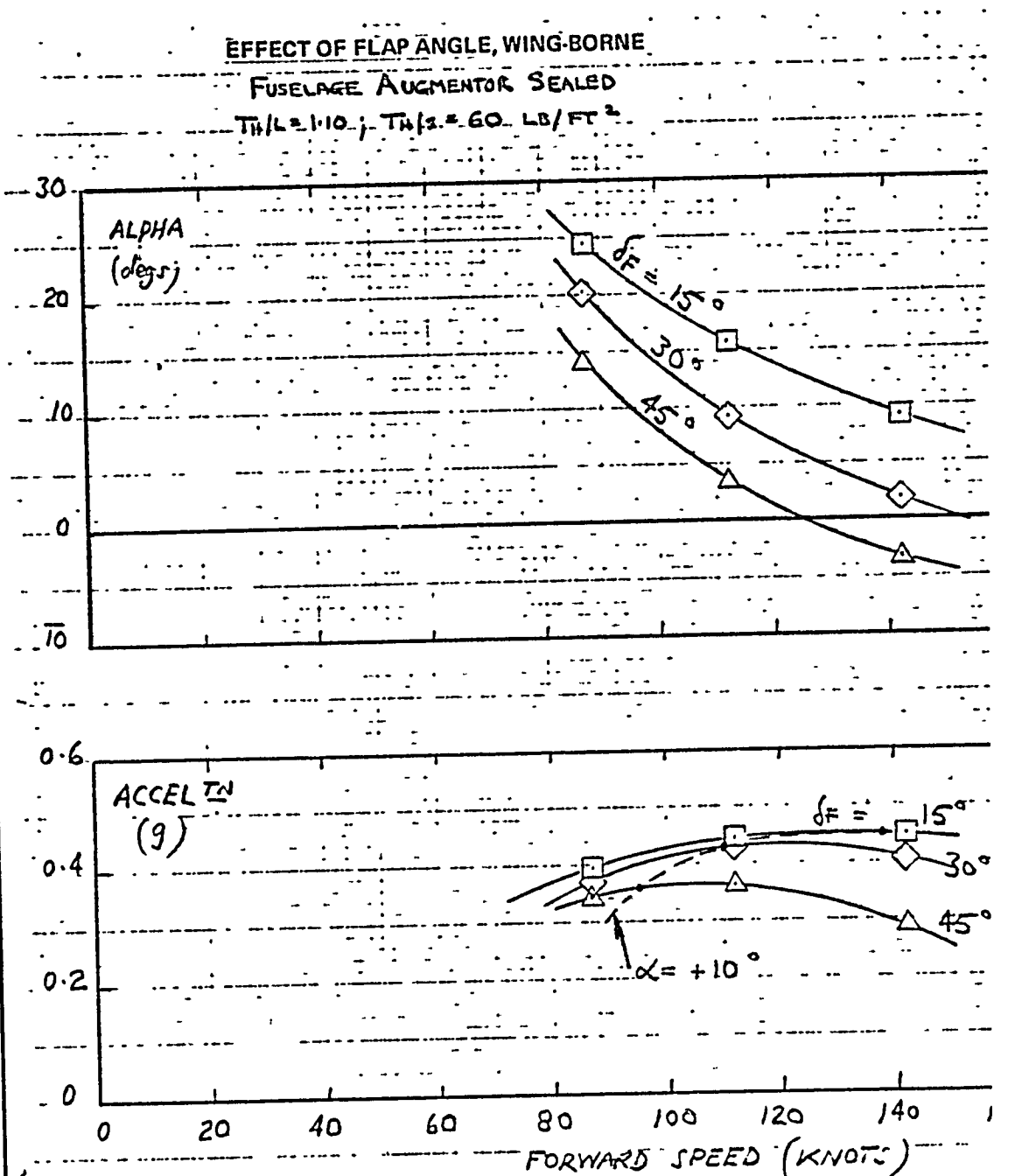
EFFECT OF FLAP ANGLE, WING-BORNE
FUSELAGE AUGMENTOR SEALED
TH/L = 1.10 ; TH/S = 60 LB/FT²
ALPHA (degs)
30
20
10
0
10
δF = 15°
30°
45°
ACCEL TN (g)
0·6
0·4
0·2
0
δF = 15°
30°
45°
α = +10°
0
20
40
60
80
100
120
140
FORWARD SPEED (KNOTS)

Fig. 58

DEMONSTRATED ACCELERATION CAPABILITY

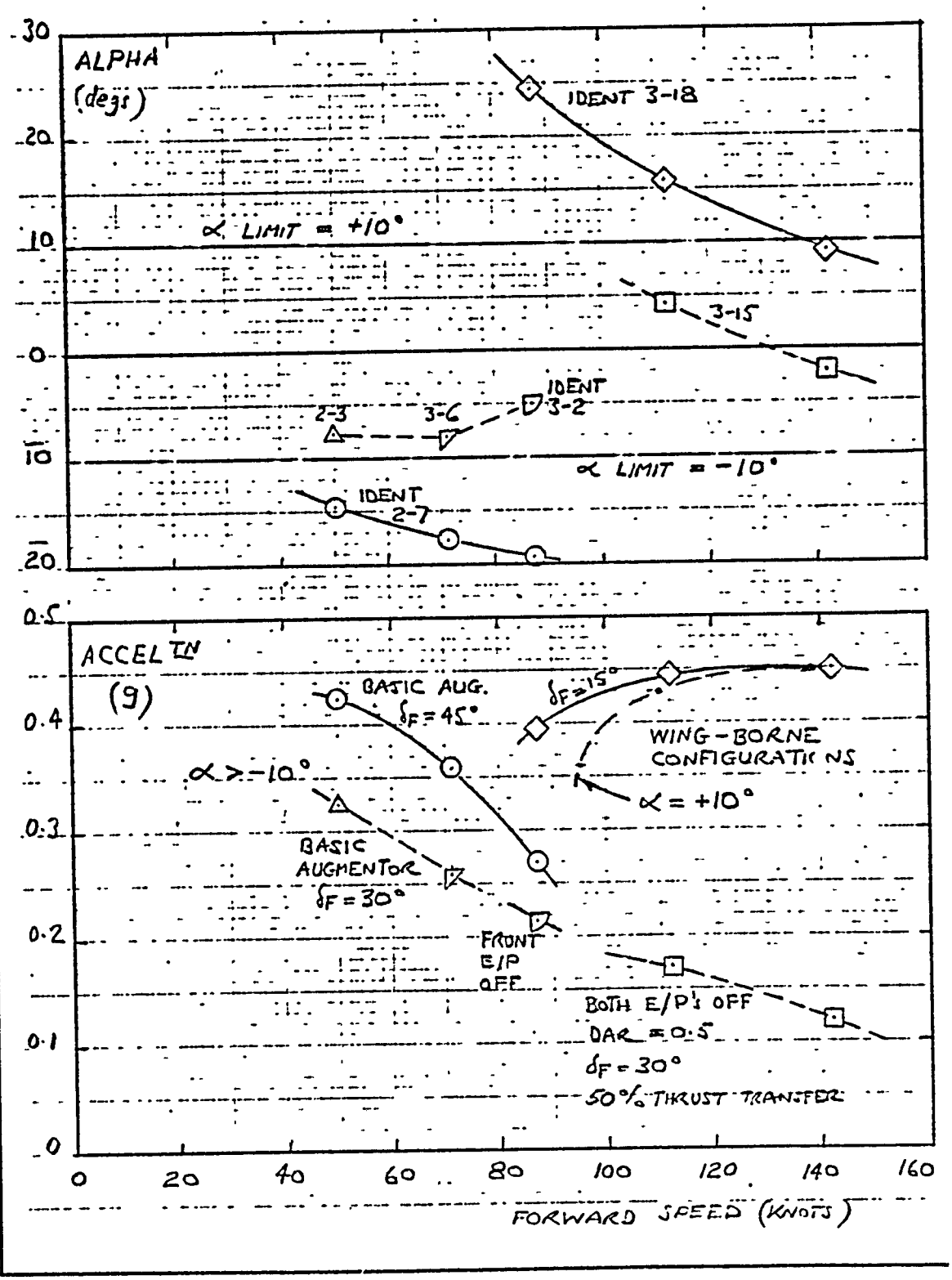

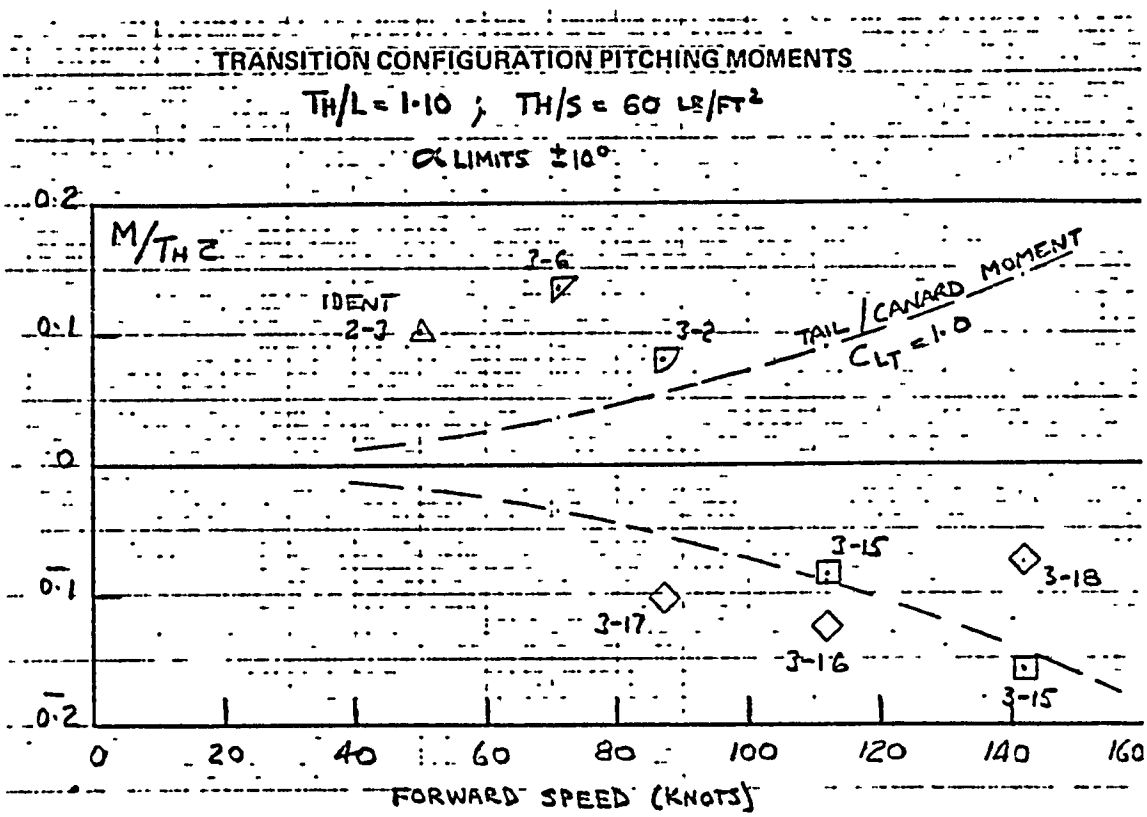

EFFECT OF WING LEADING-EDGE SLAT ON LONGITUDINAL CHARACTERISTICS

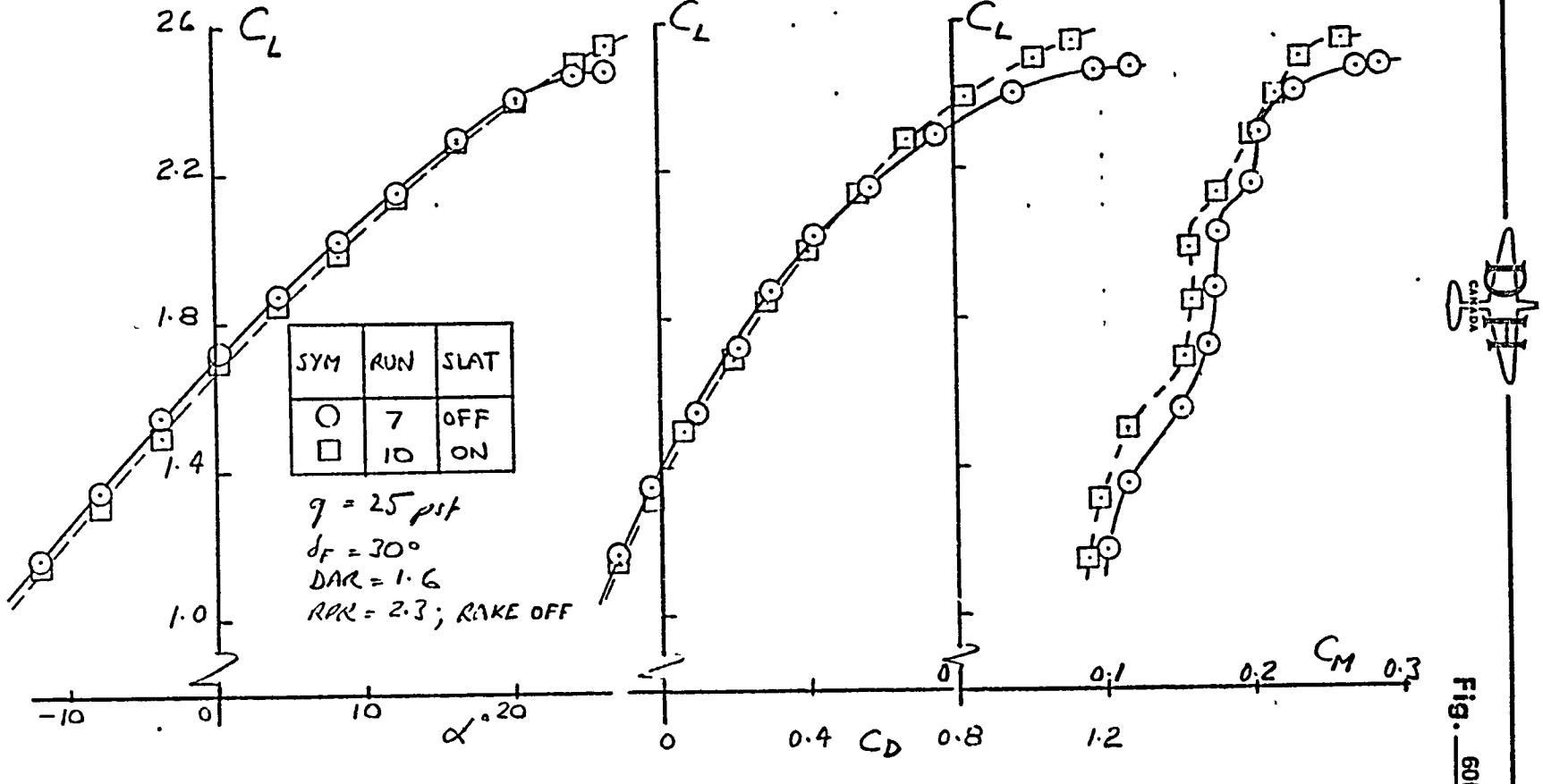

Fig. 60(a)

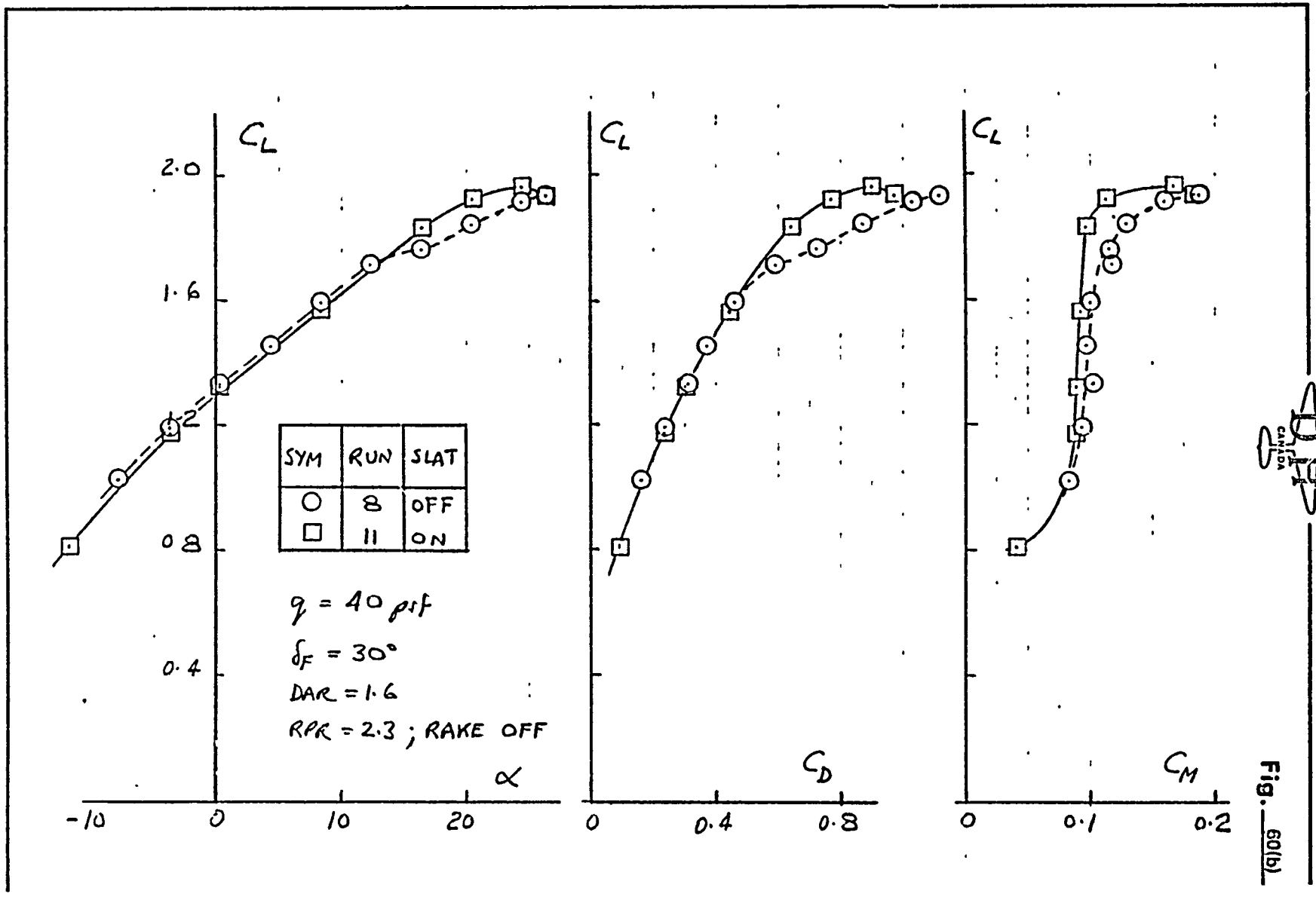
C_L
2.0
1.6
1.2
0.8
0.4
-10
0
10
20
α
SYM | RUN | SLAT
○ | 8 | OFF
□ | 11 | ON
q = 40 psf
δ_F = 30°
DAR = 1.6
RPR = 2.3 ; RAKE OFF
C_L
0
0.4
0.8
C_D
C_L
0
0.1
0.2
C_M

Fig. 60(b)

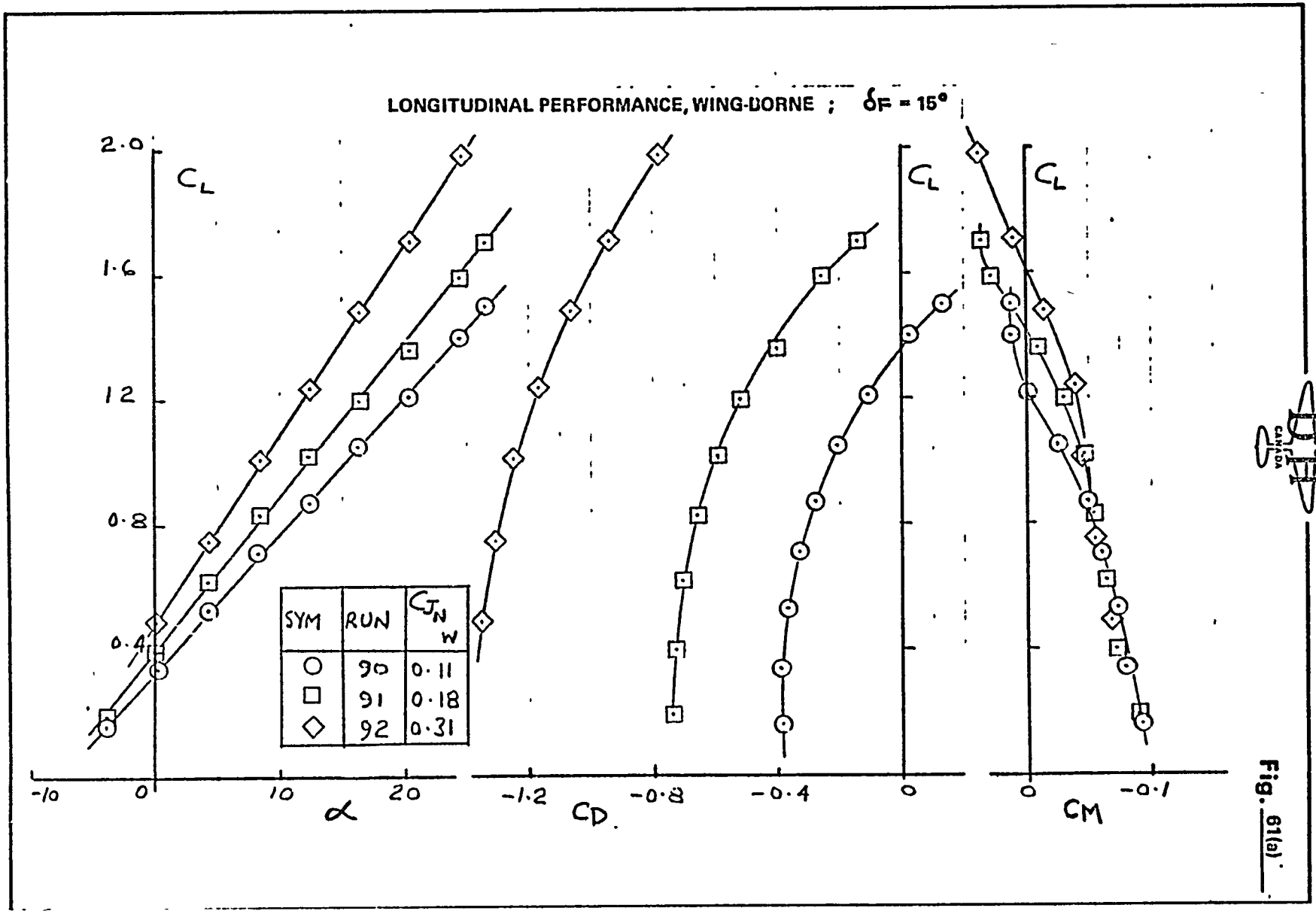
LONGITUDINAL PERFORMANCE, WING-BORNE ; δF = 15°
2·0
1·6
1·2
0·8
0·4
CL
-10
0
10
20
α
SYM
RUN
CJN W
90
0·11
91
0·18
92
0·31
-1·2
-0·8
-0·4
0
CD
CL
0
-0·1
CM
CL

Fig. 61(a)

Fig. 61(b)

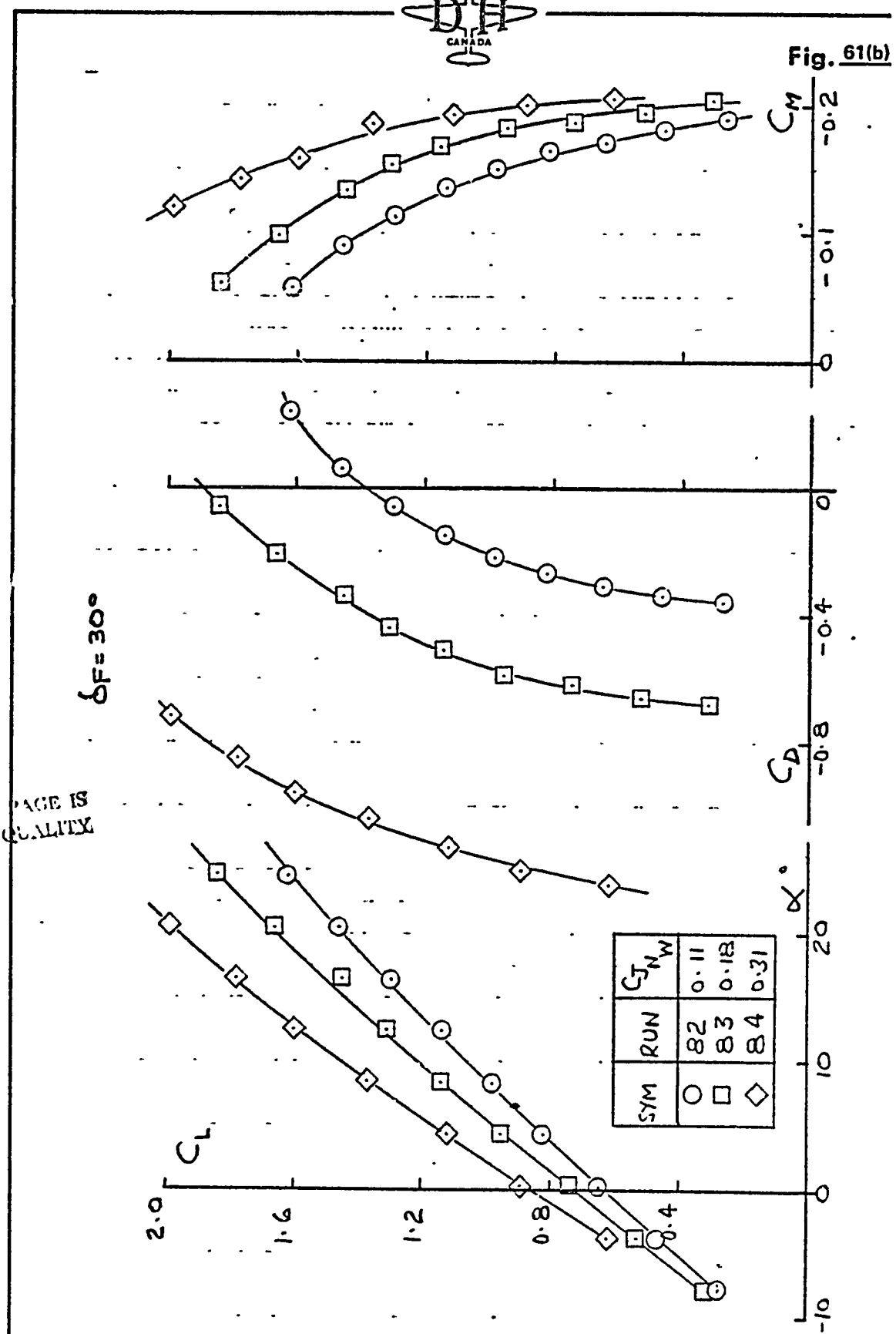

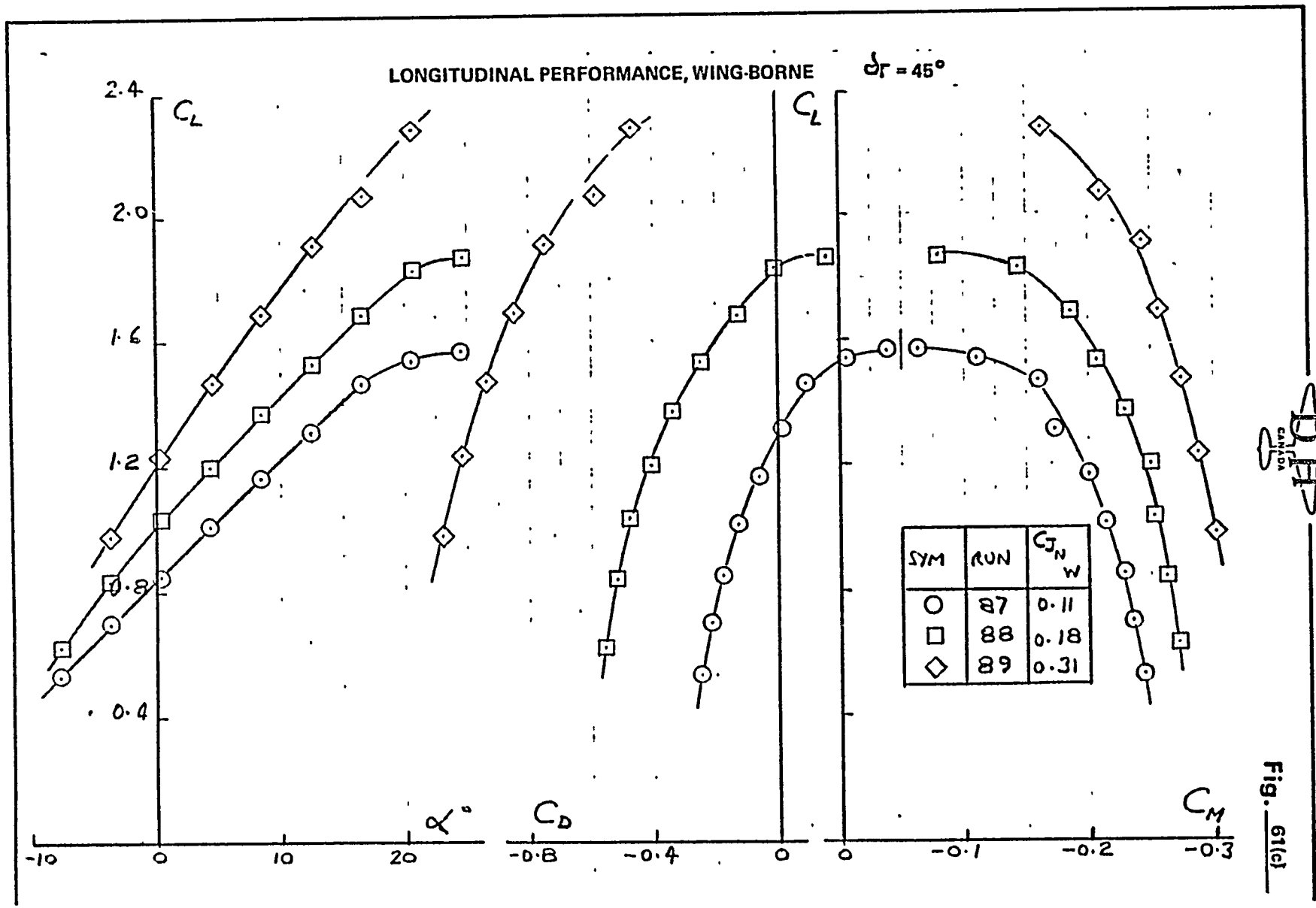
LONGITUDINAL PERFORMANCE, WING-BORNE
δ_T = 45°
C_L
2.4
2.0
1.6
1.2
0.8
0.4
α°
-10
0
10
20
C_D
-0.8
-0.4
0
C_L
C_M
0
-0.1
-0.2
-0.3
SYM
RUN
$C_{J_{N_W}}$
87
0.11
88
0.18
89
0.31

Fig. 61(c)

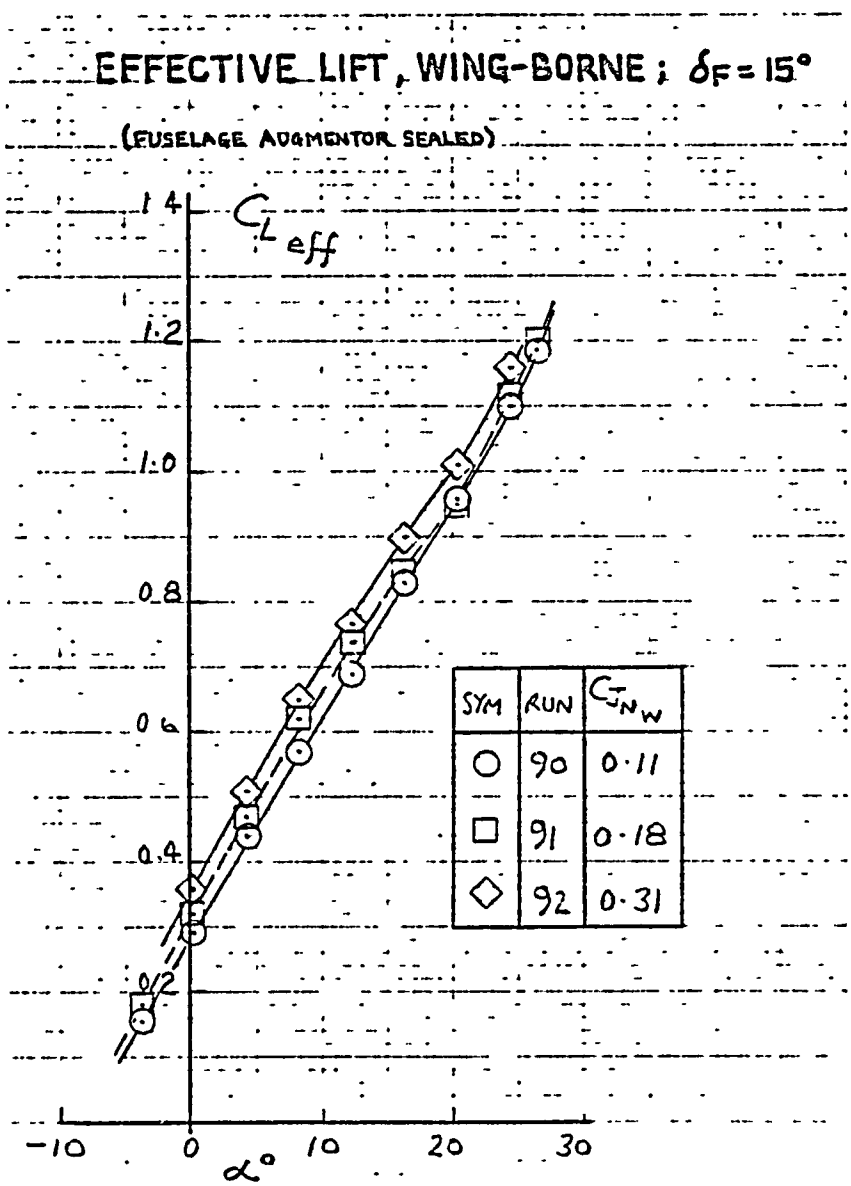
EFFECTIVE LIFT, WING-BORNE; $\delta_F = 15°$
(FUSELAGE AUGMENTOR SEALED)
$C_{L\,eff}$
1.4
1.2
1.0
0.8
0.6
0.4
0.2
−10
0
10
20
30
$\alpha°$
SYM | RUN | $C_{J_{N_W}}$
○ | 90 | 0·11
□ | 91 | 0·18
◇ | 92 | 0·31

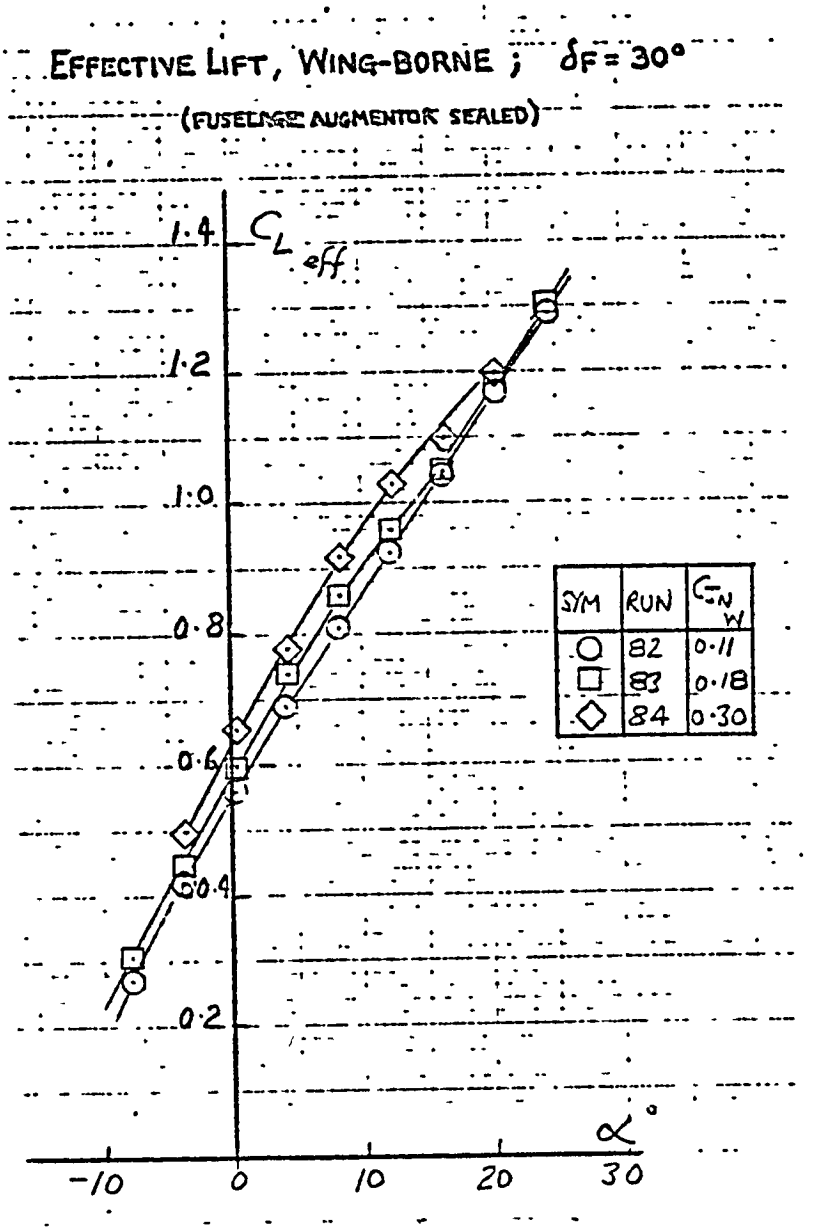

Fig. 62(c)

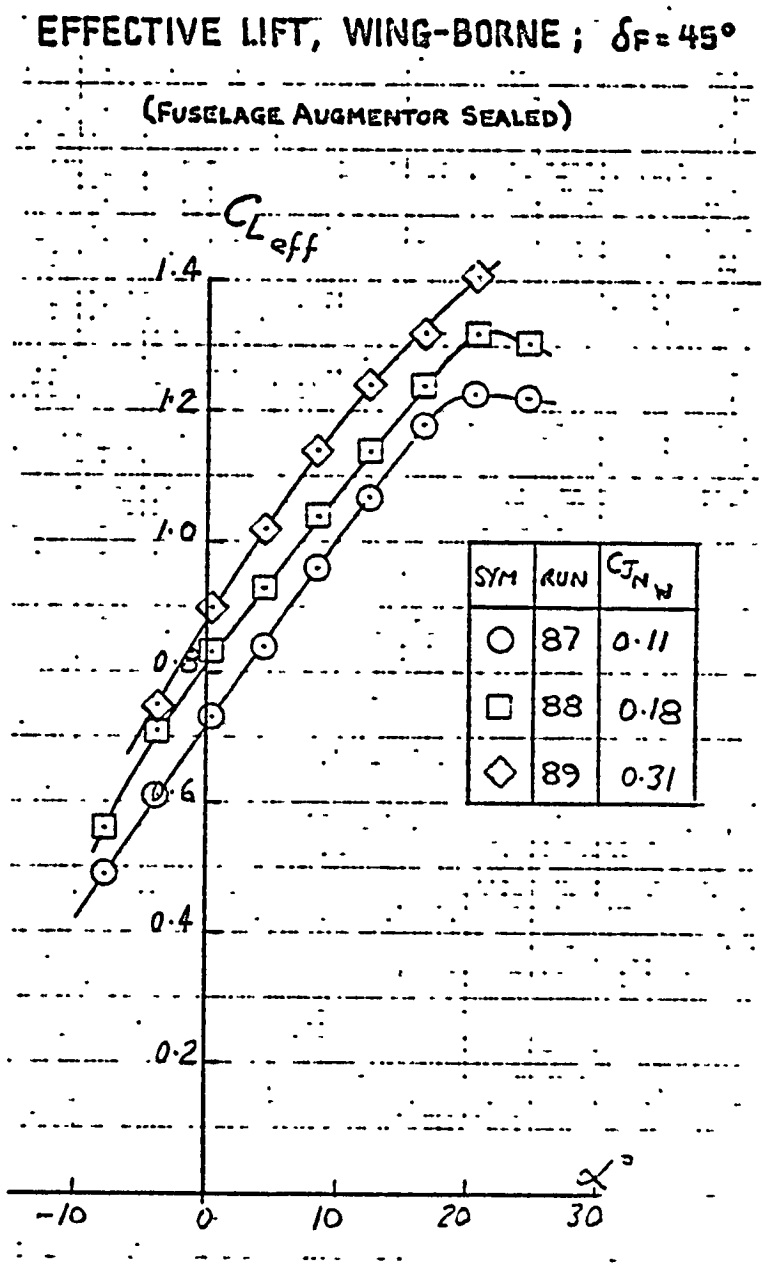
EFFECTIVE LIFT, WING-BORNE ; $\delta_F = 45°$
(FUSELAGE AUGMENTOR SEALED)
$C_{L_{eff}}$
1.4
1.2
1.0
0.8
0.6
0.4
0.2
$\alpha°$
-10
0
10
20
30
SYM | RUN | $C_{J_{N_W}}$
○ | 87 | 0.11
□ | 88 | 0.18
◇ | 89 | 0.31

Fig. 63

EFFECT OF FLAP ANGLE ON EFFECTIVE LIFT

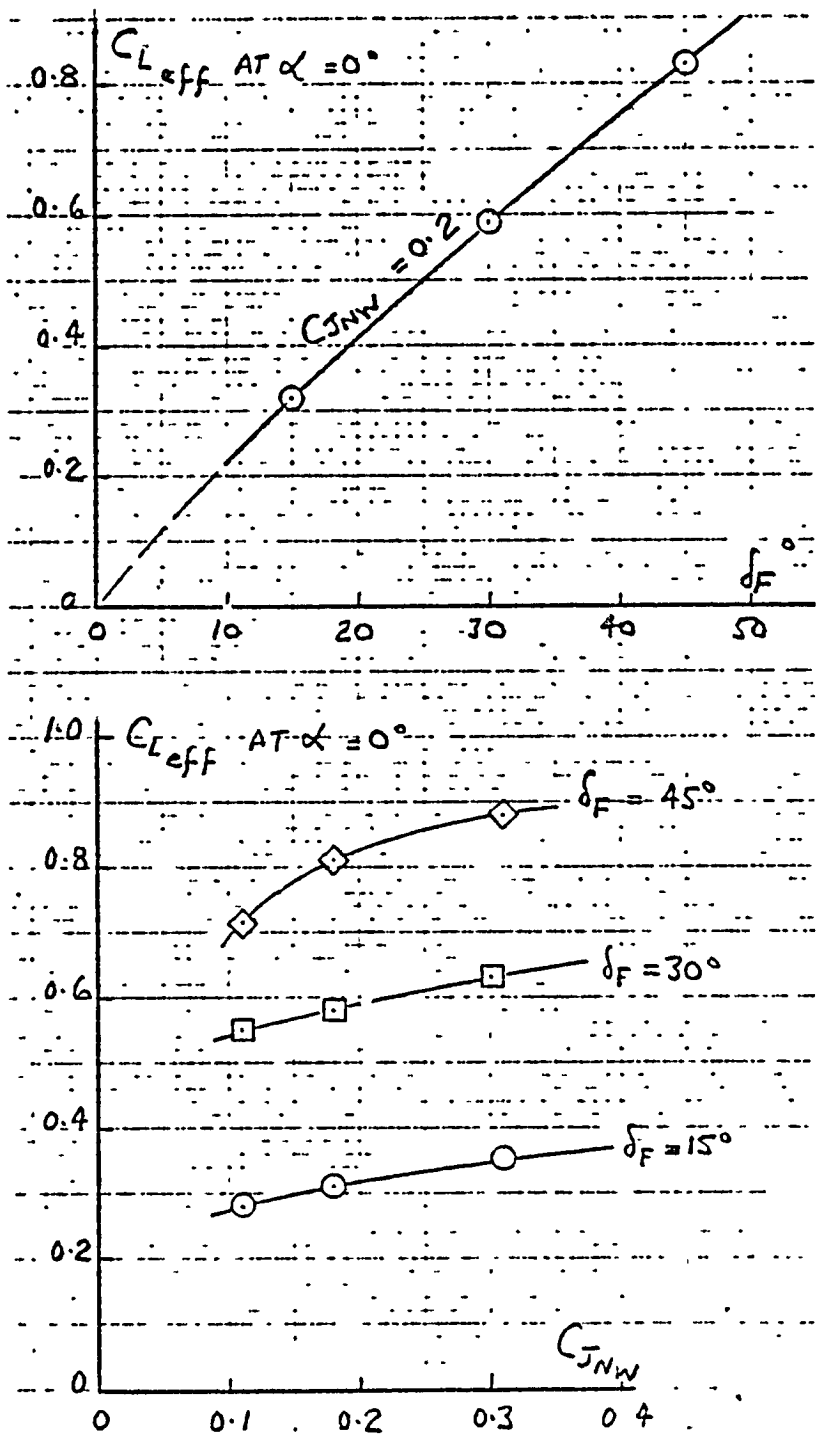

EFFECT OF FLAP ANGLE ON LIFT CURVE SLOPE

$(\partial C_{L_{EFF}}/\partial\alpha)_{\alpha=0^\circ}$ [WING-BORNE]

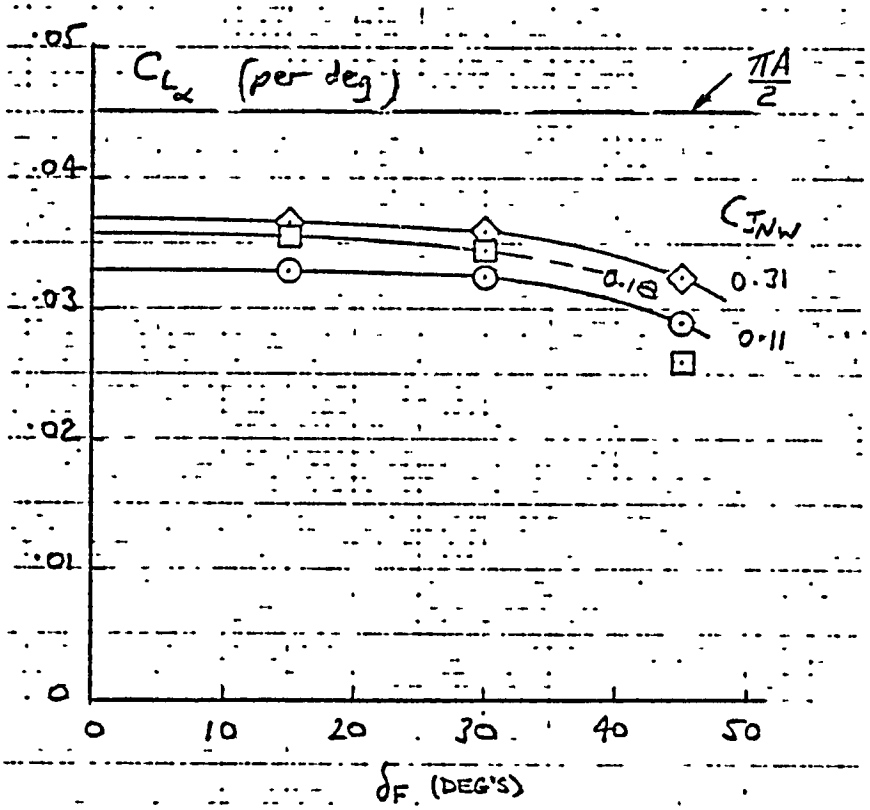

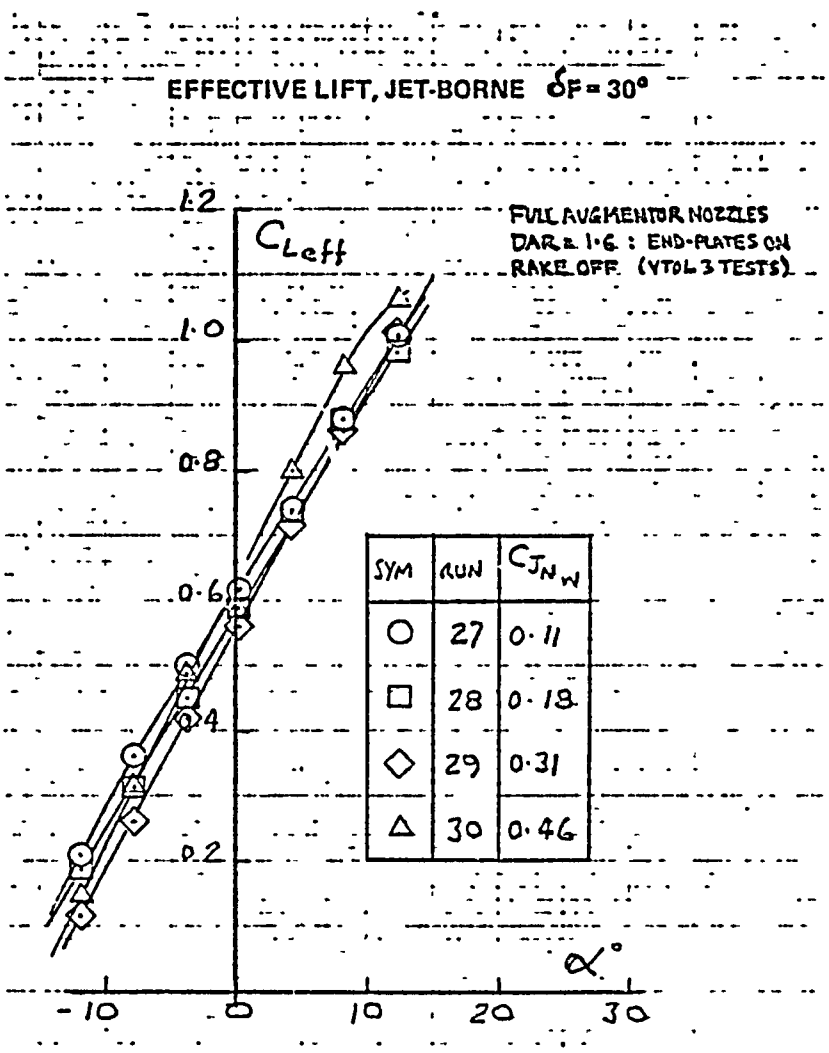

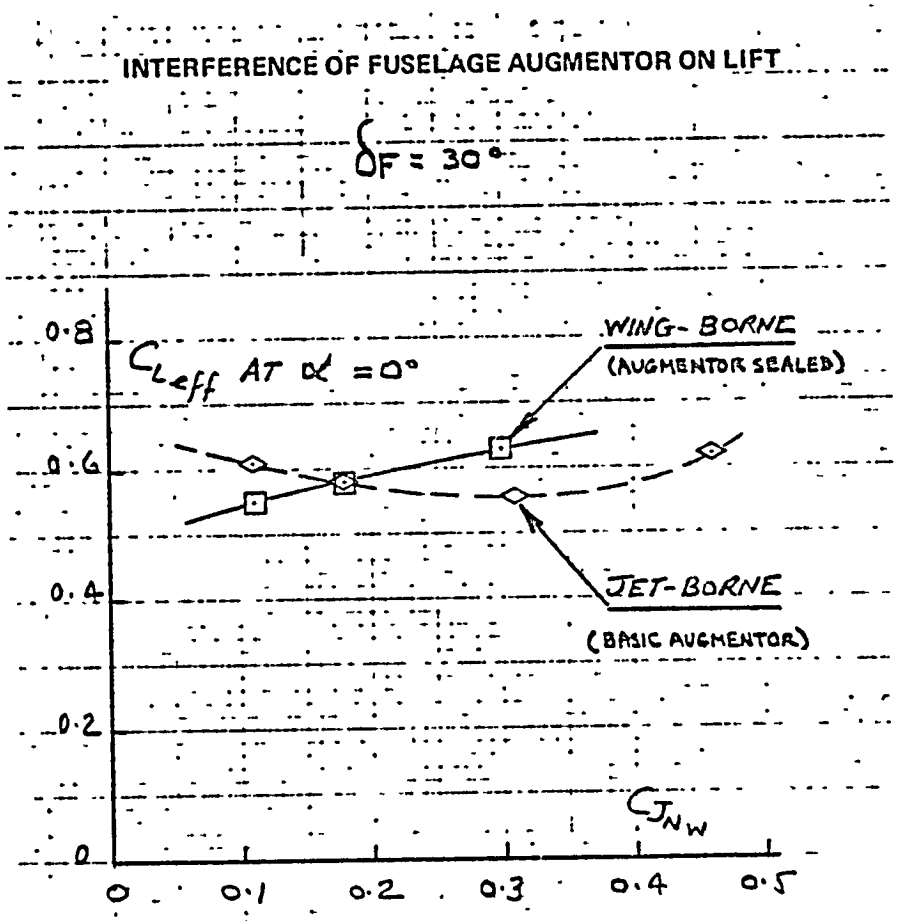
INTERFERENCE OF FUSELAGE AUGMENTOR ON LIFT
$\delta_F = 30°$
$C_{L_{eff}}$ AT $\alpha = 0°$
WING-BORNE
(AUGMENTOR SEALED)
JET-BORNE
(BASIC AUGMENTOR)
$C_{J_{NW}}$
0.8
0.6
0.4
0.2
0
0
0.1
0.2
0.3
0.4
0.5

INTERFERENCE OF FUSELAGE AUGMENTOR ON LIFT CURVE

$\delta_F = 30°$

$C_{J_{NW}} = 0.18$

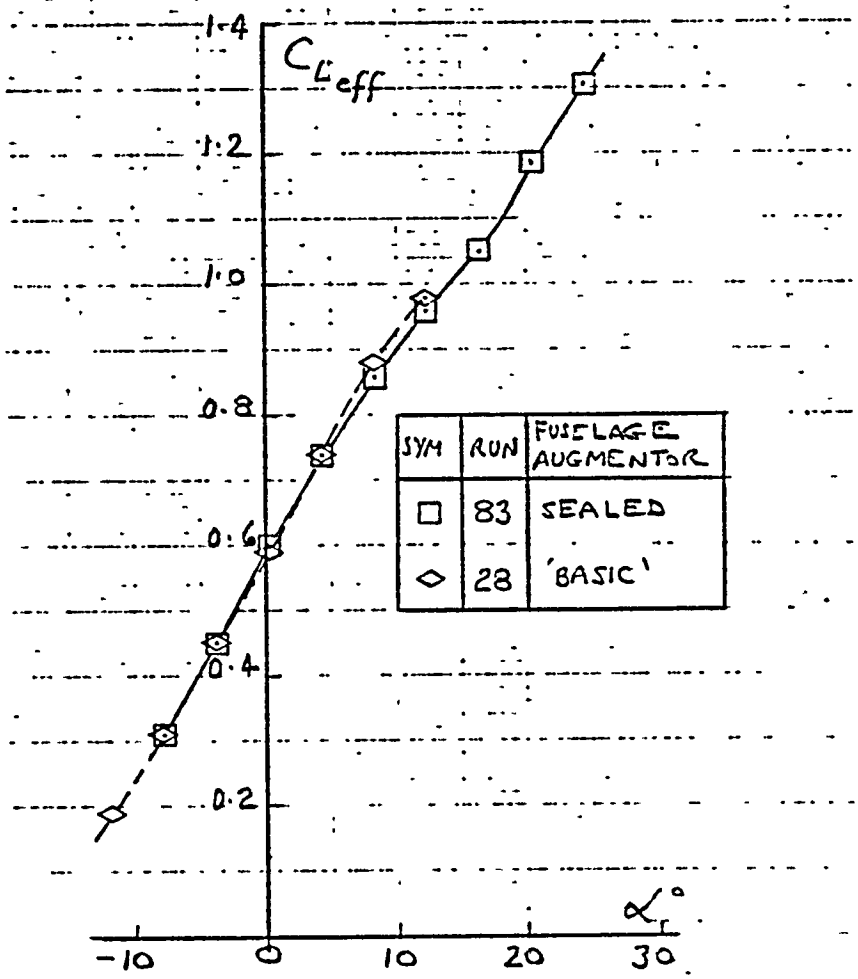

EFFECTIVE DRAG, WING-BORNE $\delta_F = 15°$ (FUSELAGE AUGMENTOR SEALED)

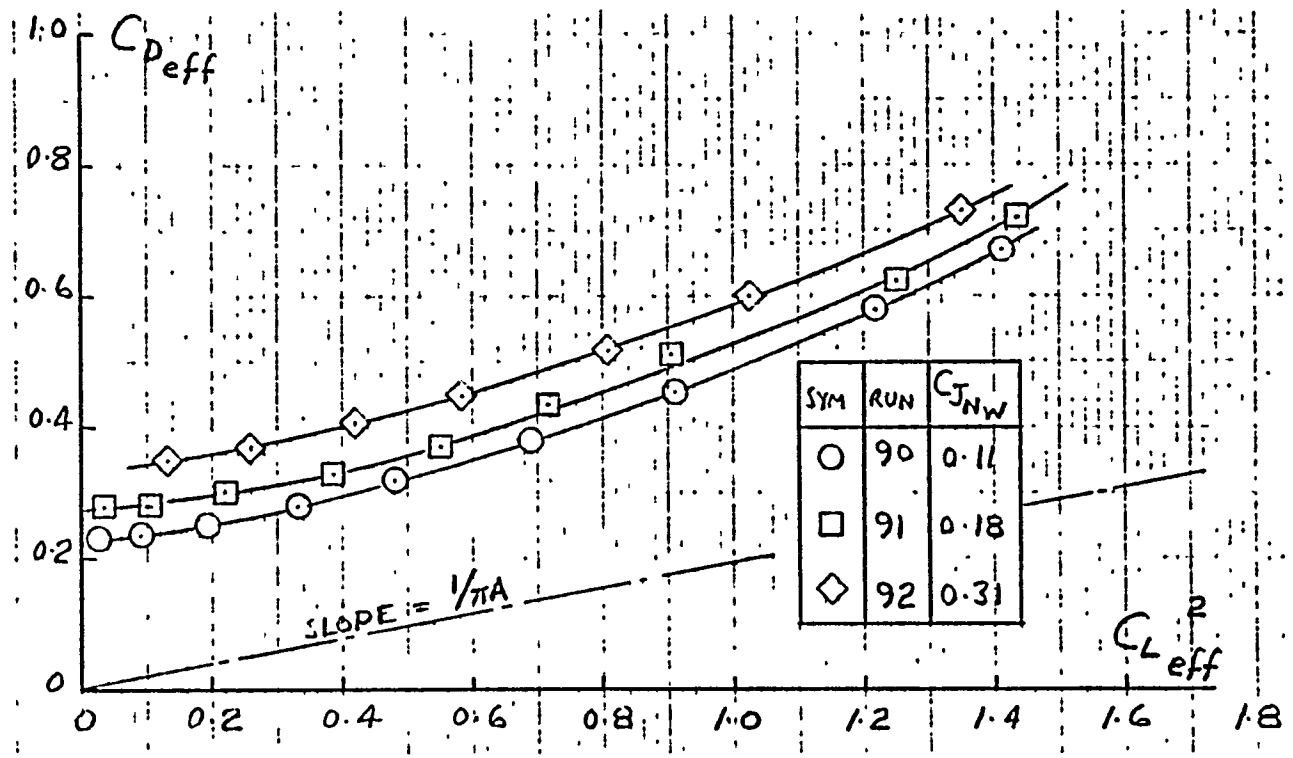

Fig. 68(a)

EFFECTIVE DRAG, WING-BORNE $\delta_F = 30°$ (FUSELAGE AUGMENTOR SEALED)

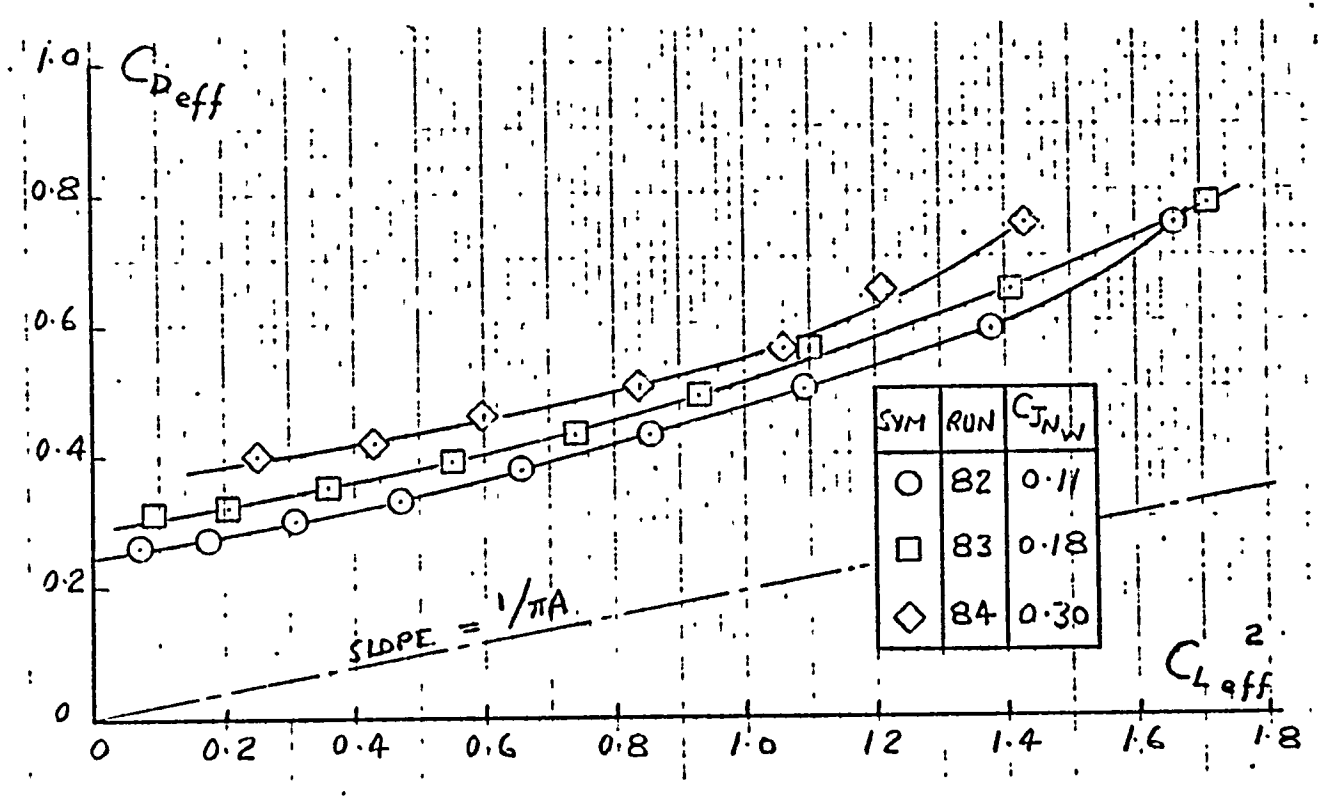

Fig. 68(b)

EFFECTIVE DRAG, WING-BORNE

δ_F = 45° (FUSELAGE AUGMENTOR SEALED)

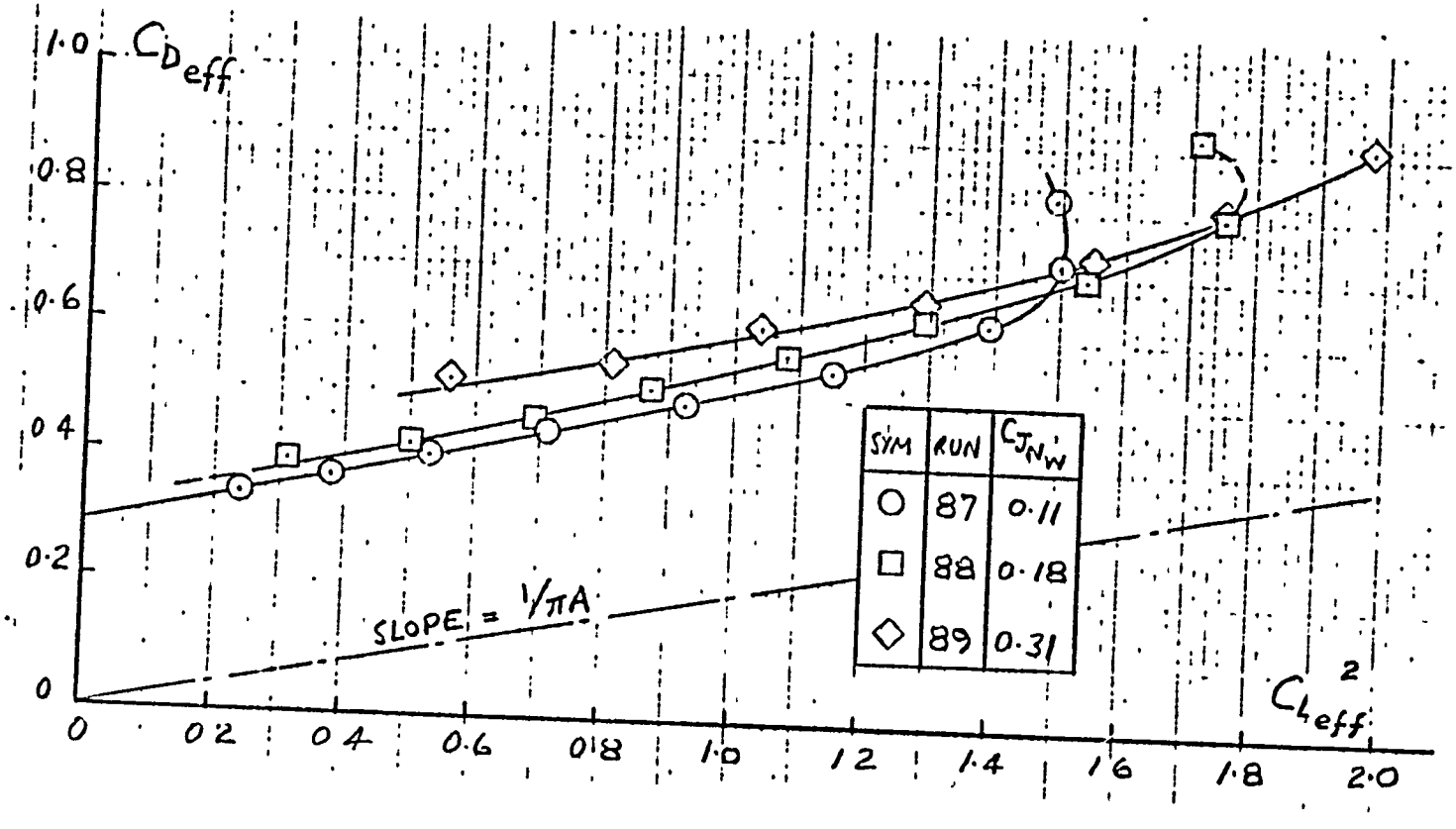

Fig. 68(

EFFECT OF FLAP ANGLE ON EFFECTIVE DRAG, WING-BORNE (FUSELAGE AUGMENTOR SEALED) $C_{J_{NW}} = 0.18$

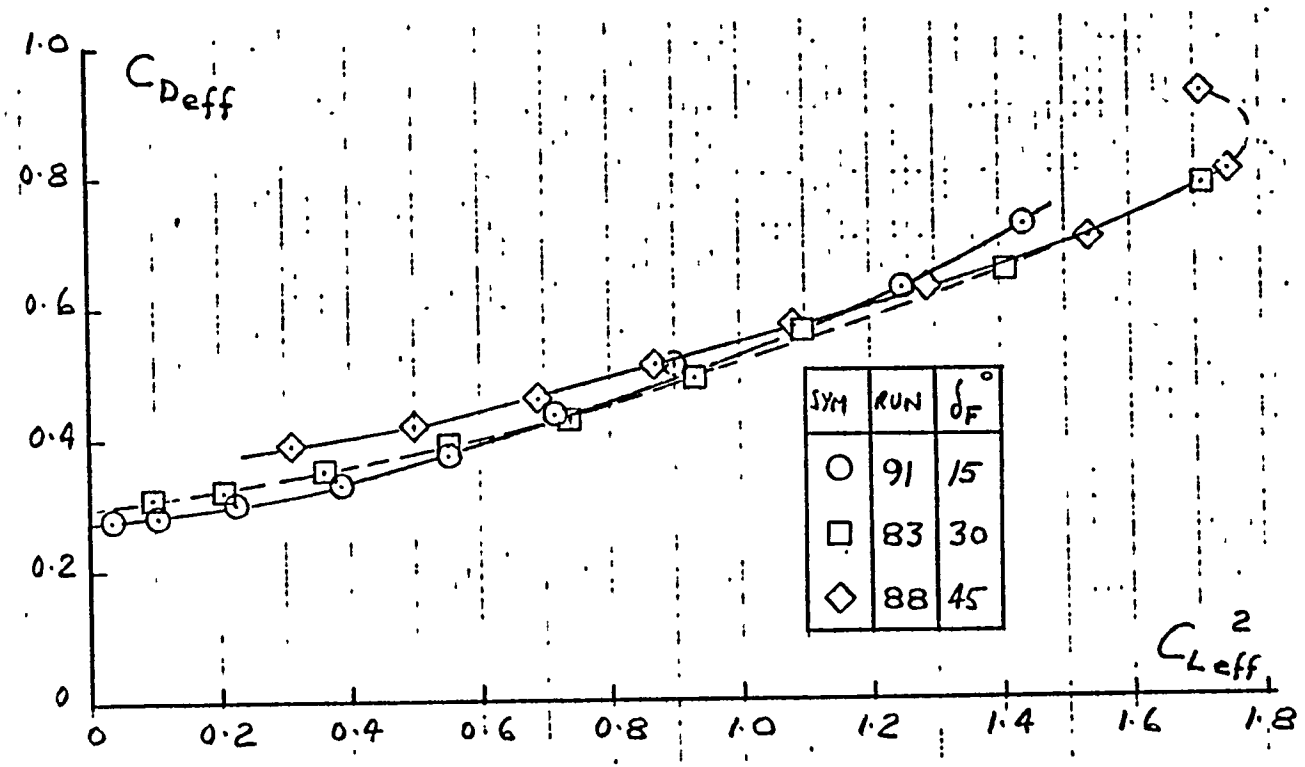

Fig. 69

Fig. 70

EFFECTIVE DRAG, JET-BORNE; $\delta_F = 30$; VTOL 1 TESTS

FULL AUGMENTOR NOZZLES
DAR = 1·6, END-PLATES ON
RAKE OFF; L/E SLAT OFF
$\delta_N = 0°$

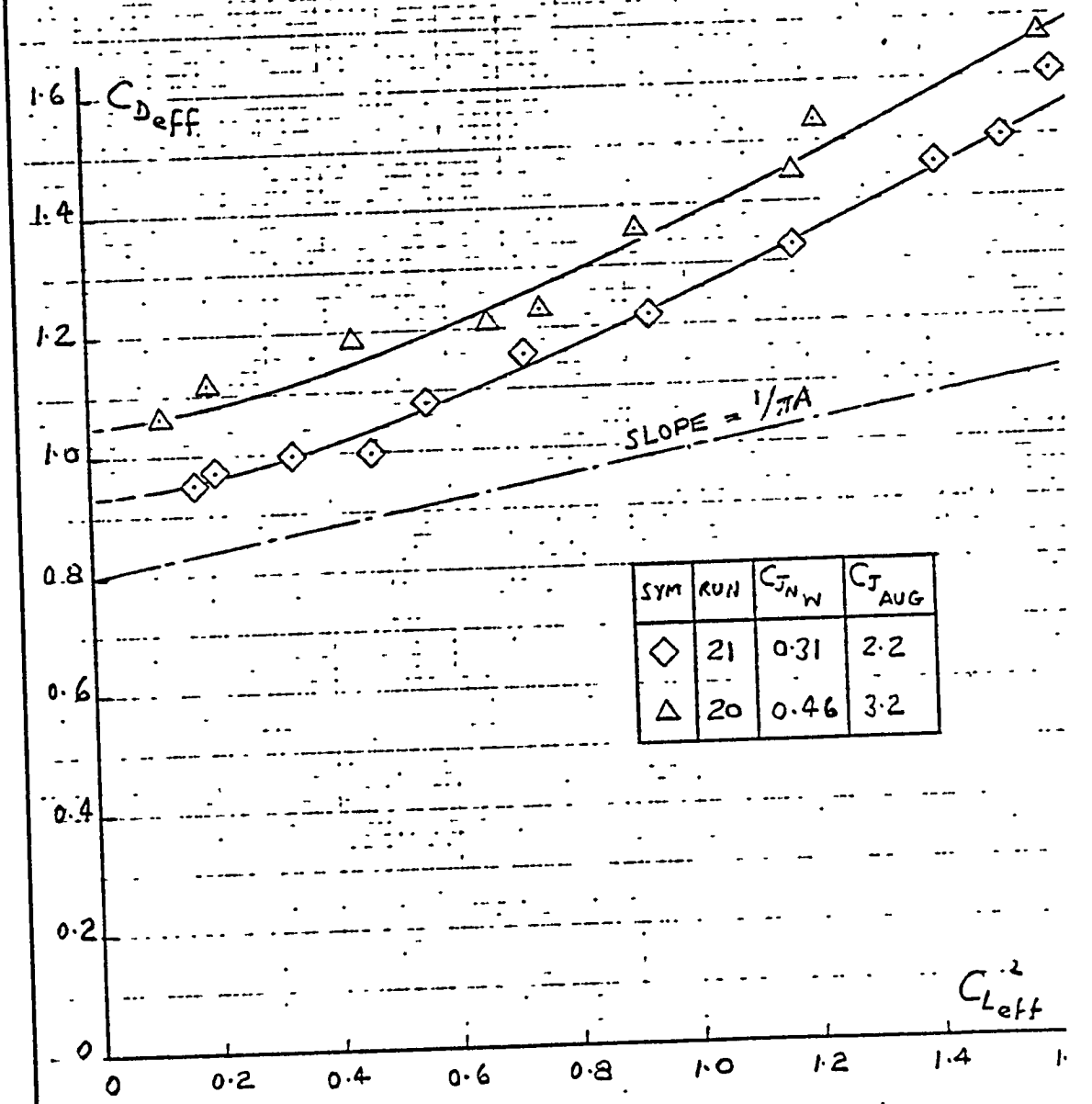

SYM	RUN	$C_{J_{NW}}$	$C_{J_{AUG}}$
◇	21	0·31	2·2
△	20	0·46	3·2

Fig. 71

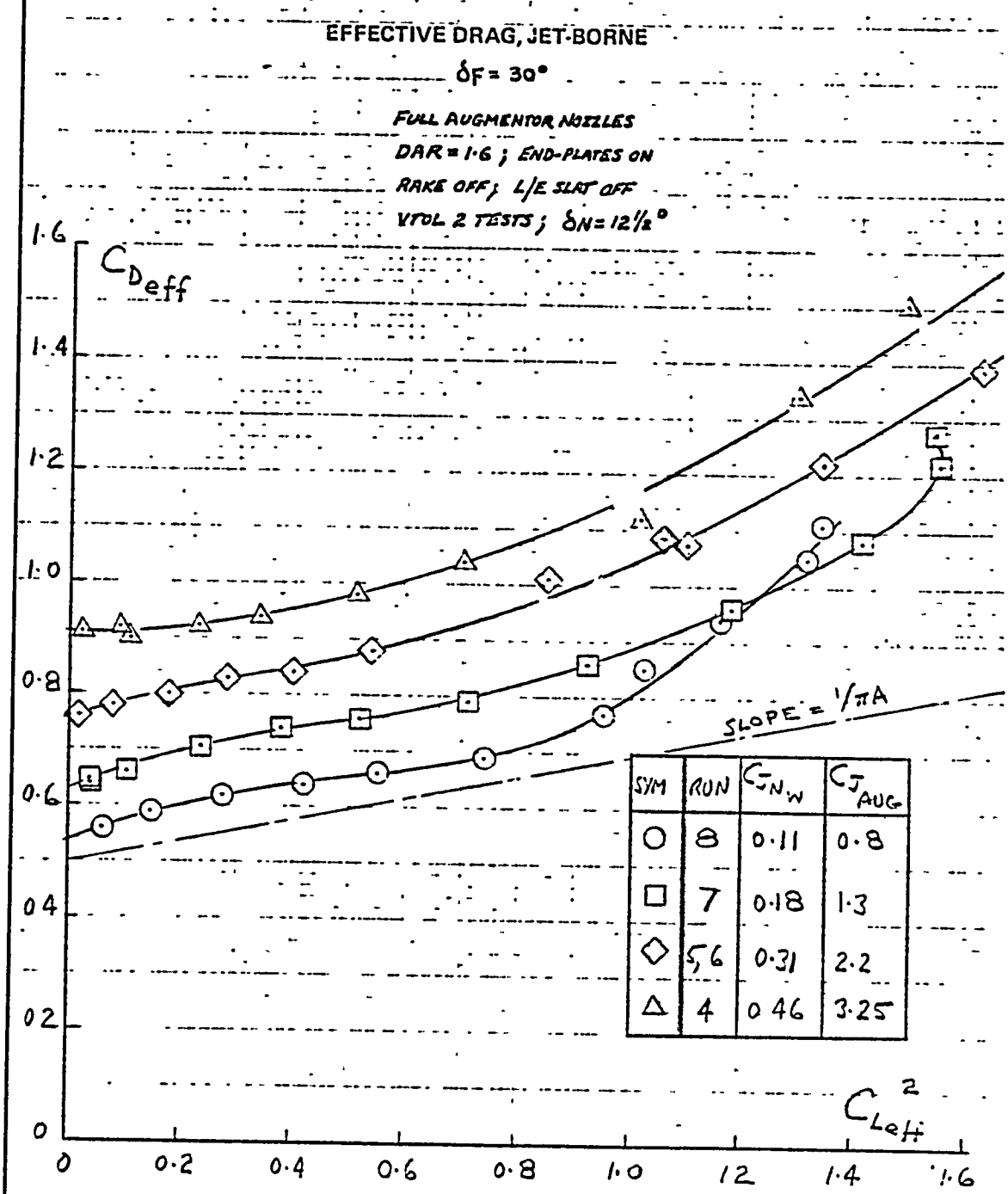
EFFECTIVE DRAG, JET-BORNE
$\delta_F = 30°$
FULL AUGMENTOR NOZZLES
DAR = 1·6 ; END-PLATES ON
RAKE OFF; L/E SLAT OFF
VTOL 2 TESTS; $\delta_N = 12\frac{1}{2}°$
$C_{D_{eff}}$
$C_{L_{eff}}^2$
SLOPE = $1/\pi A$
1·6
1·4
1·2
1·0
0·8
0·6
0·4
0·2
0
0
0·2
0·4
0·6
0·8
1·0
1·2
1·4
1·6
SYM | RUN | $C_{T_{N_W}}$ | $C_{T_{AUG}}$
○ | 8 | 0·11 | 0·8
□ | 7 | 0·18 | 1·3
◇ | 5,6 | 0·31 | 2·2
△ | 4 | 0·46 | 3·25

EFFECTIVE DRAG, JET-BORNE

$\delta_F = 30°$

FULL AUGMENTOR NOZZLES
DAR = 1·6 ; END-PLATES ON
RAKE OFF (VTOL 3 TESTS)
L/E SLAT ON

SYM	RUN	$C_{J_{N_W}}$
○	27	0·11
□	28	0·18
◇	29	0·31
△	30	0·46

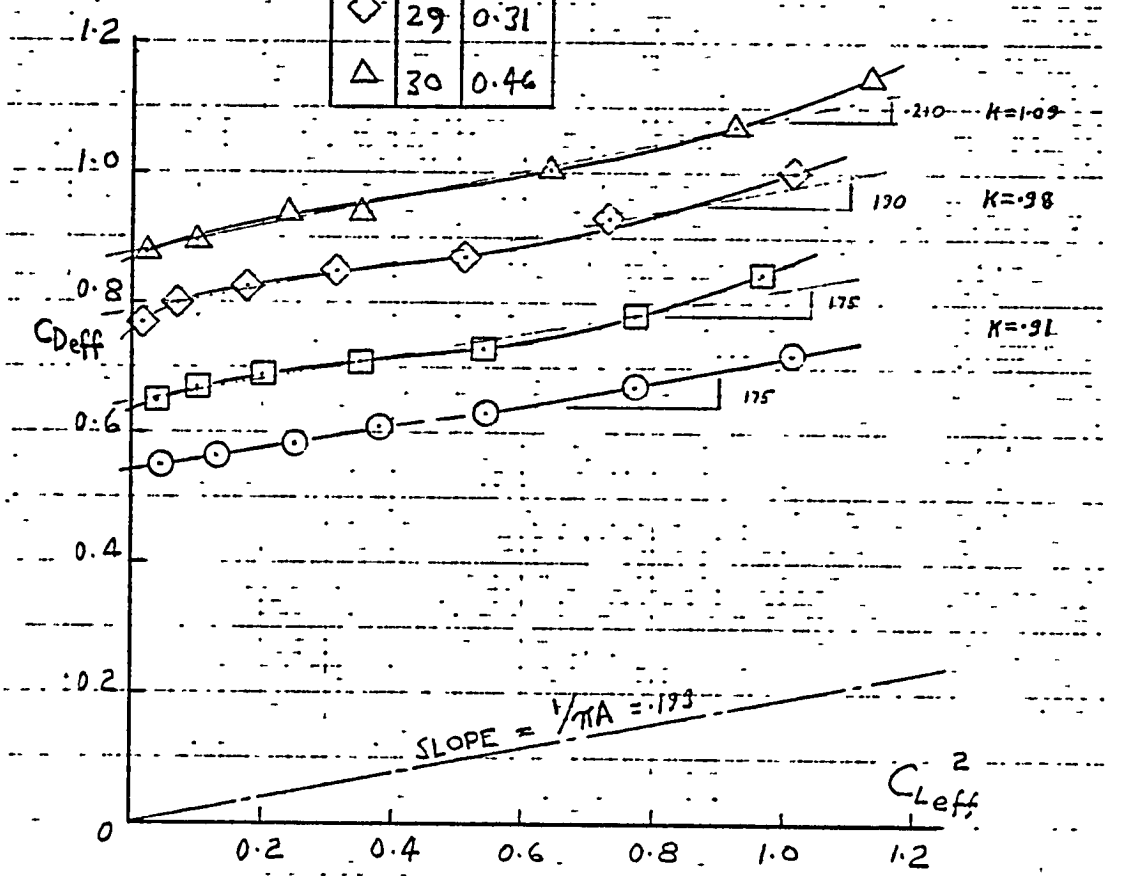

EFFECT OF FUSELAGE AUGMENTOR NOZZLE ANGLE ON EFFECTIVE DRAG

$\delta_F = 30°$; $C_{J_{NW}} = 0.31$; $C_{J_{AUG}} = 2.2$

FULL AUGMENTOR NOZZLES

DAR = 1.6 ; END-PLATES ON

RAKE OFF

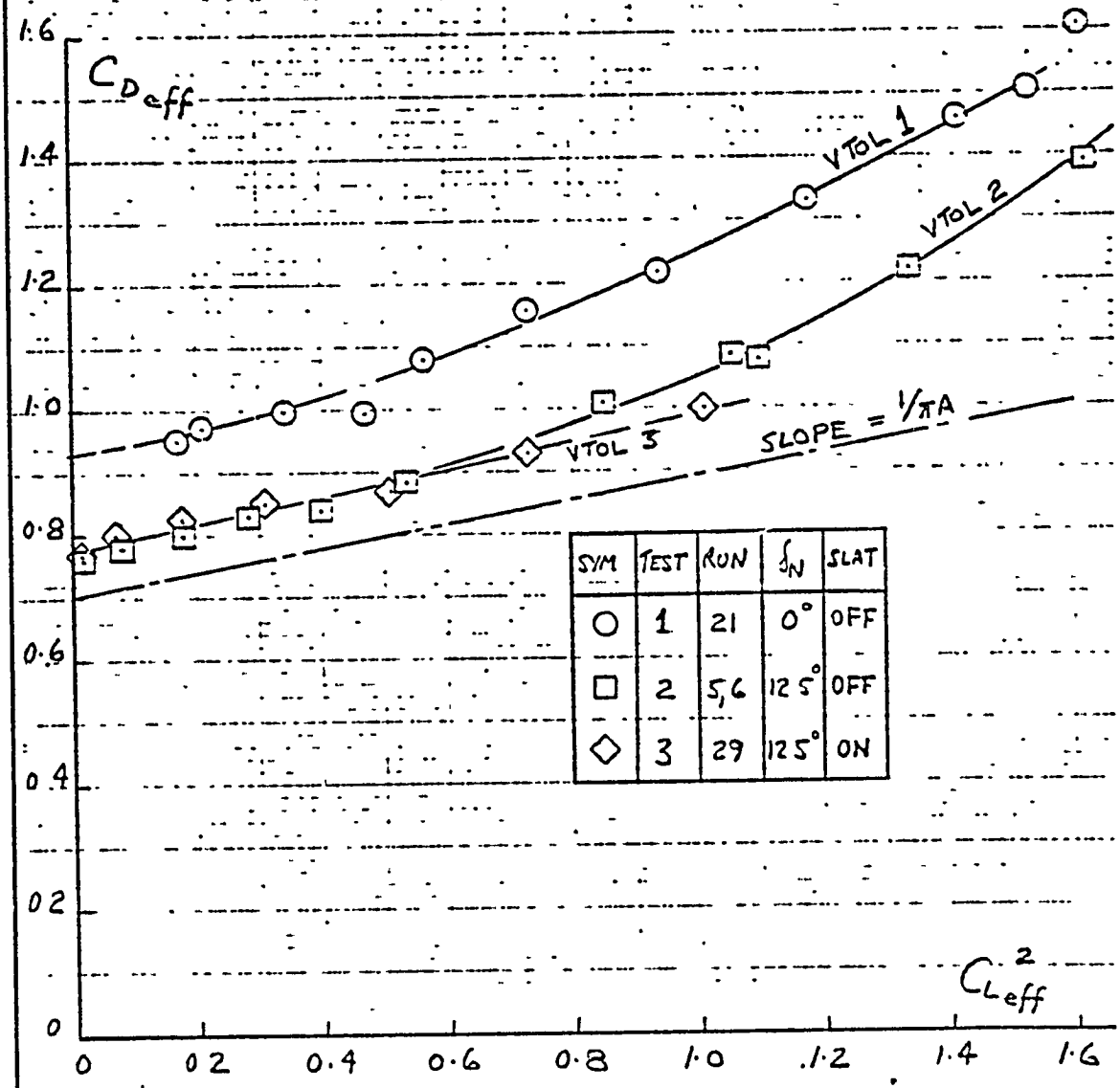

SYM	TEST	RUN	δ_N	SLAT
○	1	21	0°	OFF
□	2	5,6	12.5°	OFF
◇	3	29	12.5°	ON

Fig. 74

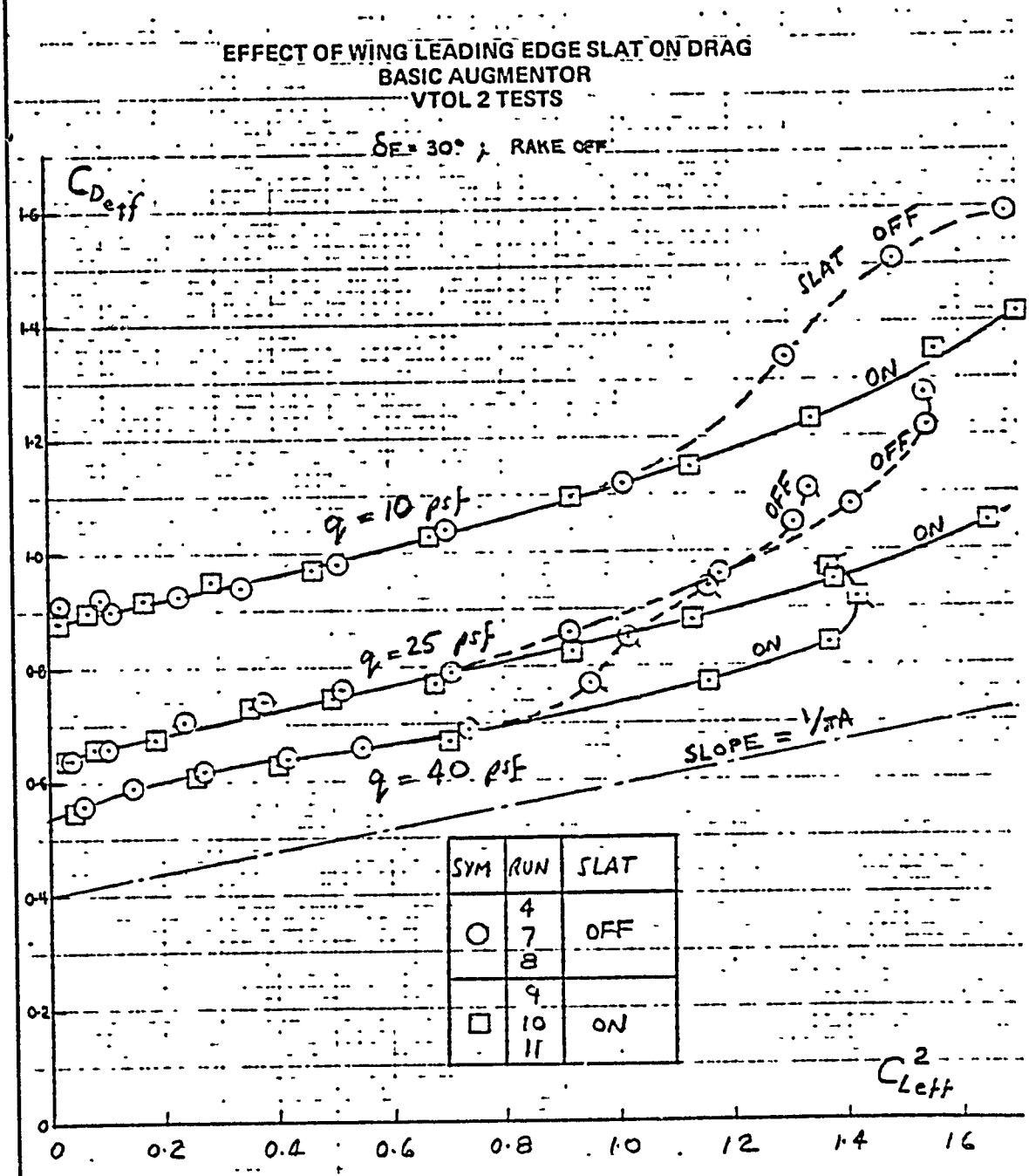
EFFECT OF WING LEADING EDGE SLAT ON DRAG
BASIC AUGMENTOR
VTOL 2 TESTS
δE = 30° ; RAKE OFF
CDeff
SLAT OFF
ON
OFF
OFF
ON
ON
q = 10 psf
q = 25 psf
q = 40 psf
SLOPE = 1/πA
SYM | RUN | SLAT
○ | 4, 7, 8 | OFF
□ | 9, 10, 11 | ON
C²Leff
0
0.2
0.4
0.6
0.8
1.0
1.2
1.4
1.6

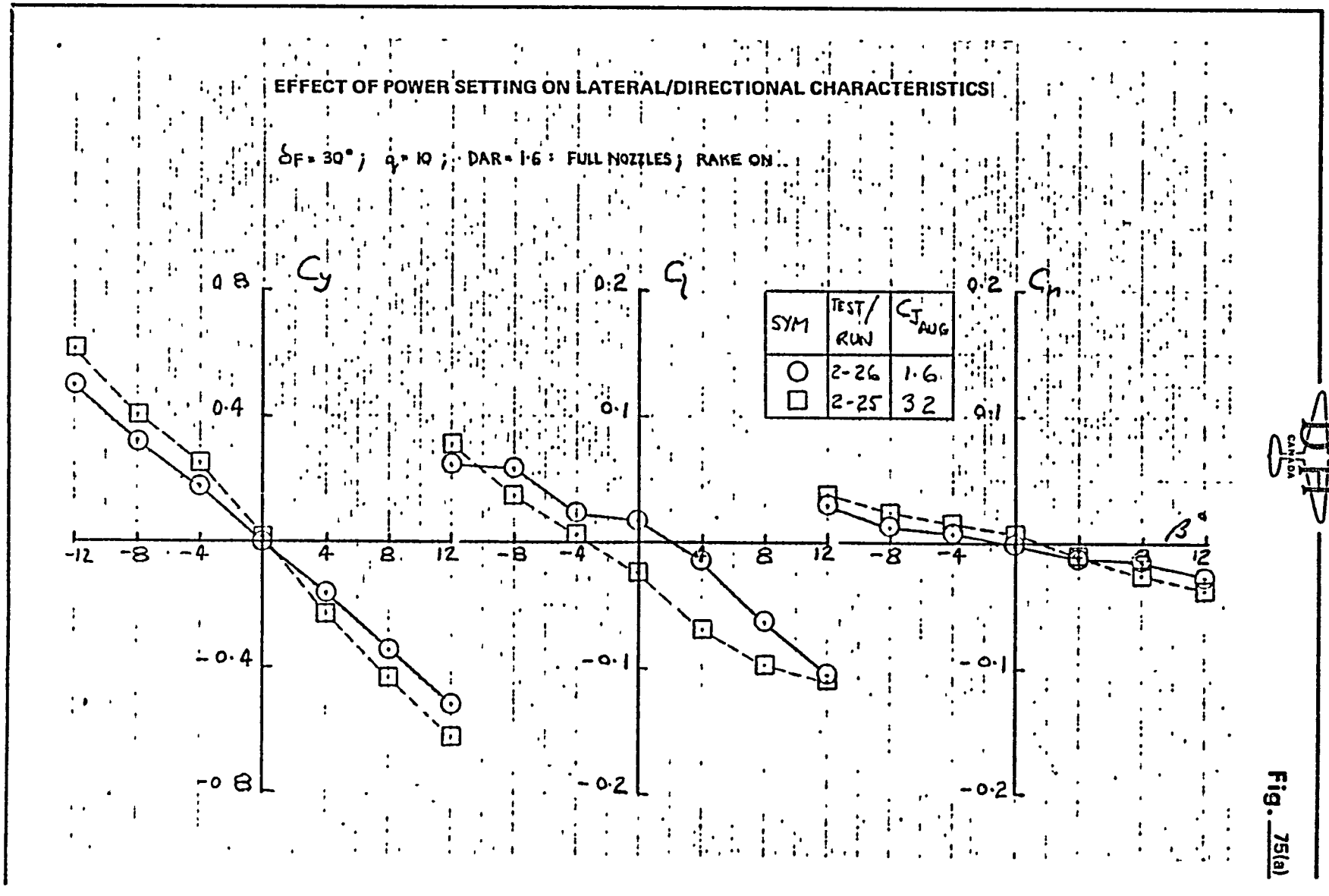
EFFECT OF POWER SETTING ON LATERAL/DIRECTIONAL CHARACTERISTICS
δF = 30° ; q = 10 ; DAR = 1·6 : FULL NOZZLES ; RAKE ON
Cy
Cl
Cn
β
SYM
TEST/RUN
CJAUG
2-26
1·6
2-25
3 2
0·8
0·4
-0·4
-0·8
0·2
0·1
-0·1
-0·2
-12
-8
-4
4
8
12

Fig. 75(a)

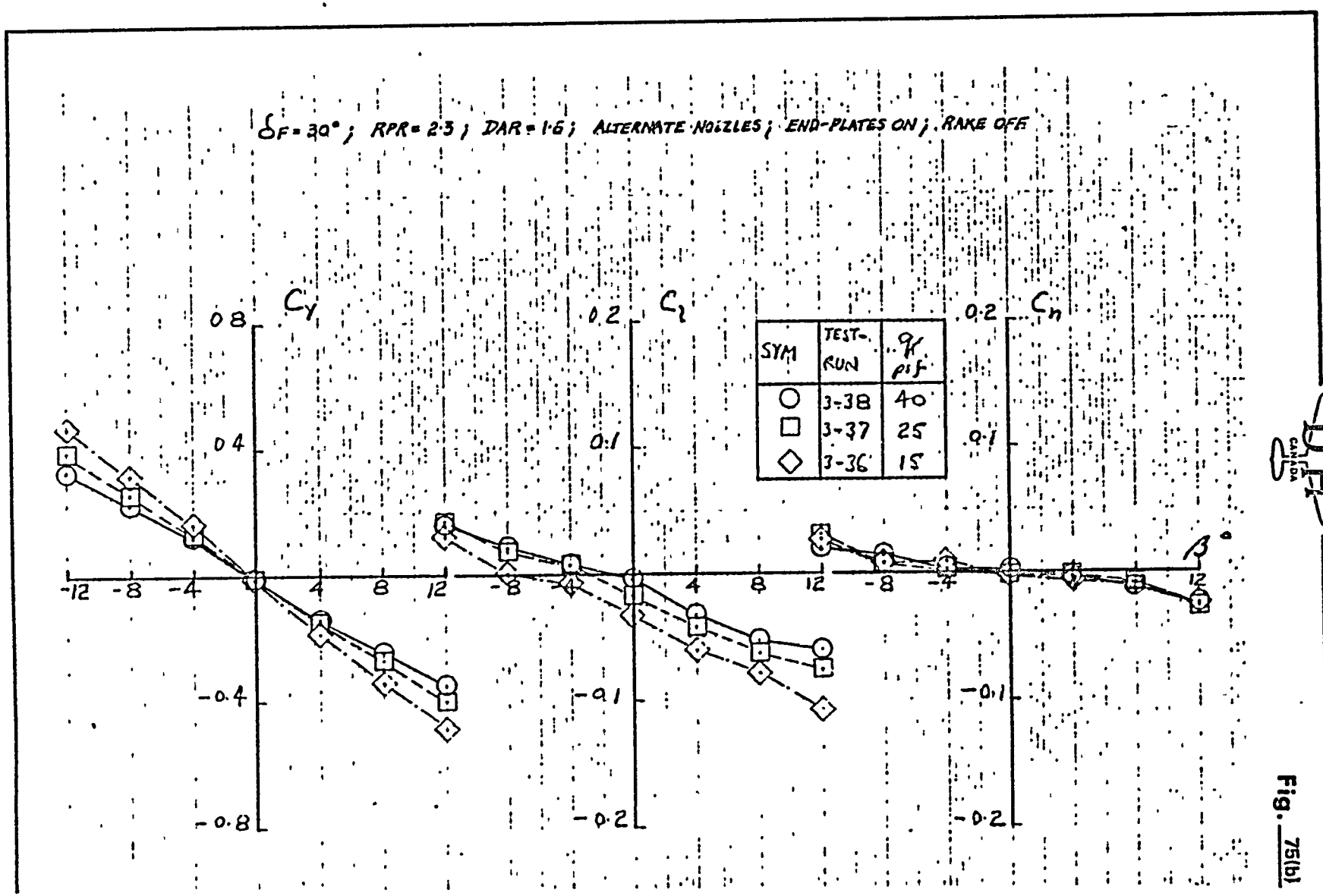
$\delta_F = 30°$; RPR = 2·3; DAR = 1·6; ALTERNATE NOZZLES; END-PLATES ON; RAKE OFF
C_Y
C_l
C_n
SYM
TEST-RUN
q psf
3-38 40
3-37 25
3-36 15
0·8
0·4
-0·4
-0·8
0·2
0·1
-0·1
-0·2
-12 -8 -4 4 8 12
β

Fig. 75(b)

EFFECT OF FUSELAGE AUGMENTOR NOZZLE ANGLE ON LATERAL/DIRECTIONAL CHARACTERISTICS

$\delta_F = 30°$; RPR = 2.3 ; q = 10 ; DAR = 1.6 ; FULL NOZZLES; RAKE ON .

Fig. 76

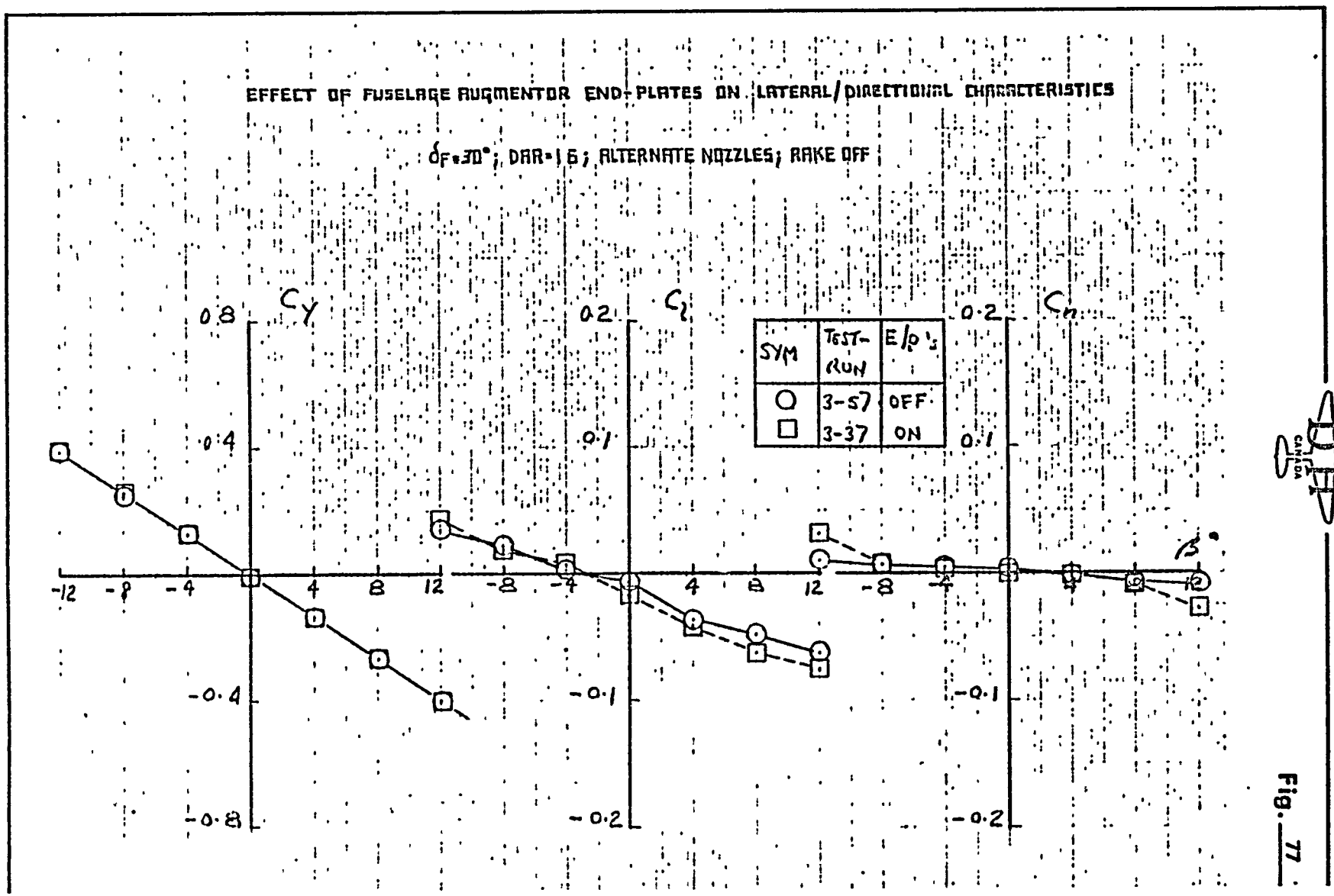
EFFECT OF FUSELAGE AUGMENTOR END-PLATES ON LATERAL/DIRECTIONAL CHARACTERISTICS
δ_F=30°; DAR=1.6; ALTERNATE NOZZLES; RAKE OFF
C_Y
C_l
C_n
SYM
TEST-RUN
E/D
3-57
OFF
3-37
ON
0.8
0.4
-0.4
-0.8
0.2
0.1
-0.1
-0.2
-12
-8
-4
4
8
12
β

Fig. 77

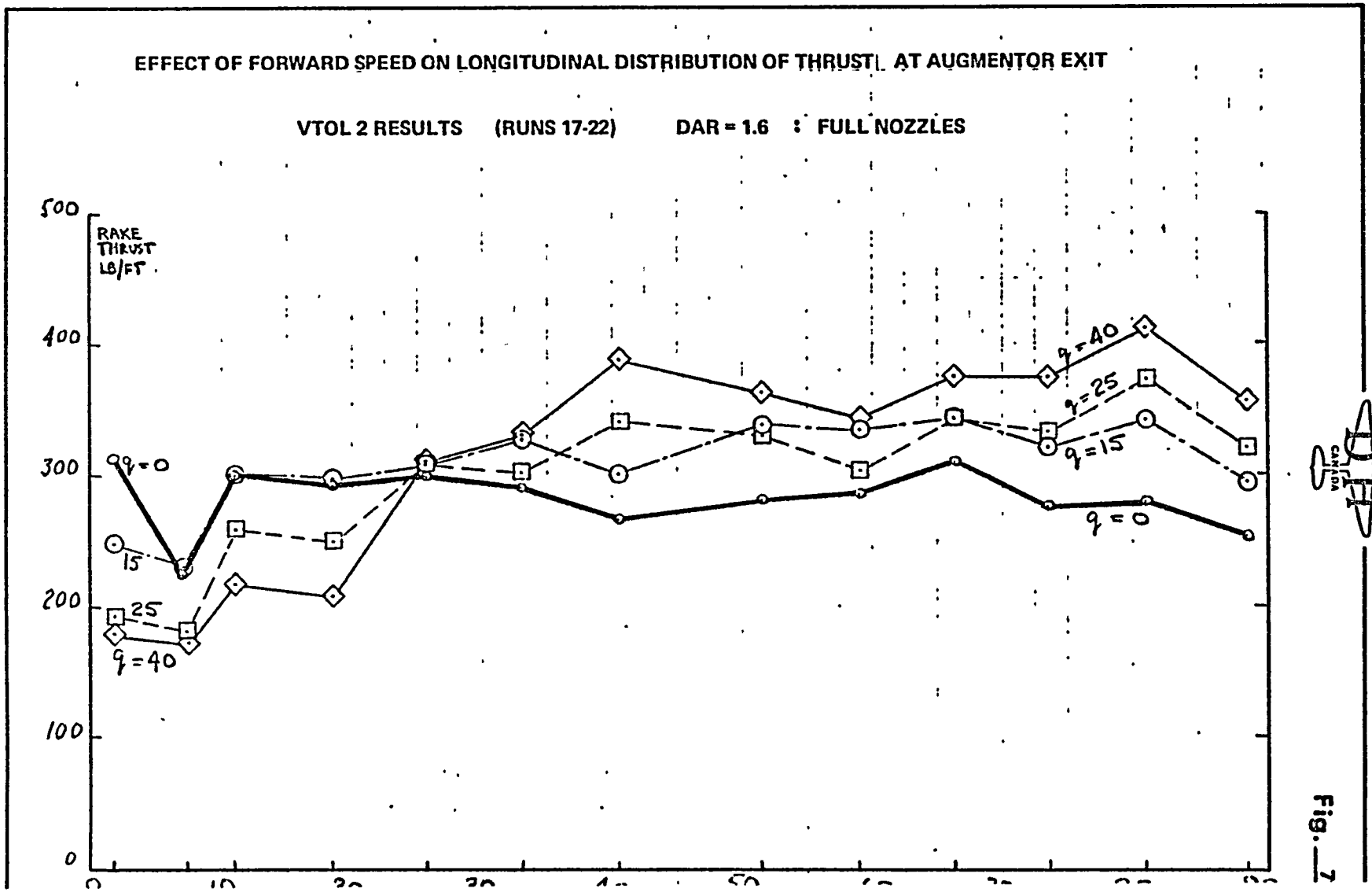
EFFECT OF FORWARD SPEED ON LONGITUDINAL DISTRIBUTION OF THRUST AT AUGMENTOR EXIT
VTOL 2 RESULTS (RUNS 17-22) DAR = 1.6 : FULL NOZZLES
RAKE THRUST LB/FT
500
400
300
200
100
0
q=40
q=25
q=15
q=0
15
25
q=40
q=0

Fig. 7

EFFECT OF FORWARD SPEED ON LONGITUDINAL DISTRIBUTION OF THRUST
AT AUGMENTOR EXIT
VTOL 3 RESULTS (RUNS 1-4) DAR = 1.6 : FULL NOZZLES

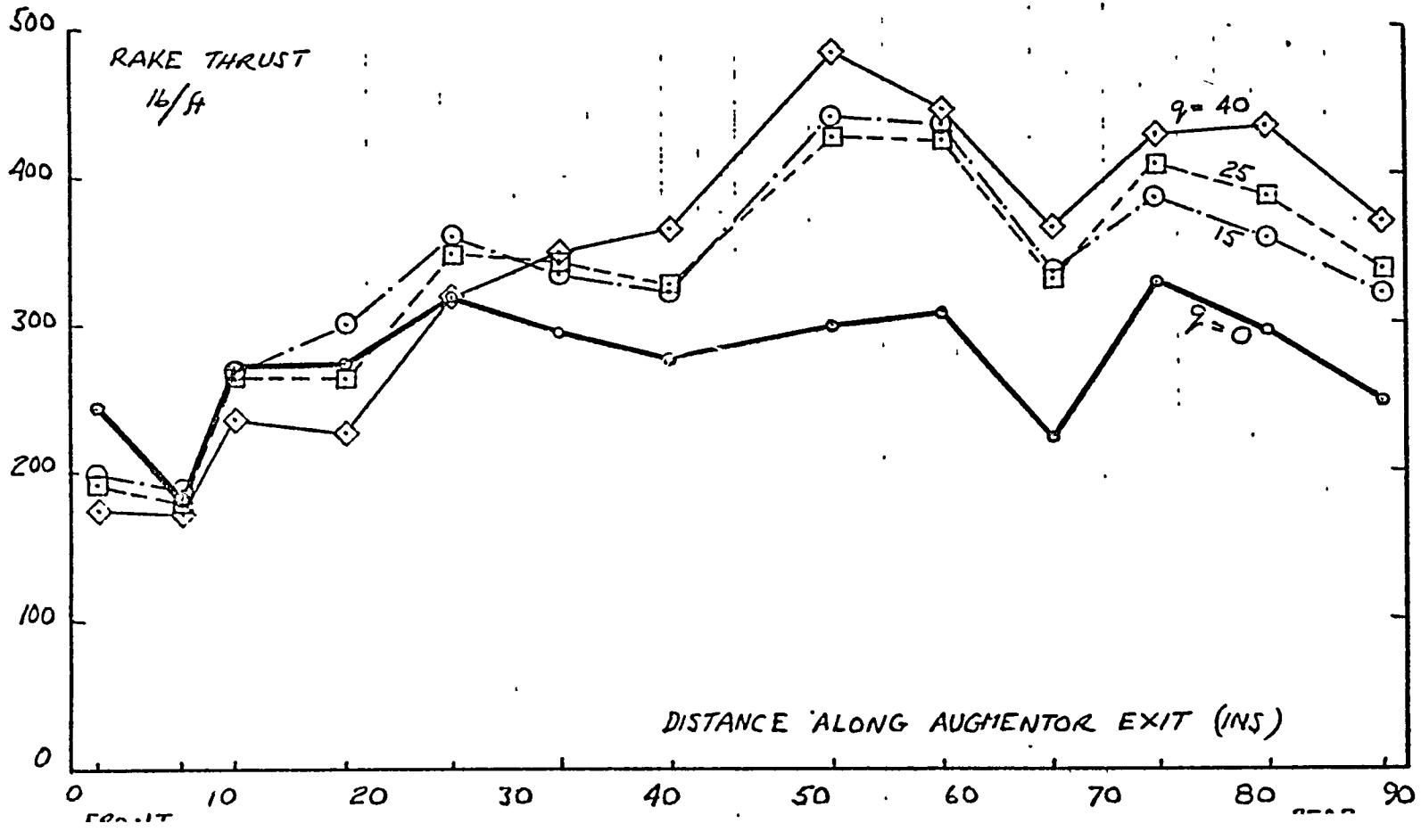

Fig. 79

Fig. 80

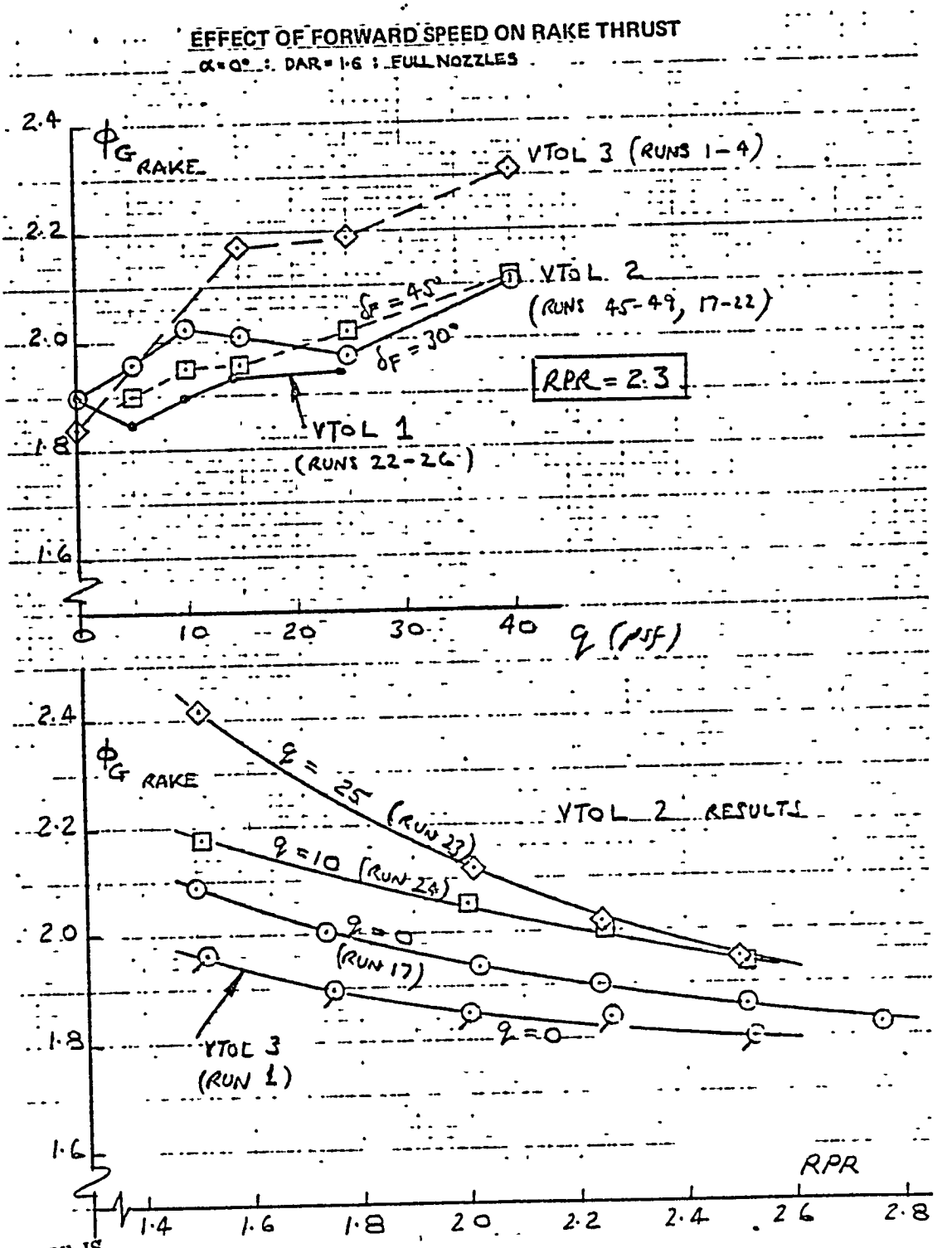

Fig. 81

EFFECT OF ANGLE OF ATTACK ON RAKE THRUST
DAR = 1.6 FULL NOZZLES RPR = 2.3

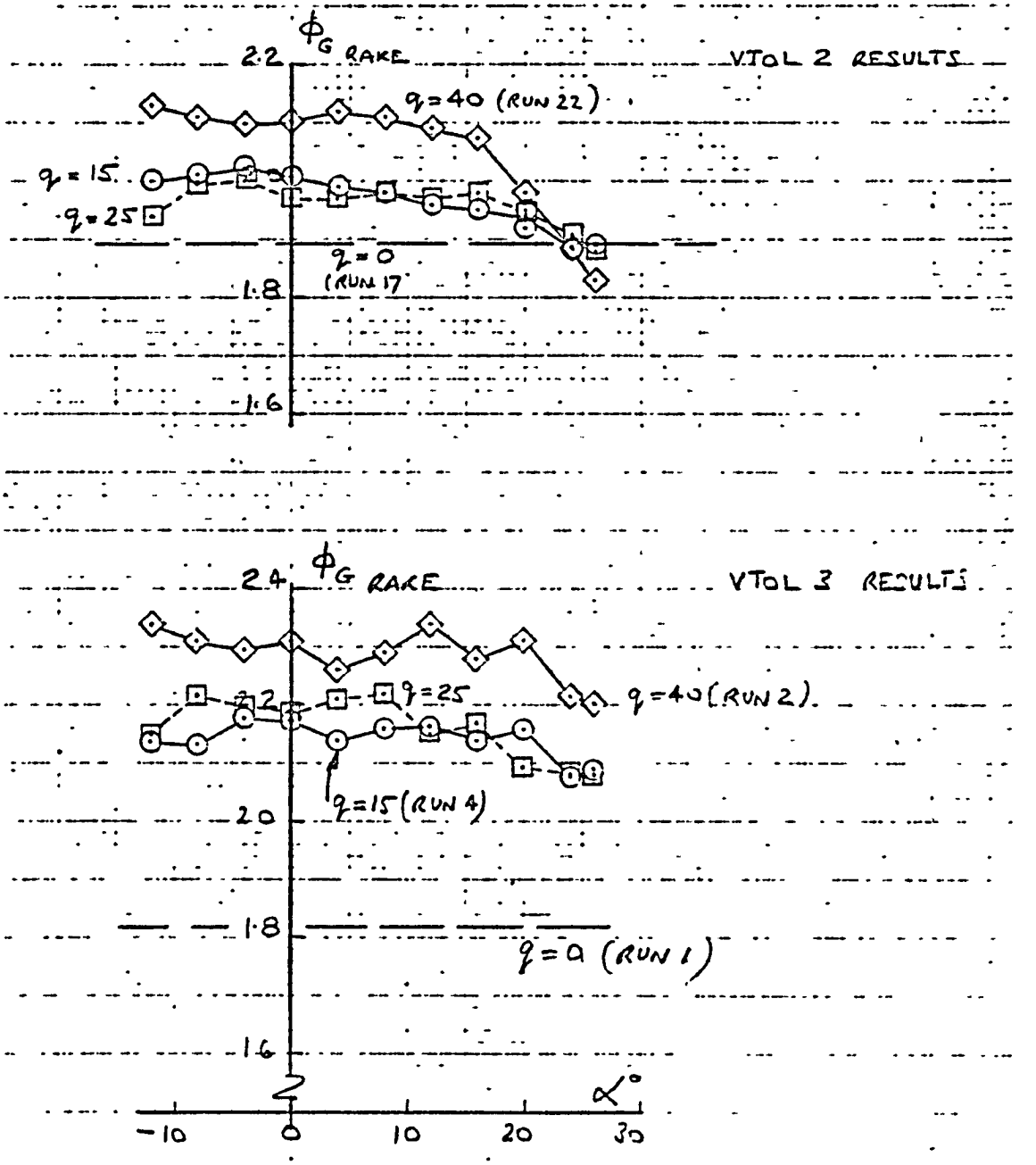

Fig. 82

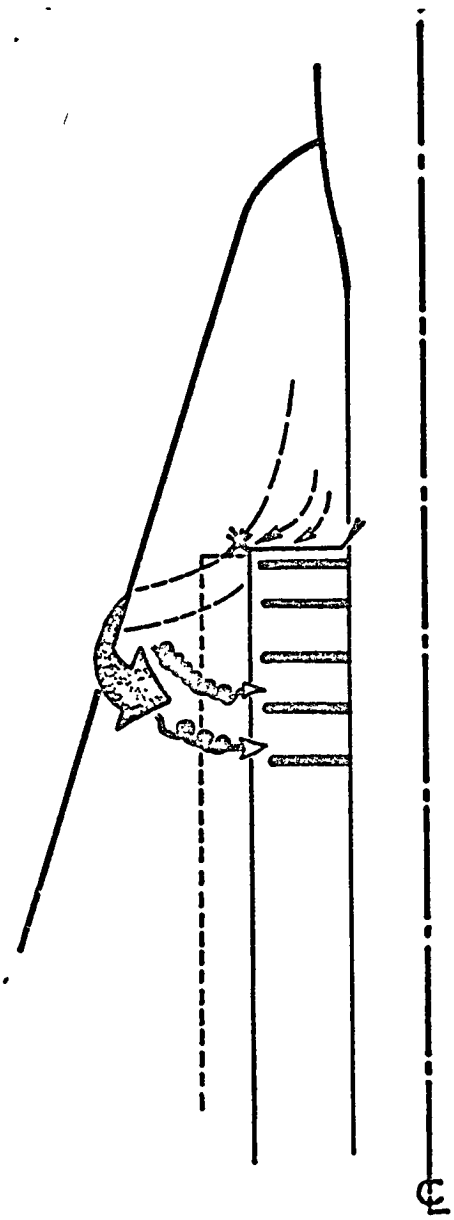

PLAN
VIEW

FLOW SEPARATION FROM FRONT -
END-PLATE AND INGESTION BY AUGMENTOR

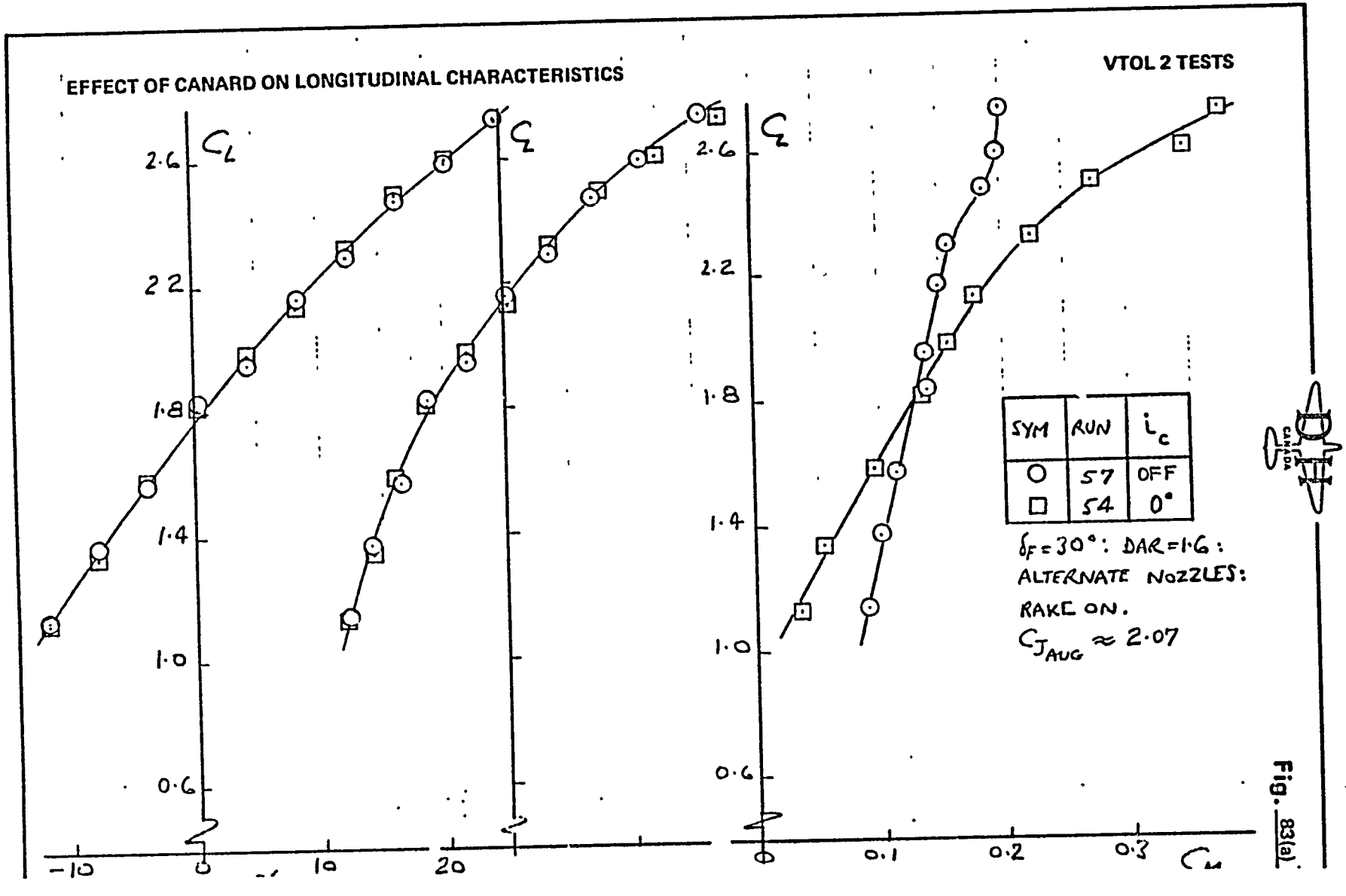
EFFECT OF CANARD ON LONGITUDINAL CHARACTERISTICS
VTOL 2 TESTS
C_L
2.6
2.2
1.8
1.4
1.0
0.6
-10
0
10
20
C_L
2.6
2.2
1.8
1.4
1.0
0.6
0
0.1
0.2
0.3
C_D
SYM | RUN | i_c
○ | 57 | OFF
□ | 54 | 0°
$\delta_F = 30°$: DAR=1·G:
ALTERNATE NOZZLES:
RAKE ON.
$C_{J_{AUG}} \approx 2.07$
CANARD

Fig. 83(a).

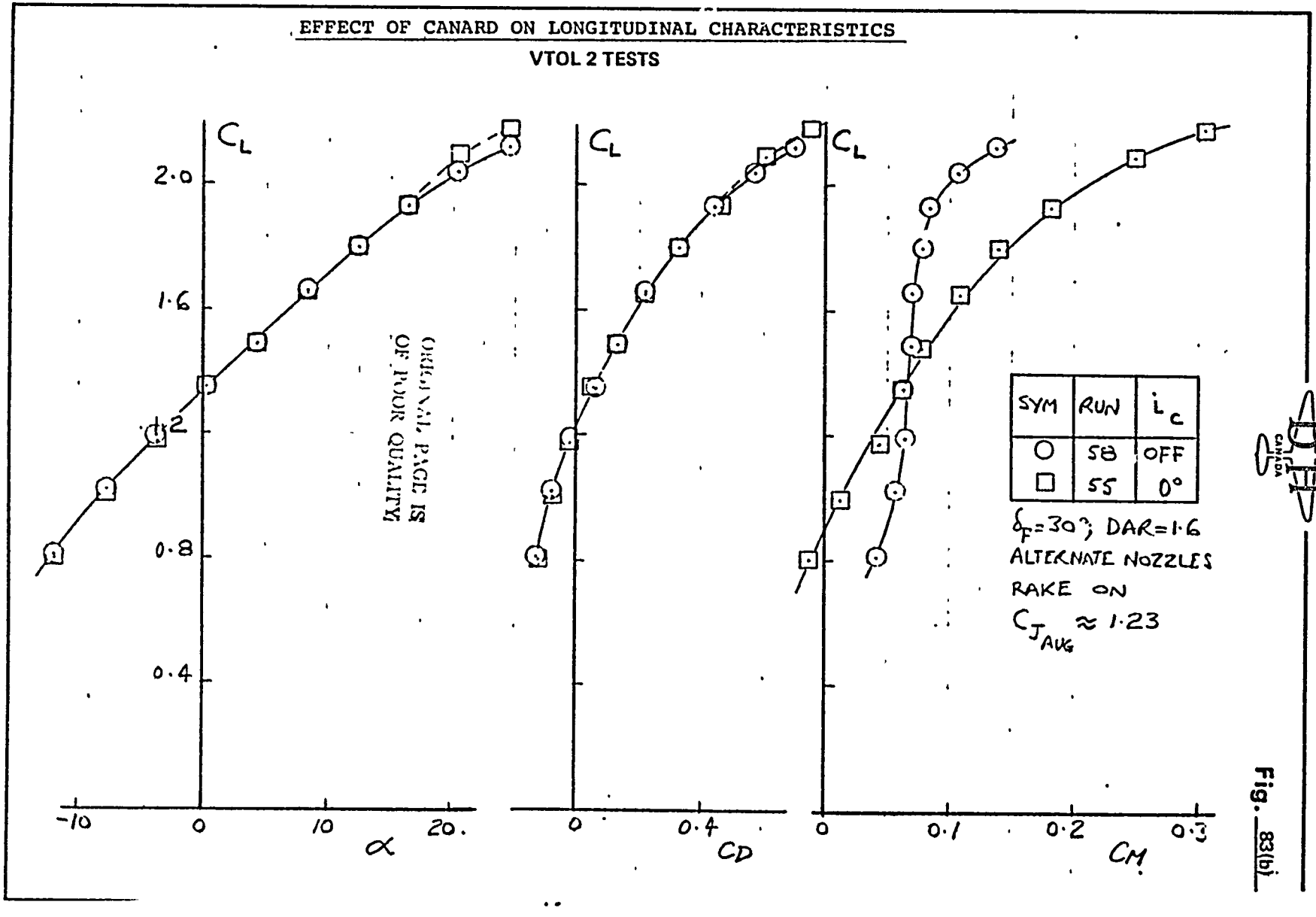
EFFECT OF CANARD ON LONGITUDINAL CHARACTERISTICS
VTOL 2 TESTS
C_L
2.0
1.6
1.2
0.8
0.4
-10
0
10
20.
α
C_L
0
0.4
C_D
C_L
0
0.1
0.2
0.3
C_M
SYM | RUN | i_c
O | 58 | OFF
□ | 55 | 0°
$\delta_F = 30°$; DAR = 1.6
ALTERNATE NOZZLES
RAKE ON
$C_{J_{AVG}} \approx 1.23$
CANARD
ORIGINAL PAGE IS
OF POOR QUALITY

Fig. 83(b)

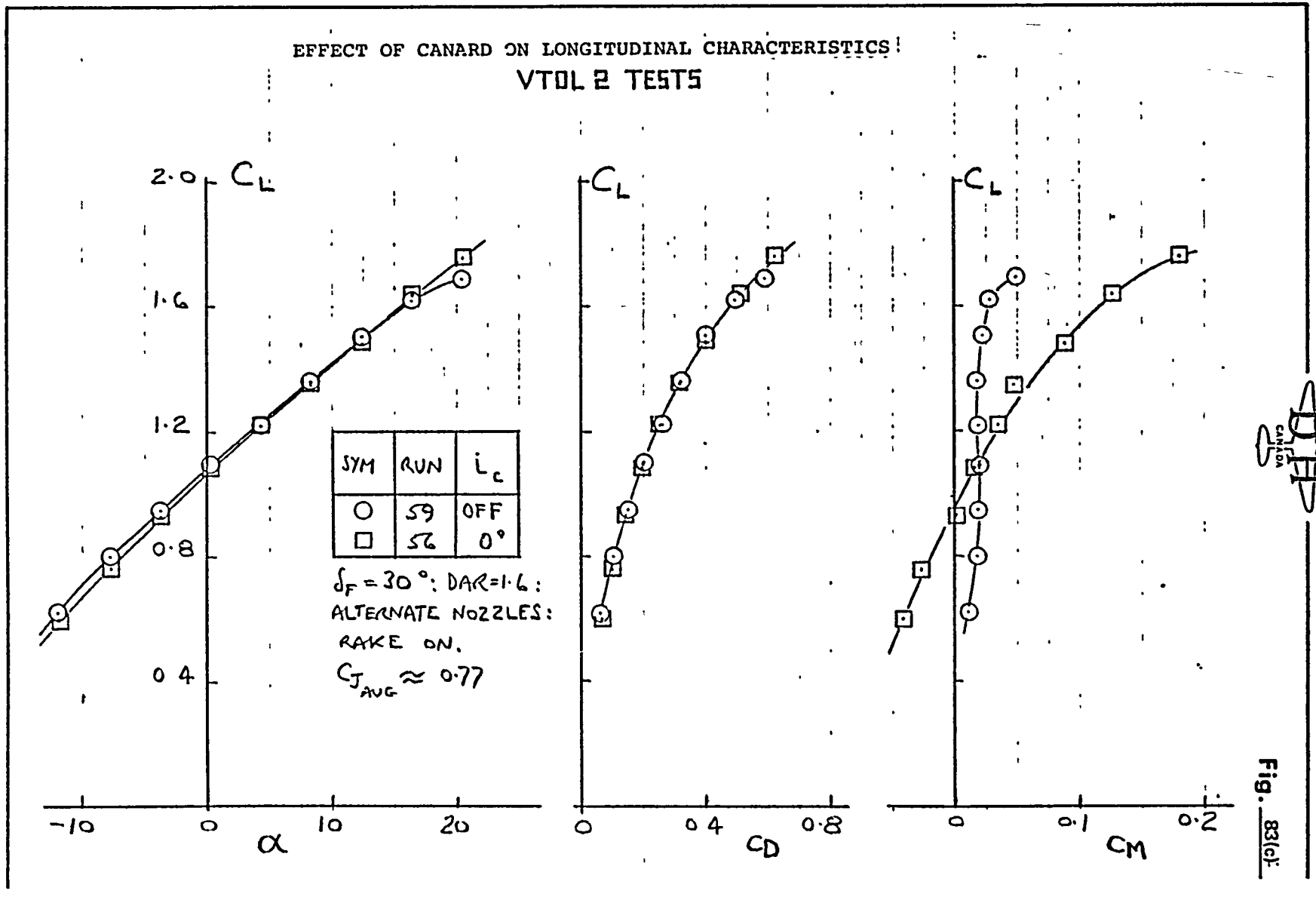
EFFECT OF CANARD ON LONGITUDINAL CHARACTERISTICS
VTOL 2 TESTS
C_L
2·0
1·6
1·2
0·8
0 4
SYM
RUN
i_c
59
OFF
56
0°
$\delta_F = 30°$: DAR=1·6:
ALTERNATE NOZZLES:
RAKE ON.
$C_{J_{AVG}} \approx 0.77$
−10
0
10
20
α
C_L
0
0 4
0·8
C_D
C_L
0
0·1
0·2
C_M
CANARD

Fig. 83(c)

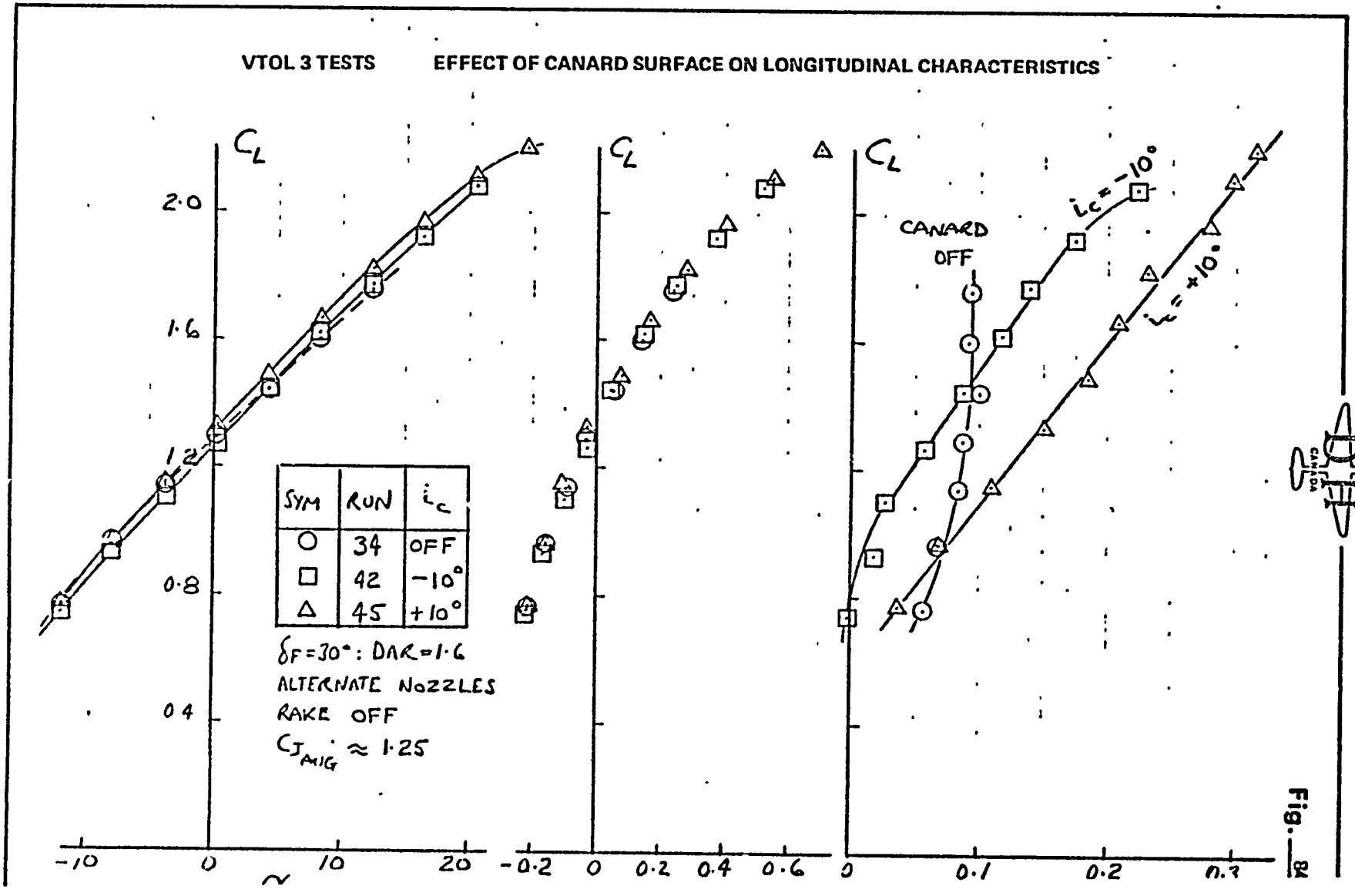
VTOL 3 TESTS
EFFECT OF CANARD SURFACE ON LONGITUDINAL CHARACTERISTICS
C_L
2·0
1·6
1·2
0·8
0·4
-10
0
10
20
α
SYM | RUN | i_c
○ 34 OFF
□ 42 −10°
△ 45 +10°
$\delta_F = 30°$: DAR = 1·6
ALTERNATE NOZZLES
RAKE OFF
$C_{J_{AMG}} \approx 1·25$
-0·2
0
0·2
0·4
0·6
CANARD OFF
$i_c = -10°$
$i_c = +10°$
0
0·1
0·2
0·3

Fig. 8

Fig. 85

LIFT AND PITCHING MOMENT DUE TO CANARD INCIDENCE CHANGE

$C_{J_{AUG}} \approx 1.25$; $\delta_F = 30°$

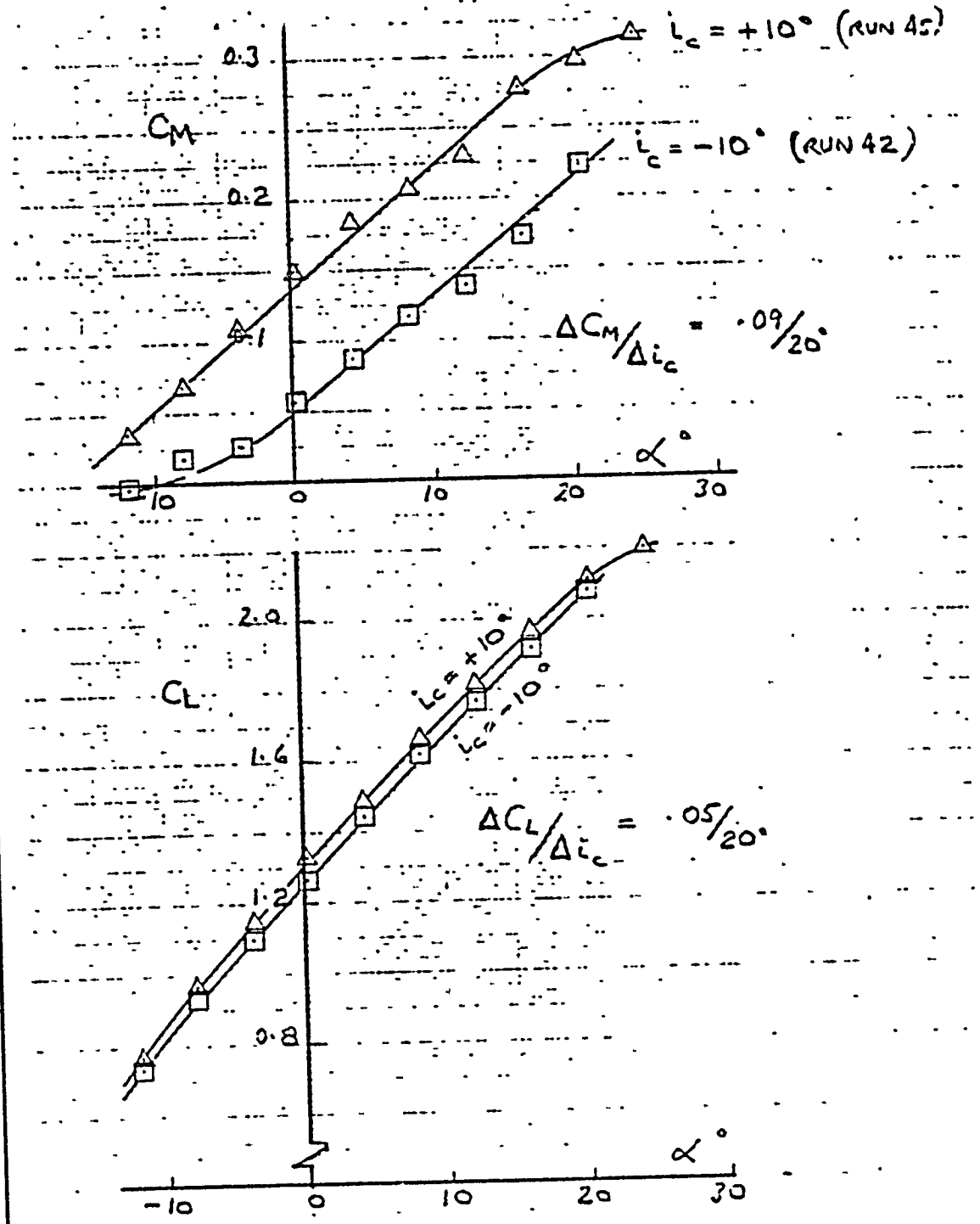

Fig. 8

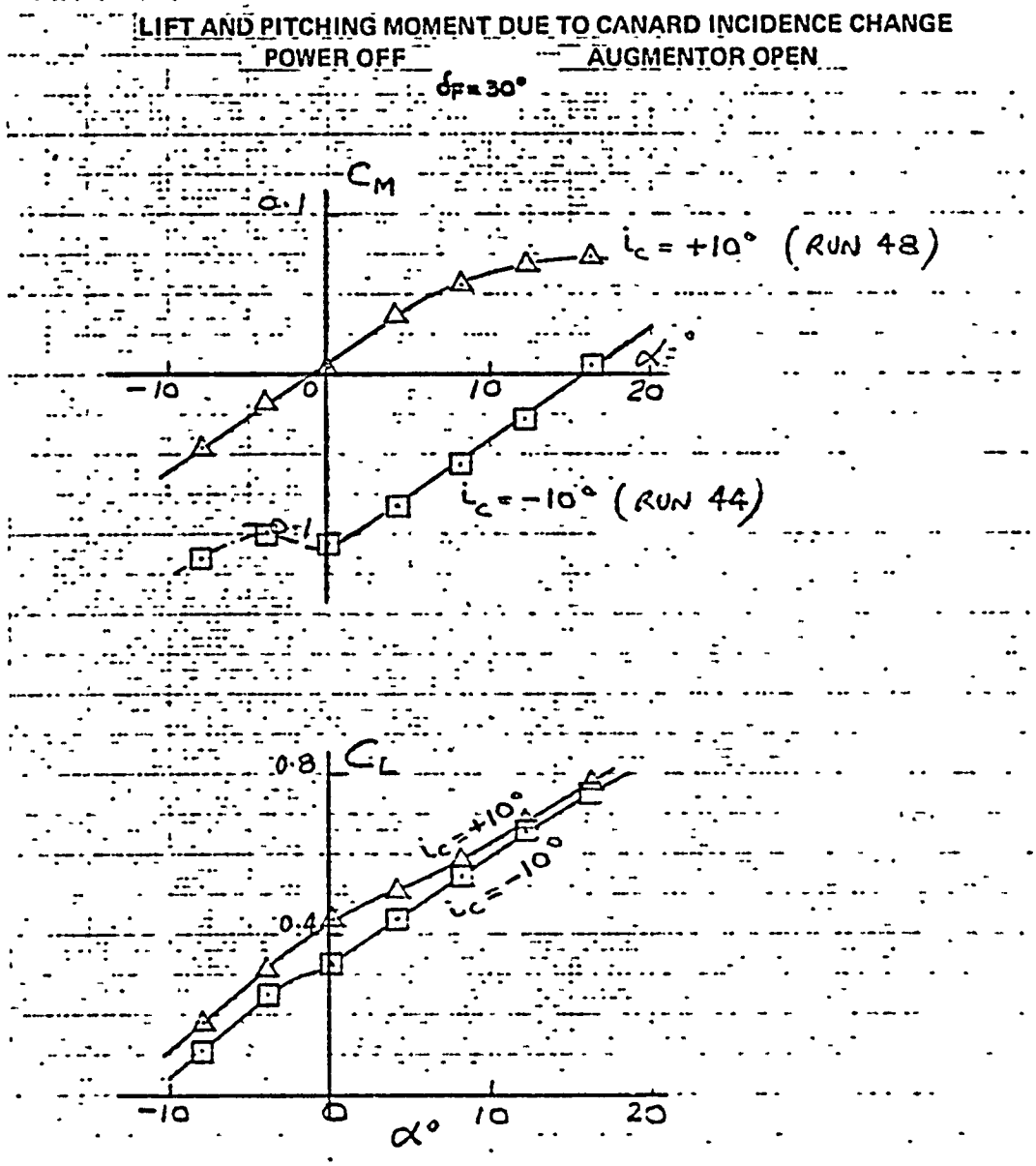
LIFT AND PITCHING MOMENT DUE TO CANARD INCIDENCE CHANGE
POWER OFF
AUGMENTOR OPEN
$\delta_F = 30°$
C_M
0.1
$i_c = +10°$ (RUN 48)
$i_c = -10°$ (RUN 44)
-10
0
10
20
$\alpha°$
C_L
0.8
0.4
$i_c = +10°$
$i_c = -10°$
-10
0
10
20
$\alpha°$

Fig. 87 :

UPWASH AT CANARD LOCATION

$\delta_F = 30°$; $C_{J\,min} \approx 1.25$

ALTERNATE NOZZLES

DAR = 1.6 ; E/P's ON

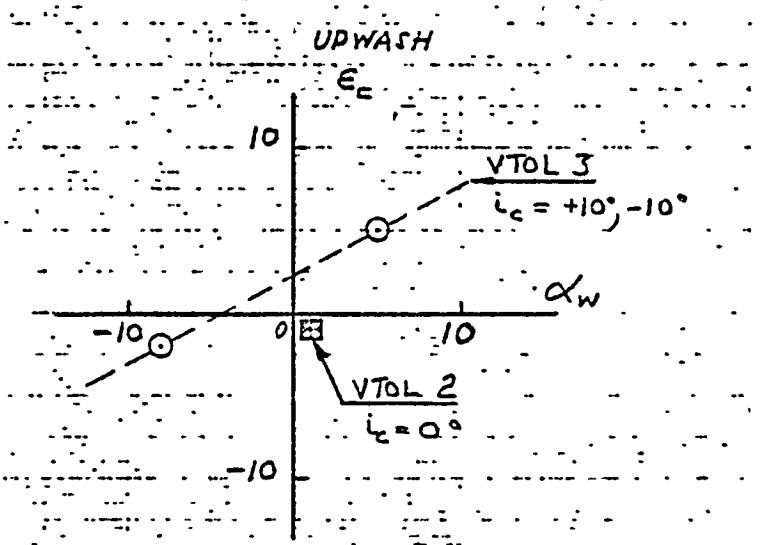

EFFECT OF CANARD FLAP ON C_L, C_D, C_m

RUN 45, VTOL 3 TESTS; $\delta_F = 30°$

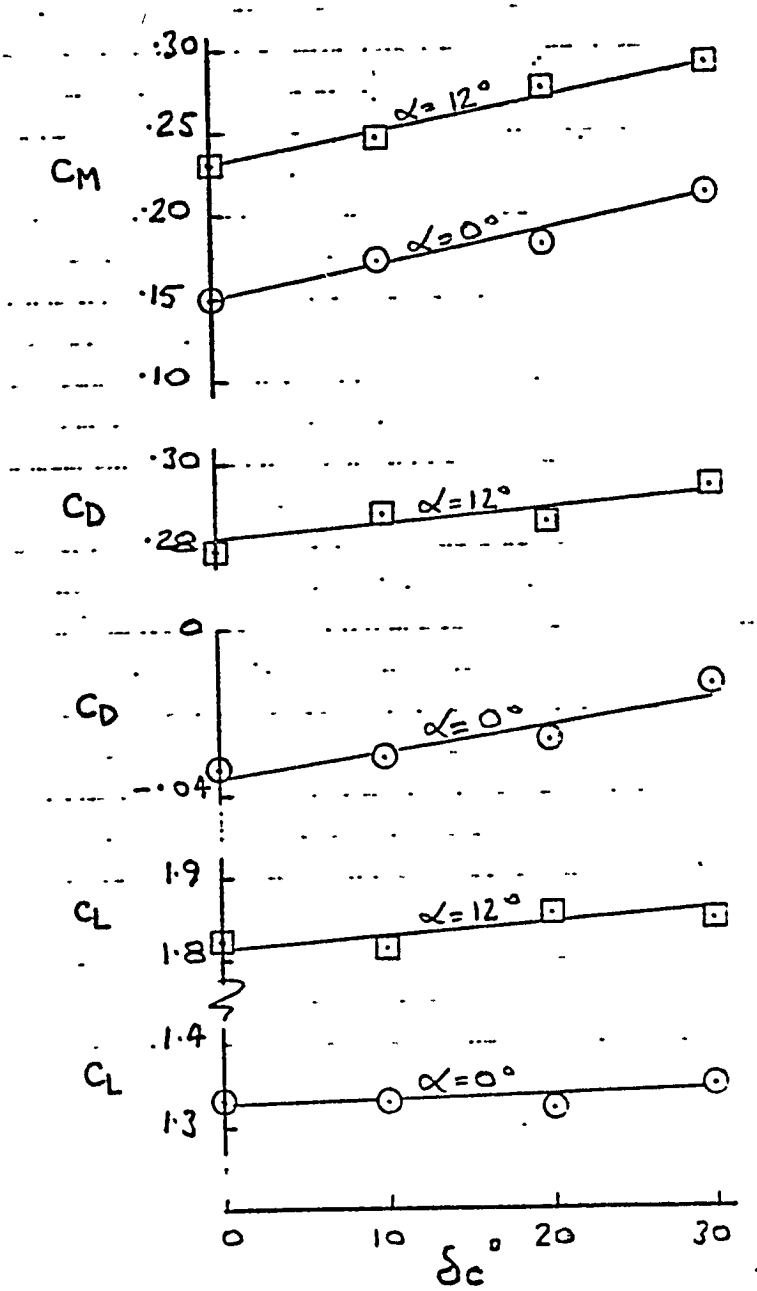

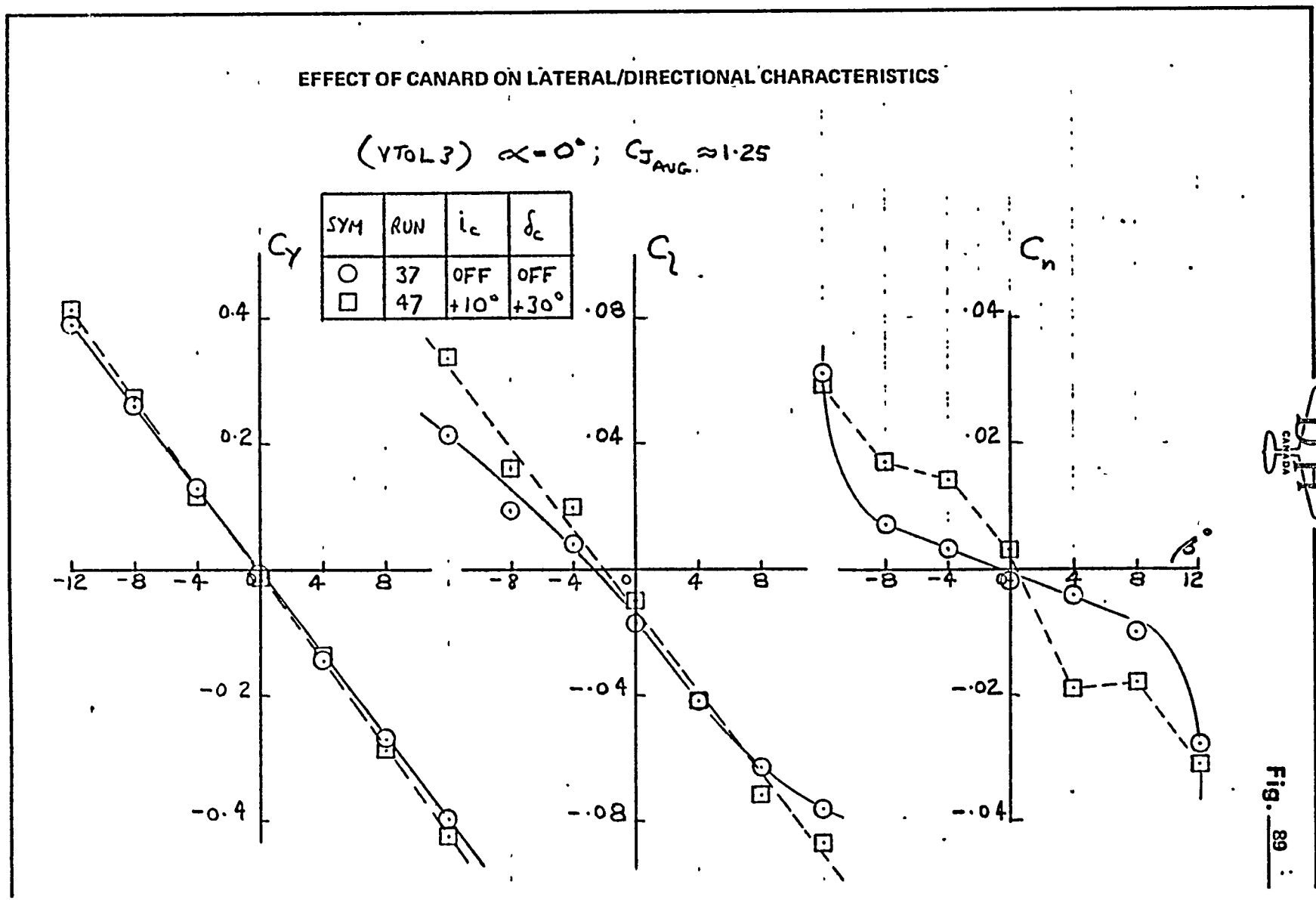
EFFECT OF CANARD ON LATERAL/DIRECTIONAL CHARACTERISTICS
(VTOL 3) α=0°; $C_{J_{AVG.}} \approx 1.25$
SYM | RUN | i_c | δ_c
○ | 37 | OFF | OFF
□ | 47 | +10° | +30°
C_Y
C_l
C_n
β°
0.4
0.2
-0.2
-0.4
.08
.04
-.04
-.08
.04
.02
-.02
-.04
-12 -8 -4 0 4 8 12

Fig. 89

SYM	RUN	i_c	δ_c
○	3-37	OFF	OFF
□	3-47	+10°	+30°
◇	3-43	-10°	0°

$\alpha = 0°$: $C_{J_{AUG}} \approx 1.25$

$\delta_F = 30°$

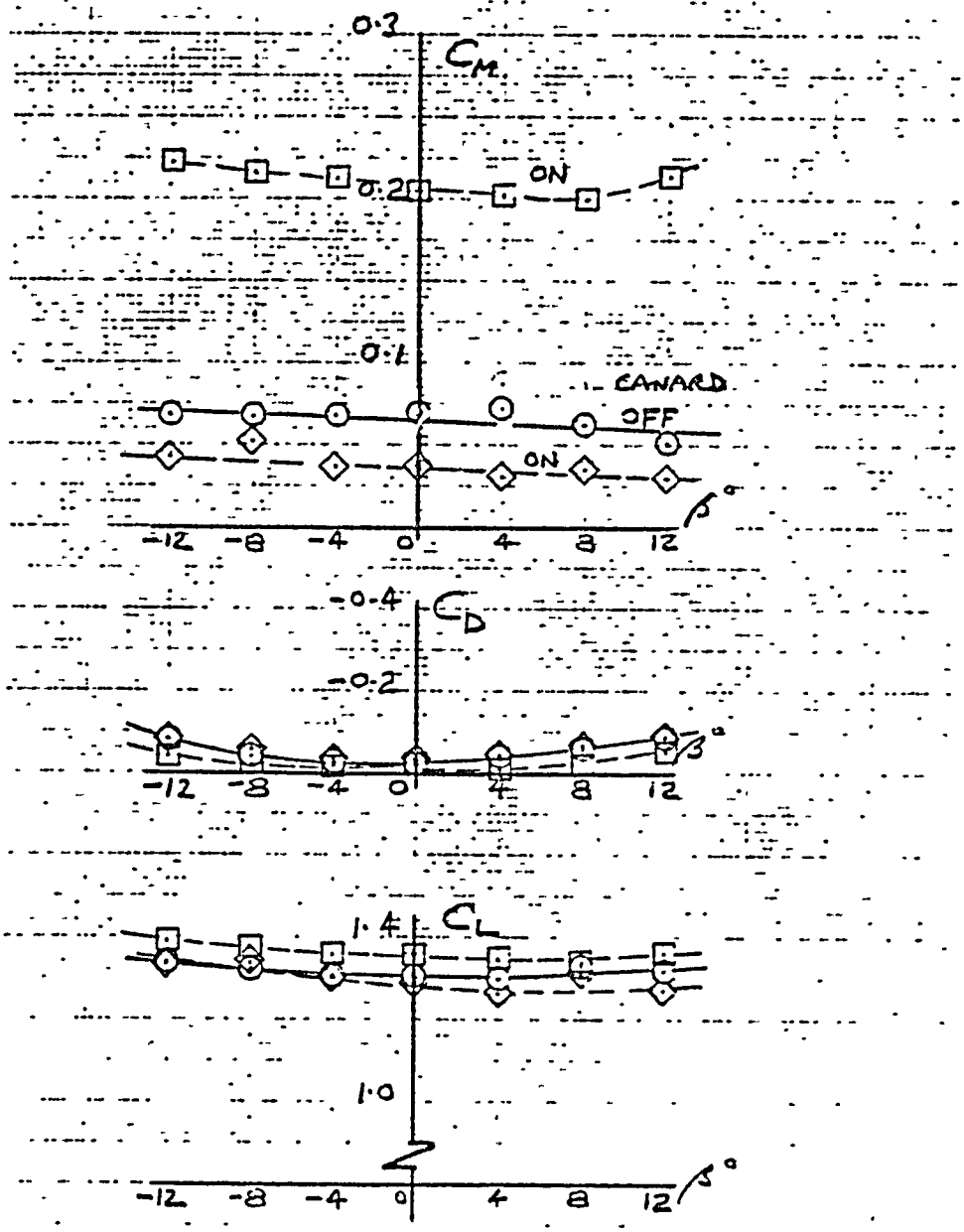

EFFECT OF CANARD ON LONGITUDINAL CHARACTERISTICS WITH YAW ANGLE

End of Document